APPENDIX 2.10.3

TABLE OF CONTENTS



LIST OF TABLES

## LIST OF FIGURES

# APPENDIX 2.10.3

# NUHOMS®-61BT DSC (CANISTER AND BASKET) STRUCTURAL EVALUATION

## 2.10.3.1 Introduction

Each NUHOMS®-61BT DSC consists of a fuel basket and a canister body (shell, canister inner bottom and top cover plates and shield plugs). The confinement vessel for the NUHOMS®-61BT DSC consists of a shell which is a welded, stainless steel cylinder with an integrally-welded, stainless steel bottom closure assembly, and a stainless steel top closure assembly.

The Canister shell thickness is 0.50 inches, and the bottom and top shield plugs are 5.0 and 7.0 inches. The Canister is constructed from SA-240 Type 304 stainless steel and A-36 carbon steel. There are no penetrations through the confinement vessel. The draining and venting systems are covered by the seal welded outer top closure plate and vent port plug. To preclude air in-leakage, the canister cavity is pressurized above atmospheric pressure with helium.

The basket structure consists of assemblies of stainless steel fuel compartments held in place by basket rails and a hold down ring. The four and nine compartment assemblies are held together by welded stainless steel boxes wrapped around the fuel compartments, which also retain the neutron poison plates between the compartments in the assemblies. The borated aluminum or boron carbide/aluminum metal matrix composite plates (neutron poison plates) provide the necessary criticality control and provide the heat conduction paths from the fuel assemblies to the cask cavity wall. This method of construction forms a very strong structure of compartment assemblies which provide for storage of 61 fuel assemblies. The open dimension of each fuel compartment is 6.0 in. × 6.0 in., which provides clearance around the fuel assemblies.

The Fuel Basket and Canister are analyzed independently. The Fuel Basket is analyzed in Section 2.10.3.2, while the Canister is analyzed in Section 2.10.3.3. Three separate finite element models are constructed for the structural evaluation of the basket and canister. A 3-dimensional cross-section finite element model is utilized to evaluate the effect of transverse impact loads on both the basket and canister. A 3-dimensional model of a Fuel Basket section is used to perform a buckling evaluation for the basket during lateral impact loads. A 2-dimensional axisymmetric model of the canister is used to evaluate the effects of axial impact loads as well as internal and external pressures on the canister alone. Analytical calculations are utilized in order to evaluate axial impact loads applied to the basket, and to perform buckling and fatigue evaluations for the canister.

## 2.10.3.2 Fuel Basket Structural Analysis

### 2.10.3.2.1 Approach

The Fuel Basket is evaluated for normal and accident condition impact and thermal loads. The basket stress analysis is performed using a finite element method for the side drop and thermal load cases and analytical calculations for the end drop load cases. Buckling analysis of the basket plates when subjected to lateral impact loads is evaluated by collapse load analysis using a finite element model to generate a relationship between displacement and applied load. A summary of the basket load cases is provided in Section 2.10.3.2.2. Stress and buckling analyses are provided in Sections 2.10.3.2.3 and 2.10.3.2.4 respectively.

Material Properties

The mechanical properties of structural materials used in the basket, rail and canister are shown in the Table 2.10.3-1 as a function of temperature. The materials are identified by reference to ASME Code specifications [3]. The yield and ultimate strengths of the structural steel, shown in Table 2.10.3-1, are the minimum values specified in the material specifications. The following table shows the maximum calculated temperatures from Chapter 3 and the selected allowable stress temperatures for the fuel basket components analyzed.

| Component | Max. Calculated Temperature, °F | Selected Allowable Stress Temperature, °F |
|---|---|---|
| Basket Rail | 482 | 500 |
| Basket | 578 | 600 |

Design Criteria

For normal conditions, the basis for the basket allowable stress is the ASME Code, Section III, Subsection NG [1]. The primary membrane stress intensity and membrane plus bending stress intensities are limited to $S_m$ ($S_m$ is the code allowable stress intensity) and 1.5 $S_m$, respectively, at any location in the basket for Level A (Normal Service) load combinations. The average shear stress is limited to 0.6 $S_m$.

The ASME Code provides a $3S_m$ limit on primary plus secondary stress intensity for Level A conditions. That limit is specified to prevent ratcheting of a structure under cyclic loading and to provide controlled linear strain cycling in the structure so that a valid fatigue analysis can be performed.

For accident conditions, stresses are evaluated as short duration Level D conditions as per ASME B&PV Code, Section III, Appendix F [2]. When evaluating the results from the non-linear elastic-plastic analysis, the general primary membrane stress intensity, $P_m$, shall not exceed $0.7S_u$ and the maximum stress intensity at any location ($P_l$ or $P_m + P_b$) shall not exceed 0.9 $S_u$. The average shear stress is limited to 0.42 $S_u$.

The allowable stresses for both normal and accident conditions are summarized in the following table.

| Loading Condition | Stress Category | Stress Criteria* [10] | Basket Plate Allowable Stress At 600° F (ksi.) | Support Rail Allowable Stress At 500° F (ksi.) |
|---|---|---|---|---|
| Normal Conditions, Elastic Analysis | Membrane Stress, $P_m$ | $S_m$ | 16.40 | 17.50 |
| | Membrane + Bending Stress, $P_m + P_b$ | 1.5 $S_m$ | 24.60 | 26.25 |
| | Average Shear Stress | 0.6 $S_m$ | 9.84 | 10.50 |
| | Primary + Secondary Stress, $P_m + P_b + Q$ | 3 $S_m$ | 49.20 | 52.50 |
| Accident Conditions, Elastic-Plastic Analysis | Membrane Stress, $P_m$ | 0.7 $S_u$ | 44.38 | 44.38 |
| | Membrane + Bending Stress, $P_m + P_b$ | 0.9 $S_u$ | 57.06 | 57.06 |
| | Average Shear Stress | 0.42 $S_u$ | 26.63 | 26.63 |

2.10.3.2.2 Loading Conditions

The basket normal and accident condition transport loads are summarized in the tables below.

**Basket Normal Condition Loads**

| Loading | Basket Orientation | Service Level | Load | Analysis Method |
|---|---|---|---|---|
| Thermal Load | Horizontal | A | 100° F Ambient | Finite Element Analysis |
| 1 Foot Side Drop | Horizontal | A | 30*g* Lateral Load | Finite Element Analysis |
| 1 Foot End Drop | Horizontal | A | 30*g* Axial Load | Analytical Hand Calculation |

**Basket Accident Condition Loads**

| Loading | Basket Orientation | Service Level | Load | Analysis Method |
|---|---|---|---|---|
| 30 Foot Side Drop | Horizontal | D | 75*g* Lateral Load | Finite Element Analysis |
| 30 Foot End Drop | Horizontal | D | 75*g* Axial Load | Analytical Hand Calculation |

Each normal and accident condition side and end drop load case is combined with the hot environment thermal load case.

2.10.3.2.3 Fuel Basket Stress Analysis

A. Finite Element Model Description

A three-dimensional ANSYS [4] finite element model of the basket, rails and canister is constructed using SHELL 43 elements. The overall finite element model of the basket, rails and canister is shown in Figure 2.10.3-1. The strength of poison plates is conservatively neglected by excluding these plates from the finite element model. However, the weight of the aluminum plates is accounted for by increasing the stainless steel basket plate density. Because of the large number of plates in the basket and large size of the basket, certain modeling approximations are necessary. Because the rails provide continuous support along the entire length of the basket during a side drop, only a 3 inch long slice of the basket, rail and canister is modeled. At the two cut faces of the model, symmetry boundary conditions are applied (UZ = ROTX = ROTY = 0). The fuel compartment tubes, outer 3 × 3 and 2 × 2 wraps, and basket rails are included in the model and are shown individually in Figures 2.10.3-2 to 2.10.3-4.

The connections between the stainless steel fuel compartments (with intermediate aluminum poison plates) and the outer stainless steel wraps, and between the outer wraps and the stainless steel rails, are made with node couplings. The nodes of various plates are coupled together in the out-of-plane direction so that they will bend in unison under surface pressure or other lateral loads, and to simulate "through the thickness" support provided by the poison plates. Node couplings also simulate the bolt connections between the support rails and the outer boxes.

The canister shell is resting on four sliding rails inside the transport cask (0.12" thick continuous pad) at approximately 18° and 52° on either side of canister/basket centerline (see Figure 2.10.3-5). The basket and canister are analyzed for two side drop scenarios. For each drop scenario, the gap elements between the outside of the canister and inside of the transport cask are simulated in the following way.

Impact Away From the Transport Cask Sliding Rails (Figure 2.10.3-5, 45°, 60° and 90°)

The gap elements (CONTACT 52) are used to simulate the interface between the basket support rails and the inner side of the canister as well as between the outer side of the canister and inside of the cask. Each gap element contains two nodes; one on each surface of the structure. The gap nodes specified at the inner side of cask are restrained in the *x*, *y* and *z* directions. The gap size at each gap element is determined by the difference between the basket rails radius and the inside radius of the canister shell, and by the difference between the canister outer radius and the inside radius of the transport cask. Gap sizes for the gap elements, at each radial location, are determined and inputed into the model as real constants using a small ANSYS macro. This macro accepts the drop orientation and model geometry as inputs and then determines the circumferential position of each gap element. The macro then computes the appropriate real constants and applies to it appropriate gap elements. The gap sizes between the rails and the canister; and between the canister and the cask (over 5° interval up to 90° and 10° interval beyond) are shown in Figures 2.10.3-6 and Figure 2.10.3-7. The finite element model of the canister and gaps is shown in Figure 2.10.3-8 and Figure 2.10.3-9.

Impact On Transport Cask Sliding Rails (Figure 2.10.3-5, 180°)

During the drop on the transport cask sliding rails (180° azimuth side drop), the initial gaps between the canister and the cask are modified. The gaps at the sliding rail locations are assumed to be closed. Between the sliding rail locations, the initial gap size is assumed to be 0.12 inches. The remaining initial gaps are suitably modified (0.12 in. to 0.63 in.) using the ANSYS macro.

During each side drop orientation, some fuel boxes and rails may have a tendency to separate or slide. Gap elements are used to model the connections at such locations. Since the basket is symmetric about the drop axis, for the 90°and 180° side drops, only a one-half model is used for these orientations.

Gap Element Nonlinearities

Gap elements (CONTACT 52) are used to model the actual surface clearance between the basket rails and the inside surface of the canister as well as between the outer surface of the canister and the inside surface of the transport cask. The gap elements also introduce nonlinearities into the model, because the reaction force generated by the gap elements depends on their status (open or closed). The typical gap sizes are shown in Figures 2.10.3-6 and 2.10.3-7. Actual gap sizes at each rail nodal location are computed using an ANSYS macro. The gap element spring constant, $K_n$, is calculated in the following way.

$$K_n = f E h \quad [4]$$

Where $f$ is a factor usually between 0.01 and 100, $E$ is the material modulus of elasticity ($25.8\times10^6$ psi), and $h$ and is a typical "target length" or typical element size [typical element length ≈ 1.16 in., typical target length = $(1.16\times3.0)^{0.5}$ = 1.86 in.]. Therefore,

$$K_n = 25.8\times10^6 \times 1.860 \times f = 0.48\times10^6 \text{ to } 4{,}800\times10^6 \text{ lb./in.}$$

In view of the large range in spring constant values, various spring constants were evaluated. Since the structure responded well with a spring constant value of $0.5\times10^6$ lb./in., this value of $K_n$ is used.

LINK8 elements, coincident to the CONTACT52 elements, were inserted into the ANSYS model to increase model stability. To assure that these elements do not transfer substantial load between the surfaces, a very low modulus of elasticity ($E$ =1,000 psi for radial gaps and $E$ = 100 psi for gaps between boxes), a small area (0.1 $in^2$), and a density of zero were used as material properties for the LINK8 elements.

B. Normal Condition Side Drop Stress Analysis

A nonlinear stress analysis of the basket structure is conducted in order to compute the elastic stresses for the 45°, 60°, 90°, and 180° drop orientations. The nonlinearity of analysis is due to the gaps in the model. The load resulting from the fuel assembly weight was applied as pressure

on the plates. At 90° and 180° drop orientations, the pressure acted only on the horizontal plates while at other drop orientations, it was divided in components to act on horizontal and vertical plates. The inertia load due to basket, rails and DSC dead weight is simulated using the density and appropriate acceleration. The poison plate weight is included by increasing the basket plate density. A maximum load of 30*g* is applied in each analysis. The automatic time stepping program option AUTOTS is activated. This option lets the program decide the actual size of the load-substep for a converged solution. The program stops at the load substep when it fails to result in a converged solution. In all side drop runs, ANSYS gave converged solutions up to the 30*g* applied load.

The maximum nodal stress intensities for each drop orientation in the basket plates and support rails are listed in Table 2.10.3-2. For shell elements, the middle fiber stresses are classified as membrane stresses ($P_m$) and top & bottom fiber stresses are classified as membrane plus bending stresses ($P_m + P_b$). These maximum stress intensities are also used to combined with the maximum thermal stresses calculated in Section E of this appendix and compared with the code allowable stresses as listed in Table 2.10.3-2. As shown, all stresses are within the defined allowables.

C. Normal Condition End Drop Stress Analysis

During an end drop, the fuel assemblies and fuel compartment are forced against the bottom of the cask. It is important to note that, for any vertical or near vertical loading, the fuel assemblies react directly against the bottom or top end of the cask and not through the basket structure as in lateral loading. It is the dead weight of basket only that causes axial compressive stress during an end drop. Axial compressive stresses are conservatively computed assuming that all of the basket weight will be taken by the fuel compartments and outer wrappers only. A conservative basket weight of 23,000 lb. (actual weight is 22,918 lb. Section 2.2) is used in end drop stress calculations.

Compressive Stress in the Fuel Compartment Tubes and Outer Wrappers

Total Weight = 23,000 lb.
Weight excluding hold down ring, SS inserts, aluminum plates, and rails is 12,406 lb.
Section area = $12,406/(164 \times 0.29) = 260.8$ in$^2$
Stress due to 1$g$ = -23.0 / 260.8 = - 0.09 ksi.
30$g$ compressive stress = $-.09 \times 30$ = - 2.70 ksi.

Shear Stress in Plate Insert Weld

64 Inserts support the poison plate weight (3,260 lb.).
Load/insert = 3.26 / 64 = 0.0509 kips
Weld Shear Area = $3 \times 0.125 \times \sin(45°) = 0.265$ in$^2$
Shear stress = $30g \times 0.0509 / 0.265 = 5.76$ ksi. < 9.84 ksi.

Shear Stress in Rail Stud

During 30$g$ end drop, the rail will support its own weight. However, the analysis conservatively assumes that the weight of the rail will be supported by the 224 rail studs attached to the outer wrappers.

Weight of rails = 5,350 lb.
Weld Shear Area = $\pi/4\ (0.5^2 - 0.3^2) = 0.126$ in$^2$
Shear stress (1$g$) = $5.35 / (0.126 \times 224) = 0.19$ ksi
30$g$, shear stress = $0.19 \times 30 = 5.70$ ksi

Compressive stress due to end drop on hold down ring

Weight of hold down ring = 940 lb.
Section area = $940/(14.5 \times 0.29) = 223.5$ in$^2$
Stress due to 1$g$ = -23.0/ 223.5= - 0.1 ksi.
30 $g$, compressive stress = $-0.1 \times 30$ = -3.0 ksi.

D. Thermal Expansion Analysis

In this section, the thermal expansions of various components of the NUHOMS-61B basket are evaluated. The thermal load considered is the 100° F ambient normal condition temperature distribution computed in Chapter 3. The mechanical properties of the materials, used in the basket, rail, and canister, are shown in the Table 2.10.3-1 as a function of temperature.

The normal condition thermal analysis of the basket is described in Chapter 3. The thermal analysis is performed to determine the basket temperatures for the condition with maximum solar heating, maximum decay heat from the canister contents, and 100° F daily average ambient air temperature. The temperatures at basket center, top and bottom are reproduced in Figures 2.10.3-10, 2.10.3-11 and 2.10.3-12. The results of the thermal analysis are used to evaluate the effects of axial and radial thermal expansion in the basket components. The following table summarizes the 100° F ambient thermal analysis results from Chapter 3. These results support the selection of basket component temperatures for the subsequent thermal expansion analysis.

**Summary of 100° F Ambient Normal Condition Thermal Analysis**

| Component | Max. Calculated Temperature (°F) | Selected Temperature for Thermal Expansion Analysis (°F) |
|---|---|---|
| Canister Shell | 388 | 375** |
| Basket Plate | 578 | 600 |
| Fuel Cladding | 598 | 600 |
| Cask Body | 302 | 300 |

** Conservatively using lower temperature for thermal expansion analysis. However, for thermal expansion between canister and cask, the canister temperature is assumed as 400°F.

To verify that adequate clearance exists between the basket and canister cavity for free thermal expansion, the thermal expansions between various components are calculated.

Thermal Expansion between the Length of Fuel Assembly and Canister Cavity

The spent fuel assemblies are assumed to be at 600° F and canister shell temperature at 375° F. The length of the spent fuel assembly when exposed to the hot environment is,

$$L_F = L_T + (L_Z \times \alpha_Z + L_S \times \alpha_S)\,\Delta T.$$

Where for the design basis GE 7×7 (longest BWR fuel):

$L_F$ = Hot length of BWR fuel assembly, in.
$L_T$ = Total length of fuel assembly at room temperature = 176.16 in.
$L_Z$ = Length of Zircaloy guide tube ≅160.47 in.
$\alpha_Z$ = Zircaloy coefficient of thermal expansion = $2.73\times10^{-6}$ in./in.°F at 600° F
$L_S$ = Length of stainless steel per fuel assembly ≅15.69 in.
$\alpha_S$ = Stainless steel coefficient of thermal expansion = $9.8\times10^{-6}$ in./in.°F at 600° F
$\Delta T$ = 600° F - 70° F = 530° F

Therefore,

$$L_F = 176.16 + (160.47\times2.73 + 15.69\times9.8)\times10^{-6}\times 530 = 176.47 \text{ in.}$$

Allowing 1.25 inchs for irradiation growth of the spent fuel assembly, the total assembly length including thermal expansion is 177.72 inches. The length of the canister cavity at room temperature is 179.38 inches. The minimum length of the canister cavity at 375° F is,

$$L_{CH} = L_{CC} + L_{CC}\times \alpha_C \times \Delta T.$$

Where:

$L_{CH}$ = Hot length of canister cavity, in.
$L_{CC}$ = Minimum canister cavity length at room temperature = 179.38 in.
$\alpha_C$ = Stainless steel coefficient of thermal expansion = $9.42\times10^{-6}$ in./in.°F at 375° F
$\Delta T$ = 375°F - 70°F = 305° F

Therefore,

$$L_{CH} = 179.38 + 179.38\times 9.42\times10^{-6}\times 305 = 179.90 \text{ in. } > 177.72 \text{ in.}$$

Adequate clearance has been provided between the BWR spent fuel assemblies and the canister cavity length to permit free thermal expansion.

Thermal Expansion between the Outer Diameter of the Basket and Inner Diameter of the Canister Cavity

The basket temperature is assumed to be at 600° F and canister shell temperature at 375° F. The maximum outside diameter of the basket when exposed to the hot environment is,

$$D_{BH} = D_{BC} + (D_{BC} \times \alpha_S)\, \Delta T$$

Where:

$D_{BH}$ = Hot outside diameter of basket, in.
$D_{BC}$ = Maximum outside diameter of basket at room temperature = 66.00 in.
$\alpha_S$ = Stainless steel coefficient of thermal expansion = $9.8 \times 10^{-6}$ in./in. °F at 600° F
$\Delta T$ = 600° F -70° F = 530° F

Therefore,

$$D_{BH} = 66.00 + 66.00 \times 9.8 \times 10^{-6} \times 530 = 66.34 \text{ in.}$$

The minimum inside diameter of the canister cavity at room temperature is 66.25 inches. The minimum inside diameter of the canister cavity at 375° F is,

$$D_{CH} = D_{CC} + (D_{CC} \times \alpha_c)\, \Delta T$$

Where,

$D_{CH}$ = Minimum inside diameter of canister when hot, in.
$D_{CC}$ = Minimum inside diameter of canister cavity at room temperature = 66.25 in.
$\alpha_C$ = Stainless steel coefficient of thermal expansion = $9.42 \times 10^{-6}$ in./in.°F at 375° F
$\Delta T$ = 375° F -70° F = 305° F

Therefore:

$$D_{CH} = 66.25 + 66.25 \times 9.42 \times 10^{-6} \times 305 = 66.44 \text{ in.} > 66.34 \text{ in.}$$

Adequate clearance has been provided between the outside diameter of the basket and the inside diameter of the canister cavity to permit free thermal expansion.

Thermal Expansion between the Length of Basket (including Basket hold-down Ring) and Canister Cavity

The basket temperature is assumed to be at 600°F and canister shell temperature at 375°F. The length of the basket when hot is,

$$L_{BH} = L_{BC} + (L_{BC} \times \alpha_S)\, \Delta T$$

Where,

$L_{BH}$ = Hot length of basket including basket hold-down ring, in.
$L_{BC}$ = Total length of basket including hold-down ring at room temperature = 178.50 in.
$\alpha_S$ = Stainless steel coefficient of thermal expansion = $9.8 \times 10^{-6}$ in./in. °F at 600° F
$\Delta T$ = 600 °F – 70 °F = 530 °F

Therefore,

$$L_{BH} = 178.5 + 178.5 \times 9.8 \times 10^{-6} \times 530 = 179.43 \text{ in.} < 179.90 \text{ in.}$$

Adequate clearance has been provided between the basket and the canister cavity length to permit free thermal expansion.

Thermal Expansion between the Outer Diameter of Canister and Inner Diameter of Cask body

The canister temperature is assumed to be at 400° F and cask body temperature at 300° F. The maximum outside diameter of the canister when exposed to the hot environment is,

$$D_{BH} = D_{BC} + (D_{BC} \times \alpha_S)\, \Delta T$$

Where:

$D_{BH}$ = Hot outside diameter of canister, in.
$D_{BC}$ = Maximum outside diameter of canister at room temperature = 67.35 in.
$\alpha_S$ = Stainless steel coefficient of thermal expansion = $9.5 \times 10^{-6}$ in./in.°F at 400° F
$\Delta T$ = 400° F - 70° F = 330° F

Therefore,

$$D_{BH} = 67.35 + 67.35 \times 9.5 \times 10^{-6} \times 330 = 67.56 \text{ in.}$$

The minimum inside diameter of the cask cavity at room temperature is 68.00 inches. The minimum inside diameter of the cask cavity at 300° F is,

$$D_{CH} = D_{CC} + (D_{CC} \times \alpha_c)\, \Delta T$$

Where:

$D_{CH}$ = Minimum inside diameter of cask cavity when hot, in.
$D_{CC}$ = Minimum inside diameter of cask cavity at room temperature = 68.00 in.
$\alpha_C$ = Stainless steel coefficient of thermal expansion = $9.2\times10^{-6}$ in./in. °F at 300° F
$\Delta T$ = 300 °F –70 °F = 230 °F

Therefore,

$$D_{CH} = 68.00 + 68.00 \times 9.2\times10^{-6} \times 230 = 68.14 \text{ in.} > 67.56 \text{ in.}$$

Adequate clearance has been provided between the outside diameter of the canister and the inside diameter of the cask cavity to permit free thermal expansion.

Thermal Expansion between the Length of Canister and Cask Cavity

The canister temperature is assumed to be at 400° F and cask body temperature at 300° F. The length of the canister when exposed to the hot environment is,

$$L_{BH} = L_{BC} + (L_{BC} \times \alpha_S)\, \Delta T$$

Where:

$L_{BH}$ = Hot length of canister, in.
$L_{BC}$ = Maximum length of canister at room temperature = 196.04 in.
$\alpha_S$ = Stainless steel coefficient of thermal expansion = $9.5\times10^{-6}$ in./in.°F at 400° F
$\Delta T$ = 400° F - 70° F = 330° F

Therefore,

$$L_{BH} = 196.04 + 196.04 \times 9.5\times10^{-6} \times 330 = 196.65 \text{ in.}$$

The length of the cask cavity at room temperature is 196.88 inches. The minimum length of the canister cavity at 300 °F is,

$$L_{CH} = L_{CC} + L_{CC} \times \alpha_C \times \Delta T$$

Where:

$L_{CH}$ = Hot length of cask cavity, in.
$L_{CC}$ = Minimum cask cavity length at room temperature = 196.88 in.
$\alpha_C$ = Stainless steel coefficient of thermal expansion = $9.2 \times 10^{-6}$ in./in.°F at 300° F
$\Delta T$ = 300° F –70° F = 230° F

Therefore,

$$L_{CH} = 196.88 + 196.88 \times 9.2 \times 10^{-6} \times 230 = 197.30 \text{ in.} > 196.65 \text{ in.}$$

Adequate clearance has been provided between the canister and the cask cavity length to permit free thermal expansion.

Summary of Thermal Expansion Analysis

Based on the results of the above analyses, there is adequate clearance between the various components of the basket, fuel assemblies, canister and cask to allow free thermal expansion. Consequently, no significant stress will develop in the NUHOMS®-61B Fuel Basket due to thermal expansion. The following table summarizes the thermal expansion calculation results from the above analyses.

Thermal Expansion of 61BT Components

| **Fuel Assembly/Canister Cavity Axial Thermal Expansion** | | | | | |
|---|---|---|---|---|---|
| F.A. Length at 70°F (in.) | Max. F.A. Temp (°F) | F.A. Length Hot | Canister Cavity Length at 70°F (in) | Min. Canister Cavity Temp (°F) | Canister Cavity Length Hot (in) |
| 176.16 | 600 | 177.72 | 179.38 | 375 | 179.90 |
| **Basket/Canister Diametrical Thermal Expansion** | | | | | |
| Basket O.D. at 70°F (in.) | Basket Temp (°F) | Basket O.D. Hot (in) | Canister Cavity I.D. at 70°F (in) | Min. Canister Cavity Temp (°F) | Canister Cavity I.D. Hot (in) |
| 66.0 | 600 | 66.34 | 66.25 | 375 | 66.44 |
| **Basket(Including Hold Down Ring)/Canister Cavity Axial Thermal Expansion** | | | | | |
| Basket Length at 70°F (in.) | Basket Temp (°F) | Basket Length Hot (in) | Canister Cavity Length at 70°F (in) | Min. Canister Cavity Temp (°F) | Canister Cavity Length Hot (in) |
| 178.50 | 600 | 179.43 | 179.38 | 375 | 179.90 |
| **Canister/Cask Diametrical Thermal Expansion** | | | | | |
| Canister O.D. at 70°F (in.) | Canister Temp (°F) | Canister O.D. Hot (in) | Cask Cavity I.D. at 70°F (in) | Min. Cask Cavity Temp (°F) | Cask Cavity I.D. Hot (in) |
| 67.35 | 400 | 67.56 | 68.00 | 300 | 68.14 |
| **Canister/Cask Axial Thermal Expansion** | | | | | |
| Canister Length at 70°F (in.) | Canister Temp (°F) | Canister Length Hot (in) | Cask Cavity Length at 70°F (in) | Min. Cask Cavity Temp (°F) | Cask Cavity Length Hot (in) |
| 196.04 | 400 | 196.65 | 196.88 | 300 | 197.30 |

E. Thermal Stress Analysis

In this section, the thermal stresses due to thermal gradients of various components of the NUHOMS-61B basket are evaluated. The thermal load considered is the 100° F ambient normal condition temperature distribution computed in Chapter 3. The mechanical properties of the materials, used in the basket, rail, and canister, are shown in the Table 1 as a function of temperature.

Thermal stresses in the basket can only be developed if free thermal expansion of the basket is constrained by the peripheral rails or canister. The thermal expansion calculations provided in Section 2.10.3.2.3.D, show that the basket rails are free to grow during maximum operating temperature in the canister. The rails are attached to the basket with bolts in slotted holes. Therefore, the rails also permit free thermal growth of basket boxes. However, the welded spacers at the top and bottom of the basket connect the fuel compartments and outer wrappers to each other. Thermal stresses are calculated at these locations due to radial temperature gradients. Furthermore, thermal stresses are also investigated in the outer wrapper due to thermal growth of the fuel compartments and poison plates and due to axial thermal gradients.

Thermal Stresses in Basket due to Radial Thermal Gradient

Since the basket inserts are located at the top and bottom of the basket, only these sections are analyzed. Figures 2.10.3-11 and 2.10.3-12 show that the radial thermal gradient at the top of the basket is higher than at the bottom of the basket. Also, the maximum temperature at the top of the basket is higher than at the bottom of the basket. Therefore, the top basket section is selected for thermal stress analysis.

A three-dimensional ANSYS [4] finite element model of the basket is used for the thermal stress analyses of the basket. The model used to conduct the side drop structural analysis of the basket is also used for the thermal stress analysis. This finite element model is described in Section 2.10.3.2.3.A. Due to the symmetry of the temperature distribution, only ¼ model of the model is used (see Figure 2.10.3-13). The rails and canister shell are removed since they have no effect on the basket stresses. The CONTACT52 and LINK8 elements are also removed from the model.

An elastic stress analysis of the basket structure is conducted for computing the thermal stresses. The finite element model, along with displacement boundary conditions and couplings, is shown in Figure 2.10.3-14. The nodal temperature distribution from the thermal analysis is applied to obtain the thermal stress model. The resulting shell middle surface nodal stress intensities are the membrane stress intensities, and the top or bottom surface stress intensities are the membrane plus bending stress intensities. The maximum membrane plus bending stress intensity, due the thermal gradient, is 8,799 psi.

Stresses in Outer Wrap due to Thermal Expansion of Inner Boxes and Aluminum Plates

Stresses in the 3-compartment outer wrap will be higher since the 3-compartment contains two aluminum poison plates (see Figure 2.10.3-15). Tensile stress in outer wrap is generated by the differential thermal growth of outer wrapper and aluminum poison plates. The maximum basket plate temperature in the basket plates is 600° F.

The difference in thermal growth, $\delta L$, between the outer stainless steel wrap and the aluminum poison plates is,

$$2\times0.31\times(600 - 70)[\alpha_a - \alpha_s] = 2\times0.31\times(600 - 70)[14.2\times10^{-6} - 9.8\times10^{-6}] = 1719\times10^{-6}\text{ in.}$$

Where $\alpha_a$ and $\alpha_s$ are the coefficients of thermal expansion of aluminum and SA-240 Type 304 stainless steel respectively. The inside length of the outer wrap, L, is 19.43 inches ($6 \times 3 + 6 \times 0.135 + 2 \times 0.31$). Conservatively assuming that outer wrap elongates by $\delta L$, the tensile stress in the outer wrap is 2,238 psi. ($1719 \times 10^{-6} \times 25.3 \times 10^{6} / 19.43$).

Stresses in Outer Wrap due to Axial Thermal Gradient

The maximum temperature at the axial center of the basket is roughly 600° F (see Figure 2.10.3-10), while the minimum temperature at the bottom of the basket is roughly 450° F (see Figure 2.10.3-12). The coefficient of thermal expansion and modulus of elasticity of SA-240 Type 304 stainless steel at 450° F, $\alpha_s$ and $E$ are $9.6 \times 10^{-6}$ in./in.°F, $26.2 \times 10^{6}$ psi. respectively. The width of the 3-compartment wrap is 19.64 inches. The radial thermal growth, $\delta$L, of the outer wrap is,

$$\delta L = L\,\Delta T\,\alpha_s$$

At the axial center of the basket, the thermal growth, $\delta L_1$, is 0.10201 in. [$19.64 \times (600\,0 - 70) \times 9.8 \times 10^{-6}$], while at the bottom of the basket, the thermal growth, $\delta L_2$, is 0.07165 in. [$19.64 \times (450 - 70) \times 9.6\times10^{-6}$].

Therefore, the difference in thermal growth between the bottom and center of the outer wrap is 0.10201 in. – 0.07165 in. = 0.01518 in.

In order to calculate the stresses due to the axial thermal gradient, a single side of the outer wrap is analyzed as a plate 19.64 in. × 164 in., fixed on all sides. Equations used in this analysis are taken from Roark [5], Table X, Case 41, and are as follows.

$a$ = 164 in. $\quad b$ = 19.64 in. $\quad a/b$ = 8.35 $\quad \alpha$=0.0284 $\quad \beta$= 0.5

The maximum deflection, $y$, is given by,

$$y = \alpha w b^4 / (Et^3)$$

$$\Rightarrow w = yEt^3 / \alpha b^4$$

At the center of long edge of the plate, the maximum stress, $s$, is,

$$s = \beta w b^2 / t^2 = (\beta/\alpha) \times [yEt/b^2]$$

$$= (0.5/0.0284) \times [0.01518 \times 26.2 \times 10^6 \times 0.105/19.64^2] = 1{,}907 \text{ psi}$$

The combined stress at the center of the wrap is therefore, 2238 psi. + 1907 psi. = 4,145 psi.

Summary of the Basket Thermal Stress Analysis

The following table summarizes and combines the thermal stresses calculated above. The combination is conservative, since the maximum stresses due to each individual case at different basket locations are added, irrespective of their locations. This thermal stress is combined with stresses, from side drop and end drop load cases, and compared with the code allowable stresses for normal conditions in Table 2.10.3-2 and for accident conditions in Table 2.10.3-3.

**Thermal Stresses in Basket Compartment**

| Stress due to radial thermal gradient (ksi) (Top) | Stress due to poison plate thickness growth (ksi) (Center) | Stress due to poison plate length growth (ksi) (Center) | Stress due to axial thermal gradient (ksi) (Center) | Combined Stress (ksi) |
|---|---|---|---|---|
| 8.80 | 2.24 | 0 | 1.91 | 12.95 |

Basket Rail Thermal Stress Analysis

This section evaluates the thermal stresses in NUHOMS-61B basket rails, generated by temperature distributions resulting from the 100° F. normal condition ambient environment. Thermal stresses can develop in the rails if free thermal expansion of the rails is constrained by the canister. The thermal expansion analysis provided in Section 2.10.3.2.3.D show that the basket rails are free to grow when subjected to the maximum normal condition temperature in the canister. The rails are attached to the basket with bolts in slotted holes, so that the rails permit free thermal growth of the outer wraps. However, thermal stresses occur in the rails due to temperature gradients within the rails themselves. The rail temperatures, taken from the normal condition thermal analysis (Chapter 3), are provided in Figures 2.10.3-16 and 2.10.3-18.

Elastic 3-dimensional ANSYS [4] finite element models of the Type 1 and Type 2 Rails are constructed from the basket model described in Section 2.10.3.2.3.A, and are used to perform the thermal stress analysis. The finite element models of rails, including displacement boundary conditions, are shown in Figures 2.10.3-19 and 2.10.3-20. The mechanical properties of the

materials, used in the basket, rail, and canister, are shown in the Table 2.10.3-1 as a function of temperature.

The following table summarizes the maximum thermal stress intensities in the Rail Type 1 and the Rail Type 2, due to the normal condition temperature distribution. The shell element middle nodal stress intensity is the membrane stress intensity and the element top or bottom nodal stress intensity is the membrane plus bending stress intensity. The maximum thermal stress of 1,758 psi from the Type 2 rail is combined with the side drop and end drop load cases. These combined stresses are compared with the code allowable stresses for normal conditions in Table 2.10.3-2 and for accident conditions in Table 2.10.3-3.

**Basket Rail Thermal Stress Analysis Results**

| Rail Type | Rail Section | Stress Intensity, Top Surface (psi) | Stress Intensity, Bottom Surface (psi) |
|---|---|---|---|
| Type 1 | Top ($P_m + P_b$) | 1,057 | 1,084 |
| | Middle ($P_m$) | 808 | 800 |
| | Bottom ($P_m + P_b$) | 716 | 717 |
| Type 2 | Top ($P_m + P_b$) | 1,758 | 1,564 |
| | Middl e ($P_m$) | 1,428 | 1,228 |
| | Bottom ($P_m + P_b$) | 1,227 | 1,060 |

F. Summary of Normal Condition Basket Stress Analysis

Table 2.10.3-2 summarizes the normal condition basket stress analysis results and allowable stresses for each individual load, as well as the combination of impact and thermal loads. The allowable for the basket components is taken at 600° F (from Chapter 3, the actual maximum temperature is 578° F). The allowable stress for the support rails is taken at 500° F (from Chapter 3, the actual maximum temperature of the rails is 488° F). All the calculated stresses are less than the ASME Code allowable stresses.

G. Accident Condition Side Drop Stress Analysis and Results

Loading Conditions

The basket is analyzed for two types of side drops using the ANSYS finite element model described in Section 2.10.3.2,3A. First, the canister is assumed to drop away from the transport cask sliding rails. Under this condition, 45°, 60°, and 90° orientation side drops are considered, because they bound all possible orientations. Second, the canister is assumed to drop directly on the transport cask sliding rails at 180° orientation. The lateral load orientation angle is defined in Figure 2.10.3-5. The load resulting from the fuel assembly weight was applied as pressure on the plates. For the 90° and 180° orientations, the pressure was applied only on the horizontal plates, while in other orientations, it was divided into components acting on both the horizontal and vertical plates. The applied 1*g* pressures for all orientations considered are summarized in the following table.

Fuel Assembly Weight Simulation Based on 1g Load

| Drop Orientations | Pressure Applied to Horizontal Plates $P \times \text{Sin}\ \theta$ (psi) | Pressure Applied to Vertical Plates $P \times \text{Cos}\ \theta$ (psi) |
|---|---|---|
| 45° | 0.4887 | 0.4887 |
| 60° | 0.5985 | 0.3456 |
| 90° and 180° | 0.6911 | - |

The inertia load due to the basket, rails, and DSC dead weight is simulated by increasing material density and by applying the appropriate acceleration. Increasing the basket plate density accounts for the poison plate weight.

The load distribution for 45, 60, 90 and 180 degree analyses are shown on Figures 2.10.3-21 to 2.10.3-23.

Material Properties

The basket, rails and canister are constructed from SA-240, 304 stainless steel. A bilinear stress-strain relationship is used to simulate the correct nonlinear material behavior for the short term during dynamic loading from the 30 foot side drop impact. The following elastic and inelastic material properties are used in the analysis:

| SA-240, 304 Stainless Steel at 500° F [3] | |
|---|---|
| Modulus of Elasticity, $E$ (psi) | $25.8 \times 10^6$ |
| Yield Strength (psi) | 19,400 |
| Tangent Modulus, $E_t$ (psi) | 5% of $E = 1.29 \times 10^6$ |

The material properties used in the analysis are taken at 500°F. However, the resulting stresses are compared with the allowable stresses at 600°F. This combination is considered conservative, because using higher values of $E$, $S_y$ and $E_t$ (properties at 500° F) in the analysis results in higher

stresses. Taking material properties at 600° F also yields higher displacements, causing more gaps to close, which reduces stresses further.

Analysis and Results

A nonlinear stress analysis of the fuel basket is conducted to compute the stresses for the 45°, 60°, 90°, and 180° drop orientations. A maximum load of 100g was applied in each analysis. The automatic time stepping program option "Autots" was activated. This option lets the program decide the actual size of the load-substep for a converged solution. Displacements, stresses and forces for each converged substep load were written on ANSYS result files. The program stops at the load substep when it fails to result in a converged solution. In all side drop cases the program gave converged solutions up to 100g load. Results were extracted at the load sub-step nearest to the maximum drop load of 75g. Maximum nodal stress intensities in the basket and rails are shown on Figures 2.10.2-24 to 2.10.2-39 and summarized in Table 2.10.3-3.

H. Accident Condition End Drop Stress Analysis

During an end drop, the fuel assemblies and fuel compartments are forced against the bottom of the cask. It is important to note that, for any vertical or near vertical loading, the fuel assemblies react directly against the bottom or top end of the cask and not through the basket structure as in lateral loading. It is the dead weight of basket only that causes axial compressive stress during an end drop. Axial compressive stresses are conservatively computed assuming that all of the basket weight will be taken by the fuel compartments and outer wraps only. A conservative basket weight of 23,000 lb. (actual weight is 22,918 lb. Section 2.2) is used in end drop stress calculations.

Compressive Stress in the Fuel Compartment Tubes and Outer Wrappers

Total Weight = 23,000 lb.
Weight excluding hold down ring, SS inserts, aluminum plates, and rails is 12,406 lb.
Section area = $12,406/(164 \times 0.29) = 260.8$ in$^2$
Stress due to $1g$ = -23.0 / 260.8 = - 0.09 ksi.
$75g$ compressive stress = $-.09 \times 75 = -6.75$ ksi.

Shear Stress in Plate Insert Weld

64 Inserts support the poison plate weight (3,260 lb.).
Load/insert = 3,260 / 64 = 50.9 lb.
Weld shear Area = $3 \times 0.125 \times \sin(45°) = 0.265$ in$^2$
Shear stress = $75g \times 50.9$ lb. / 0.265 in$^2$. = 14.41 ksi. < 26.63 ksi.

Shear Stress in Rail Stud

During 30*g* end drop, the rail will support its own weight. However, the analysis conservatively assumes that the weight of the rail will be supported by the 224 rail studs attached to the outer wrappers.

Weight of rails = 5,350 lb.
Weld Shear Area = $\pi/4\ (0.5^2 - 0.3^2) = 0.126\ in^2$
Shear stress (1*g*) = 5.35 / (0.126 × 224) = 0.19 ksi
75*g*, shear stress = 0.19 × 30 = 14.25 ksi

Compressive stress due to end drop on hold down ring

Weight of hold down ring = 940 lb.
Section area = $940/(14.5 \times 0.29) = 223.5\ in^2$
Stress due to 1*g* = -23.0/ 223.5= - 0.1 ksi.
75*g*, compressive stress = -0.1 × 75 = -7.5 ksi.

I. Summary of Accident Condition Basket Stress Analysis

Table 2.10.3-3 summarizes the accident condition basket stress analysis results and allowable stresses for each individual load, as well as the combination of impact and thermal loads. The allowable for the basket components is taken at 600° F (from Chapter 3, the actual maximum temperature is 578° F). The allowable stress for the support rails is taken at 500° F (from Chapter 3, the actual maximum temperature of the rails is 482° F). All the calculated stresses are less than the ASME Code allowables.

J. Basket Hold Down Ring Accident Condition Stress Analysis

In this section, the stresses in the NUHOMS-61B Basket Hold Down Ring and Ring Alignment Leg are evaluated for the accident condition side drop event. The computed stresses are compared the allowable stresses as per ASME B&PV Code, Appendix F [2]. For this evaluation, nominal dimensions are used, and material properties are taken at 500° F.

Alignment Leg Stress Analysis

The hold down ring is captured between the top of the basket and the inside surface of the canister's top shield plug. This prevents axial motion of the hold down ring. The hold down ring is supported in the transverse direction by the canister support ring, and by four alignment legs that mate with holes in the basket support rails.

A simple finite element model is used to calculate stresses in the alignment legs. The three-dimensional ANSYS [1] finite element model is constructed using SHELL43 plastic shell elements. The finite element model along with boundary conditions is shown in Figure 2.10.3-40.

The alignment legs are constructed from SA-240, 304 stainless steel. A bilinear stress-strain relationship is used to simulate the material behavior beyond elastic limit. The following material properties are used [3].

$E = 25.8\times10^6$ psi.
$S_y = 19.4$ ksi.
$S_u = 63.4$ ksi.
Tangent Modulus, $E_T = 5\%$ of $E = 1.29\times10^6$ psi.

The accident condition side drop subjects the basket and hold down ring to 75$g$ lateral load. During a side drop event, the entire inertial load of the hold down ring acts on one alignment leg.

For the purpose of this analysis, the weight of the hold down ring is taken to be 950 lb. (Actual computed weight from Section 2.2, is 940 lb.). Assuming that the hold down ring's inertial load acts equally on the support ring and alignment leg, the load applied to the alignment leg during a side drop event, $L$, is the following.

$$L = \tfrac{1}{2} \times (950 \text{ lb.}) \times (75g) = 35{,}625 \text{ lb.}$$

This force is applied to the alignment leg model as a uniformly distributed pressure. This pressure was applied in a number of steps. The automatic time stepping option, AUTOTS, was activated. This option lets the program decide the actual size of the load sub-step for a converged solution. The program stops at the load sub-step that fails to result in a converged solution. A converged solution was obtained for the maximum applied load.

Table 2.10.3-4 summarizes the maximum alignment leg stresses computed by ANSYS. All the calculated stresses are less than the ASME Code allowables.

Alignment Leg Weld Stress Analysis

A 3/8 inch fillet weld connects the alignment leg with the body of the hold down ring.

The methodology for the following analysis is taken from Bednar [6], Table 10.3, Case 4.

$$Z_w = bd + \frac{d^2}{3} = 6\times4 + \frac{4^2}{3} = 29.33 \text{ in}^2.$$

$$Z = 29.33 \times 0.375 = 11.0 \text{ in}^3.$$

The bending moment in the weld, $M$, is,

$$M = 35{,}625 \times (0.8 + 0.7/2 + 2.0) = 112{,}219 \text{ in.lb.}$$

Therefore, the bending Stress in the alignment leg weld is, $\sigma_b = 112{,}219/11.0 = 10{,}202$ psi., which is less than the allowable stress of 26.63 ksi.

Hold Down Ring Stress Analysis

A two-dimensional finite model is used to calculate stresses in the hold down ring during a 75*g* side drop event. The ANSYS finite element model is constructed from PLANE42 elements, with the thickness option. The finite element model is shown in Figure 2.10.3-41.

The hold down ring is constructed from SA-240, 304 stainless steel. A bilinear stress-strain relationship is used to simulate the material behavior beyond elastic limit. The following material properties are used [3].

$E = 25.8 \times 10^6$ psi.
$S_y = 19.4$ ksi.
$S_u = 63.4$ ksi.
Tangent Modulus, $E_T = 5\%$ of E = $1.29 \times 10^6$ psi.

The hold down ring is evaluated for 90° and 45° side drop orientations.

90° Orientation Side Drop:

The finite element model and displacement boundary conditions for the 90° orientation are shown in Figure 2.10.3-41. The nonlinear stress analysis was conducted using the ANSYS [4] computer code. A 100*g* load (*y* – direction) was applied in a number of steps. The automatic time stepping option, AUTOTS, was activated. This option lets the program decide the actual size of the load sub-step for a converged solution. The program stops at the load sub-step that fails to result in a converged solution. A converged solution was obtained for the maximum applied load.

Table 2.10.3-4 summarizes the maximum hold down ring stresses at the load step corresponding to 75*g*. The stresses at critical locations were linearized to obtain the membrane ($P_m$) and membrane plus bending ($P_m + P_b$) stress intensities.

45° Side Drop

The finite element model and displacement boundary conditions for the 45° orientation are shown in Figure 2.10.3-42. The nonlinear stress analysis was conducted using the ANSYS computer code. A 100*g* load (–70.7*g* in *x*-direction and 70.7*g* in *y* - direction) was applied in a number of steps. The automatic time stepping option, AUTOTS, was activated. This option lets the program decide the actual size of the load sub-step for a converged solution. The program stops at the load sub-step that fails to result in a converged solution. A converged solution was obtained for the maximum applied load.

Table 2.10.3-3 summarizes the maximum hold down ring stresses at the load step corresponding to 75*g*. The stresses at critical locations were linearized to obtain the membrane ($P_m$) and membrane plus bending ($P_m + P_b$) stress intensities.

2.10.3.2.4 Fuel Basket Buckling Analysis

A. Basket Plate Buckling Analysis

Basket assembly stability which includes a buckling evaluation of the wall between fuel compartments at the most highly loaded location for the most challenging drop orientation and a buckling evaluation of the support rails is determined in this section. Fuel compartment stability is demonstrated by performing a buckling evaluation using an ANSYS finite element analysis approach. Additionally, an order of magnitude check on the fuel compartment stability is performed using a hand calculation methodology. An ANSYS finite element analysis approach is used to evaluate support rail buckling.

Fuel Compartment Stability Demonstration Using Finite Element Analysis

Additional analyses are performed in this section to evaluate the outer basket plate stability when the lateral inertial loading is applied at various angles relative to the plates. Analyses are performed for vertical, 30°, and 45° drop angles (Figure 2.10.3-43).

The basic structural element of the basket is considered to be a wall between fuel compartments which consists of one 0.31" thick poison plate (the strength of the poison plates is neglected from the buckling load calculation, but the weight is included) sandwiched between two 0.135" thick stainless steel. The overall dimensions of this outer basket wall are 6.135" high and 6.0" wide. It is assumed that the load due to eight fuel assemblies stacked on 0.135" thick boxes is more severe than the weight of six fuel assemblies on 0.12" thick boxes. The maximum basket plate temperatures at locations 1 and 2 (Figure 2.10.3-43) are 500°F, and 578°F respectively. The buckling analysis of the basket is conservatively performed at temperatures of 550°F for location 1 and 650° F for location 2.

Finite Element Model

A three-dimensional ANSYS finite element model is constructed using a Shell 43 plastic large strain shell element to evaluate the plastic buckling loads for the basket plates at locations 1 and 2 (Figure 2.10.3-43). Shell 43 is well suited to model nonlinear, flat or warped, thin to moderately thick shell structures. The element has six degrees of freedom at each node: translations in the nodal x, y, and z directions and rotations about the nodal x, y, and z axes. The nodes of various plates are coupled together in the out of plane direction so that they will bend in unison under surface pressure loading and to simulate the through thickness support provided by the poison plates. The finite element model simulation is shown in Figure 2.10.3-44.

Geometric Nonlinearities

Since the structure experiences large deformations before buckling, the large displacement option of ANSYS is used. The deflections during each load step are used to continuously redefine the geometry of the structure, thus producing a revised stiffness matrix. If the rate of change in deflection (per iteration) is observed, an estimation of the stability of the structure can

be made. In particular, if the change of displacement at any node is increasing, the loading is above critical and the structure will eventually buckle.

Material Nonlinearities

Material properties for the basket plates, SA-240 Type 304, are taken from ASME Code [3]. The maximum temperatures at locations 1 and 2 are 500° F and 578° F respectively (Chapter 3). However, the material properties at locations 1 and 2 are conservatively taken at 550° F and 650° F respectively. The following table summarizes the material properties at location 1 (550° F), and Location 2 (650° F).

| Temperature | 550° F (Location 1) | 650° F (Location 2) |
|---|---|---|
| Modulus of Elasticity, $E$ (psi.) | $25.55 \times 10^6$ | $25.1 \times 10^{6**}$ |
| Yield Strength, $S_y$ (ksi.) | 18.9* | 18.0*** |
| Ultimate Strength, $S_u$ (ksi.) | 63.4 | 63.4 |
| Tangent Modulus, $E_T$ 5% of $E$ (psi.) | $1.2775 \times 10^6$ | $1.255 \times 10^6$ |

* A value of 18.8 ksi. for $S_y$ @ 550° F is conservatively used in the following analysis.
** A value of $25.05 \times 10^6$ psi. for $E$ @ 650° F is conservatively used in the following analysis.
*** A value of 17.9 ksi. for $S_y$ @ 650° F is conservatively used in the following analysis.

Applied Loads

The loads applied on the panel model (Figure 2.10.3-43, Locations 1 & 2) were appropriately transferred from full size basket loads. The three critical drop orientations analyzed for basket plates at both locations are the following:

- Vertical (load applied in the direction parallel to the basket plates)
- 30° (load applied at 30° relative to the basket plate direction)
- 45° (load applied at 45° relative to the basket plate direction)

The loads used in vertical, 30, and 45 degree drop analyses are summarized in Table 2.10.3-5. A maximum load of 200g was applied in each analysis. The automatic time stepping program option "Autots" was activated. This option lets the program decide the actual size of the load-substep for a converged solution. The program stops at the load substep when it fails to result in a converged solution. The last load step, with a converged solution, is the plastic instability load for the model. Figure 2.10.3-45 shows the loading conditions.

Boundary Conditions

The ANSYS finite element model conservatively assumes that both ends of column are hinged. However, the stainless steel (0.135" thick) and poison plates forming the panel extend beyond the panel and connect into other panels so that moments can be developed at the top and bottom

panel edges. These reactive end moments will keep the ends from rotating during buckling. "Formulas for Stress and Strain" by Raymond Roark [5], Fourth Edition, Table XV indicates that:

| Load Case No. (From Table XV of Roark) | Loading and Edge Condition | Formula for Critical Load ( P) |
|---|---|---|
| 2 | End Load Both Ends Hinged | $P = (1)(\pi^2 EI/L^2)$ |
| 3 | End Load Both Ends Fixed | $P = (4)(\pi^2 EI/L^2)$ |

Based on the formulas described above, the end conditions selected for the ANSYS model (both ends hinged) are conservative and the calculated allowable compressive load has a large margin of safety.

ANSYS Finite Element Analysis Results

For each orientation, the analysis is solved with successfully higher loading until convergence can no longer be obtained from the FEA model. Stress intensities and displacement patterns, at the last converged substep, are shown on Figures 2.10.3-46 to 2.10.3-51.

As per paragraph F-1340 [2], the acceptability of a component may be demonstrated by collapse load analysis. The allowable collapse load shall not exceed 100% of the plastic analysis collapse load (F-1341.3). The plastic analysis collapse load is defined as that determined by plastic analysis according to the criteria given in II-1430 (F-1321.6(c)) and NB-3213.25.

Using the methodology described in II-1430 (F-1321.6(c)) or NB-3213.25. For each solution step, the maximum displacements are used to determine the collapse load (see Figures 2.10.3-52 through 2.10.3-57). Following table summarizes the allowable buckling loads for each of the drop orientations. The analyses concludes that the maximum allowable buckling load is 96g's, which occurs for the 30° drop case.

| Location | Basket Orientation | Last converged Load (g) | Allowable Collapse Load |
|---|---|---|---|
| Location 1 (550° F) | Vertical | 112 | 112 |
| | 30° | 99 | 96 |
| | 45° | 105 | 100 |
| Location 2 (650° F) | Vertical | 187 | 185 |
| | 30° | 148 | 139 |
| | 45° | 146 | 140 |

Alternate Analysis

As an order of magnitude check, the NUHOMS 61B basket plate allowable buckling load and interaction equations as per paragraph NF-3322.1 (e) are evaluated for the 75g side drop. The

most critically loaded panel (Location 1, Figure 2.10.3-43) is evaluated for the vertical and 30° drop orientations, at a temperature of 550°F.

0°drop:

According to ASME Code, Subsection NF, Paragraph NF-3322-1(c)(2)(a) (Level A Condition) [7] and modified as per Appendix F, Paragraph F-1334 (Level D Condition) [2], the compressive stress limit under accident conditions (Level D) when $KL/r$ is less than 120 and $S_u > 1.2\ S_y$ is,

$$F_a = 2S_y\left[0.47 - \frac{KL/r}{444}\right]$$

Where, $K = 0.65$ as recommended by AISC ([8], Table C1.8.1). Since the basket plate is continuously supported, the column is assumed to have fixed ends. The basket plate length is, $L$ = 6.0 inches, and the basket plate width, $b$ = 6.0 inches. The moment of inertia of the basket plate, $I$, is,

$$I = b\,h^3/12 = 6 \times (0.58^3 - 0.31^3) / 12 = 0.0827 \text{ in.}^4$$

Therefore, the area of the plate, $A = 6 \times 2 \times 0.135 = 1.62$ in.$^2$, and the radius of gyration, $r = (I/A)^{1/2} = 0.2259$ in. So,

$$KL/r = 0.65 \times 6.0 / 0.2259 = 17.26$$

Substituting the values given above, the compressive stress limit, $F_a$, is,

$$F_a = 2 \times 18{,}800\ [0.47 - (17.26)/444] = 16{,}210 \text{ psi}$$

Total weight above bottom panel = 290 lbs.
Therefore, compressive stress at $75g$, $f_a = 290 \times 75 / 1.62 = 13{,}426$ psi

For combined axial compression and bending, equations 20 and 21 of Paragraph NF-3322.1 (e) (1) are:

$$f_a/F_a + C_{mx} f_b / [1-(f_a/F_e)]\ F_b \le 1 \qquad \text{(Eq.20)}$$

$$f_a/(1.4)(0.6)S_y + f_b/F_b \le 1 \qquad \text{(Eq.21)}$$

The allowable stresses for the above equations are determined as follows:

| | Allowable Stress | ASME Reference |
|---|---|---|
| $F_b$ | 1.5 $S_y$ = 28,200 psi | F-1334.5(c) |
| $C_{mx}$ | 0.6 | NF 3322.1(e)(1)(b) |
| Note | The allowable stress $F_a$ is multiplied by 1.4 as allowed by Paragraph F-1334 | |

Since there is no column bending during the vertical drop, the interaction equations are reduced to:

Equation 20: $f_a/F_a = 13{,}426/16{,}210 = 0.83 \leq 1$
Equation 21: $f_a/(1.4)(0.6)S_y = 13{,}426/(1.4)(0.6)28{,}200 = 0.57 \leq 1$

30° Drop (load applied at 30° relative to the basket plate direction)

The plate span is treated as a beam-column with fixed ends under axial compression and uniform transverse load ("Formulas for Stress and Strain", Ed. 4, Table VI, Case 10 [5]).
During a 30 degree side drop,

Axial load (75g), $P = 75g \times 290 \cos(30) = 18{,}836$ lb.
Transverse pressure load (75g) = $75g \times 0.8 \sin(30) = 30$ psi.
The distributed transverse load, $w = 30$ psi $\times$ 6.0 in. = 360 lb./in

Moment at beam center,

$$M = wj^2\left[\frac{U/2}{\sin(U/2)} - 1\right]$$

Where,

$$j = \left[\frac{EI}{P}\right]^{1/2} = \left[\frac{(25.55\times10^6)(0.0827)}{118{,}836}\right]^{1/2} = 10.59$$

$$U = \frac{L}{j} = \frac{6.0}{10.59} = 0.567 \text{ rad.} = 32.49°$$

$$M = (360)(10.59^2)\left[\frac{0.569/2}{\sin(32.49/2)} - 1\right] = 542 \text{ in. lb.}$$

Bending stress, $f_b = Mc/I = 542 \times 0.29 / (0.0827) = 1{,}901$ psi.
Axial compressive stress, $f_a = P/A = 18{,}836/1.62 = 11{,}627$ psi.
$C_{mx} = 0.6$ [Appendix F, F-1334.5(c)]
$F_b = 1.5\, S_y = 1.5 \times 18{,}800 = 28{,}200$ psi. (Subsection NF, NF 322.1(e)(1)(b))

The value of $F_e$ is calculated by the formula below per Paragraph F-1334.5(b):

$$F_e = \frac{\pi^2 E}{1.30\left(\frac{kl}{r}\right)^2} = \frac{\pi^2 25.55\times10^6}{1.30(17.26)^2} = 651{,}127\,\text{psi.}$$

Eq.20: $$\frac{f_a}{F_a} + \frac{C_{mx} f_b}{(1 - f_b/F_e)F_b} = \frac{11{,}627}{16{,}210} + \frac{0.6(1{,}901)}{(1 - 1{,}901/651{,}127)28{,}200} = 0.76 \le 1$$

Eq. 21: $$\frac{f_a}{(1.4)(0.6)S_y} + \frac{f_b}{F_b} = \frac{11{,}627}{(1.4)(0.6)18{,}800} + \frac{1{,}901}{28{,}200} = 0.8 \le 1$$

The results of the hand analytical calculations confirm that allowable buckling loads in the basket plates due to a 75G side drop are within acceptable limits.

B. Support Rail Buckling Analysis

There are two types of rails (type 1 & type 2 – see TN Drawing 1093-71-12 ). The type 2 rail is shorter while the type 1 rail has longer vertical panels. Consequently, the type 1 rail is limiting for buckling. The overall position of this rail and its loading, with respect to the full basket model, are shown in Figure 2.10.3-58.

A nonlinear stress analysis was conducted to evaluate the plastic buckling loads for the rail. The ANSYS computer code was utilized in this analysis. A three-dimensional finite element model of the rail was extracted from the full basket model as described in Section 2.10.3.2.3A. The finite element model of rail and displacement boundary conditions are shown in Figure 2.10.3-59. The rail is constructed from SA-240, Type 304 stainless steel and its material properties at 500° F are as follows:

Material Properties (500°F)

Stainless Steel (SA-240 Type 304)

$E = 25.8 \times 10^6$ psi.
$S_y = 19.4$ ksi.
$S_u = 63.4$ ksi.
Tangent Modulus, $E_T = 5\%$ of $E = 1.29 \times 10^6$ psi.

Applied Loads Calculations

Vertical Load due to weight on top compartments:
(All weights are calculated for a 3 in. basket length)

- Weight of 14 fuel assemblies = 180.55 lb.
- Weight of 8 SS compartment tubes, 0.12" wall = 20.45 lb.
- Weight of 6 SS compartment tubes, 0.135" wall = 17.29 lb.
- Weight of 2 × 2 outer wrapper, 0.105" wall = 4.71 lb.
- Weight of 3 × 3 outer wrapper, 0.105" wall = 4.13 lb.
- Weight of poison plates = 17.72 lb.
- Weight of Rail = 8 lbs.

Total weight = 252.85 say 265 lb.
For 200$g$, total vertical Load = 265 × 200 = 53,000 lb.
Nonlinear ANSYS runs were made for two different load cases:

In the first case: 53,000 lb. load was applied equally at six nodal locations on the rail (8,833.33 lbs at each node, see Figure 2.10.3-59). Stress intensities and displacement patterns, at the last converged substep (131.5g), are shown in Figure 2.10.3-60.

In the second case: 53,000 lb load was applied using a 2:1 ratio for two middle nodal and four end nodal locations (13,250 lbs at each middle node and 6,625 at each end node, see Figure 2.10.3-59). Stress intensity and displacement patterns, at the last converged substep (160g), are shown in Figure 2.10.3-61. Thus this load case is not bounding.

Using the methodology described earlier for the basket model, the allowable collapse load has been determined for the first load case in Figure 2.10.3-62. The allowable collapse load for the rail is 128g. For other rails and loadings, the allowable collapse load will be higher.

C. Summary of Fuel Basket Buckling Analysis

It is seen from the above basket buckling analyses, that the 30° drop at location 1 is critical, and the minimum allowable collapse load for the basket is 96g.

The results of the Fuel Basket buckling analysis indicate the allowable collapse *g* loads for the NUHOMS®-61B basket are higher than the applied 75g side drop impact load. Therefore basket and rails are structurally adequate with respect to buckling. The following table summarized the collapse loads for the Fuel Basket and rails.

| Component | Orientation and Location | Collapse Load |
|---|---|---|
| Fuel Basket Plates | 30° azimuth drop, at the periphery of the basket near the impact point. | 96*g* |
| Support Rails | 0° Azimuth drop, basket rail type 1. | 128*g* |

## 2.10.3.3 Canister Structural Analysis

### 2.10.3.3.1 Approach

A finite element analysis is performed in order to quantify stresses in the NUHOMS-61B Canister generated by transport loads. The applied loads considered are normal and accident condition front end, rear end, and side drops, combined with 50 psig internal and external pressures and 100° F and -20° F environmental conditions. A two-dimensional axisymmetric finite element model is used to evaluate the stresses generated by axisymmetric loads, such as end drop, pressure, and temperature loads. A three-dimensional cross section finite element model is used to evaluate the stresses generated by the asymmetric side drop loads. An elastic analysis is employed for both normal and accident condition axisymmetric load cases, as well as the normal condition side drop (asymmetric) load cases. However, for the accident condition side drop load case, an elastic-plastic analysis is performed.

Material Properties

Since the maximum normal condition canister temperature is 388° F (Chapter 3), the elastic material properties for the canister structural analysis are conservatively taken at 400° F. The elastic analysis canister material properties are as follows.

Canister Shell and Covers (SA-240 Type 304) at 400° F. [3] [9]

$E = 26.5\times10^6$ psi. $S_y = 20.7$ ksi.
$S_u = 64.0$ ksi. $S_m = 18.7$ ksi.
$\nu = 0.3$ $\rho = 0.29$

Temperature dependent coefficient of thermal expansion:

| Temperature °F | $\alpha_m$ (in./in. °F$^{-1}$) |
|---|---|
| 70 | $8.5\times10^{-6}$ |
| 100 | $8.6\times10^{-6}$ |
| 150 | $8.8\times10^{-6}$ |
| 200 | $8.9\times10^{-6}$ |
| 250 | $9.1\times10^{-6}$ |
| 300 | $9.2\times10^{-6}$ |
| 350 | $9.3\times10^{-6}$ |
| 400 | $9.5\times10^{-6}$ |

Top and Bottom Shield Plugs (A-36) at 400° F. [3] [9]

$E = 27.7 \times 10^6$ psi. $S_y = 30.8$ ksi.
$S_u = 58.0$ ksi $S = 16.6$ ksi.
$\nu = 0.3$ $\rho = 0.29$

Temperature dependent coefficient of thermal expansion:

| Temperature °F | $\alpha_D$ (in./in. °F$^{-1}$) |
|---|---|
| 70 | $6.4 \times 10^{-6}$ |
| 100 | $6.5 \times 10^{-6}$ |
| 150 | $6.6 \times 10^{-6}$ |
| 200 | $6.7 \times 10^{-6}$ |
| 250 | $6.8 \times 10^{-6}$ |
| 300 | $6.9 \times 10^{-6}$ |
| 350 | $7.0 \times 10^{-6}$ |
| 400 | $7.1 \times 10^{-6}$ |

For the accident condition side drop analysis, the follow elastic-plastic material properties, conservatively taken at 500° F, are the following.

| SA-240, 304 Stainless Steel at 500° F [3] | |
|---|---|
| Modulus of Elasticity, $E$ (psi) | $25.8 \times 10^6$ |
| Yield Strength (psi) | 19,400 |
| Tangent Modulus, $E_t$ (psi) | 5% of $E = 1.29 \times 10^6$ |

Design Criteria

The resulting stresses are compared with the allowable stresses set forth by ASME B&PV Code Subsection NB [10]. The allowable stresses for both normal and accident conditions are summarized in the following table.

| Loading Condition | Stress Category | Stress Criteria* [10] | Material | Allowable Stress (ksi.) |
|---|---|---|---|---|
| Normal Conditions, Elastic Analysis | Membrane Stress, $P_m$ | $S_m$ | SA-240 Type 304 | 18.7 |
| | | | A-36 | 16.6 |
| | Membrane + Bending Stress, $P_m + P_b$ | 1.5 $S_m$ | SA-240 Type 304 | 28.1 |
| | | | A-36 | 24.9 |
| Accident Conditions, Elastic Analysis | Membrane Stress, $P_m$ | Lesser of 2.4 $S_m$ or 0.7 $S_u$ | SA-240 Type 304 | 44.8 |
| | | | A-36 | 39.8 |
| | Membrane + Bending Stress, $P_m + P_b$ | Lesser of 3.6 $S_m$ or $S_u$ | SA-240 Type 304 | 64.0 |
| | | | A-36 | 58.0 |
| Accident Conditions, Elastic-Plastic Analysis | Membrane Stress, $P_m$ | 0.7 $S_u$ | SA-240 Type 304 | 44.8 |
| | Membrane + Bending Stress, $P_m + P_b$ | 0.9 $S_u$ | SA-240 Type 304 | 57.6 |

* $S$ replaces $S_m$ for class 2 materials (A-36)

2.10.3.3.2 Loading Conditions

The load cases considered in this analysis are normal and hypothetical accident condition front and rear end drops. The impact loads are combined with 50 psig internal and external pressure and the 100° F and -20° F ambient environment thermal loads. The following tables summarize both normal and accident condition Canister individual load cases.

**Canister Normal Condition Load Cases**

| Loading | Analysis Type | Service Level | Load | Analysis Method |
|---|---|---|---|---|
| Hot Environment Thermal Load | Elastic Analysis | A | 100° F Ambient | Finite Element Analysis (2D axisymmetric model) |
| Cold Environment Thermal Load | Elastic Analysis | A | -20° F Ambient | Finite Element Analysis (2D axisymmetric model) |
| Internal Pressure | Elastic Analysis | A | 50 psi. Internal Pressure* | Finite Element Analysis (2D axisymmetric model) |
| External Pressure | Elastic Analysis | A | 50 psi. External Pressure* | Finite Element Analysis (2D axisymmetric model) |
| 1 Foot Side Drop | Elastic Analysis | A | 30*g* Lateral Load | Finite Element Analysis (3D cross-section model w/basket) |
| 1 Foot Front End Drop | Elastic Analysis | A | 30*g* Axial Load | Finite Element Analysis (2D axisymmetric model) |
| 1 Foot Rear End Drop | Elastic Analysis | A | 30*g* Axial Load | Finite Element Analysis (2D axisymmetric model) |

* From Chapter 3, the actual canister internal and external pressures, are 9.8 psig. and 5.4 psig. respectively. However, for the canister stress analysis, 50 psig. is conservatively used as the normal condition internal and external pressure. 50 psig. also bounds both canister internal and external accident conditions pressures.

**Canister Accident Condition Load Cases**

| Loading | Analysis Type | Service Level | Load | Analysis Method |
|---|---|---|---|---|
| 30 Foot Side Drop | Elastic-Plastic Analysis | D | 75*g* Lateral Load | Finite Element Analysis (3D cross-section model w/basket) |
| 30 Foot Front End Drop | Elastic Analysis | D | 75*g* Axial Load | Finite Element Analysis (2D axisymmetric model) |
| 30 Foot Rear End Drop | Elastic Analysis | D | 75*g* Axial Load | Finite Element Analysis (2D axisymmetric model) |

The individual loads are combined in the following way.

## Canister Normal Condition Load Combinations

| Load Case | Individual Loads | | | | | | |
|---|---|---|---|---|---|---|---|
| | 30g Side Drop | 30g Front End Drop | 30g Rear End Drop | 50 psi. Internal Pressure | 50 psi. External Pressure | 100° F Ambient Environment | -20° F Ambient Environment |
| 1 | X | | | X | | X | |
| 2 | X | | | | X | | X |
| 3 | | X | | X | | X | |
| 4 | | X | | | X | | X |
| 5 | | | X | X | | X | |
| 6 | | | X | | X | | X |

## Canister Accident Condition Load Combinations

| Load Case | Individual Loads | | | | | | |
|---|---|---|---|---|---|---|---|
| | 75g Side Drop | 75g Front End Drop | 75g Rear End Drop | 50 psi. Internal Pressure | 50 psi. External Pressure | 100° F Ambient Environment | -20° F Ambient Environment |
| 7 | X | | | X | | X | |
| 8 | X | | | | X | | X |
| 9 | | X | | X | | X | |
| 10 | | X | | | X | | X |
| 11 | | | X | X | | X | |
| 12 | | | X | | X | | X |

2.10.3.3.3 2-Dimensional Axisymmetric Finite Element Model

A 2-dimensional axisymmetric finite element model is constructed in order to evaluate the axisymmetric load cases, which include front and rear end drop, internal and external pressure, and temperature loads. A separate 3-dimensional cross-section model, that includes the basket, and is described in Section 2.10.3.2.3.A, is used to evaluate the canister for the side drop load cases.

The 2-dimensional axisymmetric ANSYS [1] finite element model, constructed from PLANE42 elements, is used in this analysis. The elastic material properties listed above are used to model the canister materials. The Canister Lifting Lugs and Grapple are not included in the model. The effect of the unmodeled weight is assumed to be negligible.

The adjacent surfaces of the three front and three rear closure plates are coupled in the axial direction in order to simulate their interaction. Adjacent nodes in the canister shell and closure plates are coupled in both $x$ and $y$ directions at the weld locations.

A plot of the finite element model used in this analysis is shown in Figure 2.10.3-63. An enlarged view front section of the finite element model including nodal couplings and boundary conditions for the front end drop load case is provided in Figure 2.10.3-64. An enlarged view rear section of the finite element model including nodal couplings and boundary conditions for the front end drop load case is provided in Figure 2.10.3-65.

Lid End Drop Boundary Conditions

The weight of the canister internals (basket and fuel assemblies) is accounted for by applying equivalent pressures. The actual weights of the canister basket and fuel assemblies are 22,918 lb. and 43,005 lb. respectively (Section 2.2). Therefore, the total actual weight of the canister internals is 65,923 lb. The weight of the canister internals used in this analysis is conservatively increased to 66,500 lb. The canister cavity inner radius at the front internal edge is 32.375 in. The pressure equivalent to the weight of the internals under normal conditions, $P_{in}$, is,

$$P_{in} = [\ 66{,}500 / (\pi \times 32.375^2)\ ] \times 30\ gs = 605.862 \text{ psi.}$$

For accident conditions,

$$P_{ia} = [\ 66{,}500 / (\pi \times 32.375^2)\ ] \times 75\ gs = 1514.654 \text{ psi.}$$

Symmetry displacement boundary conditions are applied along the $y$-axis of the two-dimensional axisymmetric model. The front face of the canister is held in the axial direction in order to simulate the rigid support provided by the transport cask lid. Inertial loads of 30$g$s and 75$g$s in the positive $y$-direction are applied to the model for the normal and accident condition load cases respectively.

Rear End Drop Boundary Conditions

The weight of the canister internals used in this analysis is 66,500 lb. The canister cavity inner radius at the rear internal edge is 33.125 in. The pressure equivalent to the weight of the internals under normal conditions, $P_{in}$, is,

$$P_{in} = [\ 66{,}500 / (\pi \times 33.125^2)\ ] \times 30\ gs = 578.737\ \text{psi}.$$

For accident conditions,

$$P_{ia} = [\ 66{,}500 / (\pi \times 33.125^2)\ ] \times 75\ gs = 1446.845\ \text{psi}.$$

Symmetry displacement boundary conditions are applied along the y-axis of the 2-dimensionsal axisymmetric model. The rear face of the canister is held in the axial direction in order to simulate the rigid support provided by the transport cask bottom. Inertial loads of 30gs and 75gs in the negative y-direction are also applied to the model for the normal and accident condition load cases respectively.

Thermal Loads

The two temperature distributions applied correspond to the 100° F. and -20° F ambient temperature environments. The temperature distributions used for the 100° F hot environment condition and the -20° F cold environment condition are taken from Chapter 3. Temperatures were applied to the canister modal at several nodes, and a thermal equilibrium analysis was performed, using the material properties provided in Section 2.10.3.3.1, in order to solve for the temperature at the remaining nodes.

2.10.3.3.4 3-Dimensional Cross-Section Finite Element Model

Finite Element Model

A 3-dimensional cross-section finite element model is constructed in order to evaluate the canister for the side drop load cases. This model is also used to evaluate the basket, and is described in detail in Section 2.10.3.2.3.A.

The 3-dimensional finite element model of the basket, rails and canister is constructed using SHELL 43 elements. The overall model is shown in Figure 2.10.3-1. The strength of poison plates is conservatively neglected by excluding these plates from the finite element model. However, the weight of the aluminum plates is accounted for by increasing the stainless steel basket plate density. Because of the large number of plates in the basket and large size of the basket, certain modeling approximations are necessary. Because the rails provide continuous support along the entire length of the basket during a side drop, only a 3 inch long slice of the basket, rail and canister is modeled. At the two cut faces of the model, symmetry boundary conditions are applied (UZ = ROTX = ROTY = 0). The fuel compartment tubes, outer 3 × 3 and 2 × 2 boxes, and rails are included in the model and are shown individually in Figures 2.10.3-2 to

2.10.3-4. The gap elements (CONTACT 52) are used to simulate the interface between the basket rails and the inner side of the canister as well as between the outer side of the canister and inside of the cask are described in detail in Section 2.10.3.2.3.A. The model is used to analyze the canister for both normal and accident conditions.

Loading Conditions

The canister is analyzed for two types of side drops using the ANSYS finite element model described in Section 2.10.3.2.3 A. First, the canister inside the cask is assumed to drop away from the transport cask sliding rails. Under this condition, 45°, 60°, and 90° orientation side drops are assumed to bound all possible orientations. Second, the side drop occurs on the transport cask sliding rails in the 180° orientation. The lateral load orientation angle is defined in Figure 2.10.3-5. The load resulting from the fuel assembly weight was applied as pressure on the plates. In the 90° and 180° orientations, the pressure is applied only on the horizontal plates while in other orientations, it is divided into components that act on both the horizontal and vertical plates. The 1g pressures for the different orientations considered are summarized in the following table.

Fuel Assembly Weight Simulation Based on 1g Load

| Drop Orientations | Pressure Applied to Horizontal Plates $P \times \sin\theta$ (psi) | Pressure Applied to Vertical Plates $P \times \cos\theta$ (psi) |
|---|---|---|
| 45° | 0.4887 | 0.4887 |
| 60° | 0.5985 | 0.3456 |
| 90° and 180° | 0.6911 | - |

The inertia load due to basket, rails, and canister dead weight is simulated using the density and appropriate acceleration. The poison plate weight is accounted for by increasing the basket plate density.

The load distribution for the 45°, 60°, 90°, and 180° analyses are shown on Figures 2.10.3-21 to 2.10.3-23.

2.10.3.3.5 Stress Analysis Results

The maximum stress intensities in the canister are extracted from the ANSYS results, from both models, for all twelve load combinations. These stresses are compared to the normal and accident condition code allowables. Tables 2.10.3-6 and 2.10.3-7 summarize the maximum calculated and allowable stress intensities generated in the NUHOMS®-61BT Canister for normal and accident conditions respectively.

For the end drop load combinations, both normal and accident condition allowable stresses are taken to be the normal and accident condition membrane allowable stresses for SA-240 Type

304, because the maximum stresses occur in the canister shell region (SA-240, Type 304 material), and stresses in the shield plugs (A-36 material) are small.

For the accident condition side drop load combinations, the maximum calculated elastic stress intensity generated by temperature and pressure loads are conservatively added to the maximum calculated elastic-plastic stress intensity generated by the side drop load cases. The resulting combined stress intensities are conservatively compared to the accident condition plastic analysis stress limits.

2.10.3.3.6 Canister Buckling Analysis

In this section, The analytical method provided in ASME Code Case N-284-1 [11] is used to determine the adequacy of the NUHOMS®-61BT canister with respect to buckling due to axial compression and external pressure.

Since the vessel is assumed to be unstiffened, only the theoretical bhuckling calculation for unstiffened shells or local buckling between stiffeners of stiffened shells applies ([11] Section 1712.1). Code Case N-284-1, Section –1712.2, Stringer Buckling and General instability, does not apply since it analyzes the global buckling of a stinger stiffened vessel.

Applied Loads

The canister normal and accident condition buckling loads are summarized in the tables below.

**Canister Normal Condition Buckling Loads**

| Loading | Service Level | Load |
|---|---|---|
| External Pressure | A | 15 psi. external pressure* |
| 1 Foot End Drop | A | 30*g* Axial Load |

* From Chapter 3, the actual normal condition canister external pressure is 5.4 psig. However, for the normal condition buckling analysis, 15 psig. is conservatively used.

**Canister Accident Condition Buckling Loads**

| Loading | Service Level | Load |
|---|---|---|
| External Pressure | D | 22 psi. external pressure* |
| 30 Foot End Drop | D | 75*g* Axial Load |

* From Chapter 3, the actual accident condition canister external pressure is 9.4 psig. However, for the accident condition buckling analysis, 22 psig. is conservatively used.

Material Properties

Properties of Canister Shell and Covers (SA-240 Type 304) at 500° F. [3]

| | |
|---|---|
| $E = 25.8 \times 10^6$ psi. | $S_y = 19.4$ ksi. |
| $S_u = 63.4$ ksi. | $S_m = 17.5$ ksi. |
| $\nu = 0.3$ | $\rho = 0.29$ |

Notation

The following notations are taken from ASME Code Case N-284-1 [11], Section –1200.

- Subscripts $\phi$ and $\theta$ = axial (meridional) and circumferential directions respectively.
- $l_\phi$ = distances between lines of support in the axial direction, use 179.3 in.
- $R$ = shell radius, mean radius = [66.25 inner diameter + 67.25 outer diameter] / 4 = 33.375 in.
- $t$ = shell thickness, 0.5 in.
- $M_\phi = \dfrac{l_\phi}{\sqrt{(R)(t)}}$
- $C_{\phi h}$, $C_\theta$ = elastic buckling coefficient under external pressure and axial compression respectively.
- $\sigma_{heL}$, $\sigma_{\phi eL}$ = local theoretical elastic instability stress in the hoop direction for cylinders under external pressure and axial compression respectively, psi.
- $E$ = modulus of elasticity of the material at design temperature, $25.8 \times 10^6$ psi. @ 500° F, (Ref. 3).
- $\alpha_{QL}$ = capacity reduction factor to account for the difference between classical theory and predicted instability stresses for fabricated shells.
- $\sigma_y$ = tabulated yield stress of material at design temperature, 19,400 psi. @ 500° F (Ref. 3).
- $\sigma_{ha}$, $\sigma_{rc}$, allowable stresses for elastic and inelastic buckling respectively, psi.
- $FS$ = factor of Safety, 2 for normal conditions, 1.34 for accident conditions (Ref. 1, Section – 400 (a)).

Compressive Stress due to End Drop

The canister wall resists the weight of the shell plus the weight of top end components during a bottom end drop event. The total weight of these items is 14,950 lb. (Section 2.2). The corresponding applied force generated for a 1$g$ end drop, $F_{axial}$, is,

$$F_{axial} = 14{,}950 \text{ lb.} \times 1g = 14{,}950 \text{ lb.}$$

The cross sectional area, $A$, of the container shell is the following.

$$A = \frac{\pi}{4}\left[D_o^2 - D_i^2\right] = \frac{\pi}{4}\left[67.25^2 - 66.25^2\right] = 104.85 \text{ in.}^2$$

Therefore, the compressive stress applied to the canister shell for 1$g$ end drop is,

$$\sigma_a = P / A = 14{,}950 \text{ lb.} / 104.85 \text{ in.}^2 = 142.58 \text{ psi.}$$

For 30$g$ deceleration due to normal condition load, $\sigma_n = 142.58 \times 30g = 4{,}278$ psi.

For 75$g$ deceleration due to accident condition load, $\sigma_a = 142.58 \times 75 = 10{,}694$ psi.

Shell Stress due to External Pressure

The hoop stress, $\sigma_{hoop}$, generated by external pressure is governed by the following formula.

$$\sigma_{hoop} = \frac{PR}{t}$$

Where $P$ is the external pressure applied, $R$ is the mean radius of the shell, and $t$ is the shell thickness. For normal condition external pressure of 15 psi., the corresponding hoop stress, $\sigma_{np}$, is,

$$\sigma_{np} = \frac{(15)(33.375)}{0.5} = 1{,}001 \text{ psi.}$$

For accident condition external pressure of 22 psi., the corresponding hoop stress, $\sigma_{np}$, is,

$$\sigma_{ap} = \frac{(22)(33.375)}{0.5} = 1{,}469 \text{ psi.}$$

Shell Buckling due to Compressive Stress

- Theoretical Buckling Value

Local Buckling ([11] Section –1712.1.1 (a)):

$$M_\phi = \frac{l_\phi}{\sqrt{(R)(t)}} = \frac{179.3}{\sqrt{(33.375)(0.5)}} = 43.89 \text{ in.}$$

$$\Rightarrow M_\phi > 1.73$$

Therefore,

$$C_\theta = 0.605$$

$$\Rightarrow \sigma_{\phi L} = C_\theta \frac{(E)(t)}{R} = 0.605 \frac{(25.8\times10^6)(0.5)}{33.375} = 0.2338\times10^6 \text{ psi.}$$

- Capacity Reduction Factor

From Code Case N-284-1, Section –1511 (a), for local buckling of cylindrical shells, stiffened or unstiffened under Axial Compression, $\alpha_{\phi L}$ is the larger of (1) and (2).

(1) Effect of *R/t*

$$\frac{R}{t} = \frac{33.375}{0.5} = 66.75$$

$$\Rightarrow \alpha_{\phi L} = MIN\left\{\begin{array}{l} 1.52 - 0.473\log_{10}\left(\frac{R}{t}\right) = 0.657 \\ \frac{300\sigma_y}{E} - 0.033 = 0.193 \end{array}\right\} = 0.193$$

(2) Effect of Length

$$M_\phi = 43.89 > 10 \Rightarrow \alpha_{\phi L} = 0.207$$

Therefore, $\alpha_{\phi L} = 0.207$.

- Plasticity Reduction Factor

The plasticity reduction factor is computed based on the formulae provided in Code Case N-284-1, Section –1611 (b) as follows.

$$\Delta = \frac{\alpha_{\phi L}\sigma_{\phi L}}{\sigma_y} = \frac{(0.207)(0.2338\times10^6)}{19{,}400} = 2.49$$

Since 1.6 < Δ < Local Buckling ([11], Section –1712.1.1 (b) (2)): 6.25,

$$\eta_\phi = \frac{1.31}{1+1.15\Delta} = \frac{1.31}{1+1.15x2.49} = 0.34 .$$

Shell Buckling due to External Pressure

The analytical method provided in ASME Code Case N-284-1 is used to determine that the NUHOMS-61B Transportable Storage Canister is structurally adequate with respect to buckling due to external pressure with end pressure included.

- Theoretical Buckling Value

$$(\sigma_\phi = 0.5\ \sigma_\theta)$$

$$M_\phi = \frac{l_\phi}{\sqrt{(R)(t)}} = \frac{179.3}{\sqrt{(33.375)(0.5)}} = 43.89 \text{ in.}$$

$$\frac{R}{t} = \frac{33.375}{0.5} = 66.75 \quad \text{and} \quad 1.65\,\frac{R}{t} = 110.14$$

$$\Rightarrow 3.5 < M_\phi < 1.65\,\frac{R}{t}$$

Therefore,

$$C_{eh} = \frac{0.92}{M\phi - 0.636} = \frac{0.92}{43.89 - 0.636} = 0.0213$$

$$\Rightarrow \sigma_{heL} = C_{eh}\frac{(E)(t)}{R} = 0.0213\frac{(25.8\times10^6)(0.5)}{33.375} = 8{,}233 \text{ psi.}$$

- Capacity Reduction Factor

From Code Case N-284-1, Section –1511 (b), for local buckling of cylindrical shells, stiffened or unstiffened under Hoop Compression,

$$\alpha_{eL} = 0.8$$

- Plasticity Reduction Factor

The plasticity reduction factor is computed based on the formulae provided in Code Case N-284-1, Section –1611 (b) as follows.

$$\Delta = \frac{\alpha_{\alpha L}\sigma_{heL}}{\sigma_y} = \frac{(0.8)(8,233)}{19,400} = 0.340$$

Since $\Delta < 0.67$,

$$\eta_\theta = 1$$

Summary of Buckling Results

The calculated buckling results for the end drop and external pressure are summarized in the following table.

| Item | End Drop (axial direction) | | External Pressure (hoop direction) | |
|---|---|---|---|---|
| | Normal (30g) | Accident (75g) | Normal (15 psi) | Accident (22 psi) |
| Calculated Stress (psi) | 4,278 | 10,694 | 1,001 | 1,469 |
| Factor of Safety | 2.0 | 1.34 | 2.0 | 1.34 |
| F.O.S Amplified Stress (psi) | 8,556 | 14,330 | 2,002 | 1,969 |
| Capacity Reduction Factor | 0.207 | 0.207 | 0.8 | 0.8 |
| Elastic Amplified Stress (psi) | 41,333 | 69,227 | 2,503 | 2,461 |
| Plastic Reduction Factor | 0.34 | 0.34 | 1.0 | 1.0 |
| Plastic Amplified Stress (psi) | 121,568 | 203,609 | 2,503 | 2,461 |
| Theoretical Buckling Stress (psi) | 233,800 | 233,800 | 8,233 | 8,233 |

Interaction Equations for Local Buckling ([11], Section – 1713)

- Normal Condition

The combination of axial compression from the 30*g* end drop with 15 psi normal condition external pressure is analyzed using the interaction equation provided in Code Case N-284, Section –1713.

The combined axial membrane stress is, $\sigma_\phi = 4{,}278 + 1{,}001/2 = 4{,}779$ psi, and the hoop membrane stress is, $\sigma_\theta = 1{,}001$ psi. Therefore,

$$\sigma_{xa} = \frac{(\alpha_{at})(\sigma_{\phi L})}{FS} = \frac{(0.207)(0.2338\times10^{6})}{2.0} = 24{,}198 \text{ psi.}$$

$$t_\theta = t_\phi = t$$
$$t_\theta / t_\phi = 1.0$$

Since, $K > 0.5$ and $\sigma_\phi \geq 0.5\sigma_{ha}$, the interaction equations in Section –1713.1.1 (b) apply.

$$\frac{\sigma_\phi - 0.5\sigma_{ha}}{\sigma_{xa} - 0.5\sigma_{ha}} + \left(\frac{\sigma\theta}{\sigma_{ha}}\right)^2 \leq 1.0$$

$$\frac{4{,}779 - 0.5\times3{,}293}{24{,}198 - 0.5\times3{,}293} + \left(\frac{1{,}001}{3{,}293}\right)^2 = 0.231$$

Therefore, the interaction equation is satisfied.

- Accident Condition

The axial compression generated during the accident condition end drop is combined with the normal condition external pressure load using the interaction equation provided in Code Case N-284-1, Section –1713. Since the accident condition pressure load is generated during the thermal accident, which occurs subsequent to the 30 foot accident condition free drop, it need not be combined with any other load case. However, the axial compression from the 75*g* end drop is conservatively combined with an external pressure of 22 psi.

The combined axial membrane stress is, $\sigma_\phi = 10{,}694 + 1{,}469/2 = 11{,}429$ psi., and the hoop membrane stress is, $\sigma_\theta = 1{,}469$ psi. Therefore,

$$\sigma_{xa} = \frac{(\alpha_{\phi L})(\sigma_{\phi eL})}{FS} = \frac{(0.207)(0.2338\times10^{6})}{1.34} = 36{,}117 \text{ psi.}$$

$$t_\theta = t_\phi = t$$
$$t_\theta / t_\phi = 1.0$$

Since, $K > 0.5$ and $\sigma_\phi \geq 0.5\sigma_{ha}$, the interaction equations in Code Case N-284-1, Section –1713.1.1 (b) apply.

$$\frac{\sigma_\phi - 0.5\sigma_{ha}}{\sigma_{xa} - 0.5\sigma_{ha}} + \left(\frac{\sigma\theta}{\sigma_{ha}}\right)^2 \leq 1.0$$

$$\frac{11{,}429 - 0.5x4915}{36{,}117 - 0.5x4915} + \left(\frac{1{,}469}{4{,}915}\right)^2 = 0.355$$

Therefore, the interaction equation is satisfied.

Summary of Buckling Evaluation

From the analysis presented above, it can be seen that all of the stresses generated in the NUHOMS®-61BT Canister are less than their corresponding allowable buckling stresses, and all buckling interaction equation requirements are also met. Therefore the canister will not buckle when subjected to normal or accident condition loads.

2.10.3.4 References


1. American Society of Mechanical Engineers, ASME Boiler and Pressure Vessel Code, Section III, Subsection NG, 1998 with 1999 Addenda.

2. American Society of Mechanical Engineers, ASME Boiler and Pressure Vessel Code, Section III, Appendix F, 1998 with 1999 Addenda.

3. American Society of Mechanical Engineers, ASME Boiler and Pressure Vessel Code, Section II, Part D, 1998, including 1999 addenda.

4. ANSYS Engineering Analysis System, User's Manual for ANSYS Rev 5.6, Swanson Analysis Systems, Inc., Houston, PA, 1998.

5. Roark, Raymond J., *Formulas for Stress and Strain*, Fourth Edition, McGraw-Hill Book Company.

6. Bednar, Henry H., *Pressure Vessel Design Handbook*, Van Nostrand Reinhold Company, 1981.

7. American Society of Mechanical Engineers, ASME Boiler and Pressure Vessel Code, Section III, Subsection NF, 1998 with 1999 Addenda.

8. *Manual of Steel Construction*, Eighth Edition, American Institute of Steel Construction, Inc., 1980.

9. Baumeister & Marks, *Standard Handbook for Mechanical Engineers*, 7th Edition.

10. American Society of Mechanical Engineers, ASME Boiler and Pressure Vessel Code, Section III, Subsection NB, 1998 with 1999 Addenda.

11. Cases of ASME Boiler and Pressure Vessel Code, Case N-284-1, *Metal Containment Shell Buckling Design Methods*, Section III, Division 1, Class MC, 1998 with 1999 Addenda.

12. NUREG/CR-0497-Rev 2,"MATPRO-Version 11 (Revision 2), A handbook of materials properties for use in the analysis of light water reactor fuel rod behavior.

**Table 2.10.3-1**
**Temperature Dependent Material Properties**

| Component | Material | Temp. °F | Ultimate $S_u$ (ksi) | Yield $S_y$ (ksi) | Allow. $S_m$ (ksi) | $E$ ($10^6$ psi) | $\alpha$ ($10^{-6}$) |
|---|---|---|---|---|---|---|---|
| Basket, Rail and Canister | SA-240 Stainless Steel 304 [3] | 70 | 75.0 | 30.0 | 20.0 | 28.3 | 8.5 |
| | | 200 | 71.0 | 25.0 | 20.0 | 27.6 | 8.9 |
| | | 300 | 66.2 | 22.4 | 20.0 | 27.0 | 9.2 |
| | | 400 | 64.0 | 20.7 | 18.7 | 26.5 | 9.5 |
| | | 500 | 63.4 | 19.4 | 17.5 | 25.8 | 9.7 |
| | | 600 | 63.4 | 18.4 | 16.4 | 25.3 | 9.8 |
| | | 650 | 63.4 | 18.0 | 16.2 | 25.1 | 9.9 |
| Fuel Tube | Zircalloy [12] | 600 | | | | | 2.73 |

## Table 2.10.3-2
## Summary of Basket Normal Condition Stress Analysis

| Drop Orientation | Component | Stress Category | Max. Stress Due to 1 foot drop (ksi) | Max. Thermal Stress (ksi) | Combined Stress (ksi) | Allowable Stress (ksi) |
|---|---|---|---|---|---|---|
| End Drop | Fuel Compartment & Outer Wrapper | $P_m$ | 2.7 | - | 2.7 | 16.40 |
| | | $P_m+P_b+Q$ | 2.7 | 12.95 | 15.65 | 49.20 |
| | Plate Insert Weld | Shear | 5.76 | - | 5.76 | 9.84 |
| | Rail Stud | Shear | 5.70 | - | 5.70 | 9.84 |
| | Hold Down Ring | $P_m$ | 3.0 | - | 3.00 | 16.40 |
| 45° Side Drop | Basket | $P_m$ | 6.42 | - | 6.42 | 16.40 |
| | | $P_m+P_b$ | 22.72 | - | 22.72 | 24.60 |
| | | $P_m+P_b+Q$ | 29.85 | 12.95 | 42.80 | 49.20 |
| | Rails | $P_m$ | 5.81 | - | 5.81 | 17.50 |
| | | $P_m+P_b$ | 19.19 | - | 19.19 | 26.25 |
| | | $P_m+P_b+Q$ | 22.22 | 1.76 | 23.98 | 52.50 |
| 60° Side Drop | Basket | $P_m$ | 8.14 | - | 8.14 | 16.40 |
| | | $P_m+P_b$ | 21.30 | - | 21.30 | 24.60 |
| | | $P_m+P_b+Q$ | 29.25 | 12.95 | 42.20 | 49.20 |
| | Rails | $P_m$ | 9.49 | - | 9.49 | 17.50 |
| | | $P_m+P_b$ | 25.03 | - | 25.03 | 26.25 |
| | | $P_m+P_b+Q$ | 30.88 | 1.76 | 32.64 | 52.50 |
| 90° Side Drop | Basket | $P_m$ | 7.92 | - | 7.92 | 16.40 |
| | | $P_m+P_b$ | 13.75 | - | 13.75 | 24.60 |
| | | $P_m+P_b+Q$ | 13.75 | 12.95 | 26.70 | 49.20 |
| | Rails | $P_m$ | 15.17 | - | 15.17 | 17.50 |
| | | $P_m+P_b$ | 26.11 | - | 26.11 | 26.25 |
| | | $P_m+P_b+Q$ | 26.11 | 1.76 | 27.87 | 52.50 |
| 180° Side Drop, Impact on support rails | Basket | $P_m$ | 6.32 | - | 6.32 | 16.40 |
| | | $P_m+P_b$ | 11.98 | - | 11.98 | 24.60 |
| | | $P_m+P_b+Q$ | 11.98 | 12.95 | 24.93 | 49.20 |
| | Rails | $P_m$ | 13.62 | - | 13.62 | 17.50 |
| | | $P_m+P_b$ | 18.24 | - | 18.24 | 26.25 |
| | | $P_m+P_b+Q$ | 18.24 | 1.76 | 20.00 | 52.50 |

## Table 2.10.3-3
## Summary of Basket Accident Condition Stress Analysis

| Drop Orientation | Component | Stress Category | Max. Stress Due to 1 foot drop (ksi) | Max. Thermal Stress (ksi) | Combined Stress (ksi) | Allowable Stress (ksi) |
|---|---|---|---|---|---|---|
| End Drop | Fuel Compartment & Outer Wrapper | $P_m$ | 6.75 | - | 6.75 | 44.38 |
| | | $P_m+P_b+Q$ | 6.75 | 12.95 | 19.70 | 57.06 |
| | Plate Insert Weld | Shear | 14.41 | - | 14.41 | 26.63 |
| | Rail Stud | Shear | 14.25 | - | 14.25 | 26.63 |
| | Hold Down Ring | $P_m$ | 7.5 | - | 7.5 | 44.38 |
| 45° Side Drop | Basket | $P_m$ | 14.54 | - | 14.54 | 44.38 |
| | | $P_m+P_b$ | 27.12 | - | 27.12 | 57.06 |
| | | $P_m+P_b+Q$ | 27.12 | 12.95 | 40.07 | 57.06 |
| | Rails | $P_m$ | 16.52 | - | 16.52 | 44.38 |
| | | $P_m+P_b$ | 25.27 | - | 25.27 | 57.06 |
| | | $P_m+P_b+Q$ | 25.27 | 1.76 | 27.03 | 57.06 |
| 60° Side Drop | Basket | $P_m$ | 14.43 | - | 14.43 | 44.38 |
| | | $P_m+P_b$ | 27.30 | - | 27.3 | 57.06 |
| | | $P_m+P_b+Q$ | 27.30 | 12.95 | 40.25 | 57.06 |
| | Rails | $P_m$ | 20.85 | - | 20.85 | 44.38 |
| | | $P_m+P_b$ | 28.72 | - | 28.72 | 57.06 |
| | | $P_m+P_b+Q$ | 28.72 | 1.76 | 30.48 | 57.06 |
| 90° Side Drop | Basket | $P_m$ | 18.02 | - | 18.02 | 44.38 |
| | | $P_m+P_b$ | 22.78 | - | 22.78 | 57.06 |
| | | $P_m+P_b+Q$ | 22.78 | 12.95 | 35.73 | 57.06 |
| | Rails | $P_m$ | 29.03 | - | 29.03 | 44.38 |
| | | $P_m+P_b$ | 32.79 | - | 32.79 | 57.06 |
| | | $P_m+P_b+Q$ | 32.79 | 1.76 | 34.55 | 57.06 |
| 180° Side Drop, Impact on support rails | Basket | $P_m$ | 17.18 | - | 17.18 | 44.38 |
| | | $P_m+P_b$ | 22.54 | - | 22.54 | 57.06 |
| | | $P_m+P_b+Q$ | 22.54 | 12.95 | 35.49 | 57.06 |
| | Rails | $P_m$ | 19.01 | - | 19.01 | 44.38 |
| | | $P_m+P_b$ | 28.16 | - | 28.16 | 57.06 |
| | | $P_m+P_b+Q$ | 28.16 | 1.76 | 29.92 | 57.06 |

## Table 2.10.3-4
## Summary of Hold Down Ring Accident Condition Stress Analysis

| Drop Orientation | Component | Stress Category | Max. Stress Due to 1 foot drop (ksi) | Allowable Stress (ksi) |
|---|---|---|---|---|
| Side Drop (All Orientations) | Alignment Leg | $P_m$ | 14.06 | 44.38 |
| | | $P_m + P_b$ | 36.77 | 57.06 |
| | Alignment Leg Weld | $P_m + P_b$ | 10.20 | 57.06 |
| Side Drop (90° Orientations) | Hold Down Ring Body | $P_m$ | 1.52 | 44.38 |
| | | $P_m + P_b$ | 45.91 | 57.06 |
| Side Drop (45° Orientations) | Hold Down Ring Body | $P_m$ | 1.65 | 44.38 |
| | | $P_m + P_b$ | 34.71 | 57.06 |

**Table 2.10.3-5**
**Summary of Loads Used for Different Drop Orientations**

Location 1
($F_y = F\cos\theta$, $P_x = P\sin\theta$, $F = 290$ lbs, $P = 0.8$ psi)

| Drop Orientation (Degree) | 1G load (6" Length) (Weight including all SS & poison plates above the bottom panel, rails, and 8 fuel assemblies**) | | 200 G Load Computer Run | |
|---|---|---|---|---|
| | Axial Load $F_y$ (lbs) | Trans. Load $P_x$ (psi) | $F_y$ (lbs) | $P_x$(psi) |
| Vertical | 290 | 0 | 58,000 | 0 |
| 30 | 251 | 0.4 | 50,200 | 80 |
| 45 | 205 | 0.565 | 41,000 | 113 |

** This assumption is very conservative for drop orientations other than the vertical drop. For example, for 30 and 45 degree drops, the bottom panel only supports 6 fuel assemblies but was analyzed for 8 fuel assemblies.

Location 2
($F_y = F\cos\theta$, $P_x = P\sin\theta$, $F = 160$ lbs, $P = 0.8$ psi)

| Drop Orientation (Degree) | 1G load (6" Length) (Weight including all SS & poison plates above the bottom panel, rails, and 4 fuel assemblies**) | | 200 G Load Computer Run | |
|---|---|---|---|---|
| | Axial Load $F_y$ (lbs) | Trans. Load $P_x$ (psi) | $F_y$ (lbs) | $P_x$ (psi) |
| Vertical | 160 | 0 | 32,000 | 0 |
| 30 | 139 | 0.4 | 27,800 | 80 |
| 45 | 113 | 0.565 | 22,600 | 113 |

** This assumption is also very conservative for drop orientations other than vertical drop. For example, for 30 and 45 degree drops, the bottom panel only supports 3 fuel assemblies but was analyzed for 4 fuel assemblies.

## Table 2.10.3-6
## Summary of Canister Normal Condition Stress Analysis

| Load Combination | | Stress Category | Maximum Stress (ksi.) | Allowable Membrane Stress Intensity (ksi.) |
|---|---|---|---|---|
| 30*g* Front End Drop | External Pressure, Cold Environment | $P_m + P_b$ | 9.2 | 18.7* |
| | Internal Pressure, Hot Environment | $P_m + P_b$ | 9.0 | 18.7* |
| 30*g* Rear End Drop | External Pressure, Cold Environment | $P_m + P_b$ | 11.6 | 18.7* |
| | Internal Pressure, Hot Environment | $P_m + P_b$ | 10.3 | 18.7* |
| 45° Azimuth 30g Side Drop | External Pressure, Cold Environment | $P_m$ | 6.2 | 18.7 |
| | | $P_m + P_b$ | 15.1 | 28.1 |
| | Internal Pressure, Hot Environment | $P_m$ | 11.4 | 18.7 |
| | | $P_m + P_b$ | 20.4 | 28.1 |
| 60° Azimuth 30g Side Drop | External Pressure, Cold Environment | $P_m$ | 6.4 | 18.7 |
| | | $P_m + P_b$ | 19.3 | 28.1 |
| | Internal Pressure, Hot Environment | $P_m$ | 11.6 | 18.7 |
| | | $P_m + P_b$ | 24.6 | 28.1 |
| 90° Azimuth 30g Side Drop | External Pressure, Cold Environment | $P_m$ | 6.6 | 18.7 |
| | | $P_m + P_b$ | 12.4 | 28.1 |
| | Internal Pressure, Hot Environment | $P_m$ | 11.8 | 18.7 |
| | | $P_m + P_b$ | 17.7 | 28.1 |
| 180° Azimuth 30g Side Drop | External Pressure, Cold Environment | $P_m$ | 7.2 | 18.7 |
| | | $P_m + P_b$ | 15.0 | 28.1 |
| | Internal Pressure, Hot Environment | $P_m$ | 12.5 | 18.7 |
| | | $P_m + P_b$ | 20.2 | 28.1 |

*The stress intensities (membrane + bending) generated in the canister during the end drop events are conservatively compared with the membrane allowable stress, $P_m$ for SA-240, Type 304.

## Table 2.10.3-7
## Summary of Canister Accident Condition Stress Analysis

| Load Combination | | Stress Category | Maximum Stress (ksi.) | Allowable Membrane Stress Intensity (ksi.) |
|---|---|---|---|---|
| 75*g* Front End Drop | Hot Environment, Internal Pressure | $P_m + P_b$ | 13.6 | 44.8* |
| | Cold Environment, External Pressure | $P_m + P_b$ | 16.8 | 44.8* |
| 75*g* Rear End Drop | Hot Environment, Internal Pressure | $P_m + P_b$ | 17.8 | 44.8* |
| | Cold Environment, External Pressure | $P_m + P_b$ | 17.0 | 44.8* |
| 45° Azimuth 75*g* Side Drop | External Pressure, Cold Environment | $P_m$ | 7.2 | 44.8 |
| | | $P_m + P_b$ | 24.8 | 57.6 |
| | Internal Pressure, Hot Environment | $P_m$ | 12.4 | 44.8 |
| | | $P_m + P_b$ | 30.0 | 57.6 |
| 60° Azimuth 75*g* Side Drop | External Pressure, Cold Environment | $P_m$ | 7.6 | 44.8 |
| | | $P_m + P_b$ | 24.7 | 57.6 |
| | Internal Pressure, Hot Environment | $P_m$ | 12.9 | 44.8 |
| | | $P_m + P_b$ | 30.0 | 57.6 |
| 90° Azimuth 75*g* Side Drop | External Pressure, Cold Environment | $P_m$ | 8.3 | 44.8 |
| | | $P_m + P_b$ | 22.0 | 57.6 |
| | Internal Pressure, Hot Environment | $P_m$ | 13.6 | 44.8 |
| | | $P_m + P_b$ | 27.2 | 57.6 |
| 180° Azimuth 75*g* Side Drop | External Pressure, Cold Environment | $P_m$ | 8.7 | 44.8 |
| | | $P_m + P_b$ | 24.9 | 57.6 |
| | Internal Pressure, Hot Environment | $P_m$ | 13.9 | 44.8 |
| | | $P_m + P_b$ | 30.1 | 57.6 |

*The stress intensities (membrane + bending) generated in the canister during the end drop events are conservatively compared with the membrane allowable stress, $P_m$ for SA-240, Type 304.

Figure 2.10.3-1
Basket Cross Section Finite Element Model

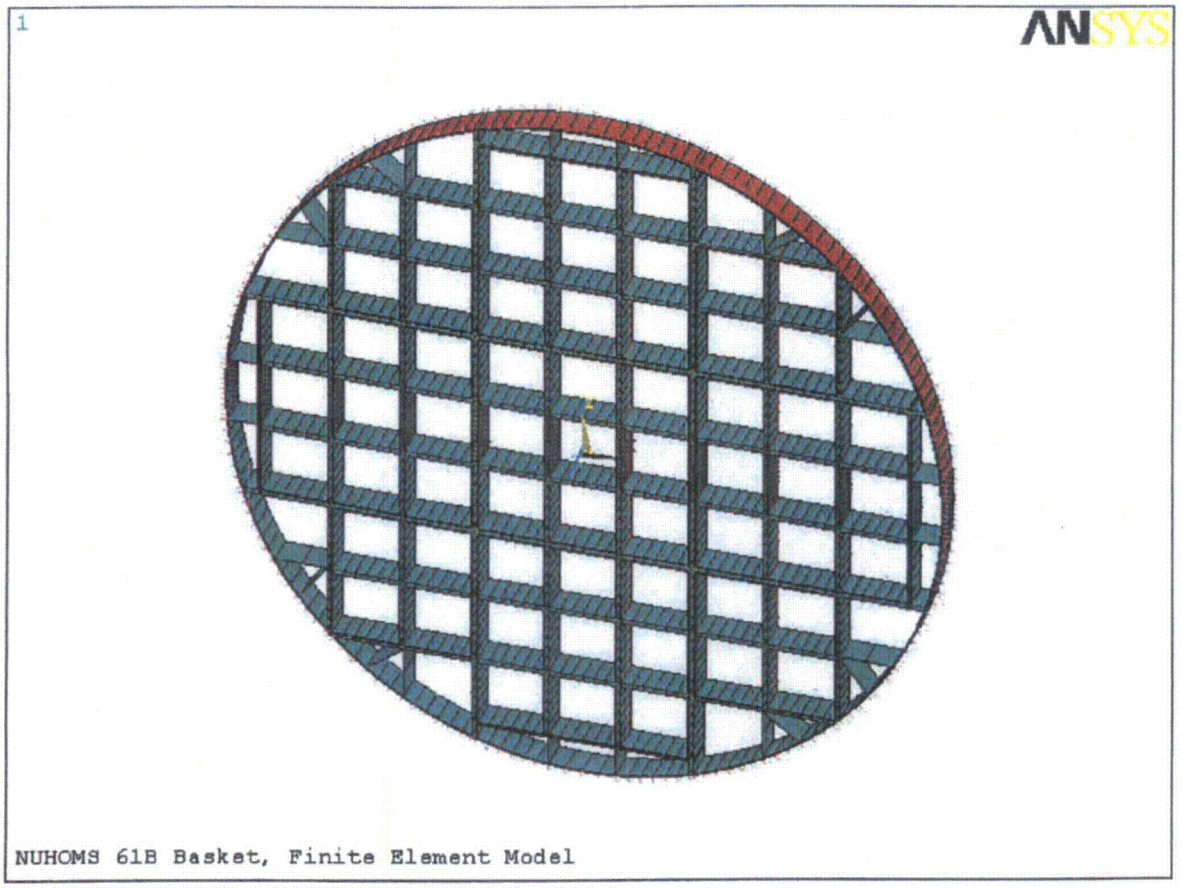

Figure 2.10.3-2
Basket Cross Section Finite Element Model – Fuel Compartments

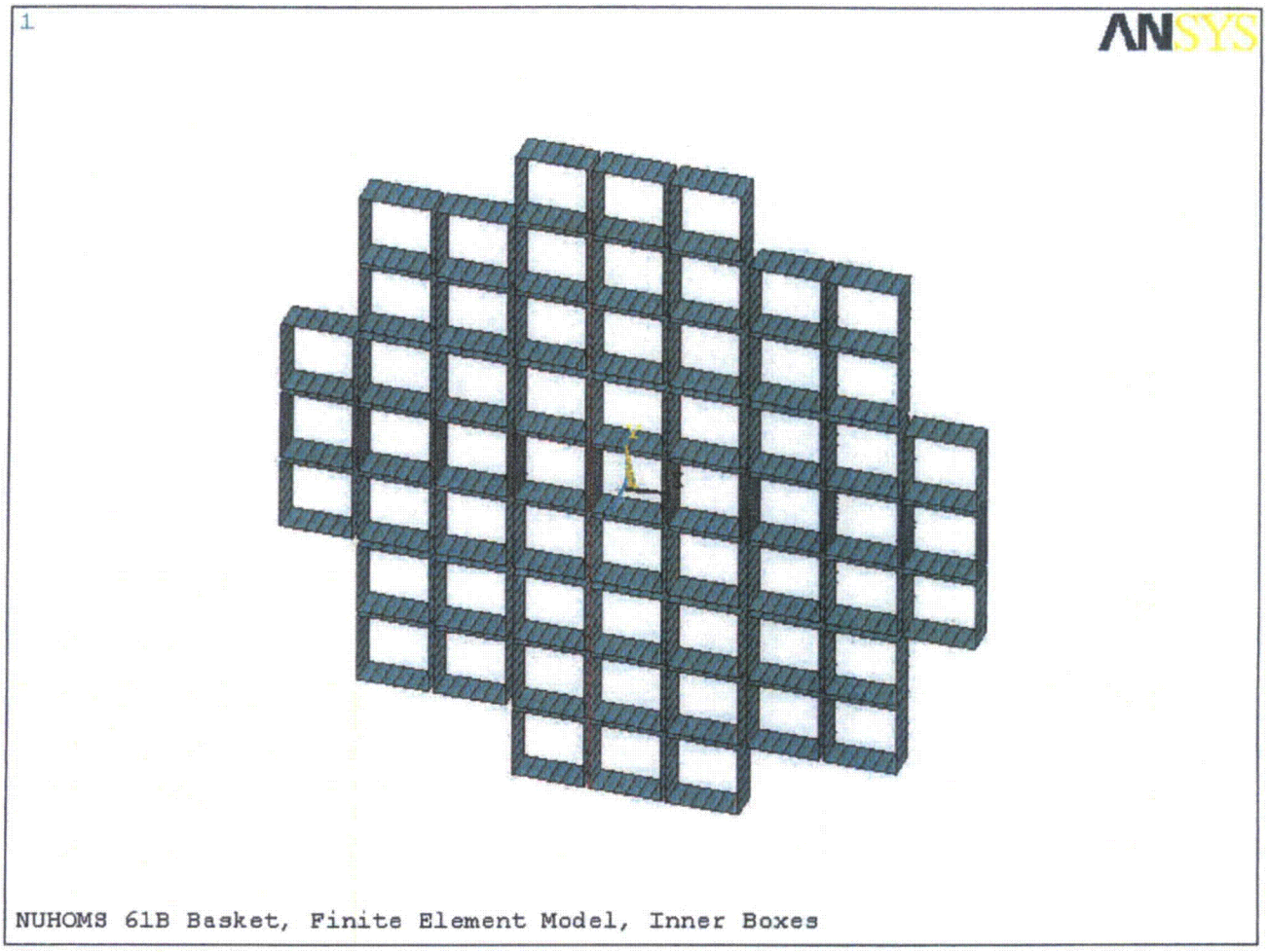

Figure 2.10.3-3
Basket Cross Section Finite Element Model – Outer Wrap

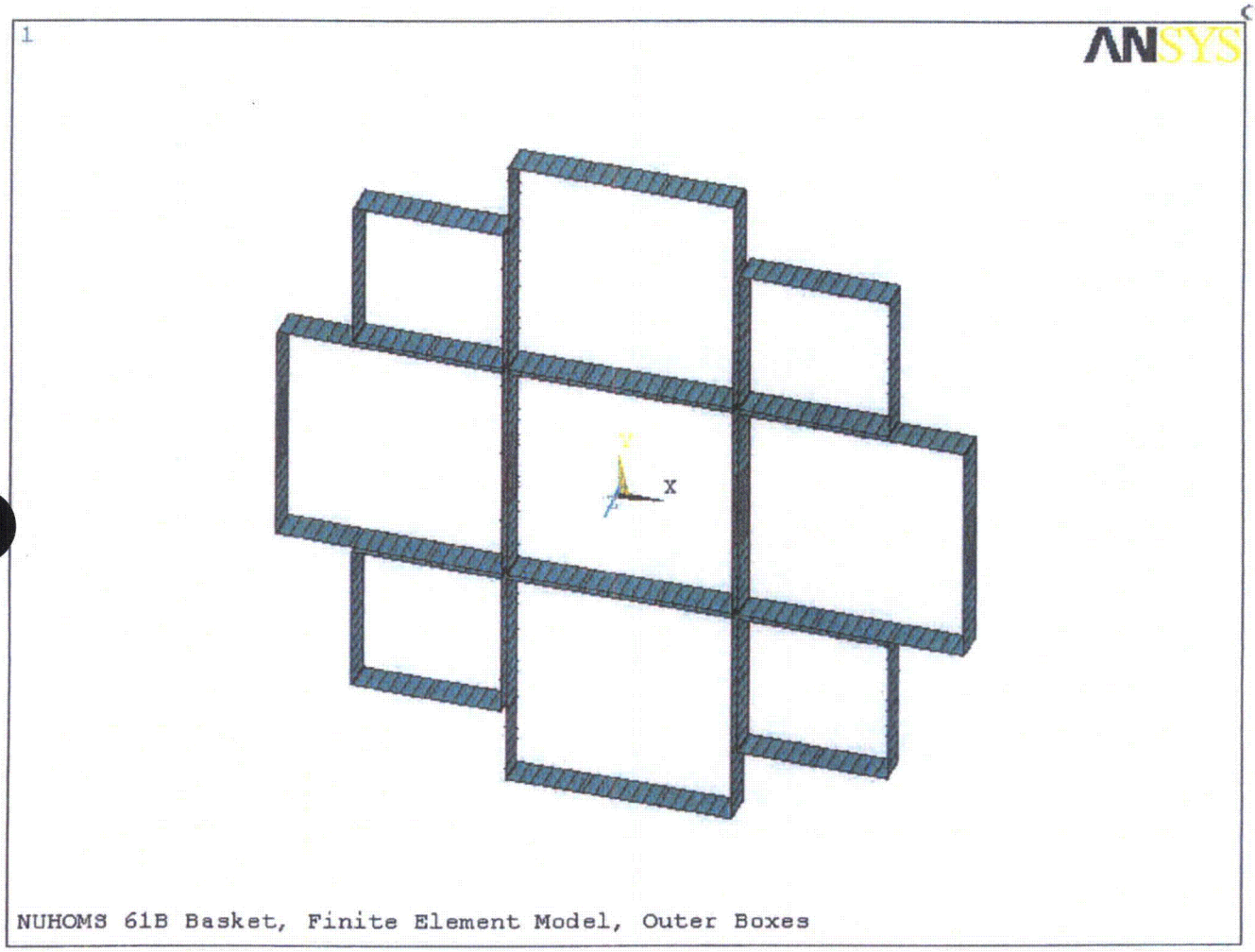

Figure 2.10.3-4
Basket Cross Section Finite Element Model – Support Rails

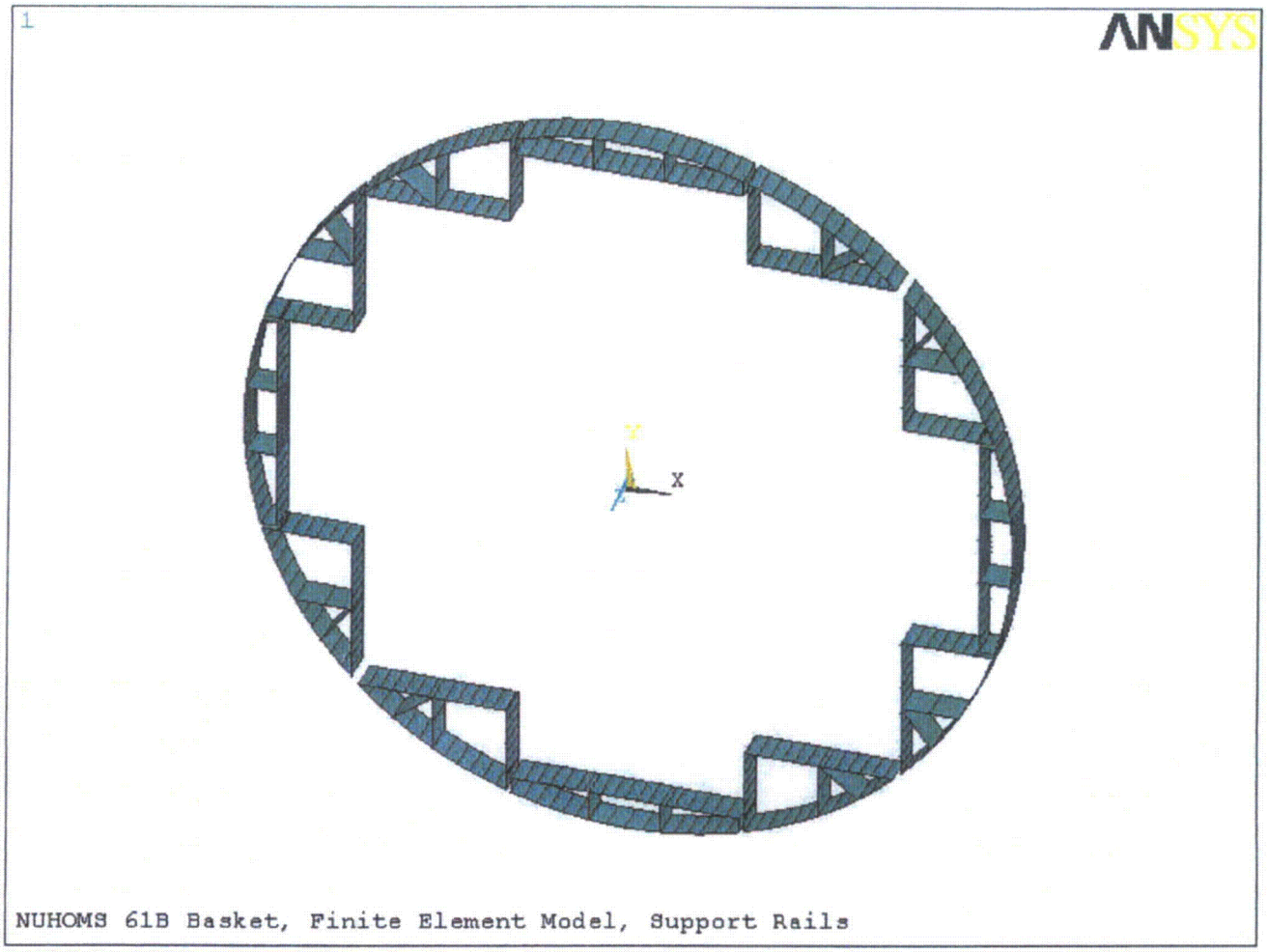

Figure 2.10.3-5
Basket Side Drop Orientations

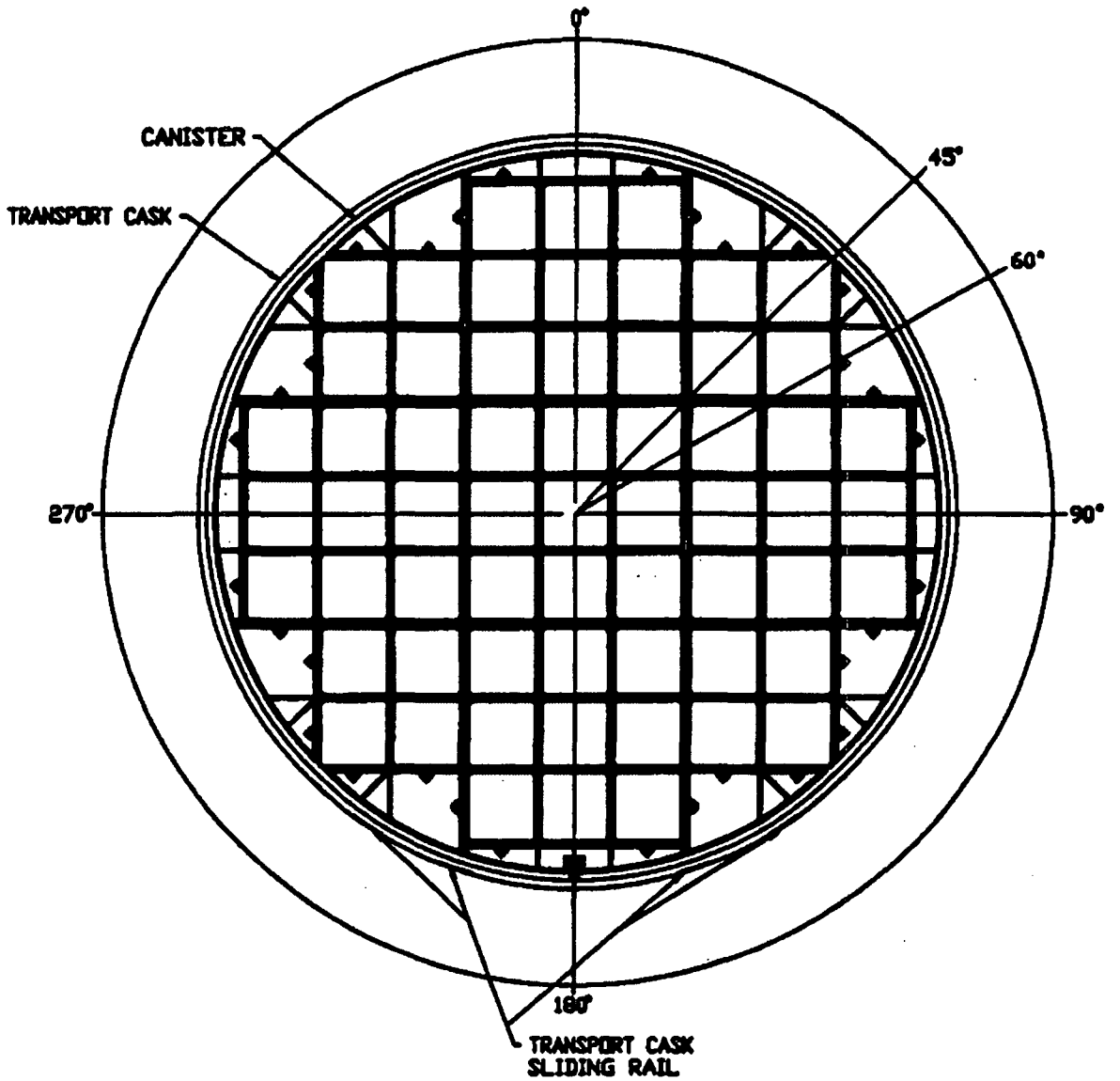

Figure 2.10.3-6
Gap Sizes between Basket Rails and Canister Inner Surface

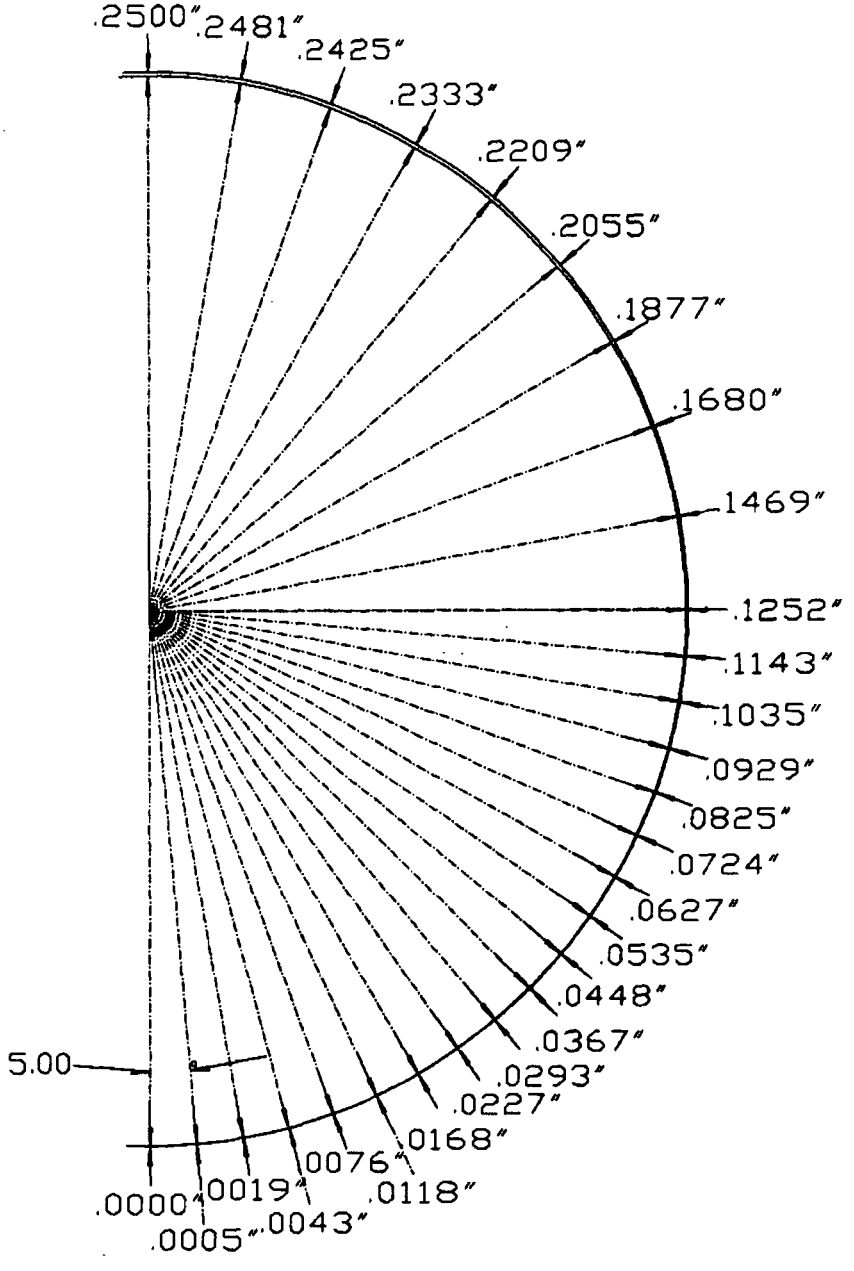

Figure 2.10.3-7
Gap Sizes between Canister Outer Surface and Transport Cask Inner Surface

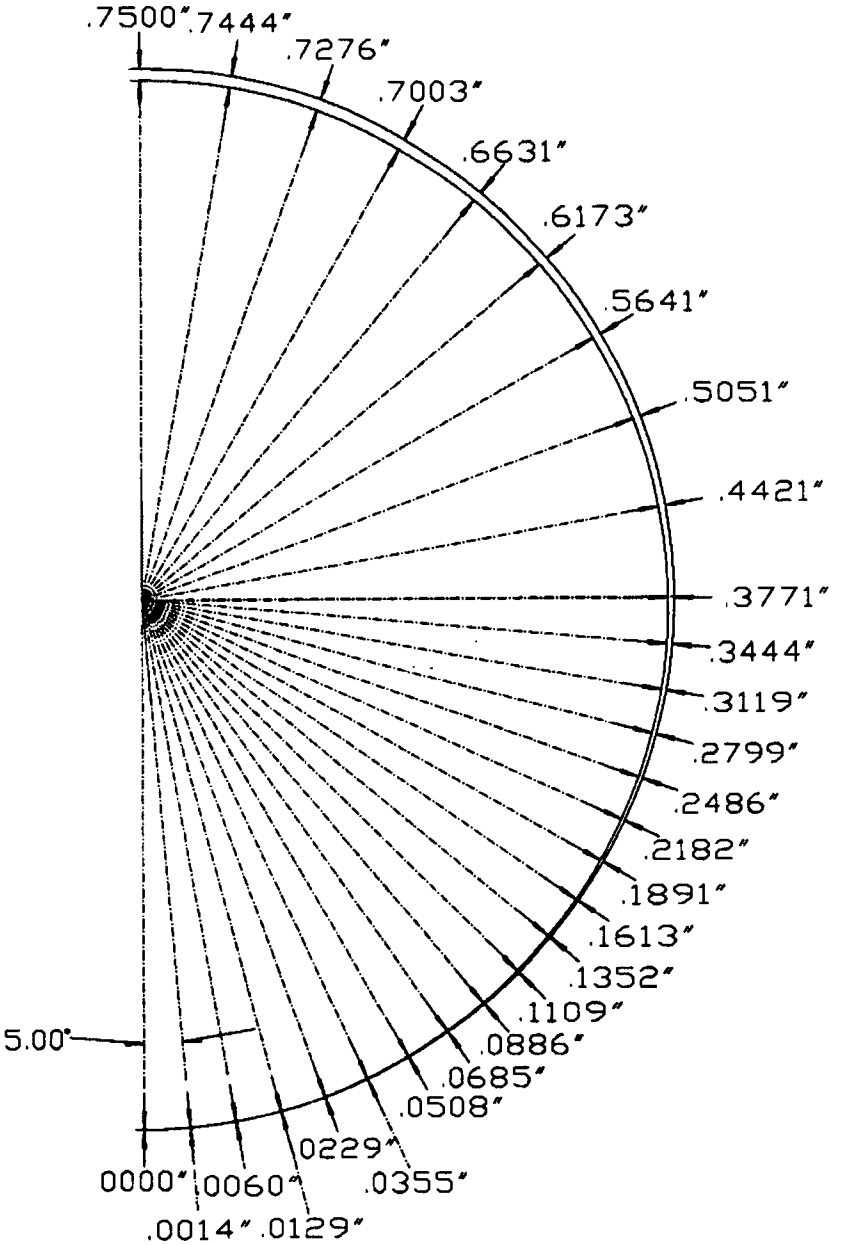

Figure 2.10.3-8
Finite Element Model – Canister & Gap Elements

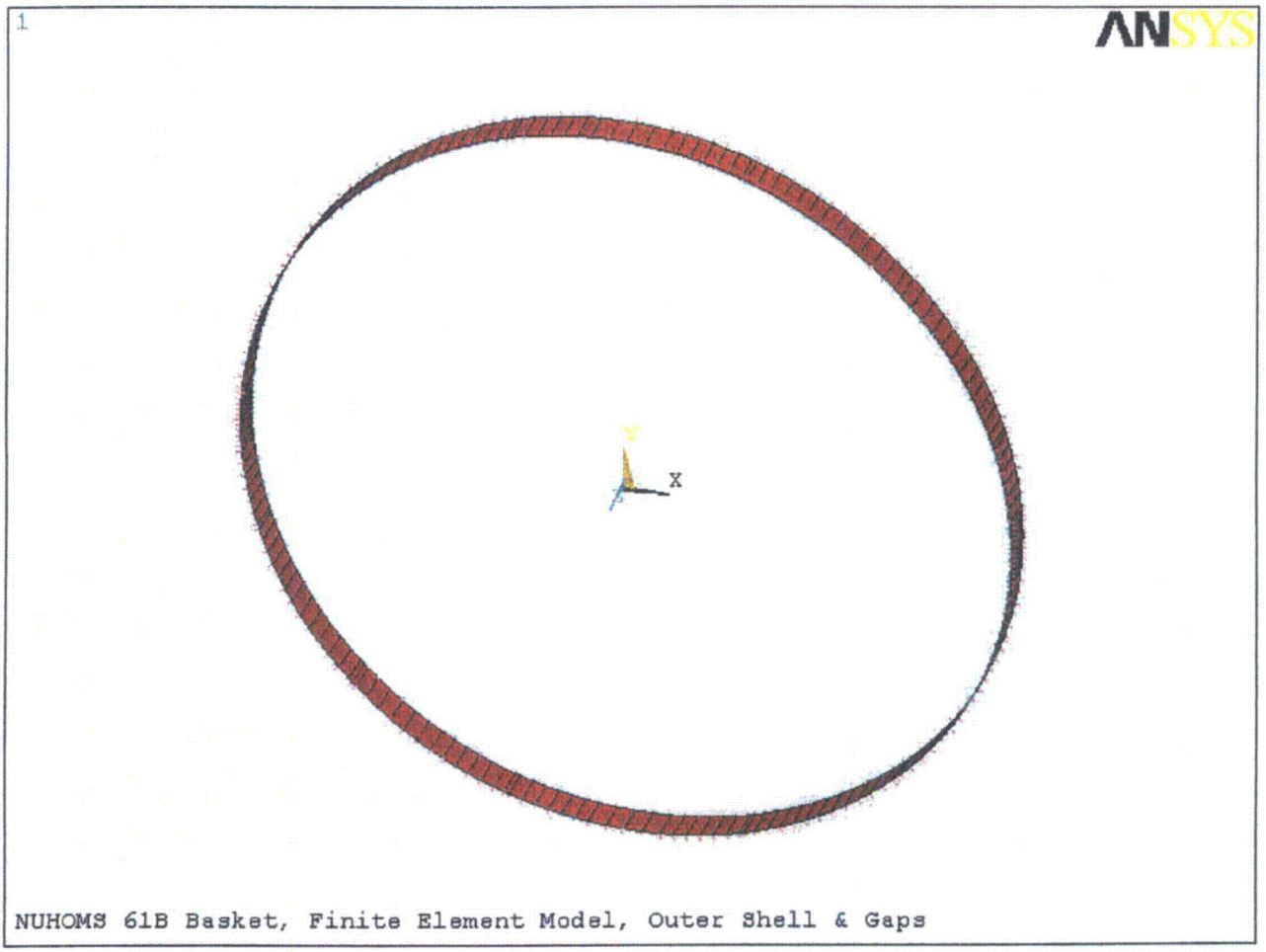

Figure 2.10.3-9
Finite Element Model – Canister & Gap Elements, Enlarged View

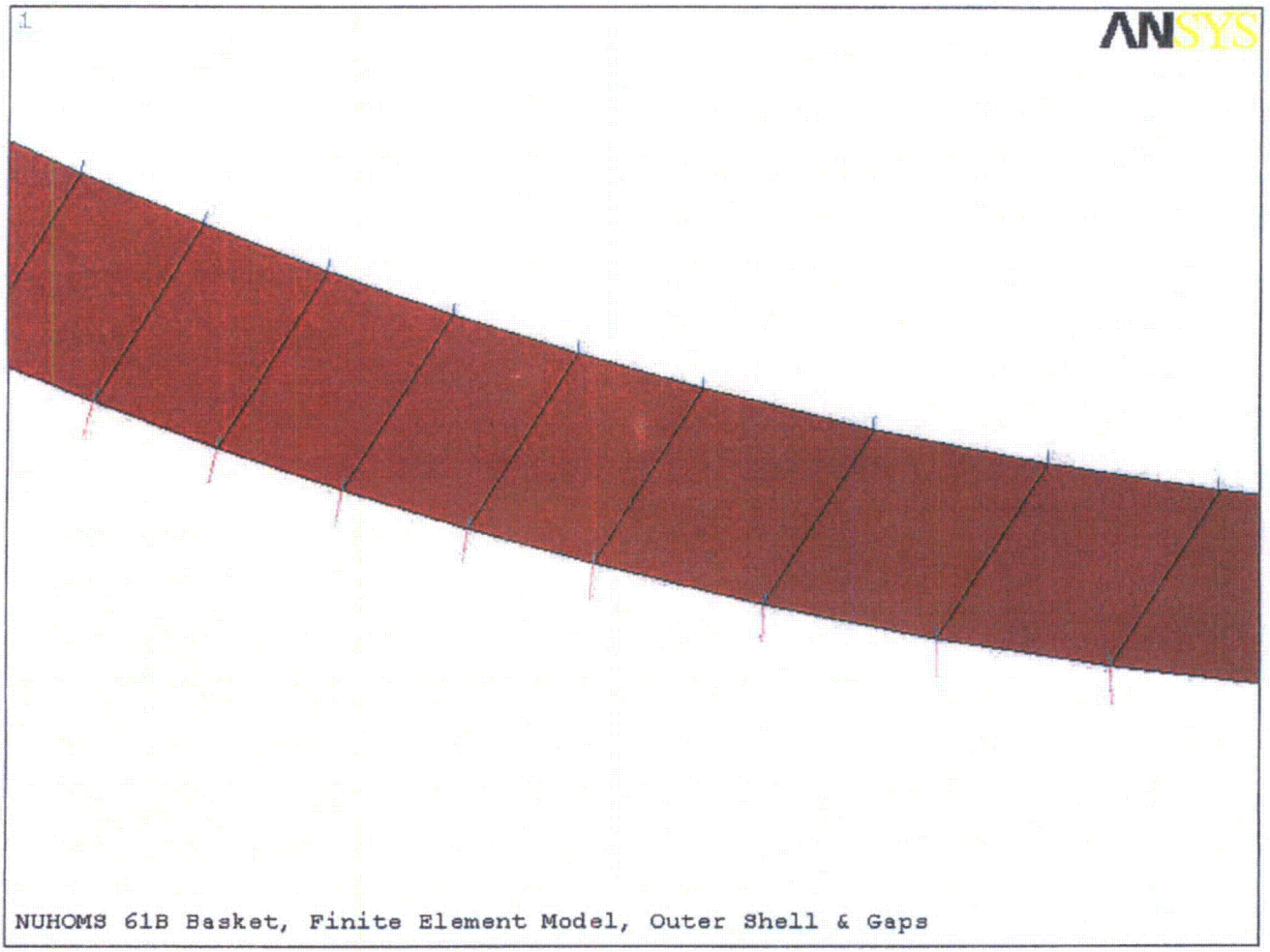

Figure 2.10.3-10
Basket Temperature Distribution at the Middle Section

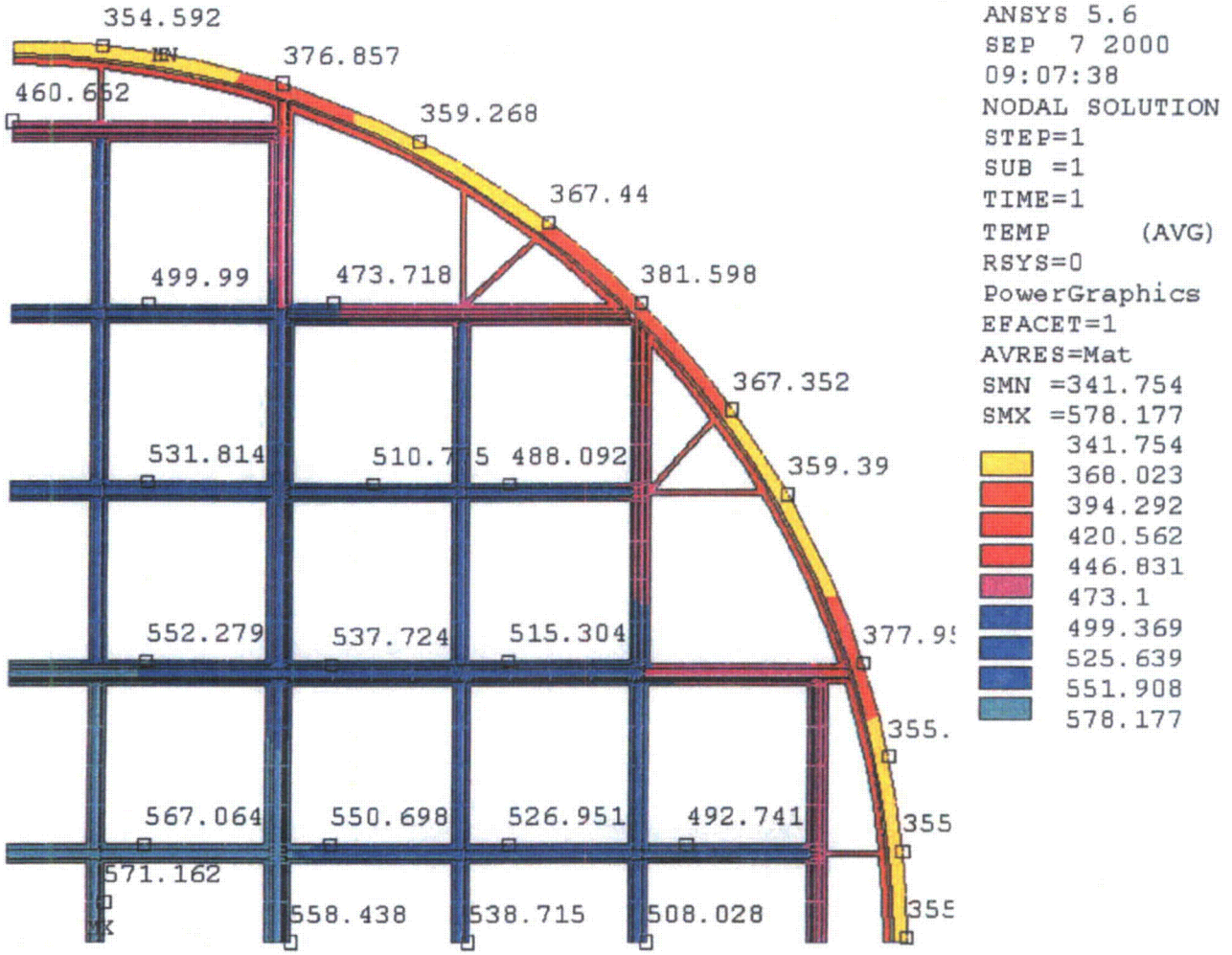


**Hottest Cross-Section**

Figure 2.10.3-11
Basket Temperature Distribution at the Top Section

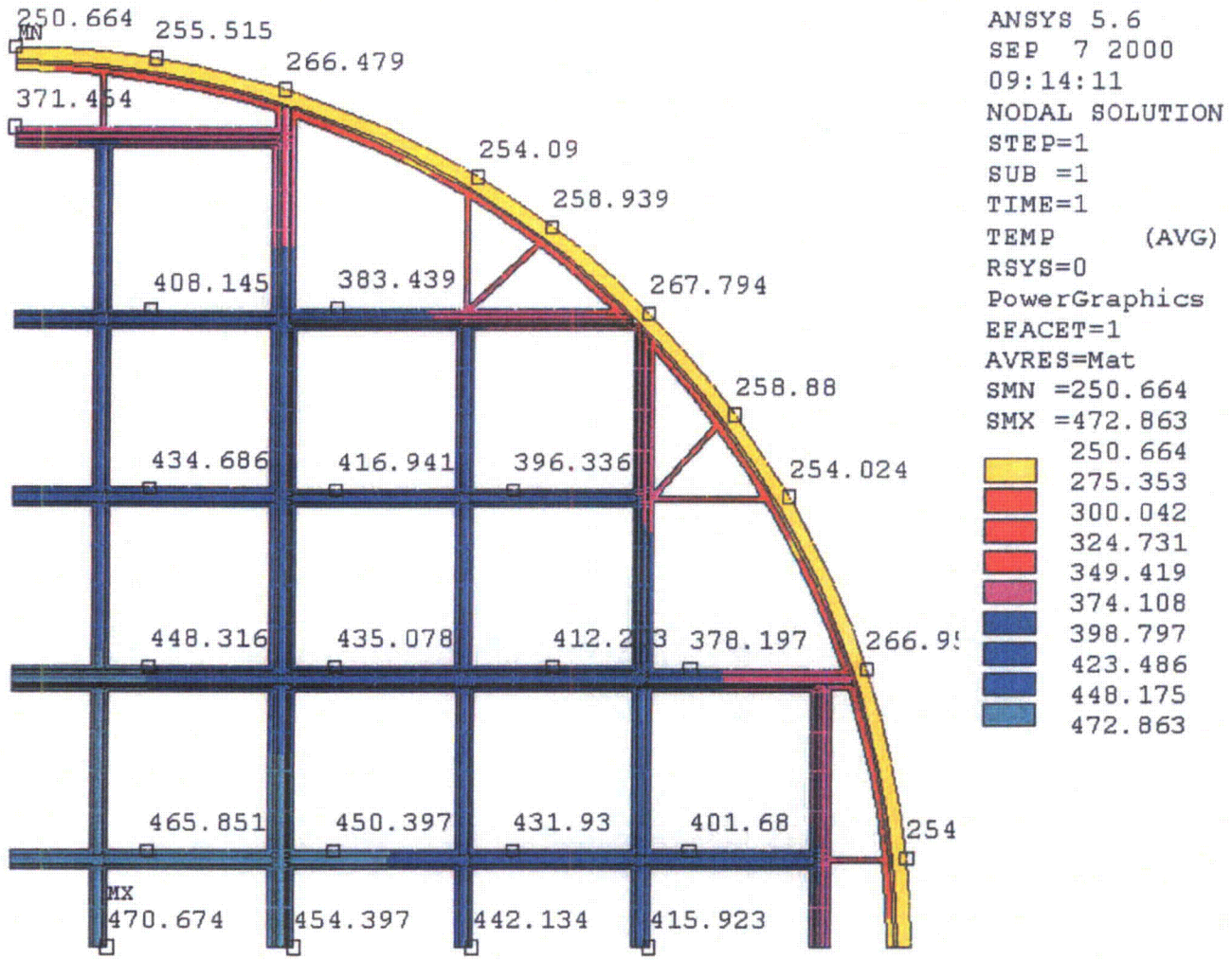


**Top Cross-Section**

Figure 2.10.3-12
Basket Temperature Distribution at the Bottom Section

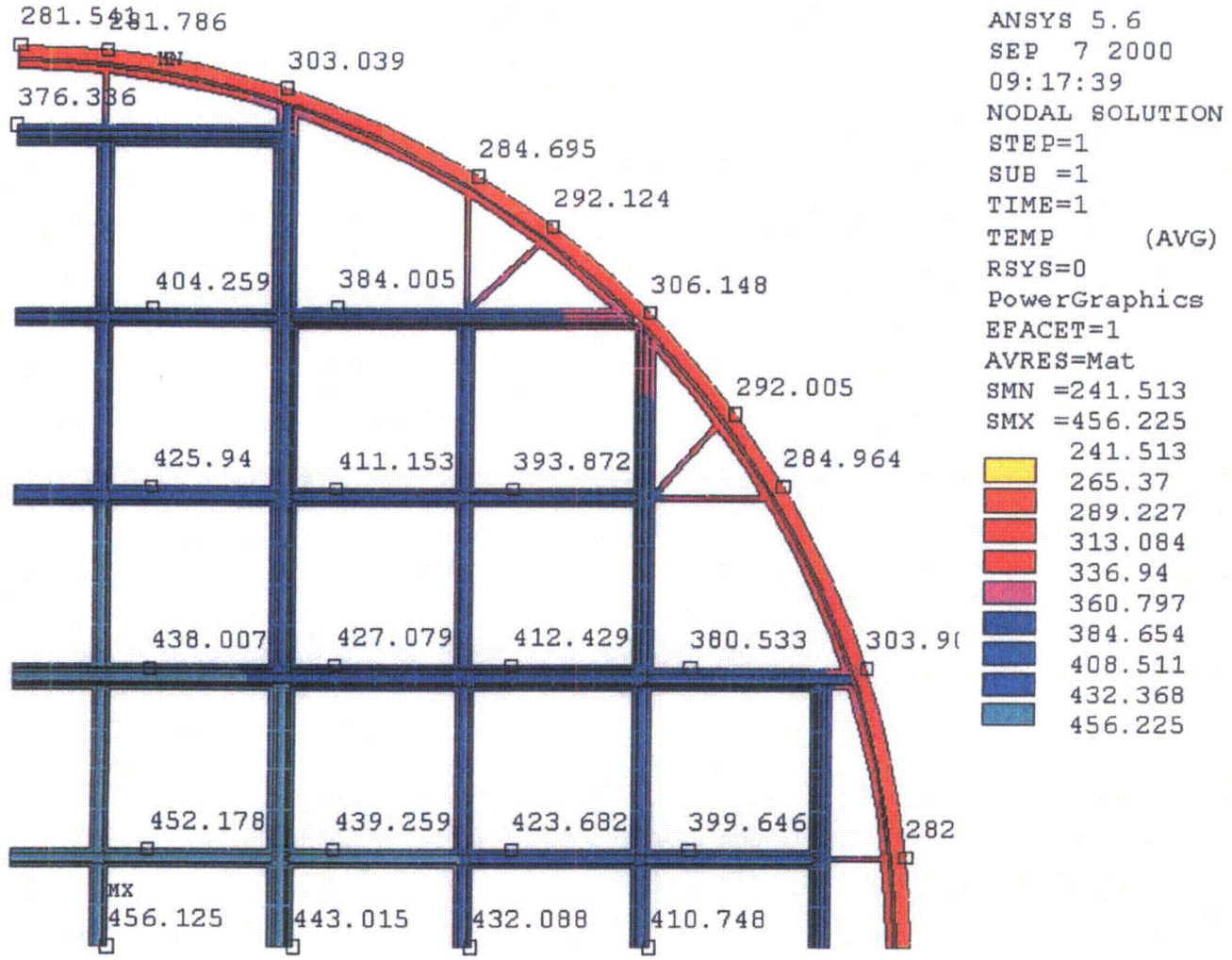


**Bottom Cross-Section**

Figure 2.10.3-13
Basket ¼ Section Finite Element Model for Thermal Stress Analysis

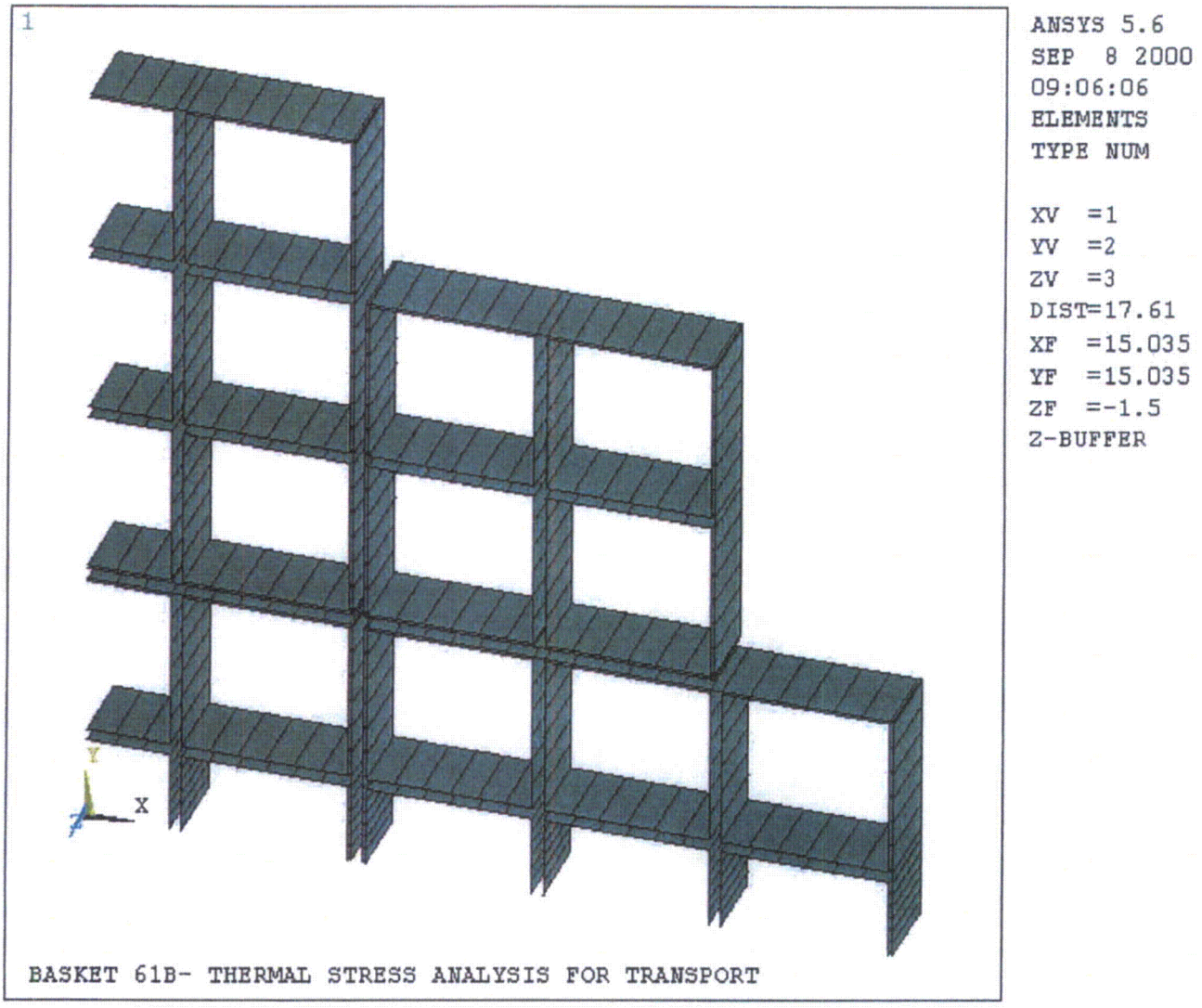

Figure 2.10.3-14
Basket ¼ Section Finite Element Model with Nodal Couplings and Boundary Conditions

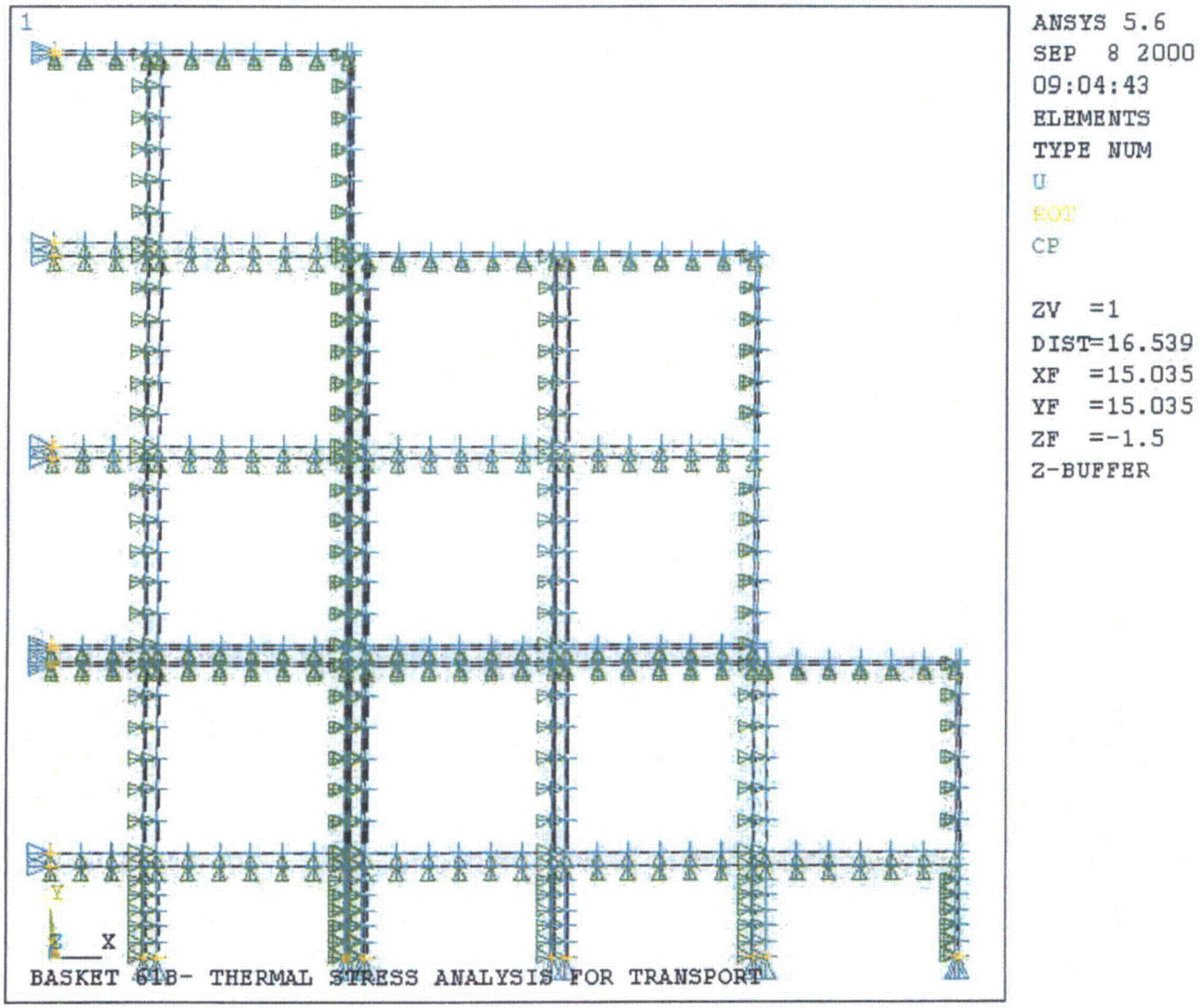

Figure 2.10.3-15
Thermal Stress Analysis Geometry

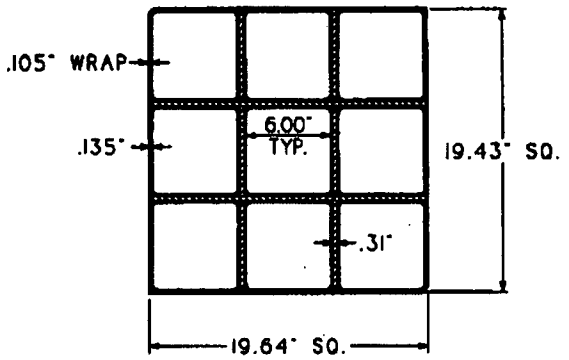


(a) 3 x 3 BOX SECTION

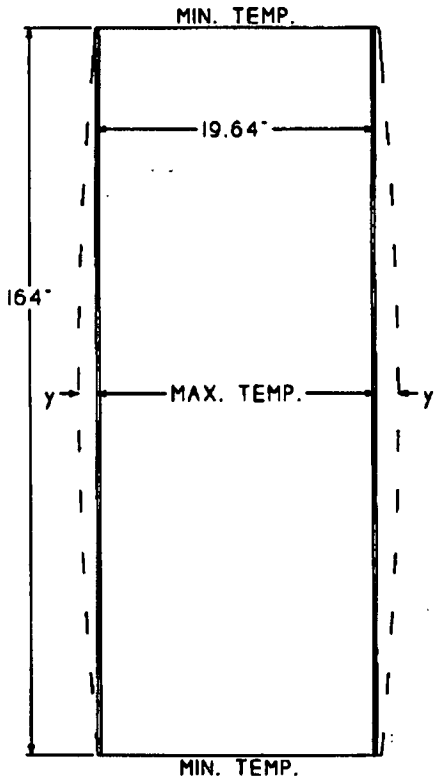


(b) 3 x 3 BOX OUTER WRAP

Figure 2.10.3-16
Support Rail Temperature Distribution at the Middle Section

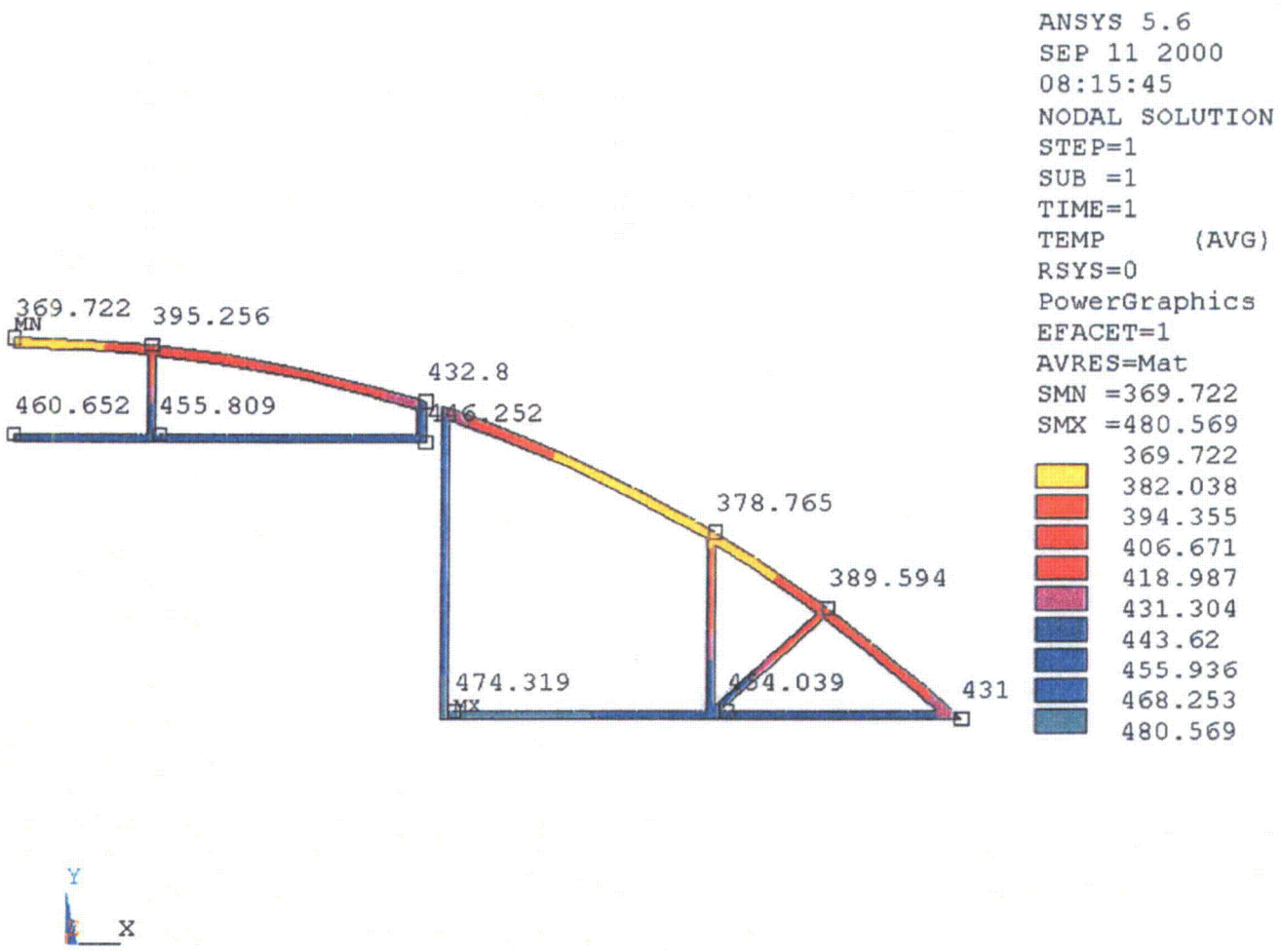


**Hottest Cross-Section**

Figure 2.10.3-17
Support Rail Temperature Distribution at the Top Section

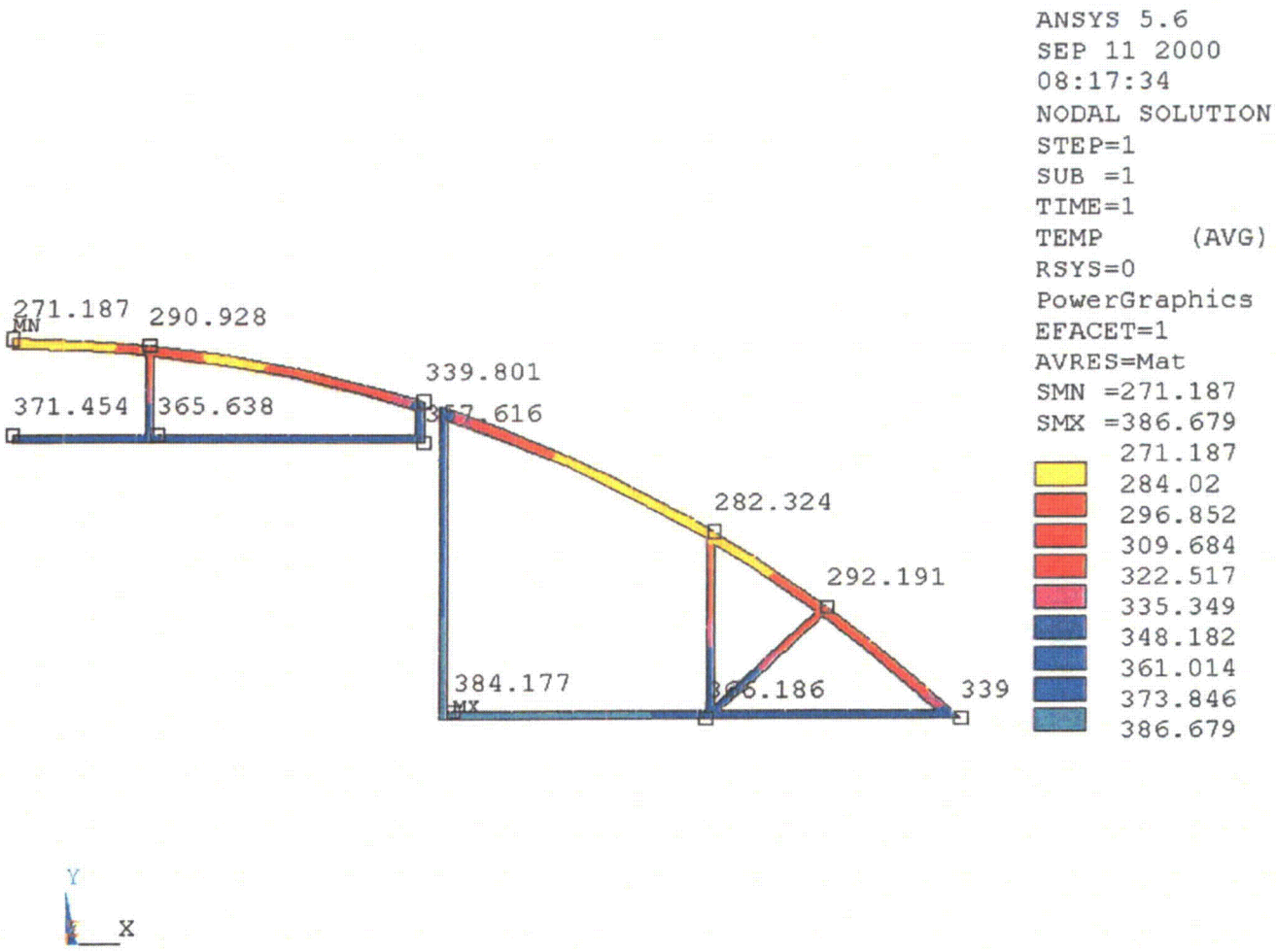


**Top Cross-Section**

Figure 2.10.3-18
Support Rail Temperature Distribution at the Bottom Section

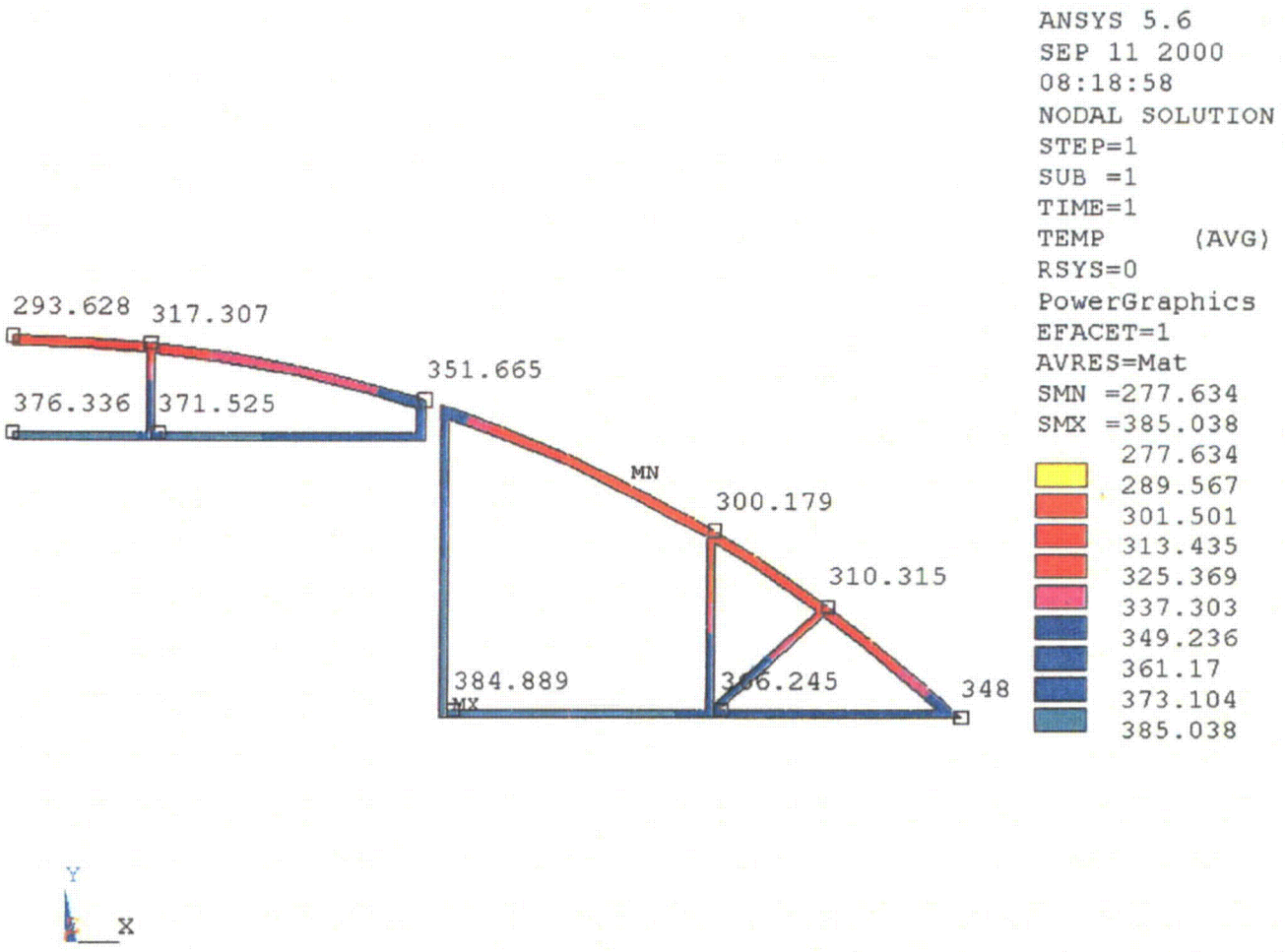


**Bottom Cross-Section**

Figure 2.10.3-19
Basket Rail Type 1 Finite Element Model

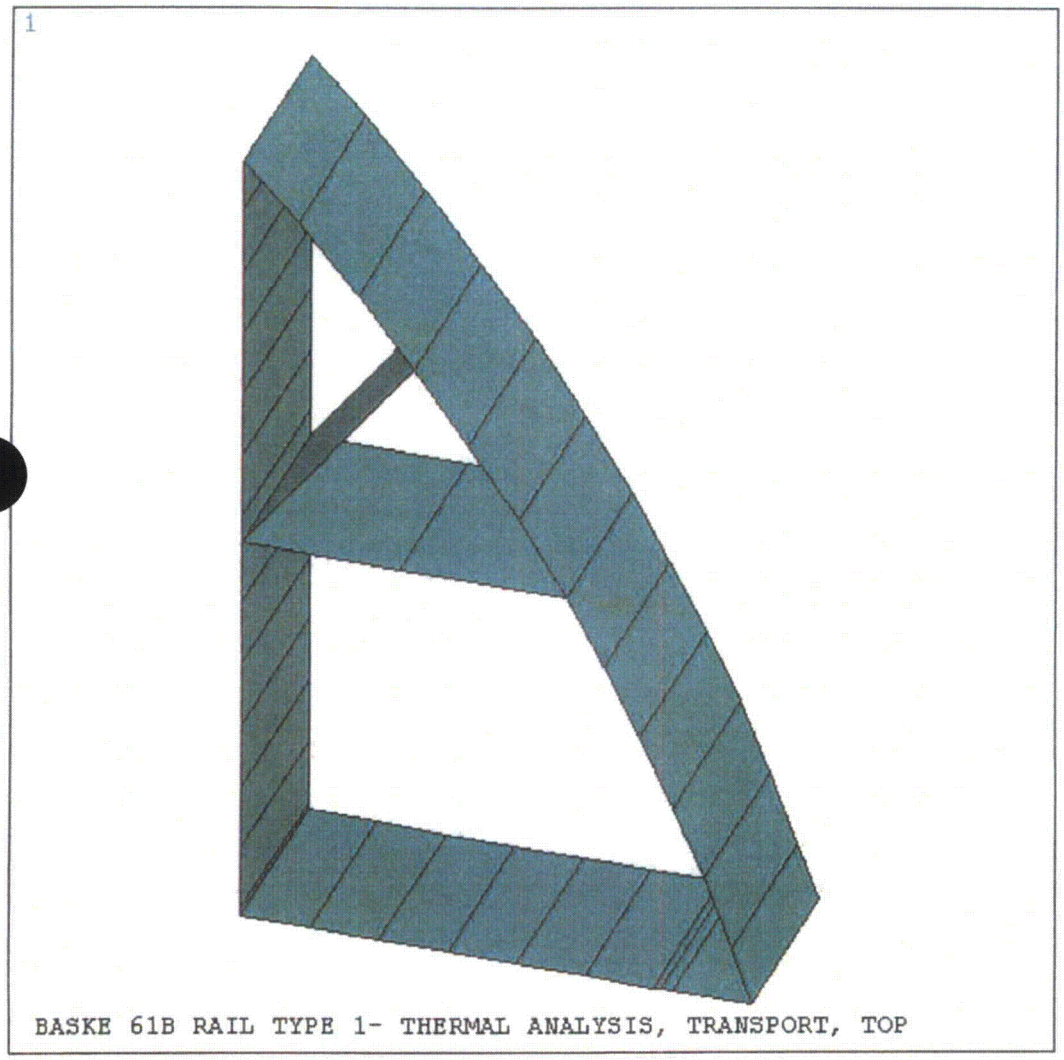

Figure 2.10.3-20
Basket Rail Type 2 Finite Element Model

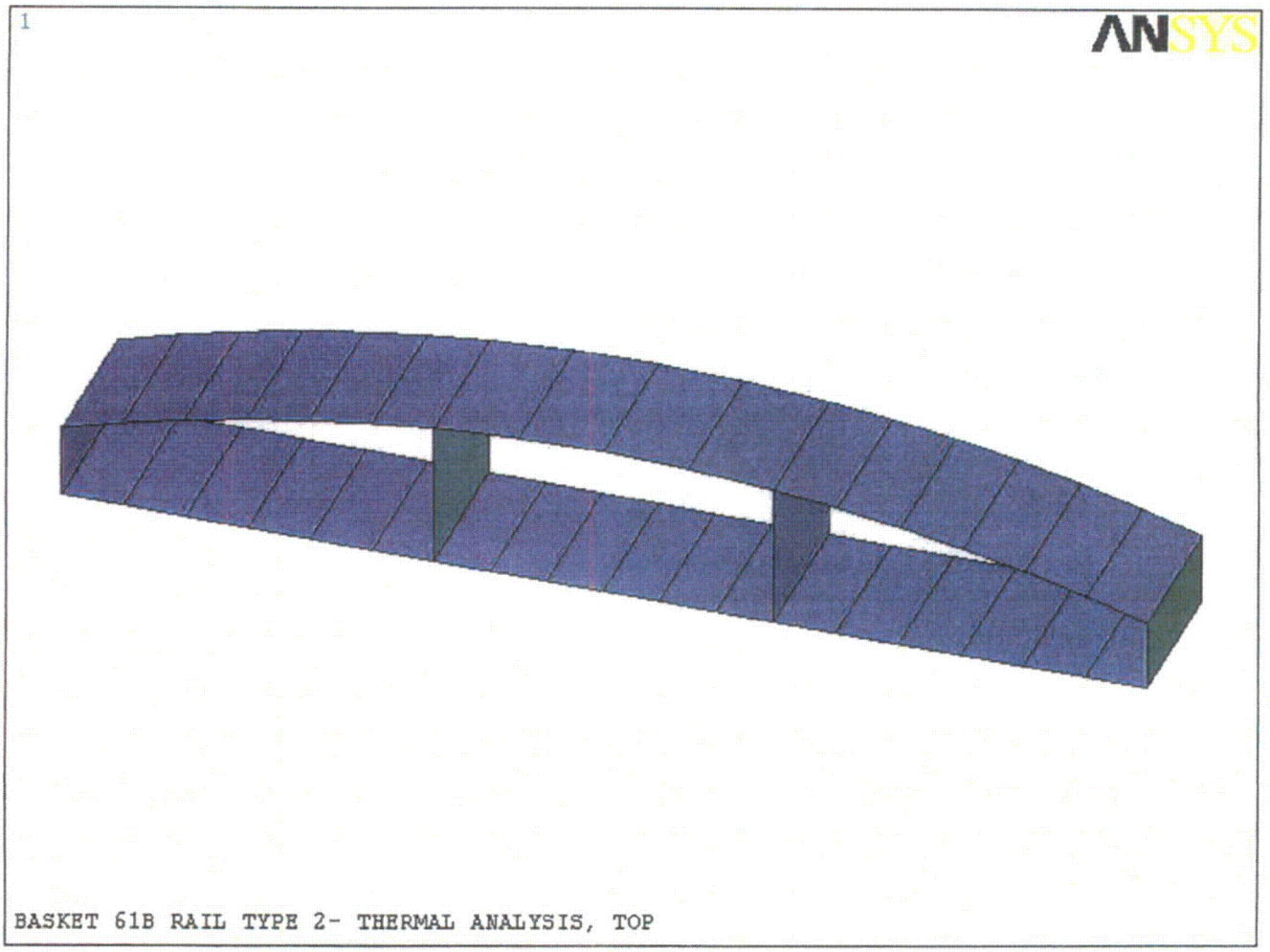

Figure 2.10.3-21
45° Orientation Side Drop – Loading Condition

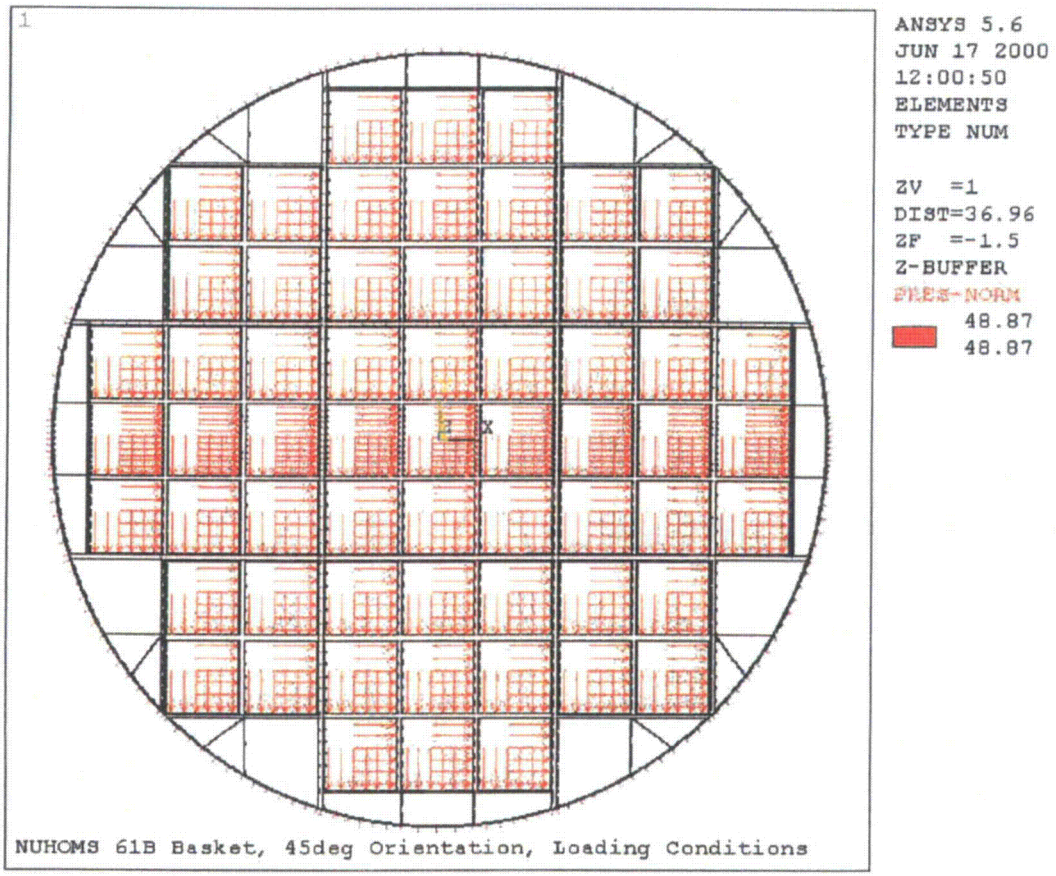

Figure 2.10.3-22
60° Orientation Side Drop – Loading Condition

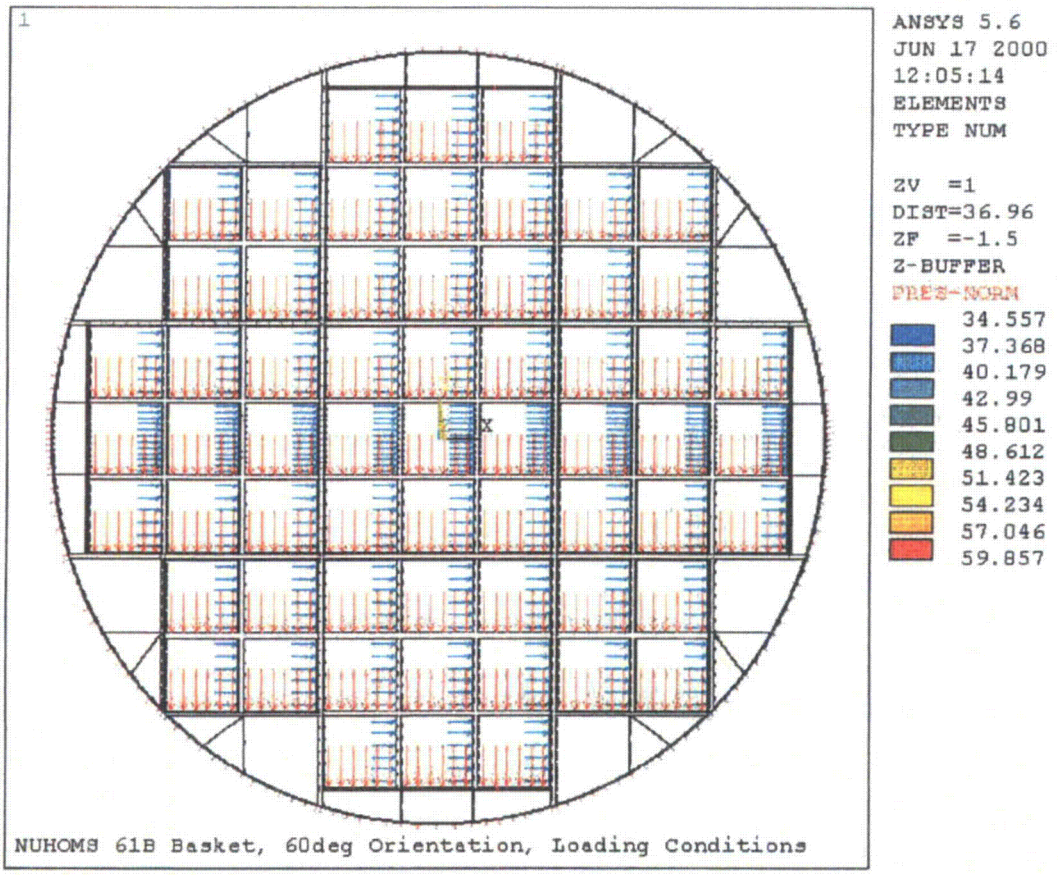

Figure 2.10.3-23
90° and 180° Orientation Side Drop – Loading Condition

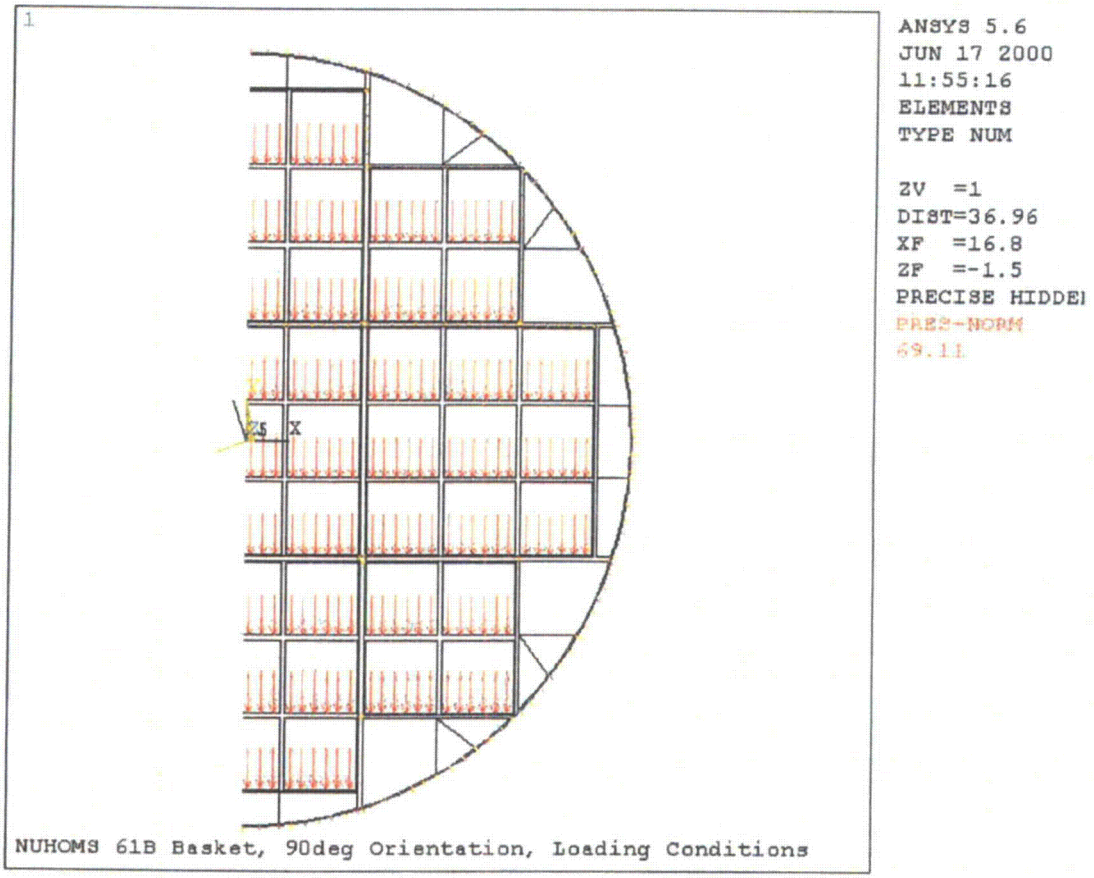

Figure 2.10.3-24
45° Orientation Side Drop – Basket, $P_m$ (75.5g)

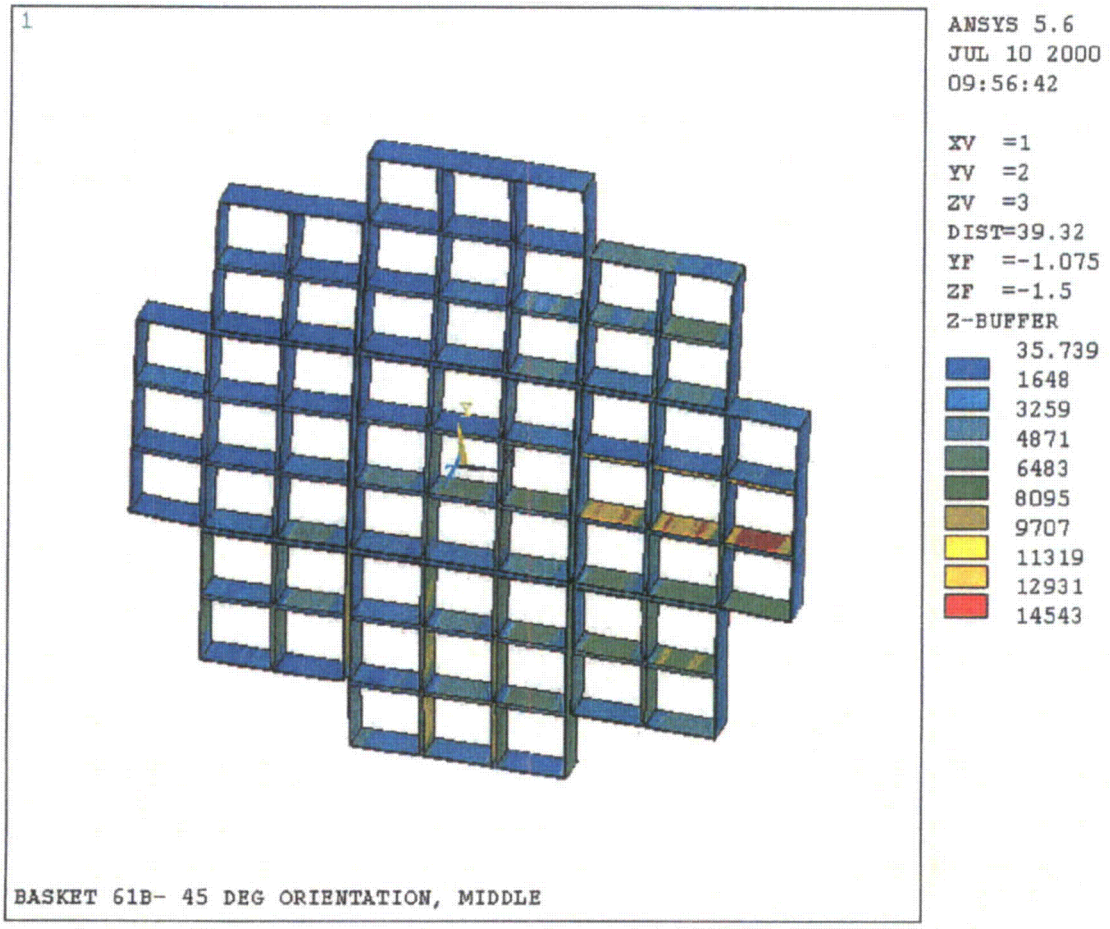

Figure 2.10.3-25
45° Orientation Side Drop – Basket, $P_m + P_b$ (75.5g)

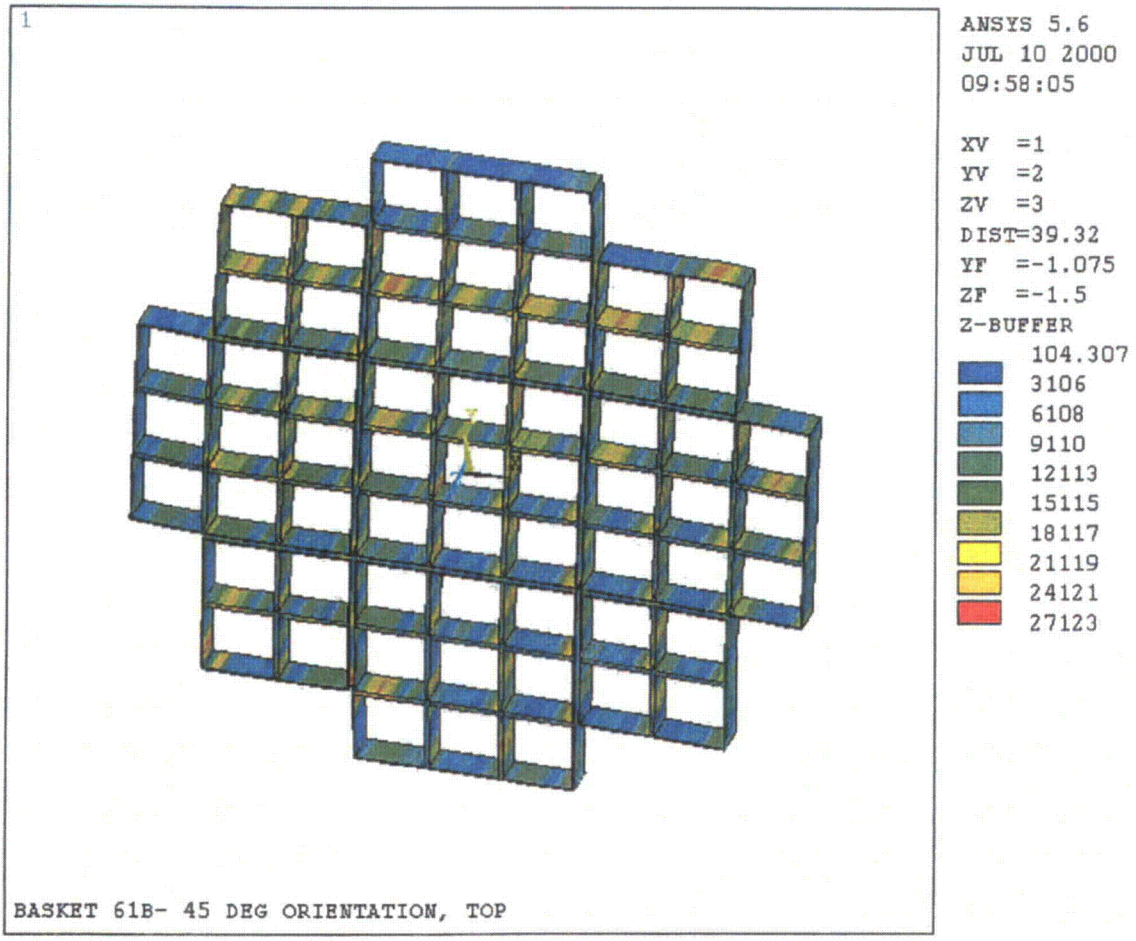

Figure 2.10.3-26
45° Orientation Side Drop – Rails, $P_m$ (75.5g)

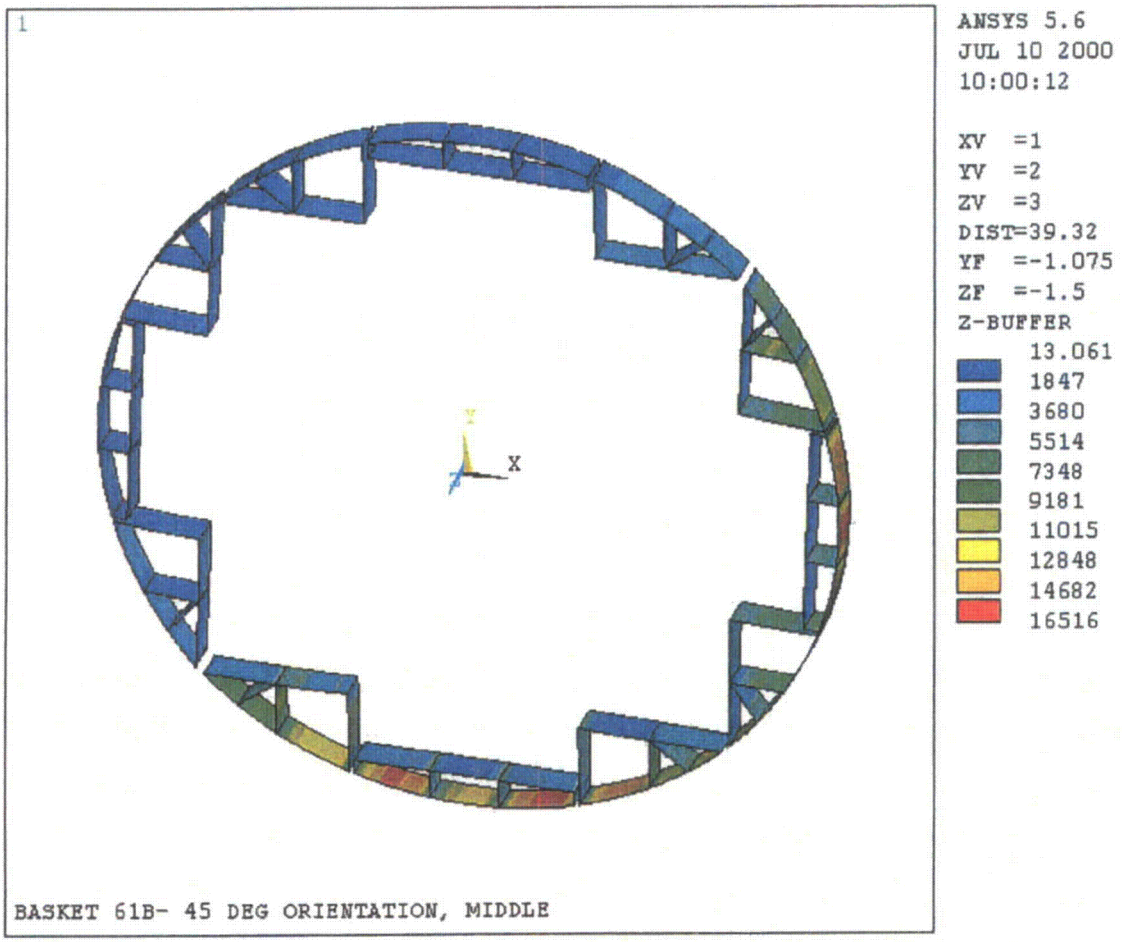

Figure 2.10.3-27
45° Orientation Side Drop – Rails, $P_m + P_b$ (75.5g)

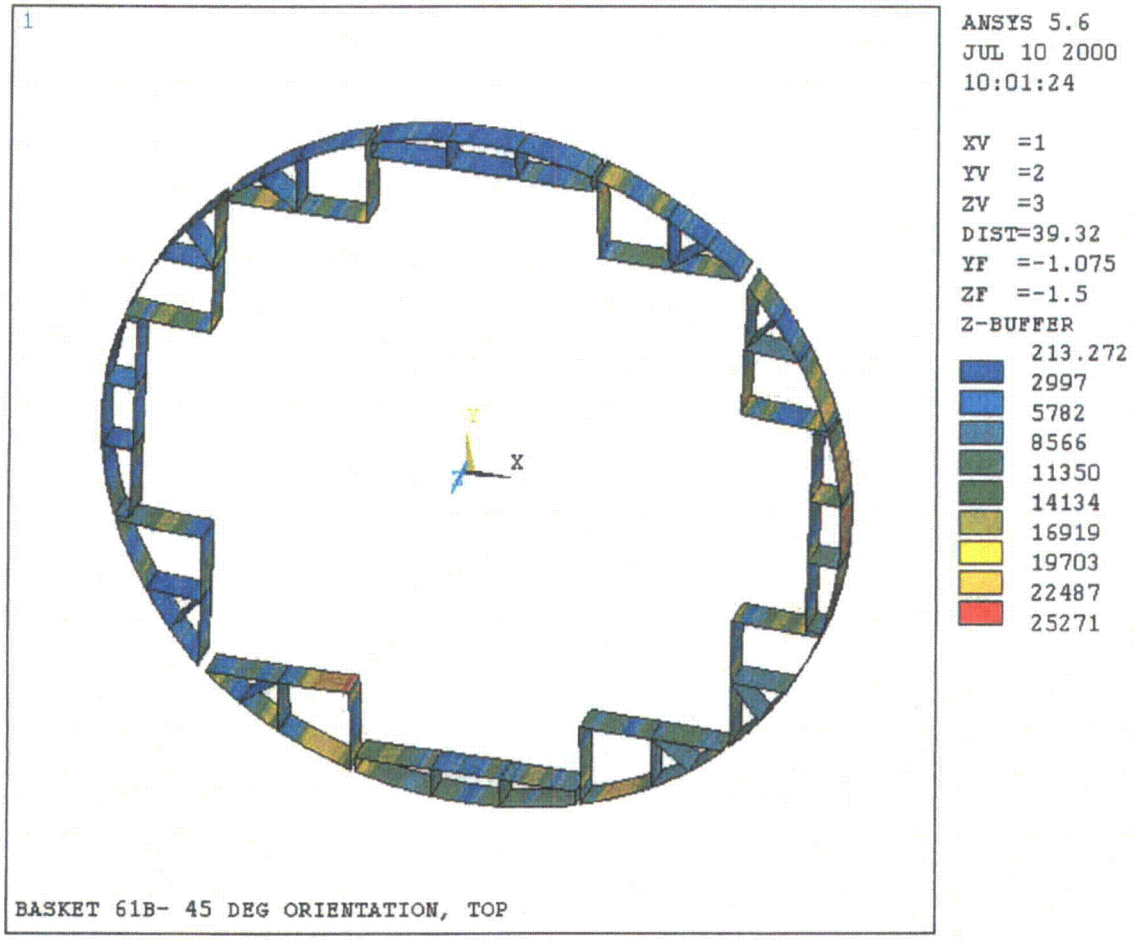

Figure 2.10.3-28
60° Orientation Side Drop – Basket, $P_m$ (75.5g)

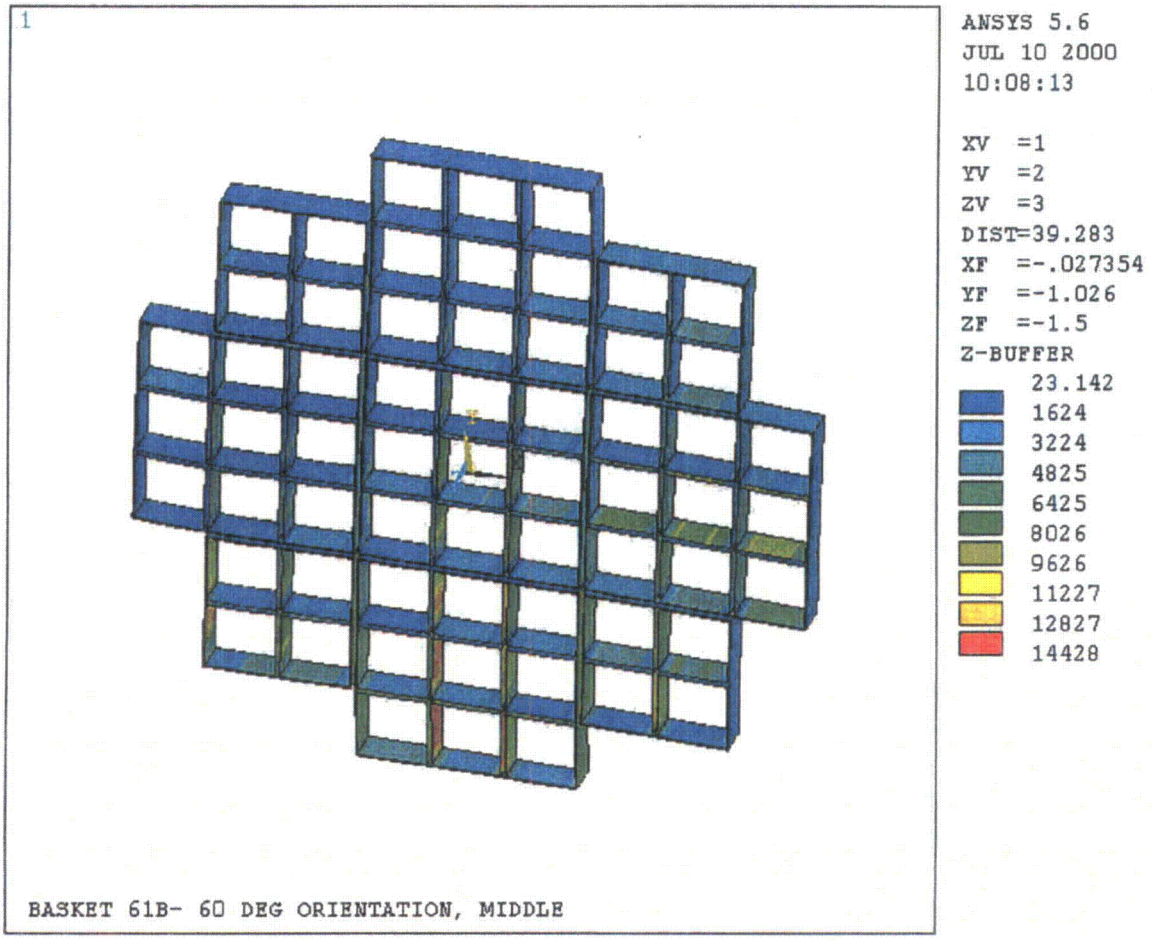

Figure 2.10.3-29
60° Orientation Side Drop – Basket, $P_m + P_b$ (75.5g)

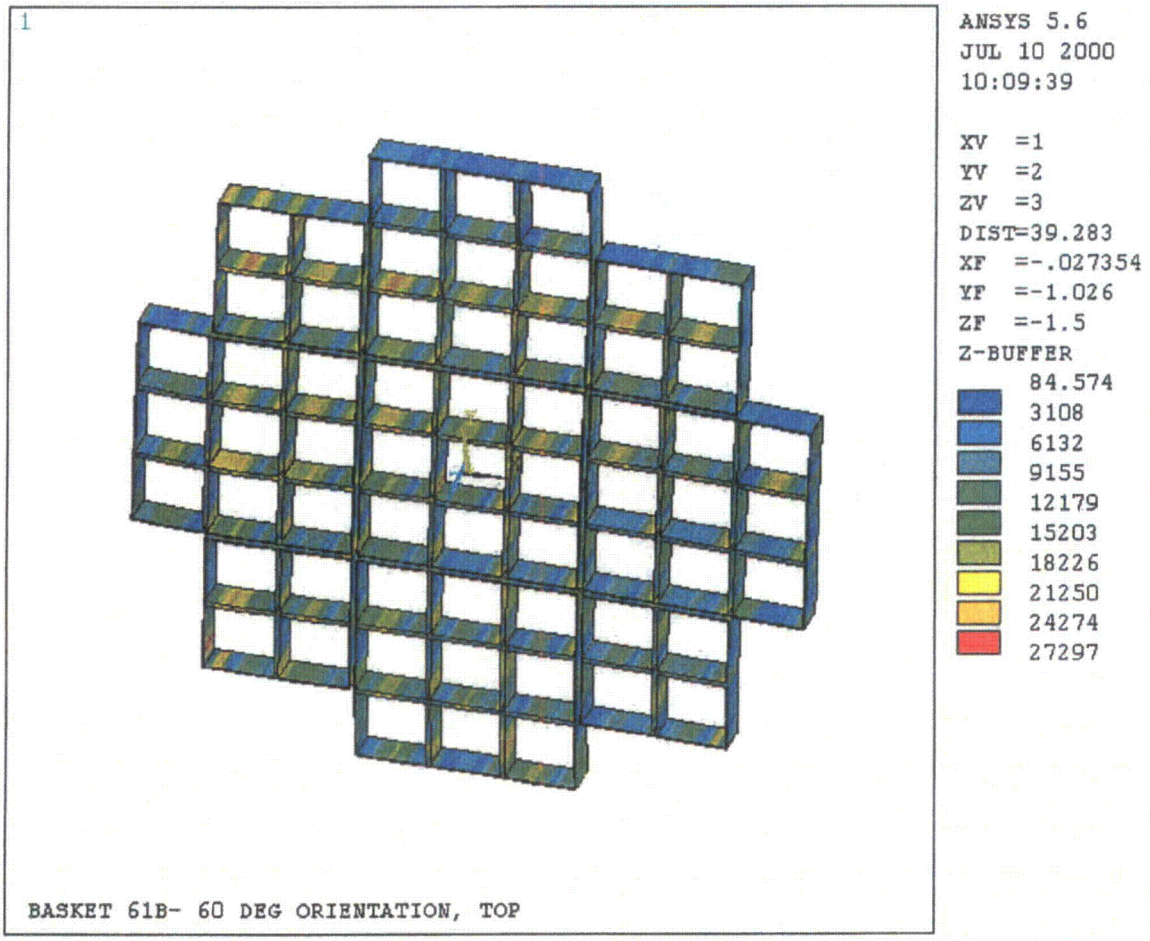

Figure 2.10.3-30
60° Orientation Side Drop – Rails, $P_m$ (75.5g)

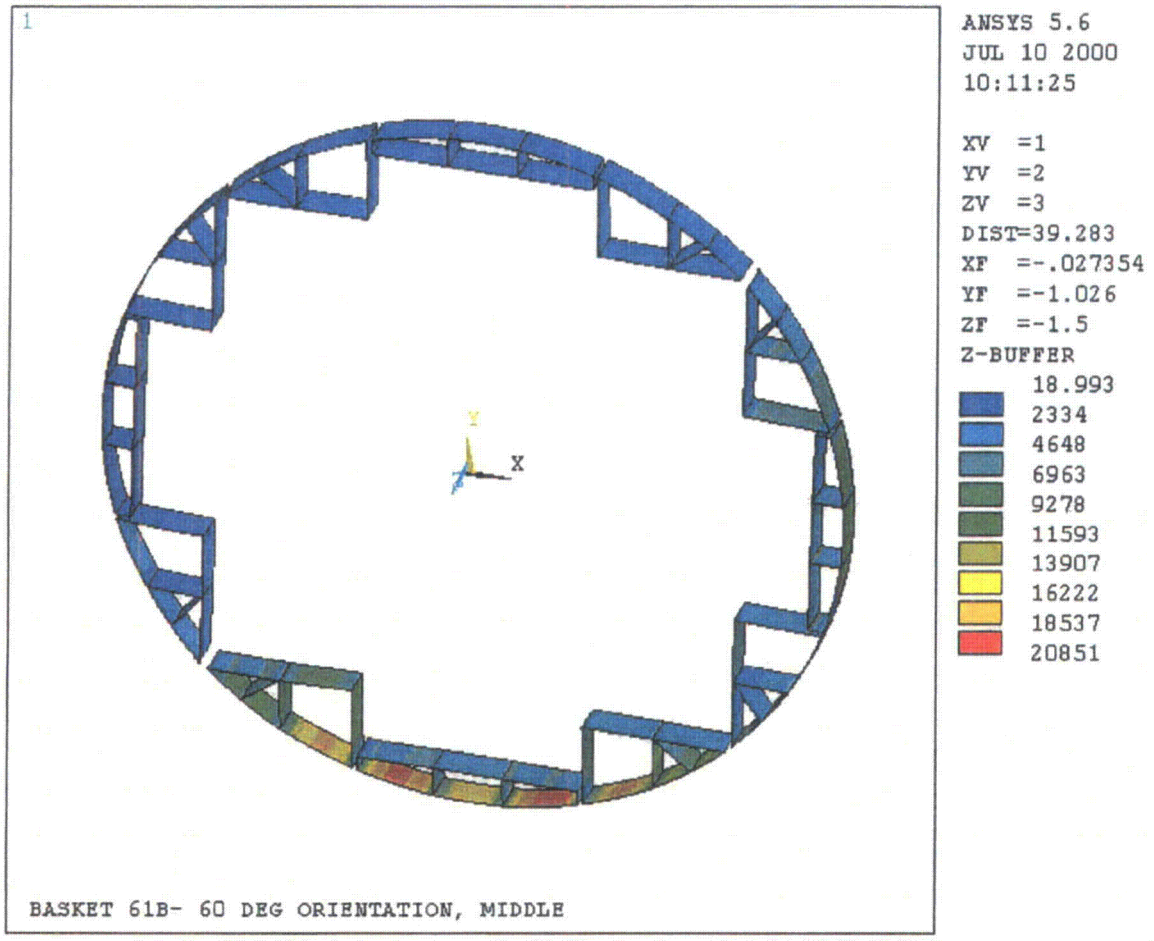

Figure 2.10.3-31
60° Orientation Side Drop – Rails, $P_m + P_b$ (75.5g)

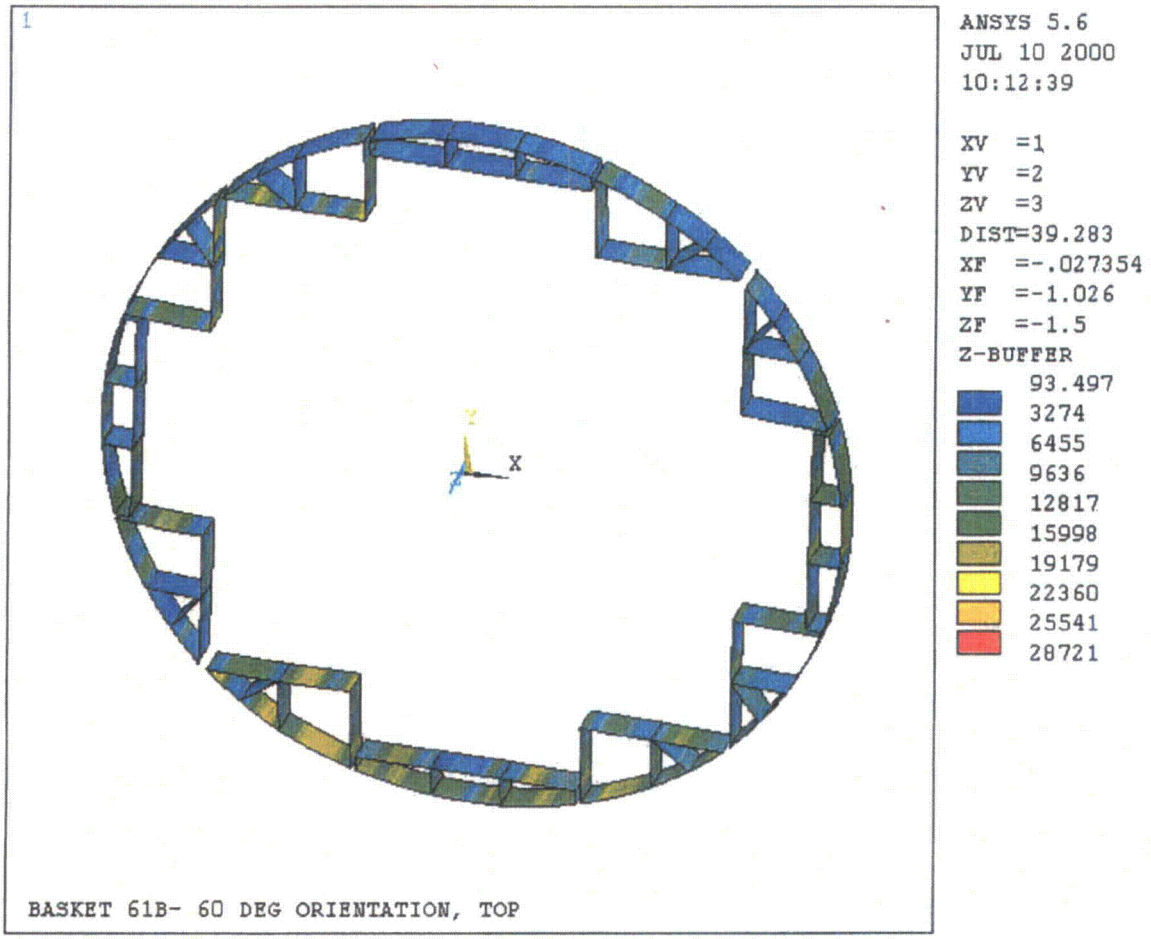

Figure 2.10.3-32
90° Orientation Side Drop – Basket, $P_m$ (75.5g)

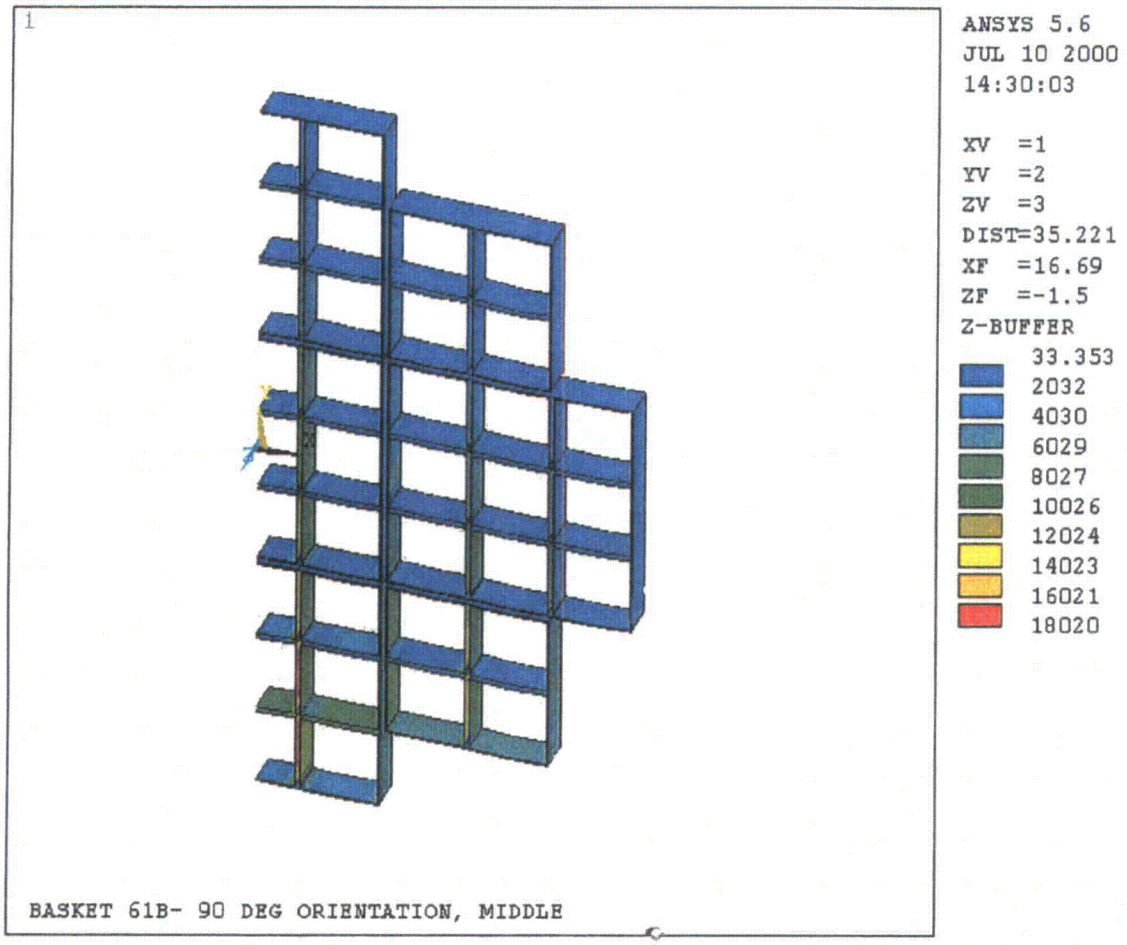

Figure 2.10.3-33
90° Orientation Side Drop – Basket, $P_m + P_b$ (75.5g)

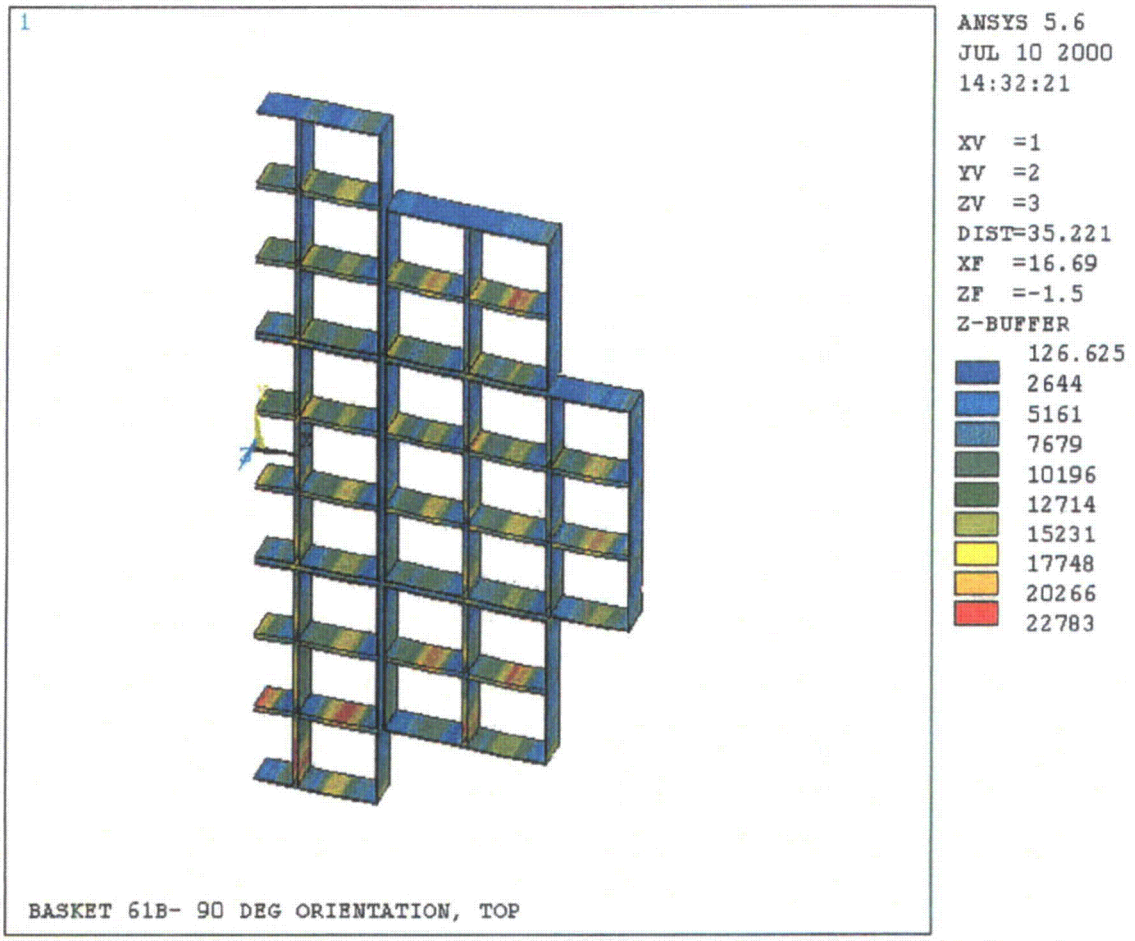

Figure 2.10.3-34
90° Orientation Side Drop – Rails, $P_m$ (75.5g)

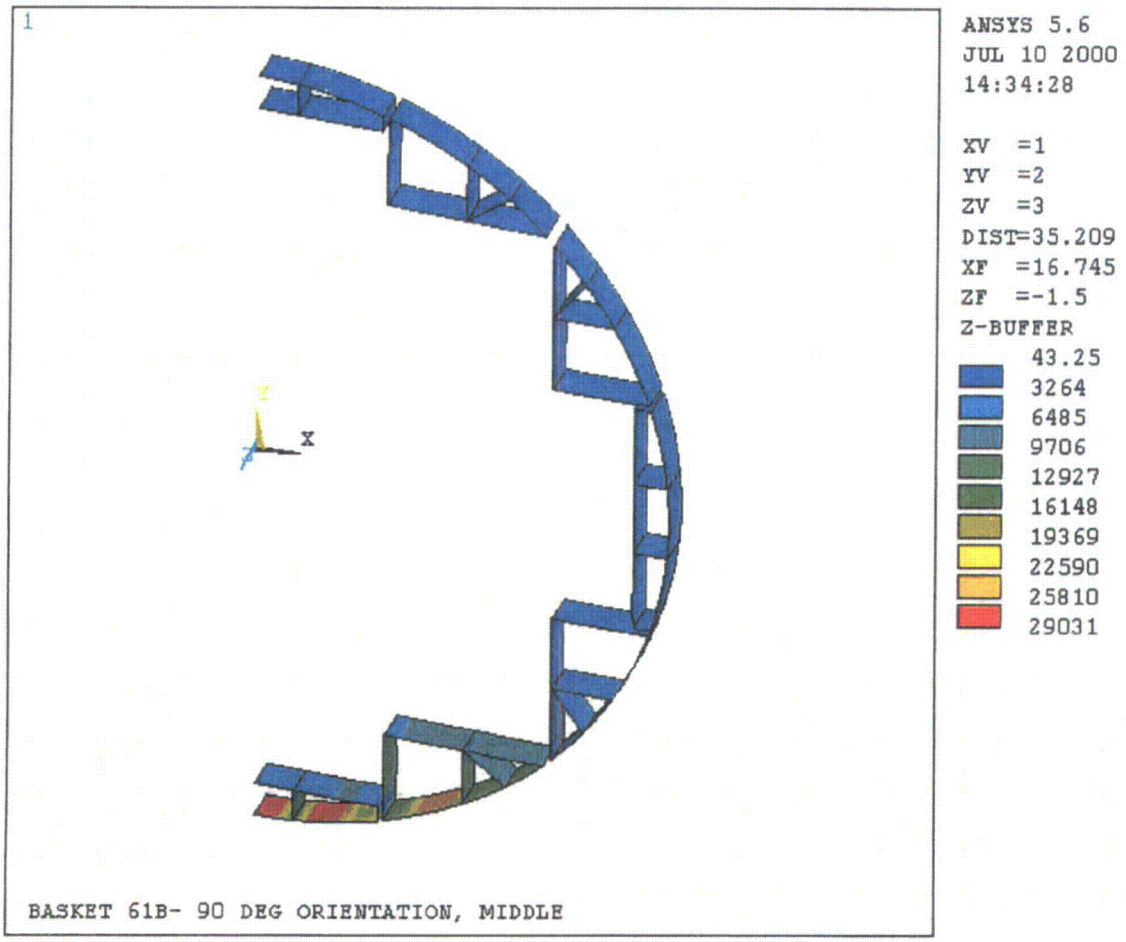

Figure 2.10.3-35
90° Orientation Side Drop – Rails, $P_m + P_b$ (75.5g)

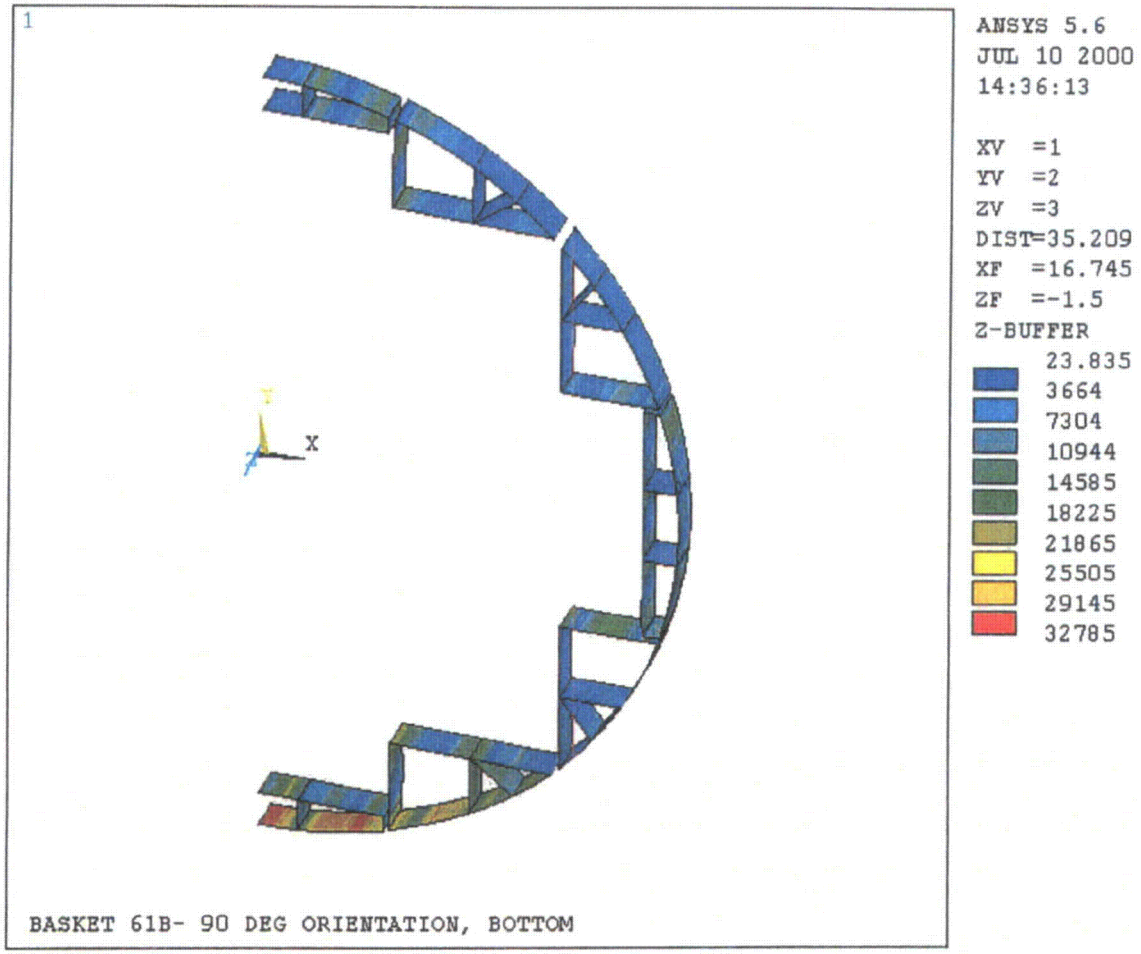

Figure 2.10.3-36
180° Orientation Side Drop – Basket, $P_m$ (75g)

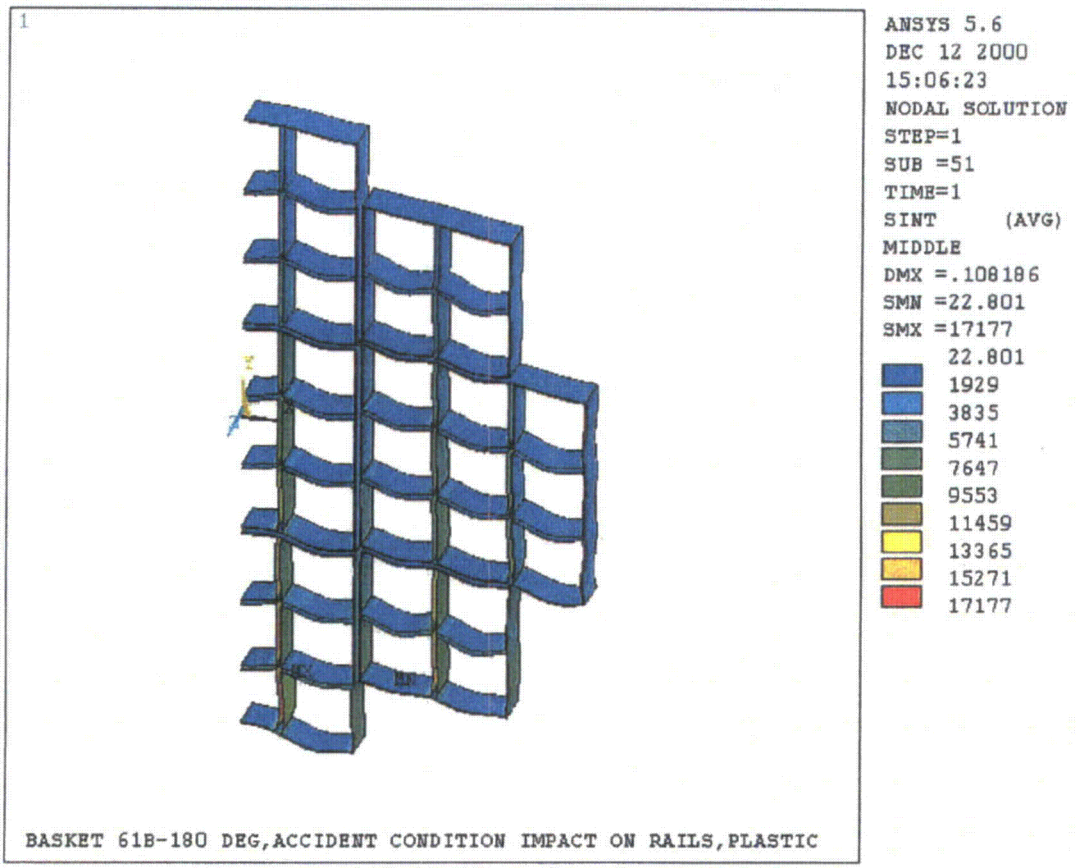

Figure 2.10.3-37
180° Orientation Side Drop – Basket, $P_m + P_b$ (75g)

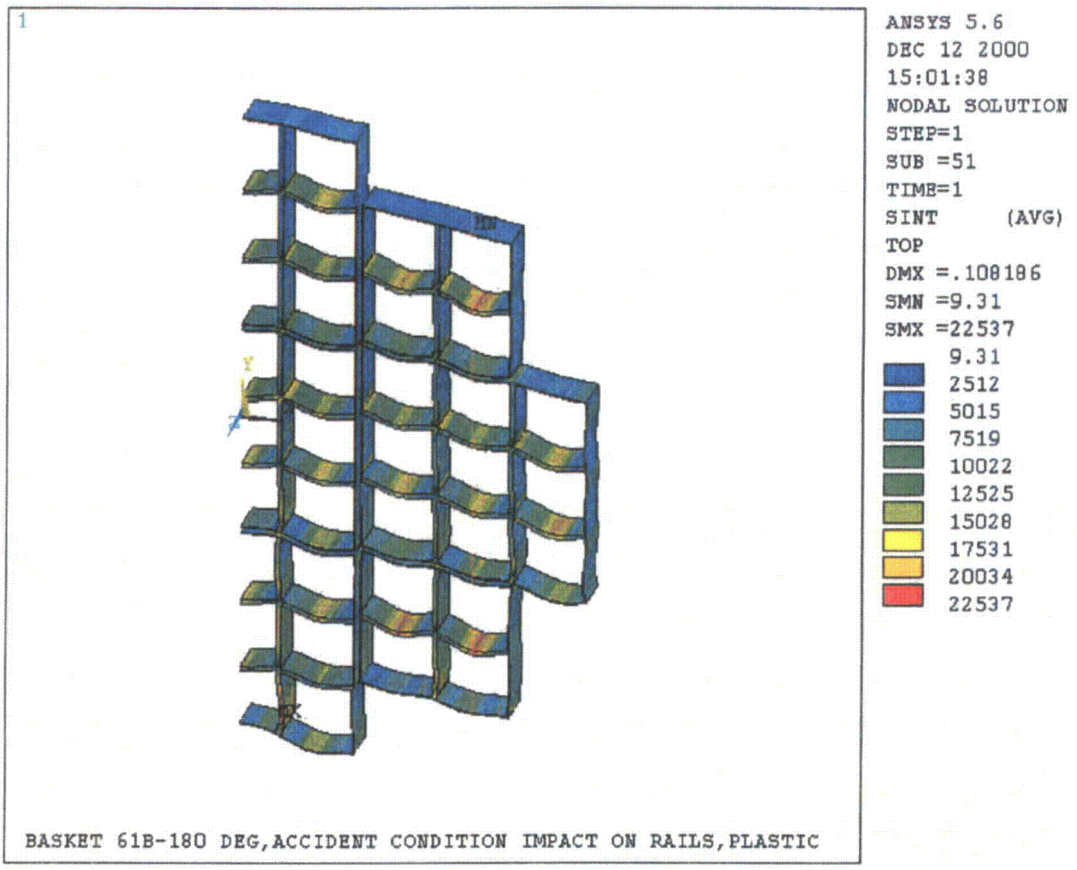

Figure 2.10.3-38
180° Orientation Side Drop – Rails, $P_m$ (75g)

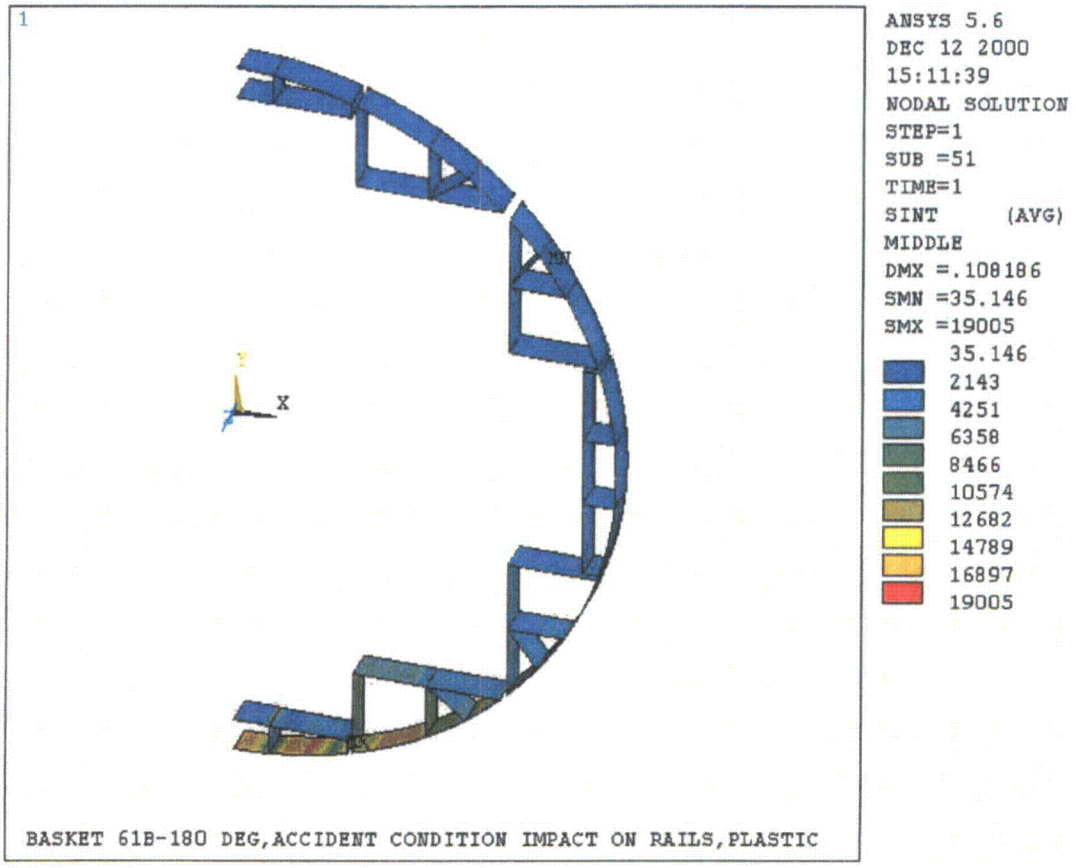

Figure 2.10.3-39
180° Orientation Side Drop – Rails, $P_m + P_b$ (75g)

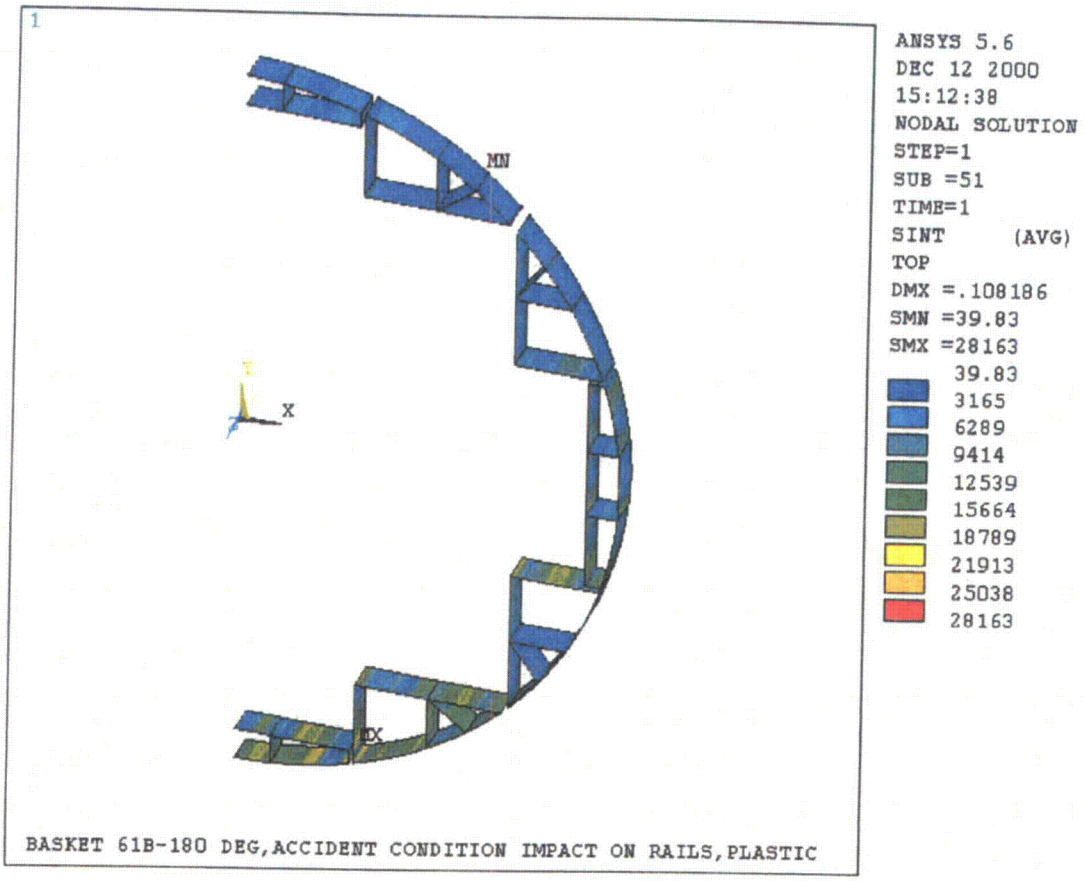

Figure 2.10.3-40
Hold Down Ring Alignment Leg Finite Element Model with Boundary Conditions

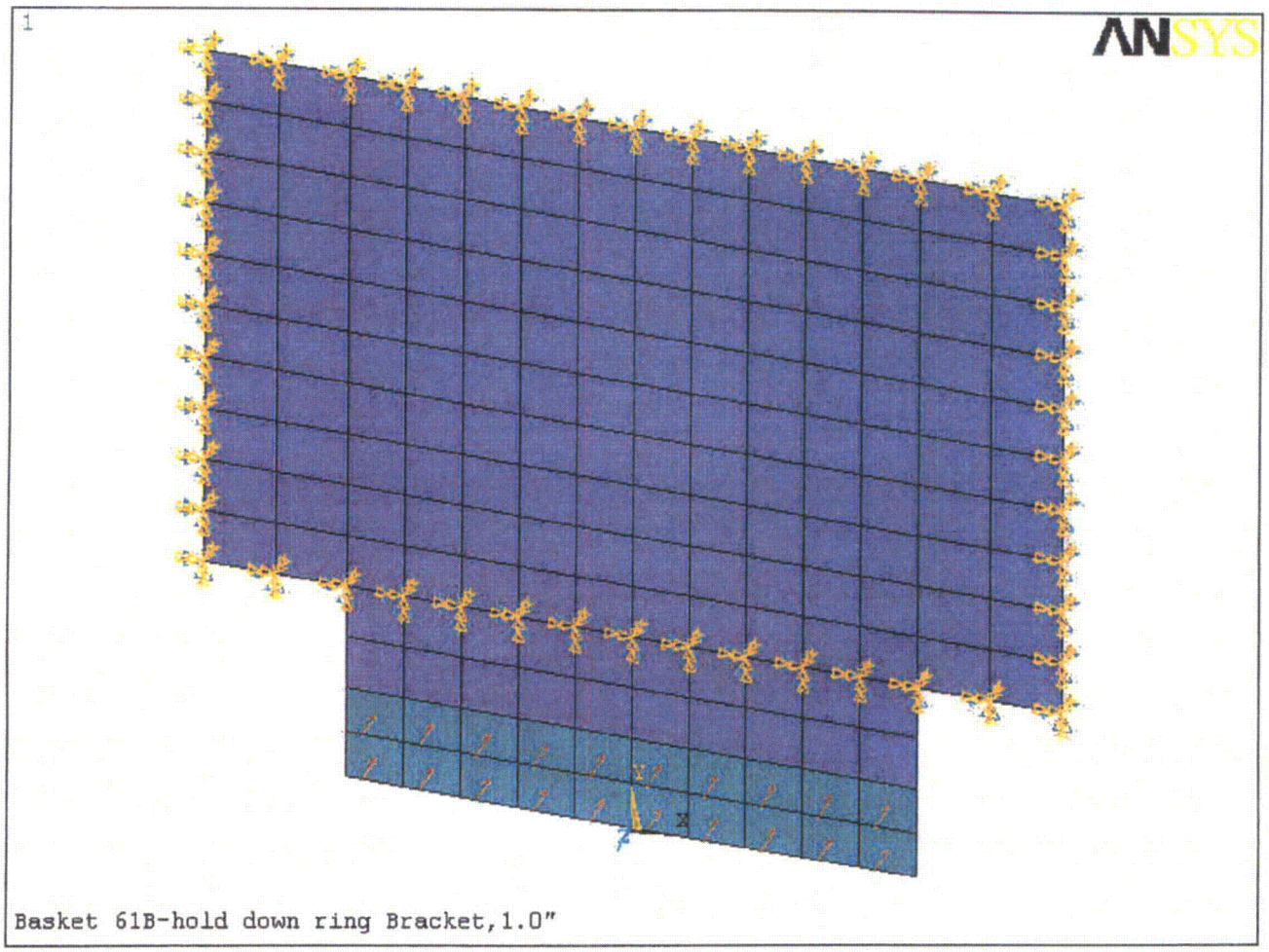

Figure 2.10.3-41
Hold Down Ring Finite Element Model with 90° Drop Orientation Boundary Conditions

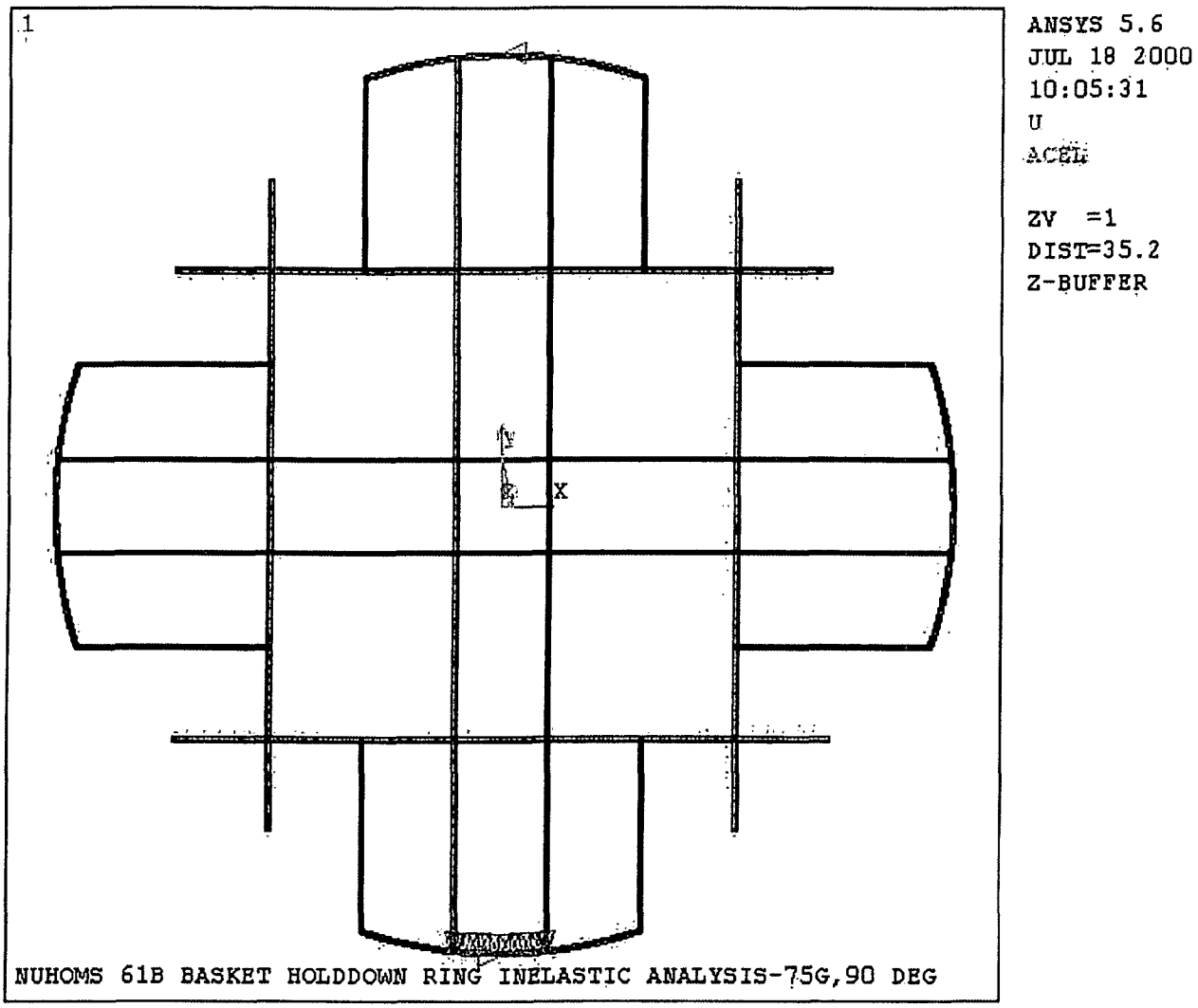

Figure 2.10.3-42
Hold Down Ring Finite Element Model with 45° Drop Orientation Boundary Conditions

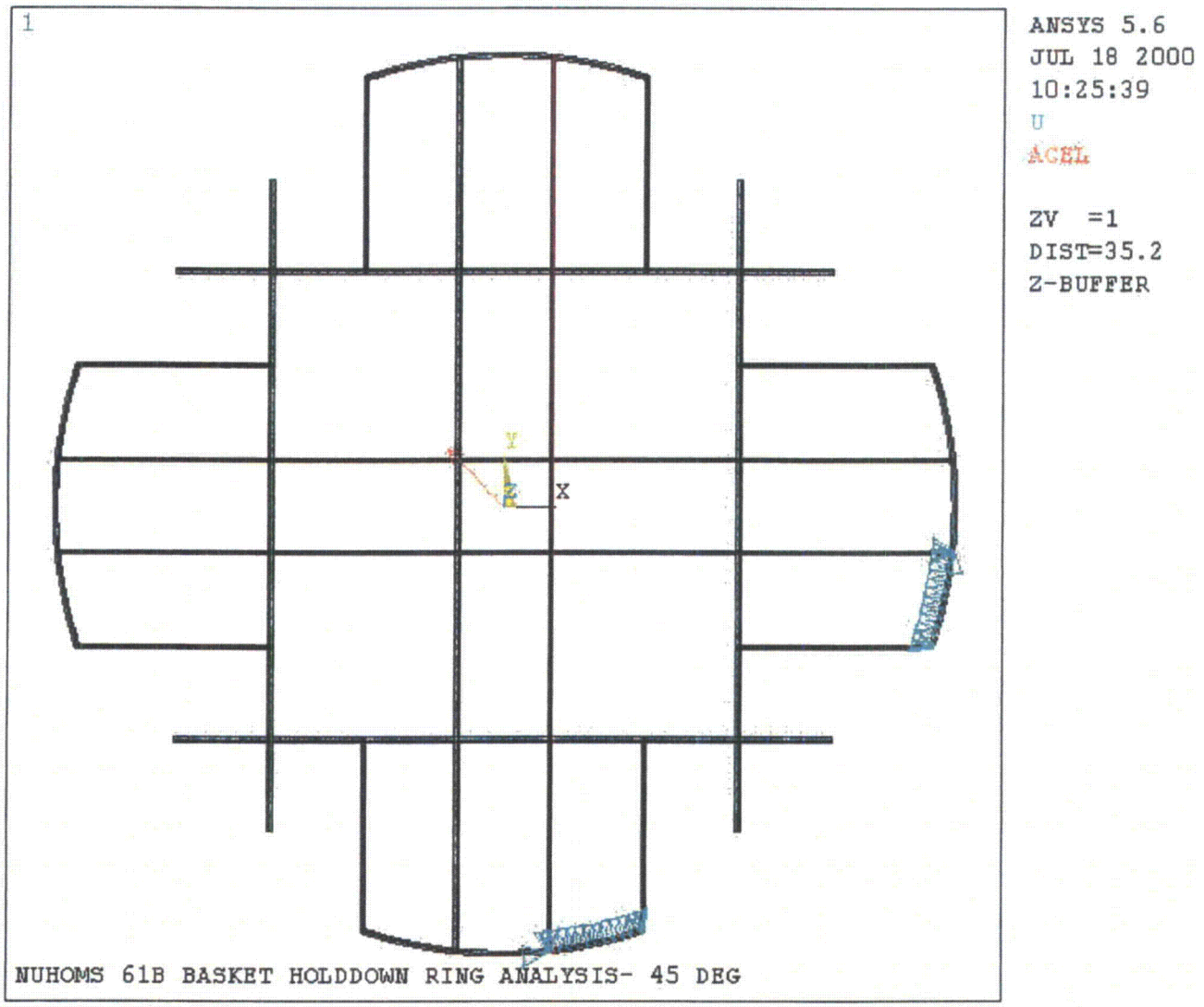

Figure 2.10.3-43
Small Basket Section Finite Element Model Locations

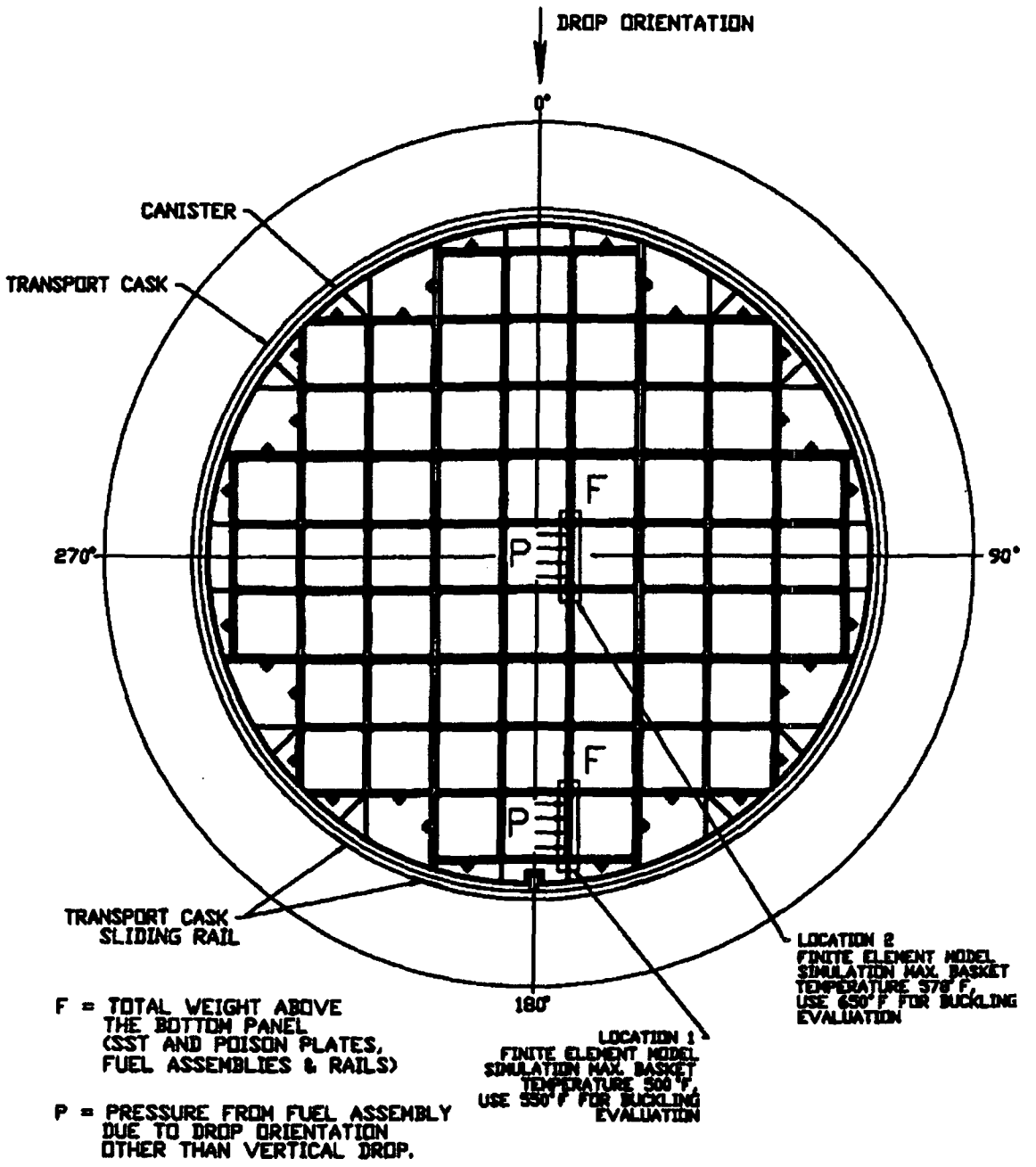


NUHOMS - 61B BASKET BUCKLING EVALUATION

Figure 2.10.3-44
Small Basket Section Finite Element Model with Boundary Conditions

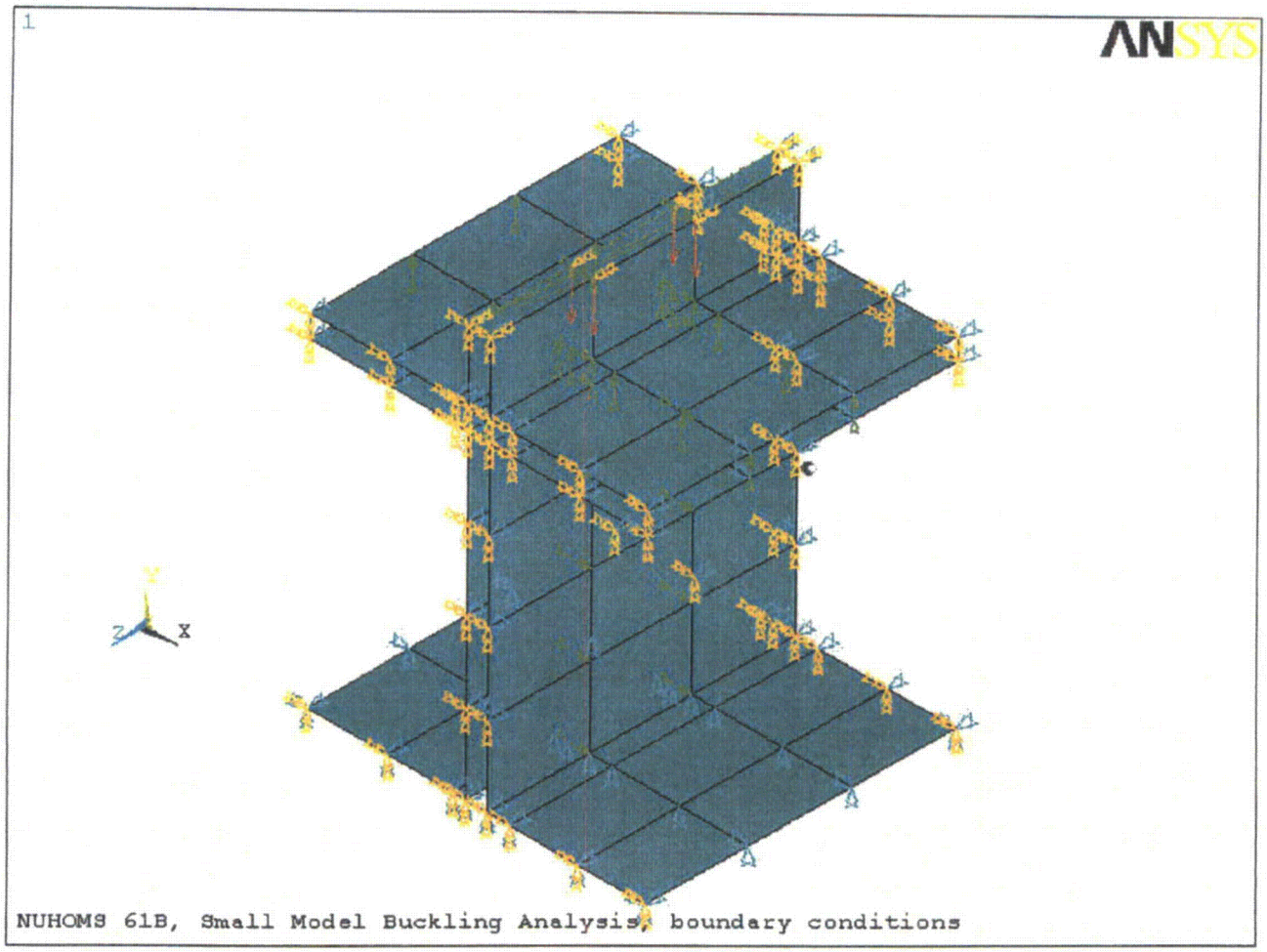

Figure 2.10.3-45
NUHOMS 61B Basket Model Geometry

F= TOTAL WEIGHT ABOVE
THE BOTTOM PANEL
(SST AND POISON PLATES,
FUEL ASSEMBLIES, AND RAILS)

P= PRESSURE FROM FUEL ASSEMBLY
DUE TO DROP ORIENTATION
OTHER THAN VERTICAL DROP.

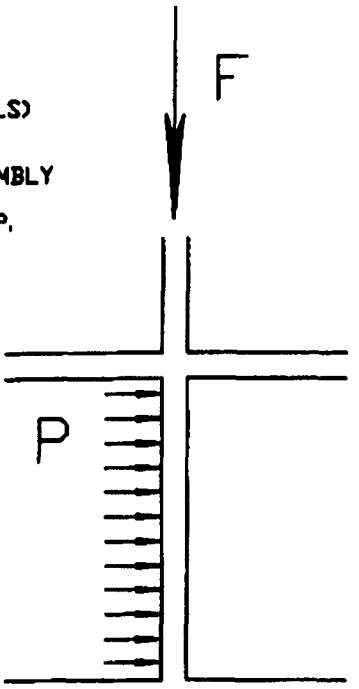


NUHOMS - 61B BUCKLING EVALUATION - LOADING CONFIGURATION

Figure 2.10.3-46
Vertical Drop Buckling Analysis, Location 1

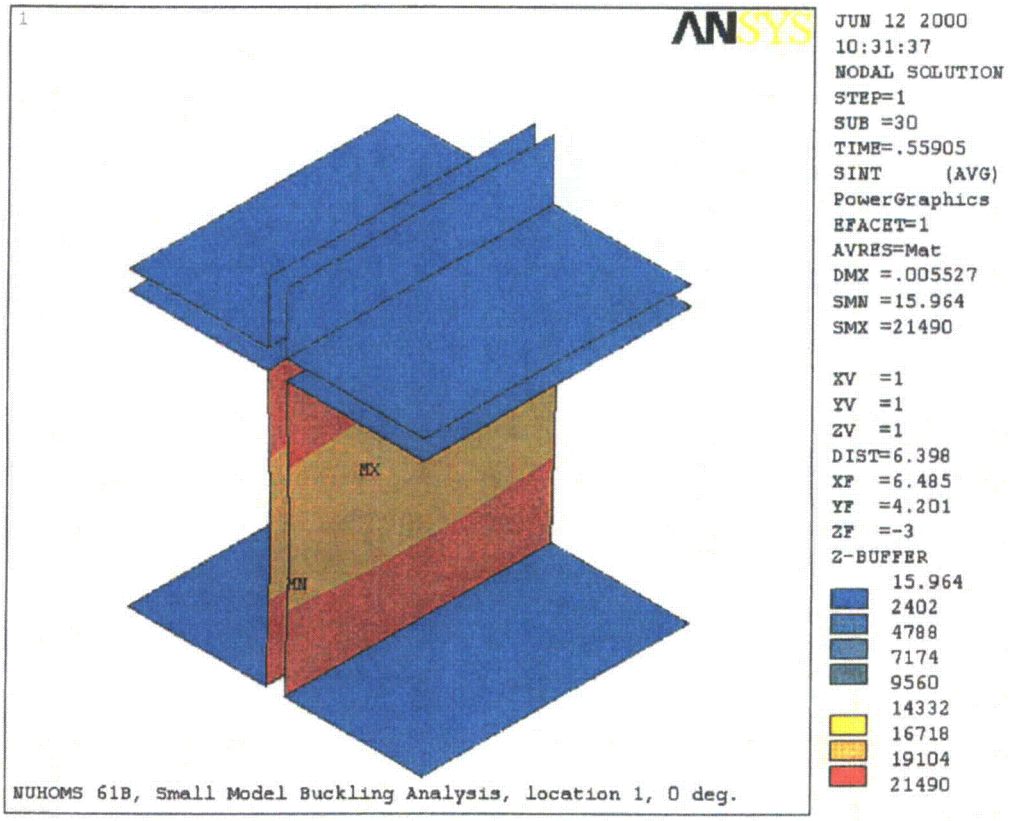

Figure 2.10.3-47
$30^0$ Drop Buckling Analysis, Location 1

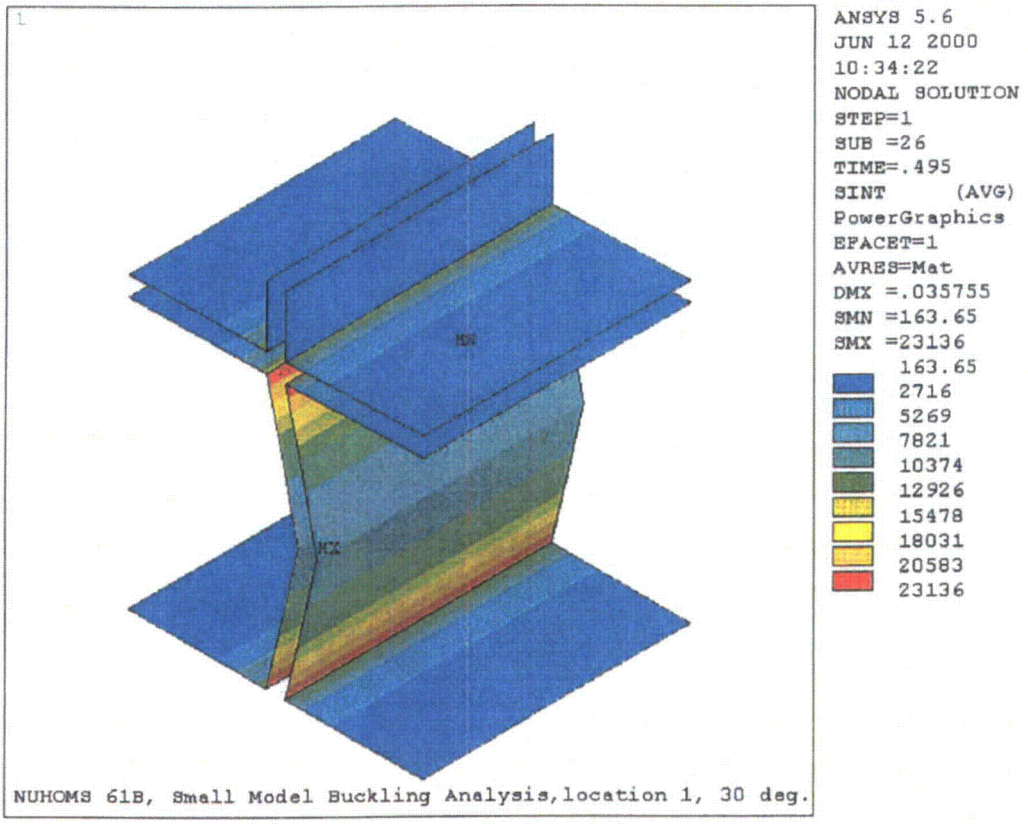

Figure 2.10.3-48
$45^0$ Drop Buckling Analysis, Location 1

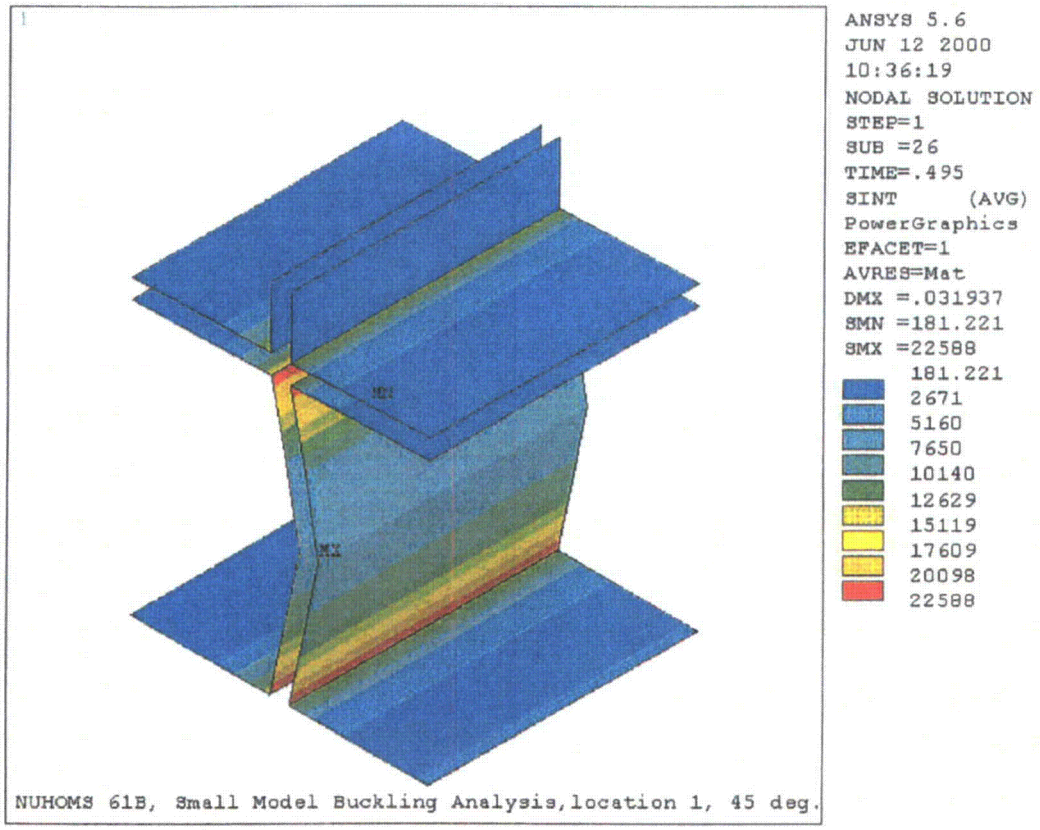

Figure 2.10.3-49
Vertical Drop Buckling Analysis, Location 2

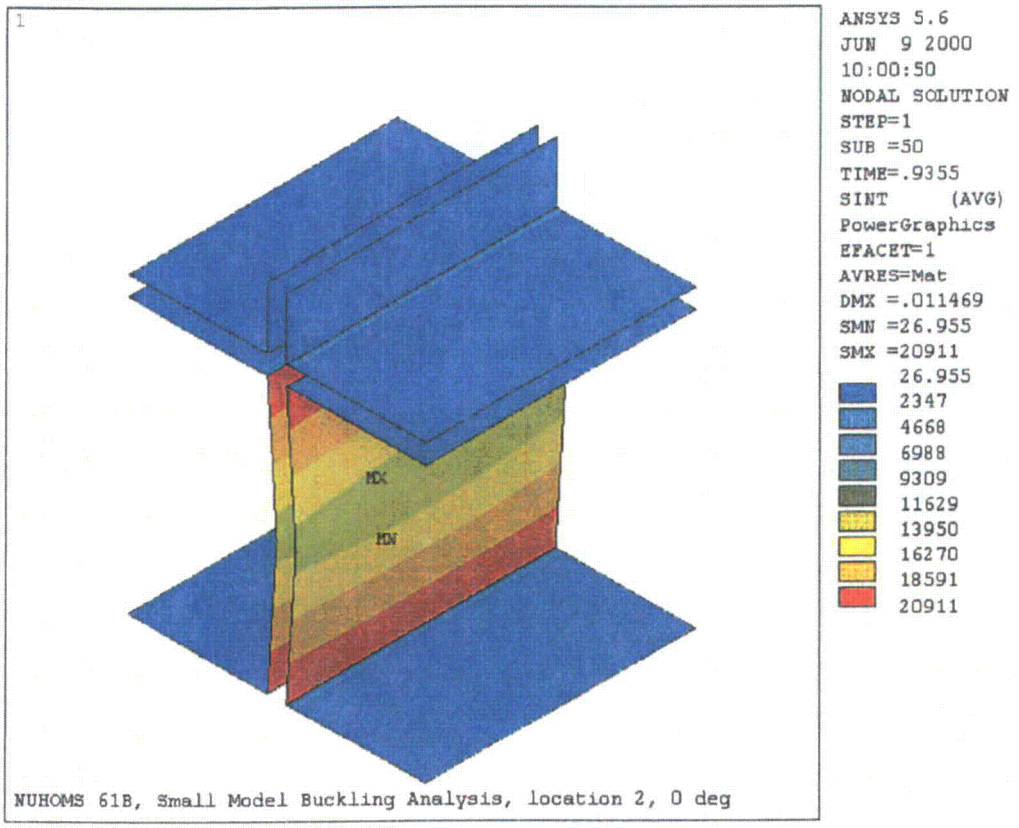

Figure 2.10.3-50
$30^0$ Drop Buckling Analysis, Location 2

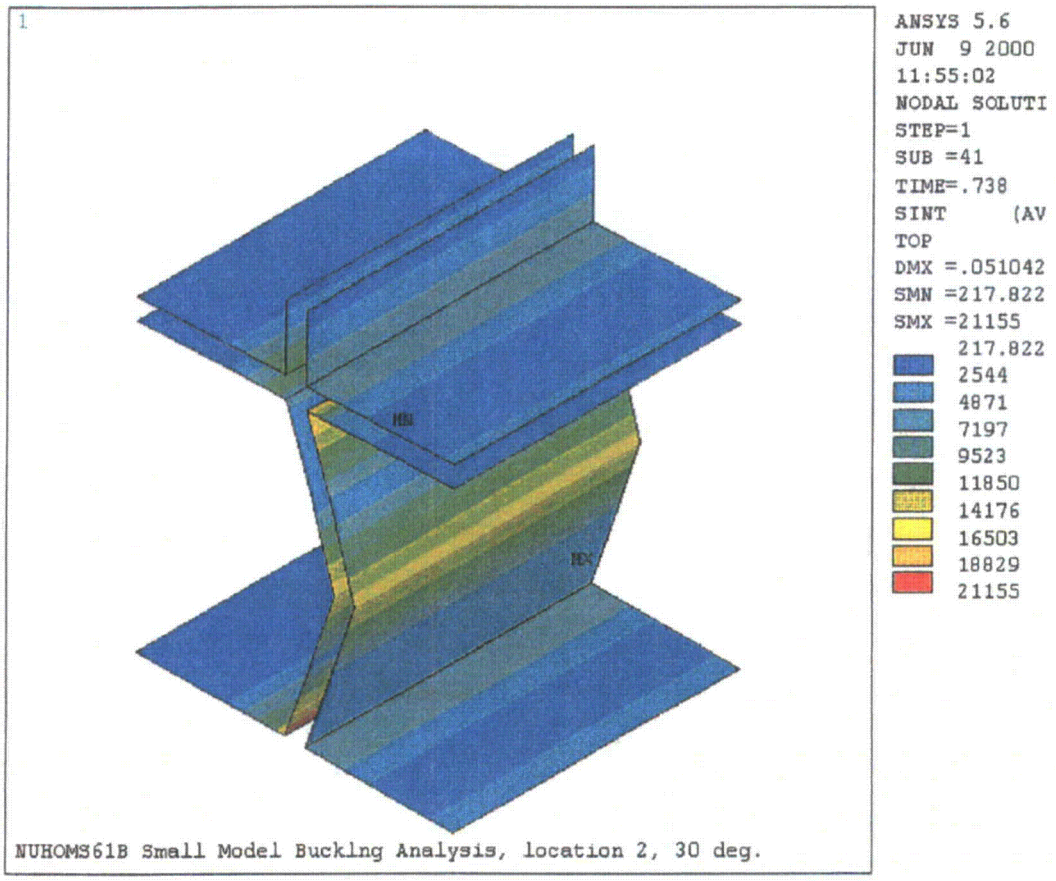

Figure 2.10.3-51
$45^0$ Drop Buckling Analysis, Location 2

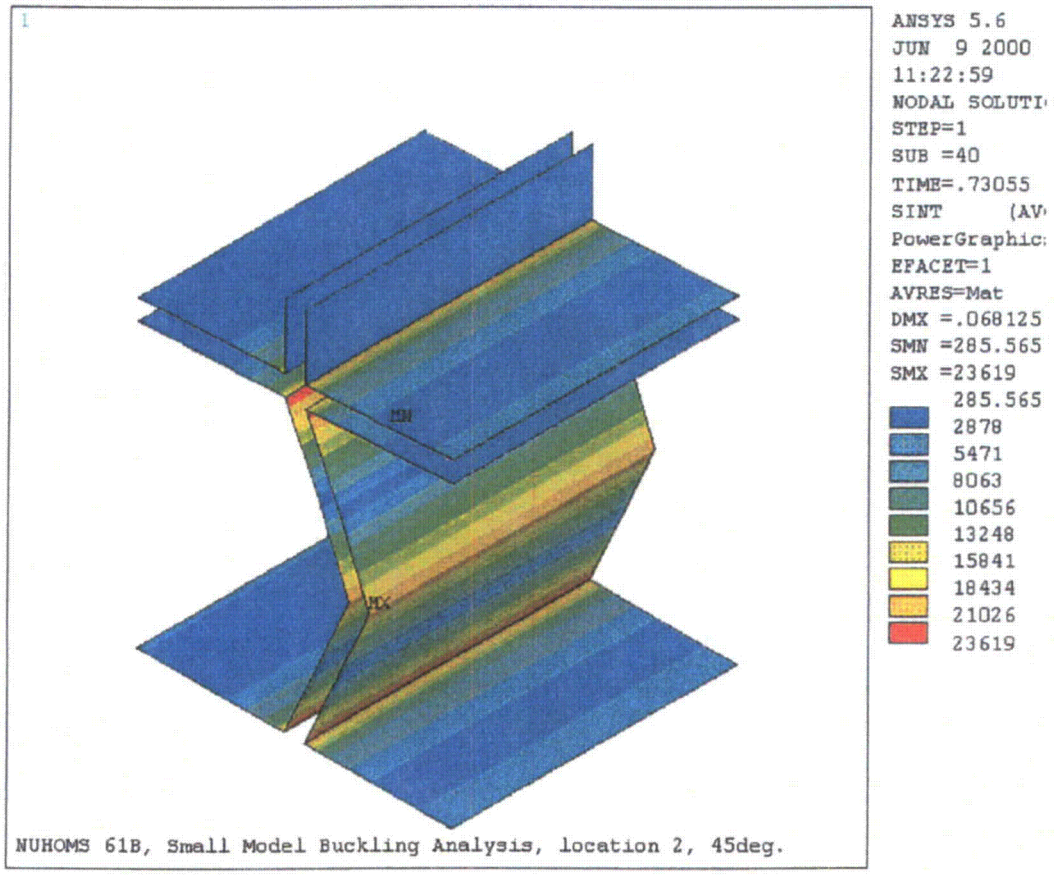

Figure 2.10.3-52
Allowable Collapse Load Determination, Location 1, Vertical Drop

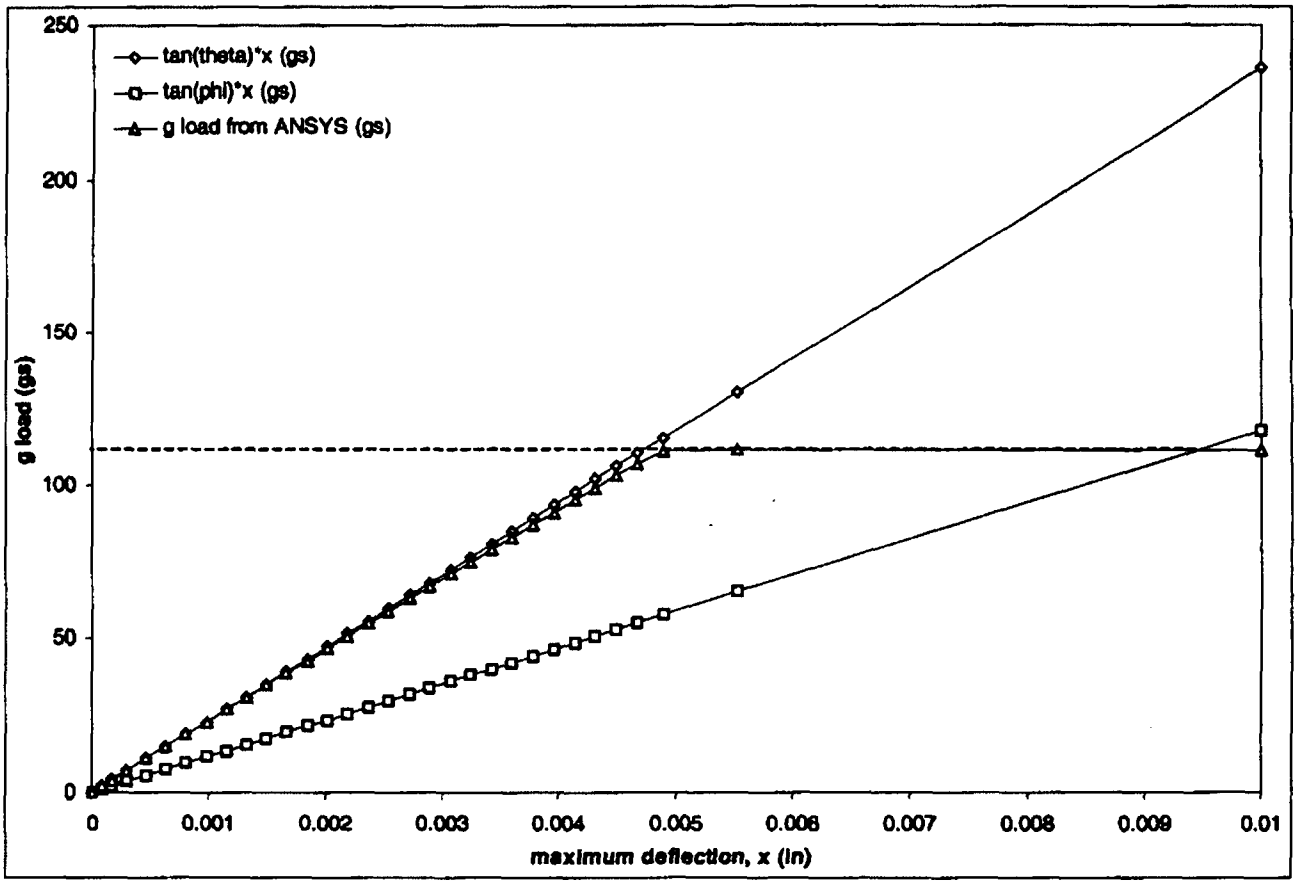

Figure 2.10.3-53
Allowable Collapse Load Determination, Location 1, 30° Drop

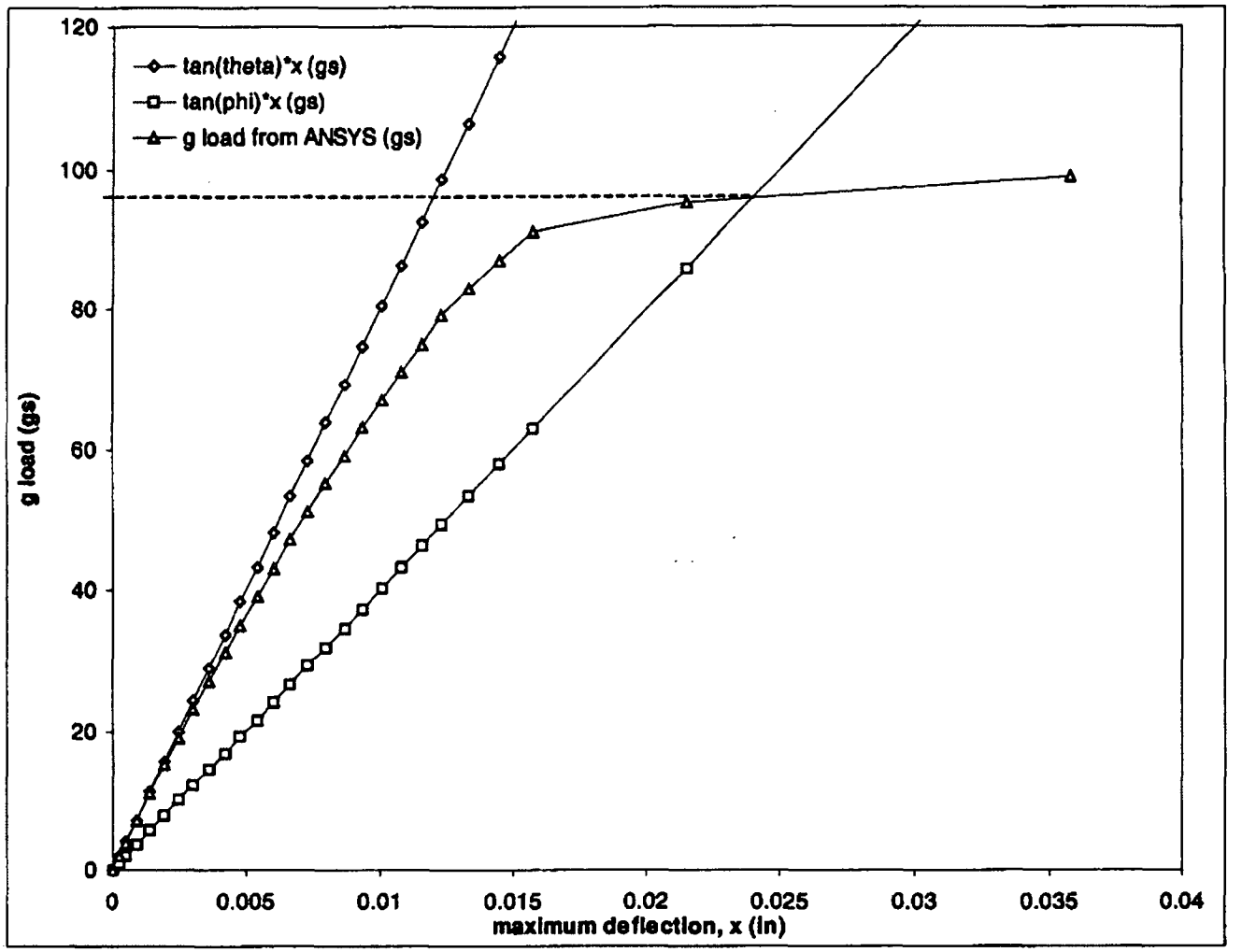

Figure 2.10.3-54
Allowable Collapse Load Determination, Location 1, 45° Drop

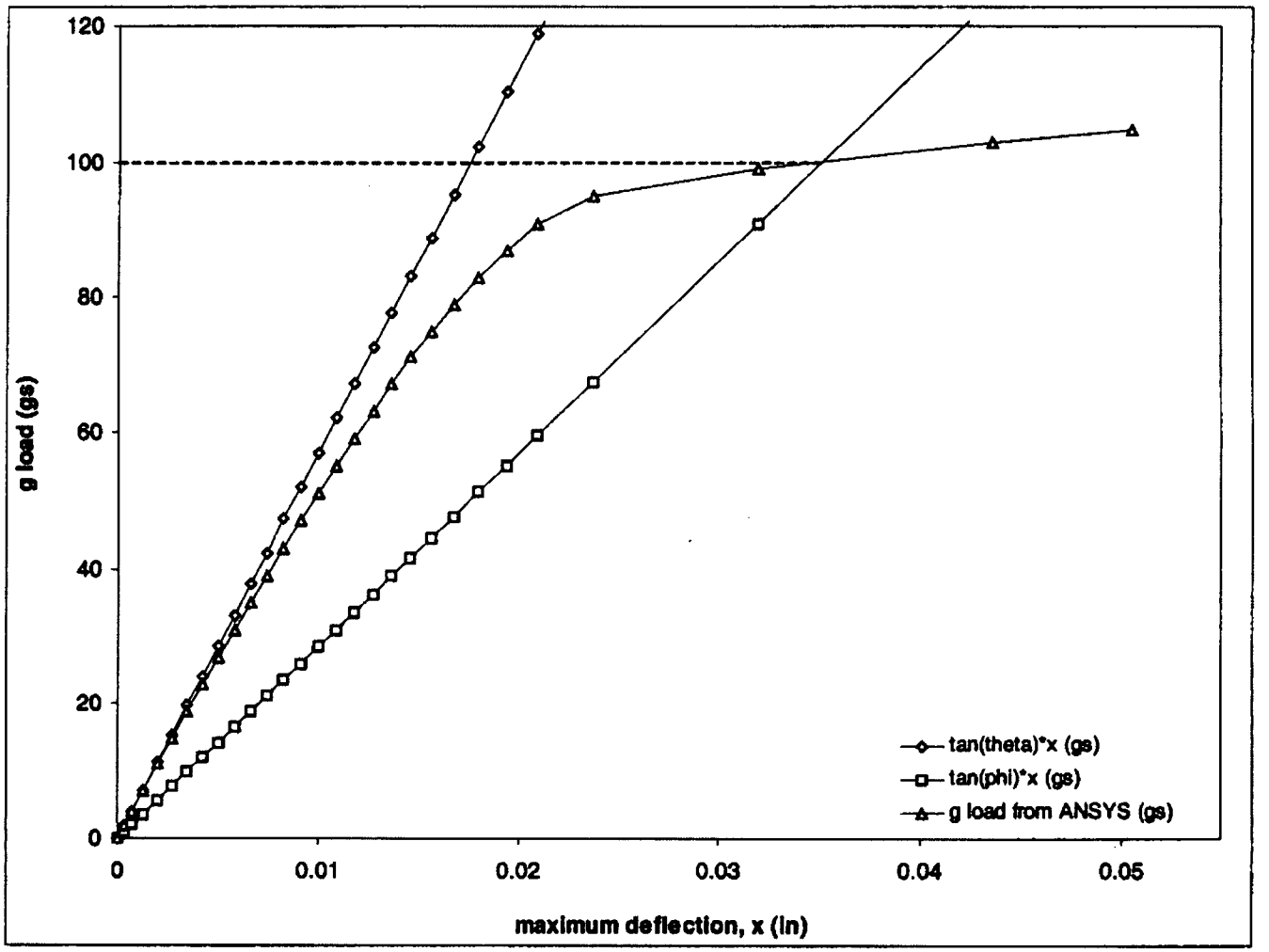

Figure 2.10.3-55
Allowable Collapse Load Determination, Location 2, Vertical Drop

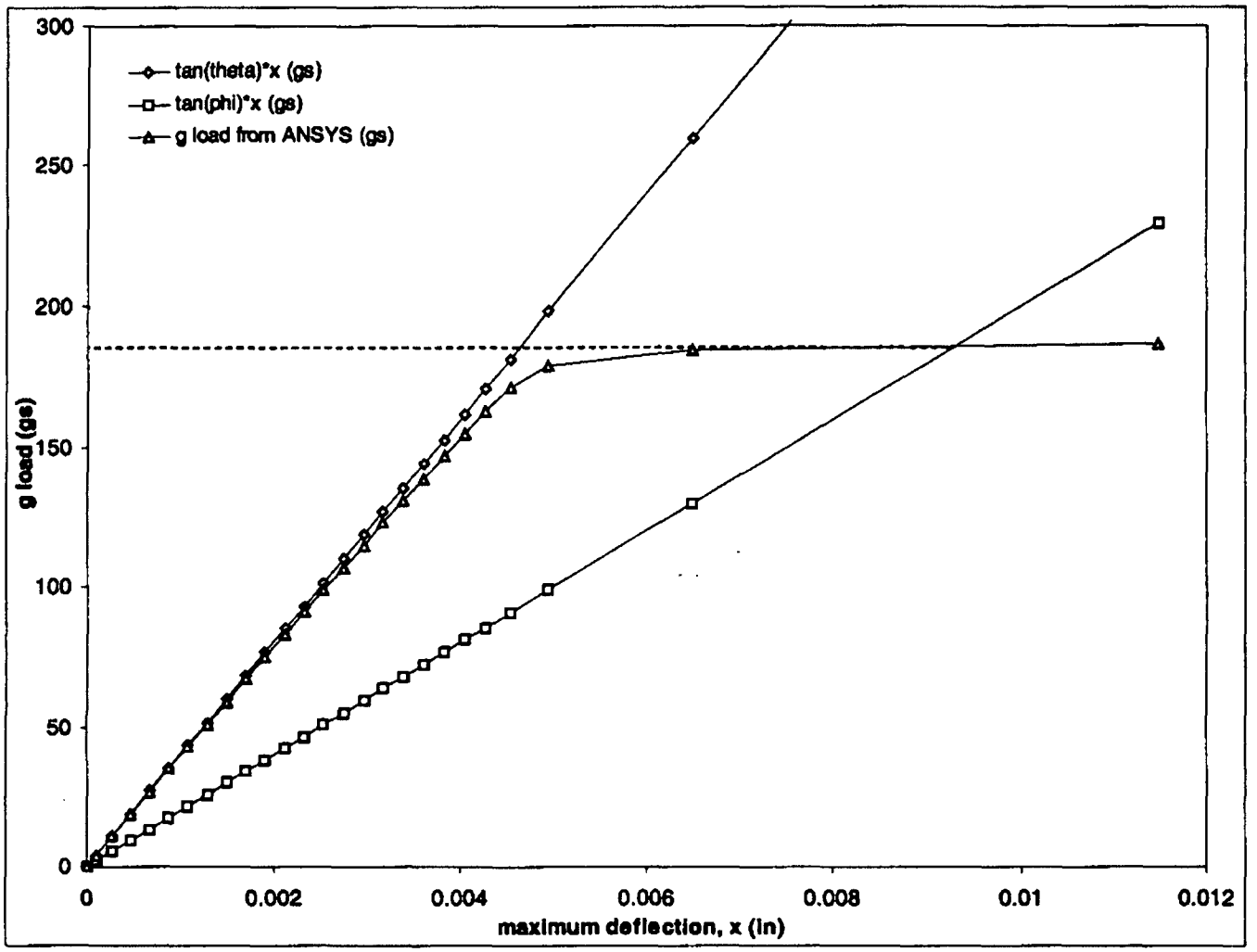

Figure 2.10.3-56
Allowable Collapse Load Determination, Location 2, 30° Drop

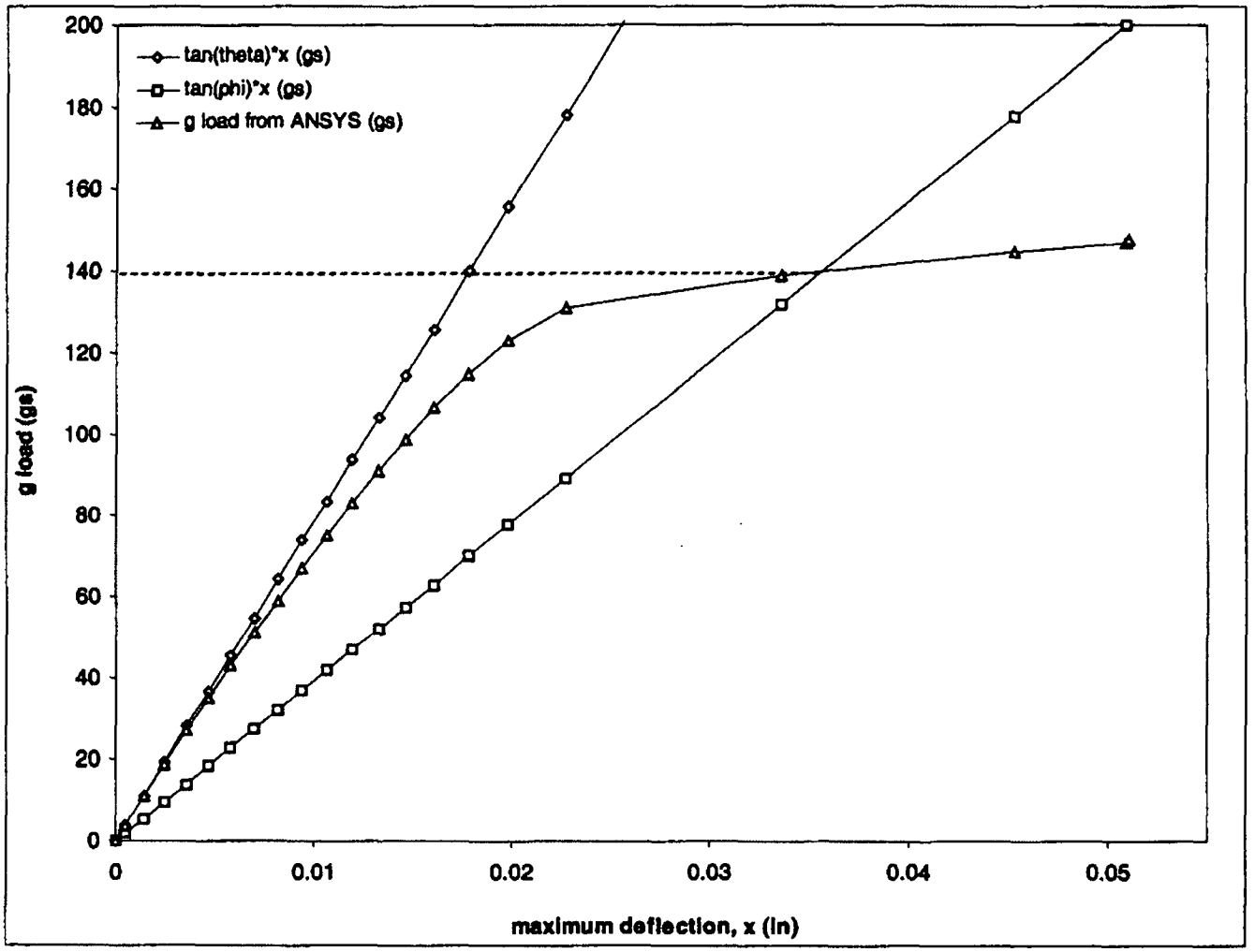

Figure 2.10.3-57
Allowable Collapse Load Determination, Location 2, 45° Drop

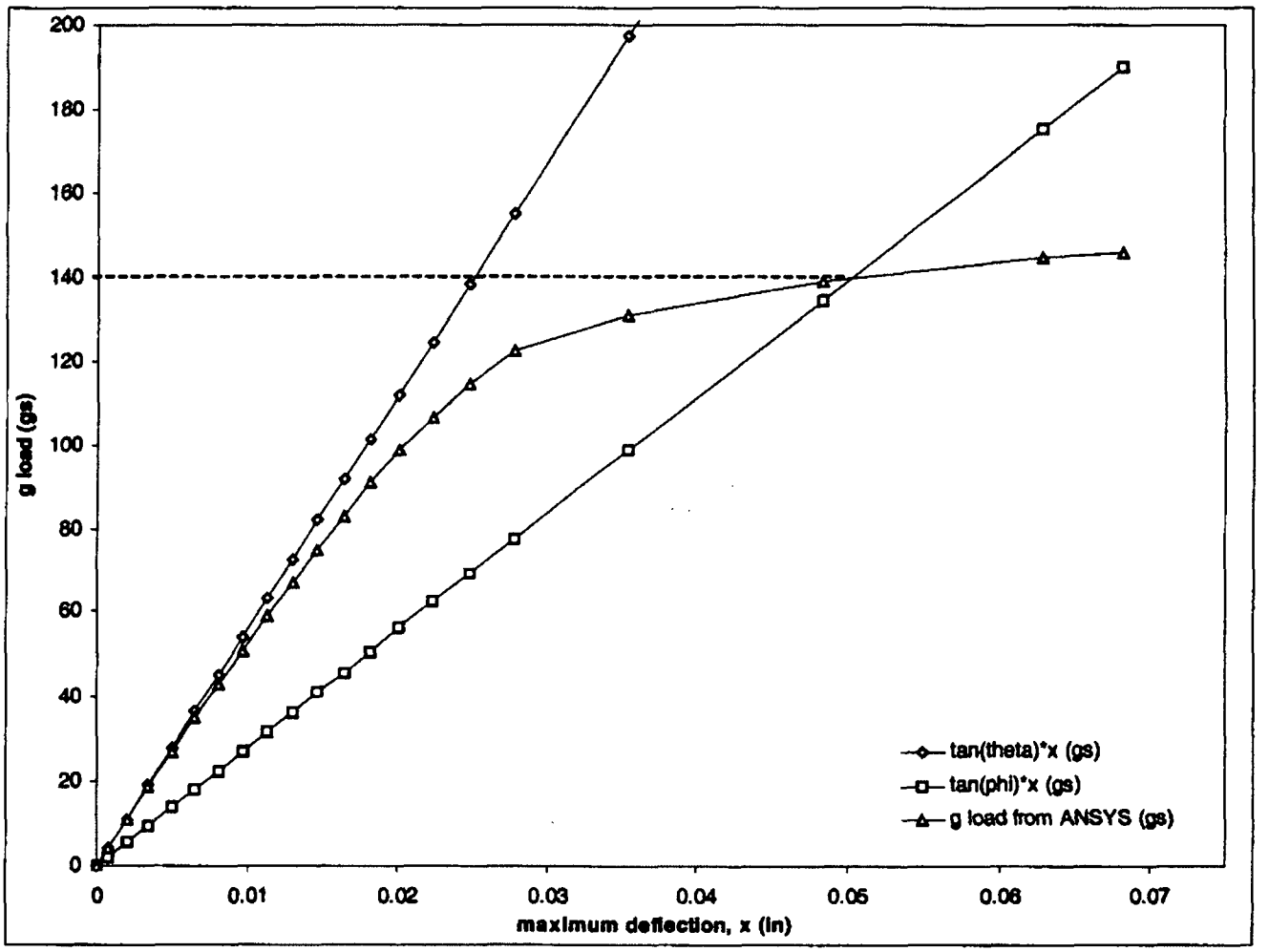

Figure 2.10.3-58
Support Rail Type 1 Location

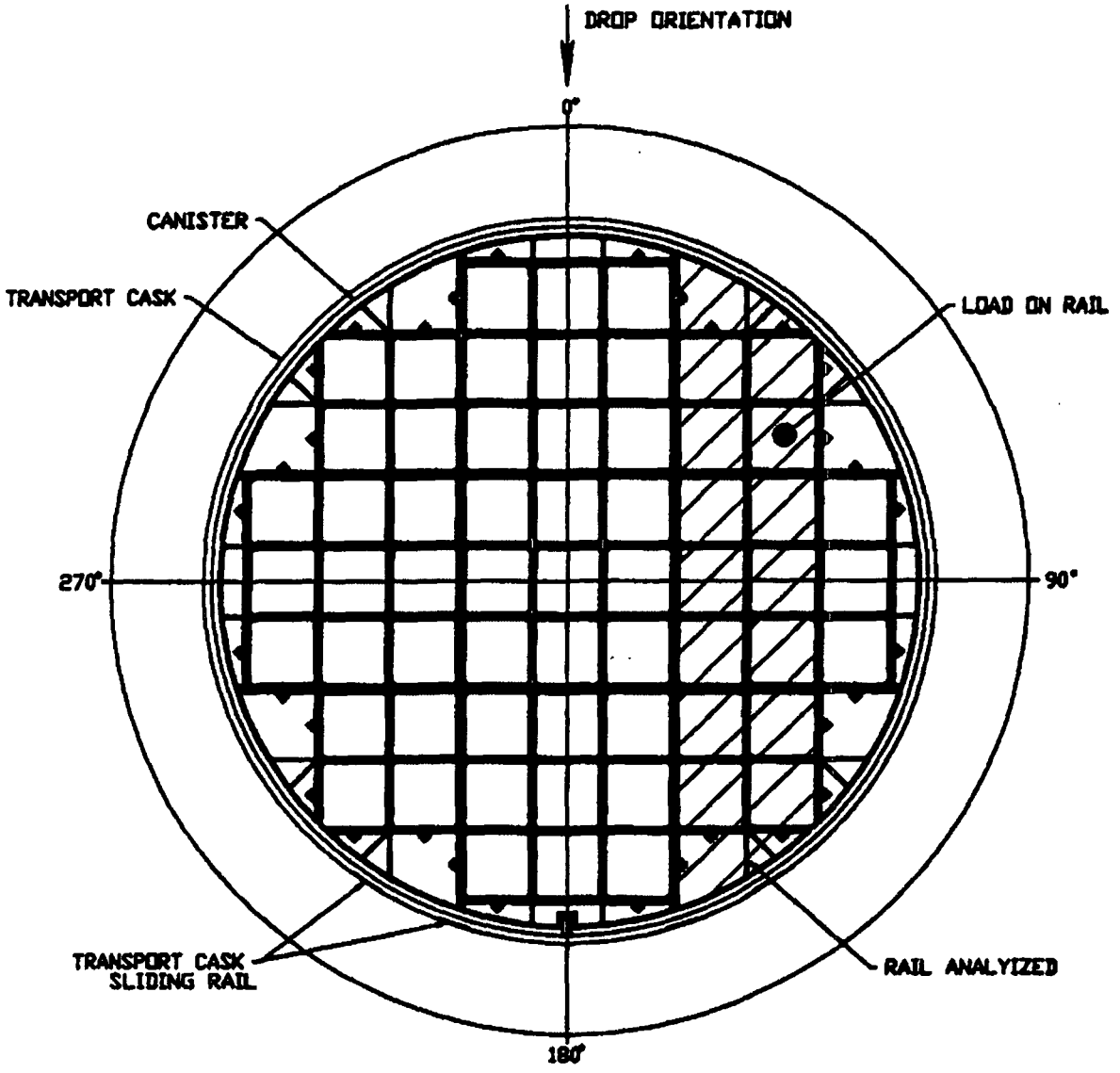


NUHOMS - 61B RAIL BUCKLING EVALUATION

Figure 2.10.3-59
Support Rail Type 1 Finite Element Model with Boundary Conditions

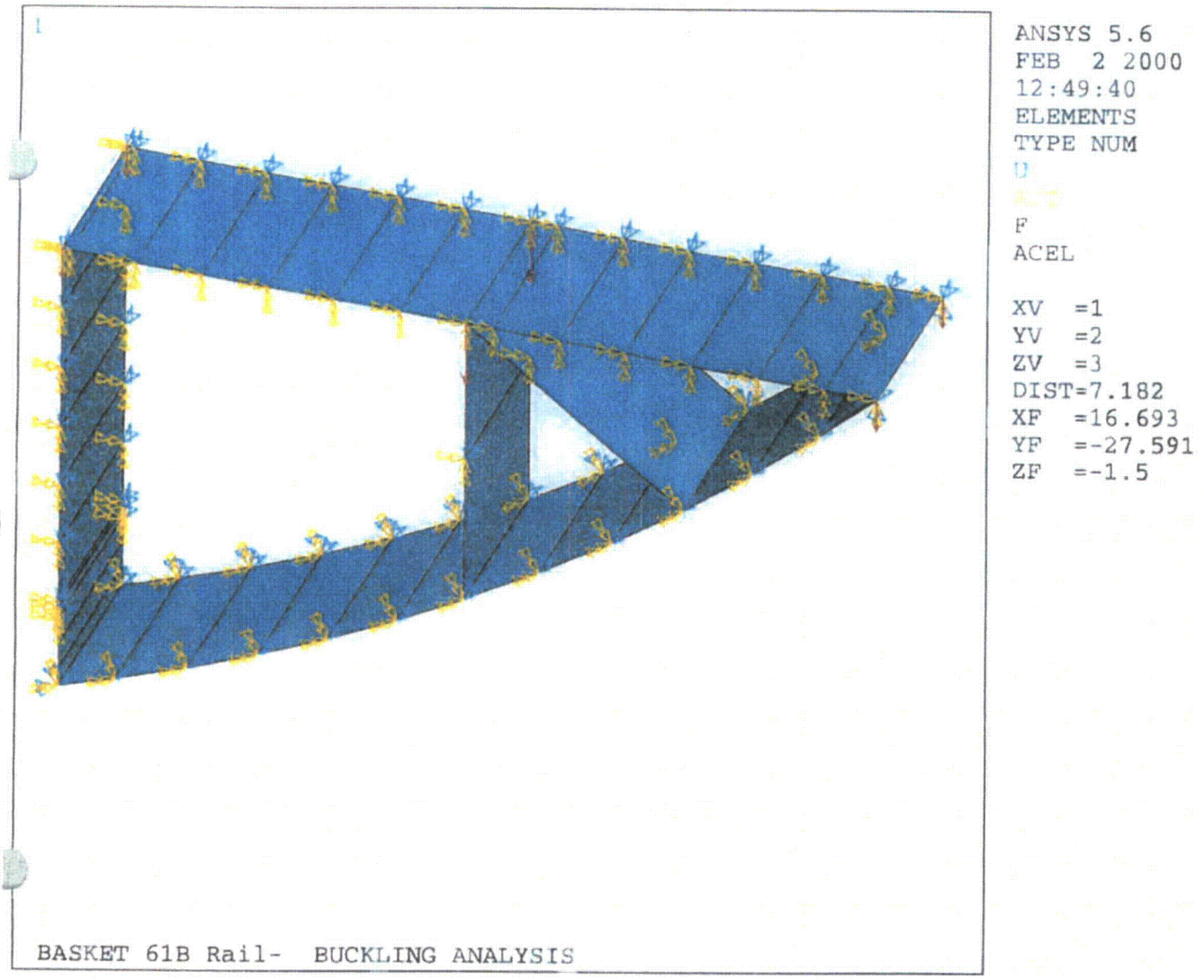

Figure 2.10.3-60
NUHOMS 61B Basket Rail Buckling Analysis, Case 1

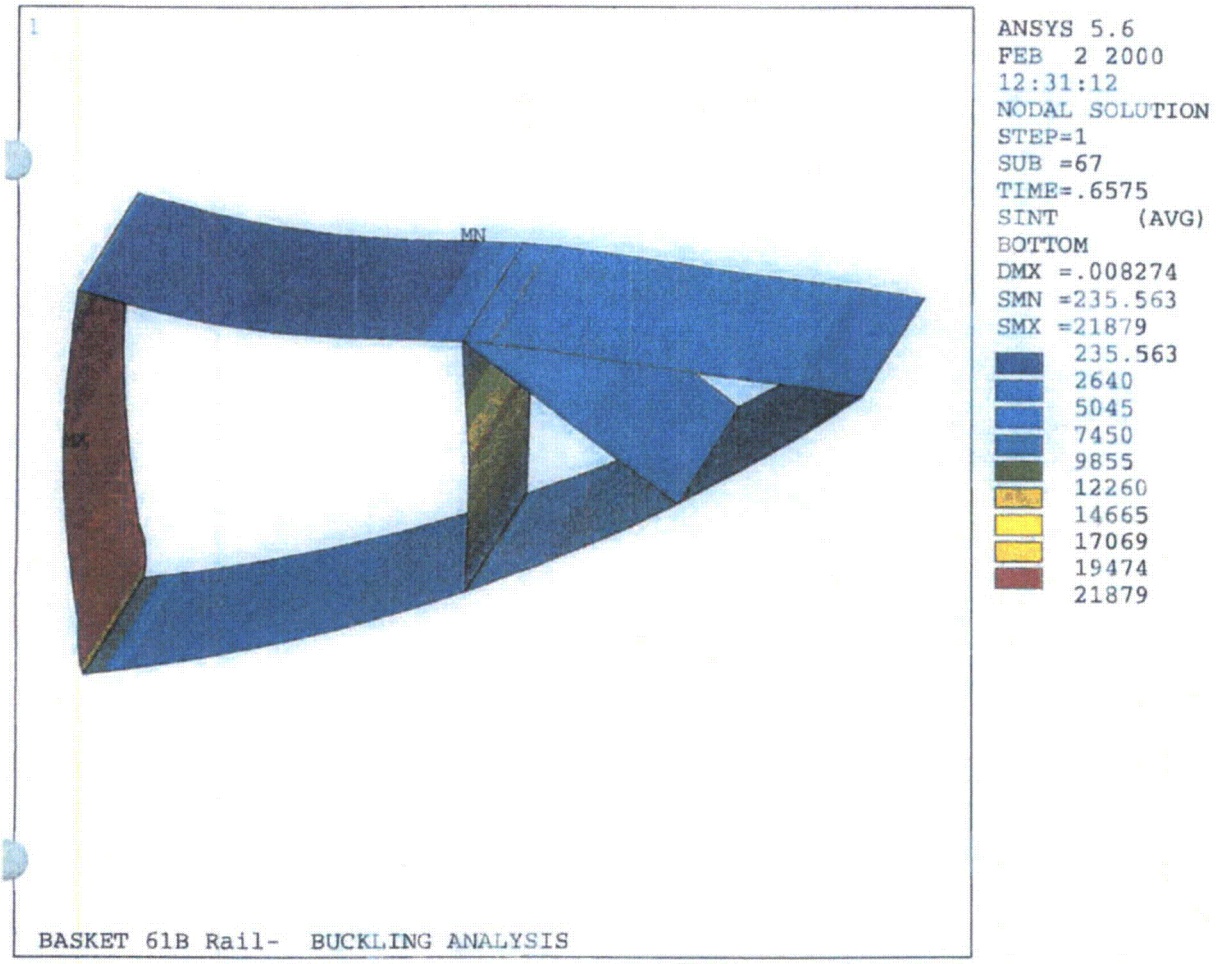

Figure 2.10.3-61
NUHOMS 61B Basket Rail Buckling Analysis, Case 2

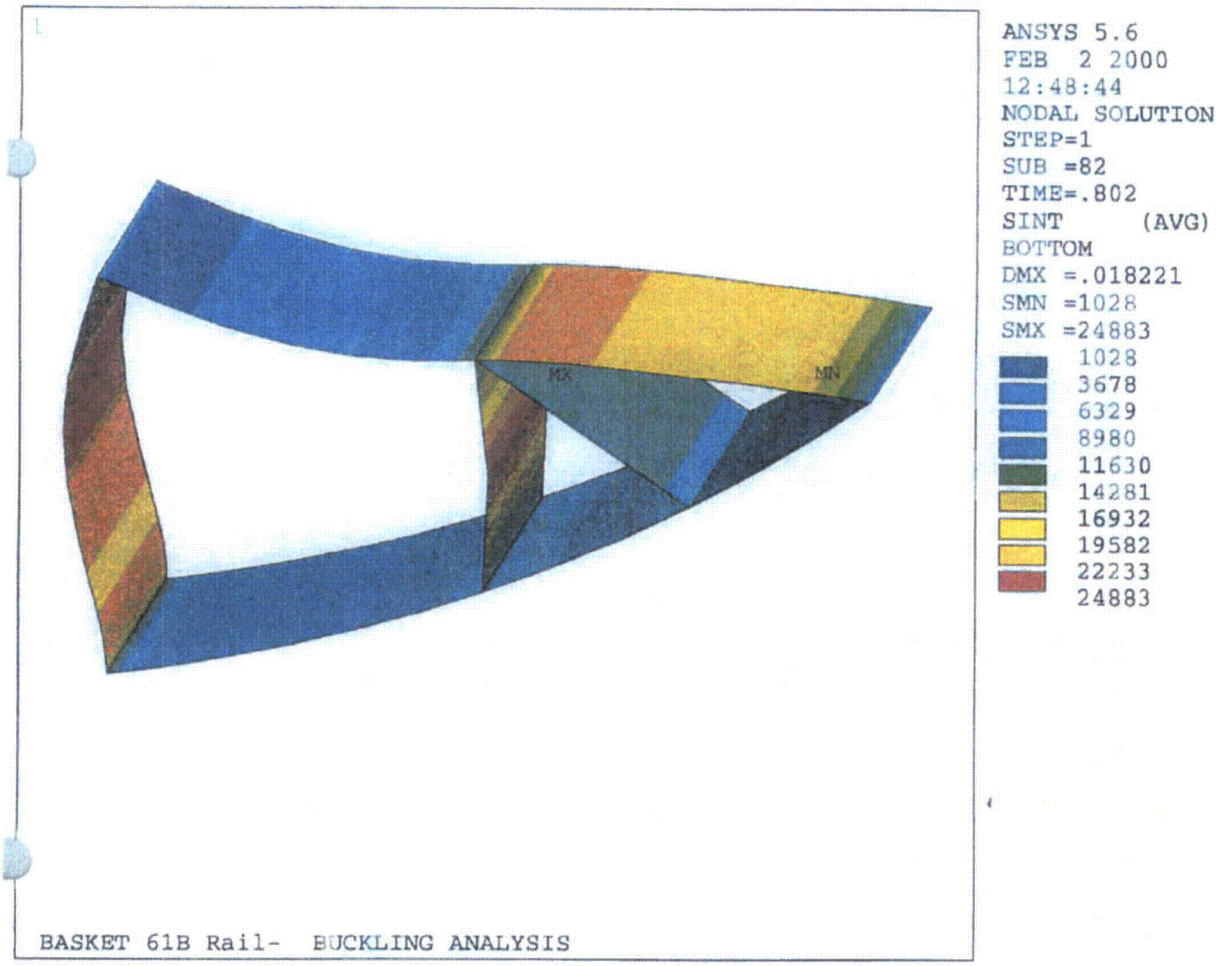

Figure 2.10.3-62
Support Rail Type 1 Allowable Collapse Load Determination

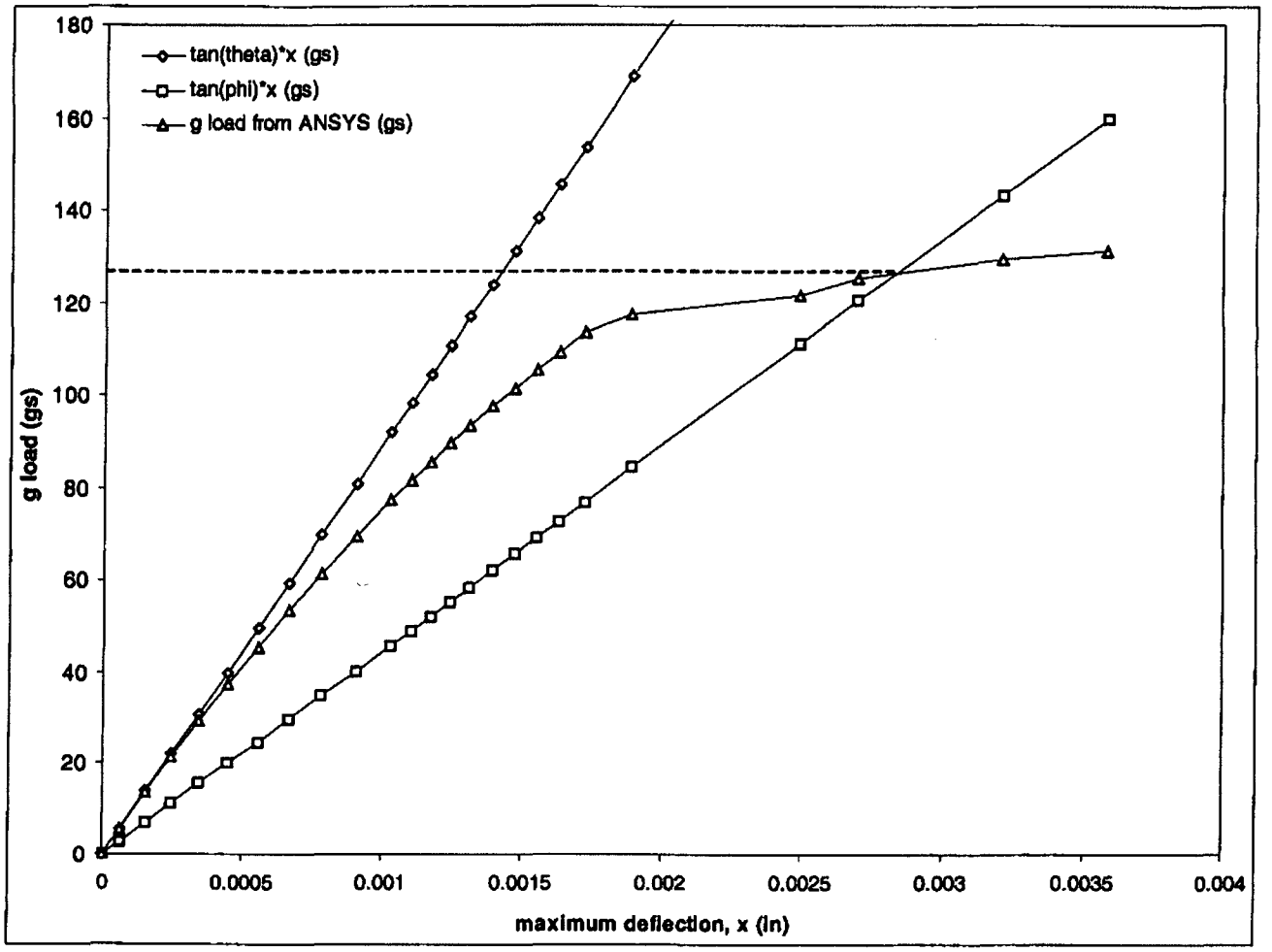

Figure 2.10.3-63
NUHOMS-61B Canister 2-Dimensional Finite Element Model

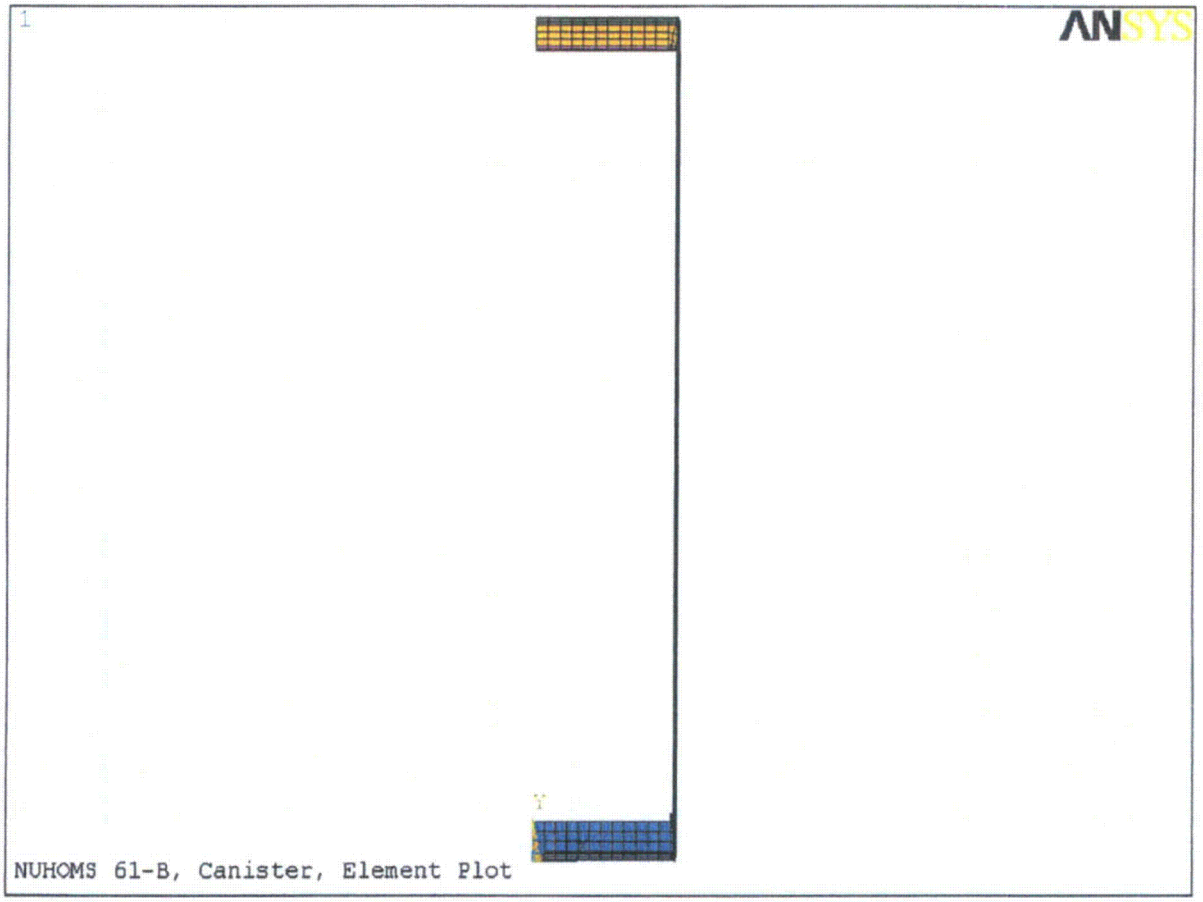

Figure 2.10.3-64
NUHOMS-61B Canister 2-Dimensional Finite Element Model,
Including Nodal Couplings and Front End Drop Boundary Conditions, Front Closure

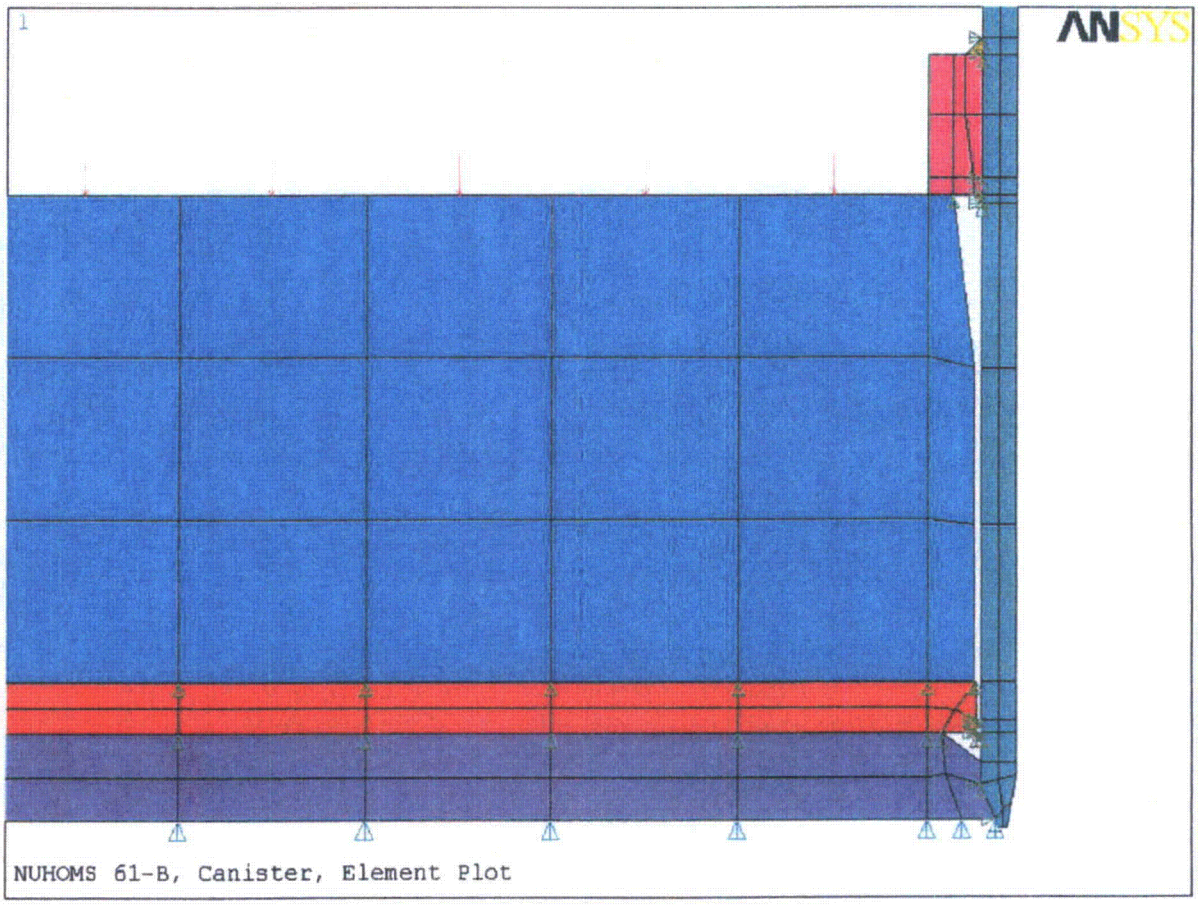

Figure 2.10.3-65
NUHOMS-61B Canister 2-Dimensional Finite Element Model,
Including Nodal Couplings and Front End Drop Boundary Conditions, Rear Closure

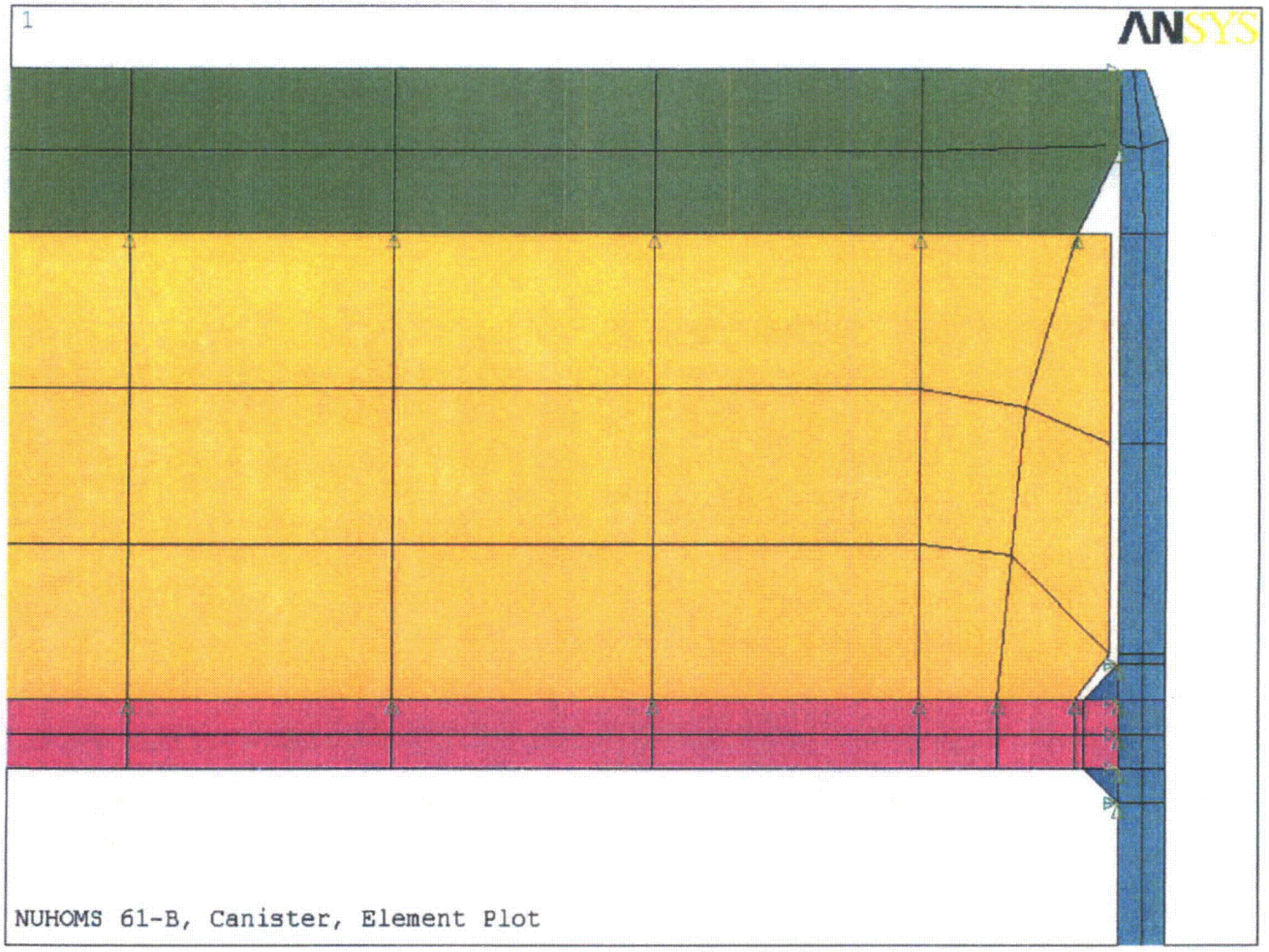

APPENDIX 2.10.4

TABLE OF CONTENTS



LIST OF FIGURES

# APPENDIX 2.10.4

# NUHOMS®-MP197 CASK LEAD SLUMP ANALYSIS

## 2.10.4.1 Introduction

The purpose of this analysis is to determine the amount of lead slump that occurs in the NUHOMS®-MP197 cask during a hypothetical accident condition end drop. The load cases considered in this calculation are hypothetical accident condition lid and bottom end drops. The impact loads are combined with thermal loads corresponding to a 100° F ambient environment and a -20° F ambient environment.

During a hypothetical accident condition end drop, permanent deformation of the lead gamma shield may occur. The lead gamma shield is supported by friction between the lead and cask shells, in addition to bearing at the end of the lead column.

A nonlinear finite element analysis is performed in order to quantify the amount of lead slump generated during an end drop event. A 2-dimensional axisymmetric ANSYS [1] finite element model is constructed for this purpose. The results of the finite element analysis provide both stresses and displacements generated during the end drop event. The displacement results are used in this section to determine the maximum size of the axial gap that develops between the lead gamma shield column and the structural shell of the cask. The effect of this cavity size on the shielding ability of the transport package is evaluated in Chapter 7. Both stress and displacement distributions computed by the finite element analysis are used to perform a buckling evaluation of inner containment shell of the NUHOMS®-MP197 cask in Appendix 2.10.5.

## 2.10.4.2 Finite Element Model

### 2.10.4.2.1 Approach

A 2-dimensional axisymmetric ANSYS [1] finite element model, constructed primarily from PLANE42 elements, is used in this analysis. LINK1 elements are used to model the lid and RAM port cover bolts. Pre-load stresses of 87 ksi. and 25 ksi. are applied to the lid and RAM port cover bolts respectively. Gap elements are used to model the interaction between the lead gamma shield and the cask inner and outer shells. The coefficient of sliding friction for lead on mild steel varies from 0.3 for lubricated surfaces to 0.95 for dry surfaces [7]. A lower bound coefficient of static friction of 0.25 is conservatively used for the buckling analysis.

In order to determine the amount of lead slump settling, an elastic plastic analysis is required. The material properties of the lid, bottom, inner shell, and outer shell of the transport cask are modeled with bilinear stress-strain curves, while the lead material is modeled with a multilinear stress-strain curve.

The neutron shield, shield shell, trunnions and bearing block are not included in the model. The effect of the unmodeled weight is accounted for by increasing the density of the outer shell in the neutron shield region. The modified density of the outer shell in this region is computed in the following way.

The weight of the section of the outer shell, $W_{os}$, that will be given an increased density is,

$W_{os}$ = $\pi$ { [41.00 in. (outer shell o.r.)]$^2$ – [38.5 in. (outer shell i.r.)]$^2$ } × 144.0 in. (section length) × 0.29 (density) = 26,075 lb.

The weight of the entire FEM prior to density modification, $W_m$, is 128,050 lb. (Section 2.2). The actual calculated weight of the transport cask, $W_{tc}$, is 150,027 lb. (Section 2.2). However, a conservative weight of 150,320 lb. is used. Therefore, the modified density used in this analysis, $\rho_m$, is

$$\rho_m = \frac{W_{os} + (W_{tc} - W_m)}{\pi(41.00^2 - 38.50^2)\times 144} = \frac{26{,}075 + (150{,}320 - 128{,}050)}{\pi(41.00^2 - 38.50^2)\times 144} = 0.538 \text{ lb.in.}^{-3}$$

2.10.4.2.2 Material Properties

The maximum temperature of the transport cask during transport in the 100° F ambient environment is 302° F (Chapter 3, Table 3-1). Properties of NUHOMS®-MP197 cask materials are taken at 300° F for both hot and cold environment cases, which is conservative. The transport cask material properties are as follows.

Outer Shell (SA-240 Type 316) @ 300° F. [1] [2] [3]

$E = 27.0\times10^6$ psi.
$S_y = 23.4$ ksi.
$S_u = 72.9$ ksi.
$\alpha_{70°F} = 8.5\times10^{-6}$ in./in. °F$^{-1}$
$\alpha_{300°F} = 9.2\times10^{-6}$ in./in. °F$^{-1}$
$\nu = 0.3$
$\rho = 0.29$
Elongation, $e = 40\%$

$\varepsilon$ @ $S_y = 23{,}400/27.0\times10^6 = 0.000867$ in. in$^{-1}$.
Tangent Modulus, $E_T = (72{,}900 - 23{,}400)/(0.40 - 0.000867) = 124{,}020$ psi.

Lid Material (SA-693 Type 630, Condition H1100) @ 300° F. [1] [2] [3]

$E = 27.2\times10^6$ psi.
$S_y = 101.8$ ksi.
$S_u = 140.0$ ksi.
$\alpha_{70°F} = 5.89\times10^{-6}$ in./in. °F$^{-1}$
$\alpha_{300°F} = 5.90\times10^{-6}$ in./in. °F$^{-1}$
$\nu = 0.3$
$\rho = 0.29$
Elongation, $e = 14\%$

$\varepsilon$ @ $S_y = 101{,}800/27.2\times10^6 = 0.003743$ in. in$^{-1}$.
Tangent Modulus, $E_T = (140{,}000 - 101{,}800)/(0.14 - 0.003743) = 280{,}353$ psi.

Lead (B-29) @ 300° F. [4] [5] [6]

$E = 2.06\times10^6$ psi.
$\nu = 0.45$
$\rho = 0.41$
$\alpha_{70°F} = 16.07\times10^{-6}$ in./in. °F$^{-1}$
$\alpha_{300°F} = 17.34\times10^{-6}$ in./in. °F$^{-1}$

Multi-linear Stress/Strain Curve:

| Strain | Stress |
|---|---|
| 0.000485 | 1000 |
| 0.030 | 1,700 |
| 0.100 | 2,380 |
| 0.300 | 2,720 |
| 0.500 | 3,060 |

Inner Shell, Flange, Bottom, RAM Closure Plate (SA-240 Type XM-19 or SA-182 Type FXM-19) @ 300° F. [1] [2] [3]

$E = 27.0\times10^6$ psi.
$S_y = 43.3$ ksi.
$S_u = 94.2$ ksi.
$\alpha_{70°F} = 8.2\times10^{-6}$ in./in. °F$^{-1}$
$\alpha_{300°F} = 8.8\times10^{-6}$ in./in. °F$^{-1}$
$\nu = 0.3$
$\rho = 0.29$
Elongation, $e = 35\%$

$\varepsilon$ @ $S_y = 43{,}300/27.0\times10^6 = 0.001604$ in. in$^{-1}$.
Tangent Modulus, $E_T = (94{,}200 - 43{,}300)/(0.35 - 0.001604) = 146{,}100$ psi.

2.10.4.2.3 Boundary Conditions

Lid End Drop Boundary Conditions

The weights of the transport cask internals and bottom impact limiter are accounted for by applying equivalent pressures. The actual weights of the transport cask internals and bottom impact limiter, including the thermal shield, are 88,390 lb. and 14,085 lb. respectively (Section 2.2). The weights of the transport cask internals and bottom impact limiter, used in this analysis, are conservatively increased to 88,500 lb. and 14,200 lb. respectively. The pressure equivalent to the weight of the internals, $P_i$, is,

$$P_i = 88{,}500 / [\, \pi \times 34.00^2 \text{ (cavity inner radius)} \,] = 24.3689 \text{ psi.}$$

The pressure equivalent to the weight of the bottom impact limiter, including the thermal shield, $P_{bil}$, is,

$$P_{bil} = 14{,}200 / [\, \pi \times 40.50^2 \text{ (cask outer radius)} \,] = 2.7577 \text{ psi.}$$

The reaction pressure at the top end of the cask in the lid region is made equivalent to the weight of the lid plus the weight of the internals. The reaction pressure at the top end of the cask in the flange region is made equivalent to the weight of the entire model plus the weight of the bottom impact limiter minus the weight of the lid. The reaction pressure at the lid, $R_l$, is,

$$R_l = \frac{88{,}500 + \pi(34^2)(4.50)(0.29)}{\pi(34^2)} = 25.67 \text{ psi.}$$

The reaction pressure at the flange, $R_f$, is,

$$R_f = \frac{150{,}320 + 14{,}200 - \pi(34^2)(4.50)(0.29)}{\pi[(37.34^2 - 34.00^2) + (40.50^2 - 37.65^2)]} = 110.32 \text{ psi.}$$

These reaction pressures are applied to the finite element model and then adjusted slightly for each load case in order to balance the reaction forces at the boundary conditions.

Symmetry displacement boundary conditions are applied along the *y*-axis of the 2-dimensionsal axisymmetric model. A single node along the *y*-axis of the model at the bottom (non-impact) end of the cask is held in the axial direction. An inertial load of 100*g*s in the negative *y*-direction is also applied to the model. A plot of the finite element model and boundary conditions for the lid end drop load case is provided in Figure 2.10.4-1.

Bottom End Drop Boundary Conditions

The weights of the transport cask internals and top impact limiter are also accounted for by applying equivalent pressures. The actual weight of the top impact limiter is 13,782 lb. The weight of the top impact limiter used in this analysis is conservatively increased to 13,900 lb. The pressure equivalent to the weight of the internals, $P_i$, is,

$$P_i = 88{,}500 / [\,\pi \times (34.00^2 - 8.75^2) \text{ (cavity inner radius)}\,] = 26.10 \text{ psi.}$$

The pressure equivalent to the weight of the top impact limiter, $P_{til}$, is,

$$P_{til} = \frac{13{,}900}{\pi[37.34^2 + (40.50^2 - 37.65^2)]} = 2.74 \text{ psi.}$$

The reaction pressure at the bottom end of the cask in the central region is made equivalent to the weight of the bottom plus the weight of the internals. The reaction pressure at the bottom end of the cask in the outer region is made equivalent to the weight of the entire model plus the weight of the top impact limiter minus the weight of the bottom. The reaction pressure in the center region, $R_c$, is,

$$R_c = \frac{88{,}500 + \pi(34^2)(6.50)(0.29)}{\pi(34^2)} = 26.25 \text{ psi.}$$

The reaction pressure at the outer edge, $R_o$, is,

$$R_o = \frac{150{,}320 + 13{,}900 - \pi(34^2)(6.50)(0.29)}{\pi(40.50^2 - 34.00^2)} = 103.45 \text{ psi.}$$

These reaction pressures are applied to the finite element model and then adjusted slightly for each load case in order to balance the reaction forces at the boundary conditions.

Symmetry displacement boundary conditions are applied along the *y*-axis of the 2-dimensionsal axisymmetric model. A single node along the *y*-axis of the model at the lid (non-impact) end of the cask is held in the axial direction. An inertial load of 100*g*s in the positive *y*-direction is also applied to the model. A plot of the finite element model and boundary conditions for the bottom end drop load case is provided in Figure 2.10.4-2.

Thermal Loads

Two thermal load cases are applied to each drop orientation load case, yielding a total of four load combinations. The two temperature distributions applied correspond to the 100° F. and -20° F ambient temperature environments. The temperature distributions applied to the finite element model for both the 100° F hot environment condition and the -20° F cold environment condition are taken from Chapter 3.

### 2.10.4.3 FEA Results

In order to quantify the axial length of the cavity that develops as a result of lead slump, the difference between the maximum axial deflections of adjacent lead and structural shell nodes, at the load step corresponding to 75 gs, is determined. This difference is taken to be the maximum cavity length caused by lead slump.

The following table summarizes the axial gap between the lead and cavity after all four load combinations analyzed. Nodal displacement distributions for the four load combinations are shown Figures 2.10.4-3 through 2.10.4-6.

| Load Combination | Gap |
|---|---|
| 75*g* Lid End Drop, Hot Environment | 0 in. |
| 75*g* Lid End Drop, Cold Environment | 0.235 in. |
| 75*g* Bottom End Drop, Hot Environment | 0 in. |
| 75*g* Bottom End Drop, Cold Environment | 0.107 in. |

### 2.10.4.4 Conclusions

The table above shows that the maximum longitudinal gap, caused by lead slump, is 0.235 inches, and occurs during accident condition lid end drop, in the cold environment. The table above, as well as the displacement plots (Figures 2.10.4-3 through 2.10.4-6) also show that in the hot environment, differential thermal expansion between the lead shield and the structural shells precludes gap formation during both lid and end drops. The effect of the gap on the shielding ability of the NUHOMS®-MP197 cask is analyzed in Chapter 6.

## 2.10.4.5 References


1. ANSYS User's Manual, Rev 5.6, 1998.

2. American Society of Mechanical Engineers, ASME Boiler and Pressure Vessel Code, Section II, Part D, 1998, including 1999 addenda.

3. American Society of Mechanical Engineers, ASME Boiler and Pressure Vessel Code, Section II, Part A, 1998, including 1999 addenda.

4. An Assessment of Stress-Strain Data Suitable for Finite-Element Elastic-Plastic Analysis of Shipping Containers, NUREG/CR-0481.

5. Cask Design Guide, ORNL-NSIC-68, February 1970.

6. A Survey of Strain Rate Effects for some Common Structural Materials Used in Radioactive Material Packaging and Transportation Systems, U.S. Energy Research and Development Administration, Battelle Columbus Laboratories, August 1976.

7. Baumeister & Marks, Standard Handbook for Mechanical Engineers, 7th Edition.

Figure 2.10.4-1
NUHOMS®-MP197 cask 2-Dimensional Finite Element Model
with Lid End Drop Boundary Conditions

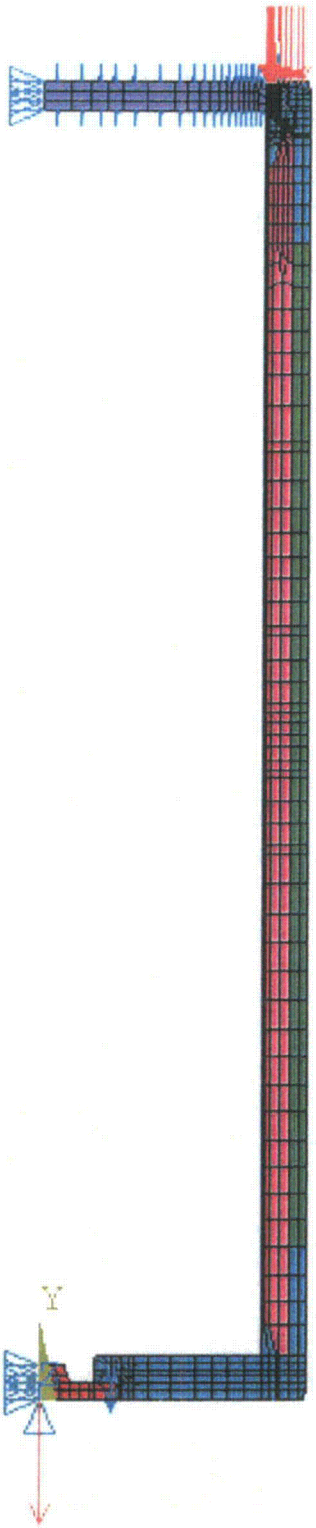

Figure 2.10.4-2
NUHOMS®-MP197 cask 2-Dimensional Finite Element Model
with Bottom End Drop Boundary Conditions

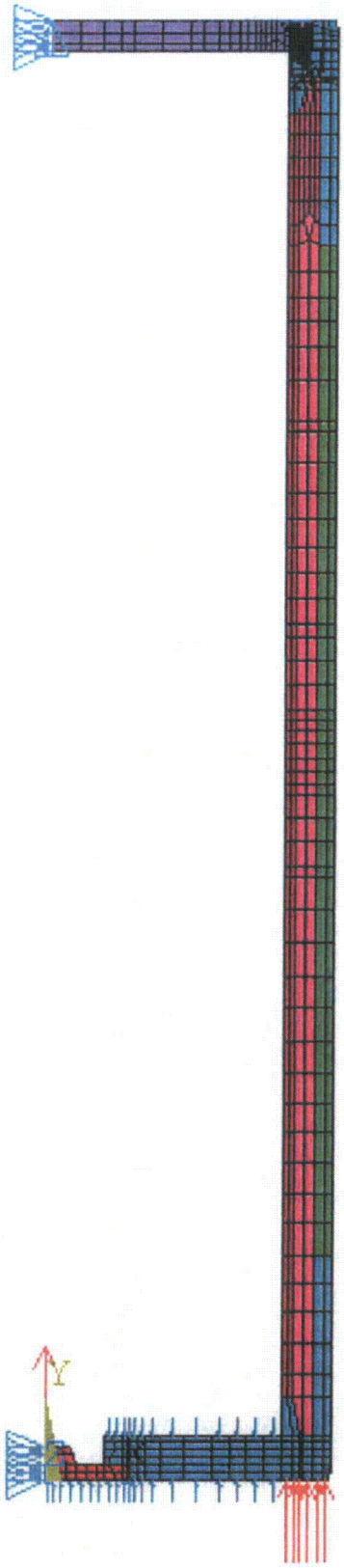

Figure 2.10.4-3
Displacement Pattern – Lid End Drop, Hot Environment Load Case

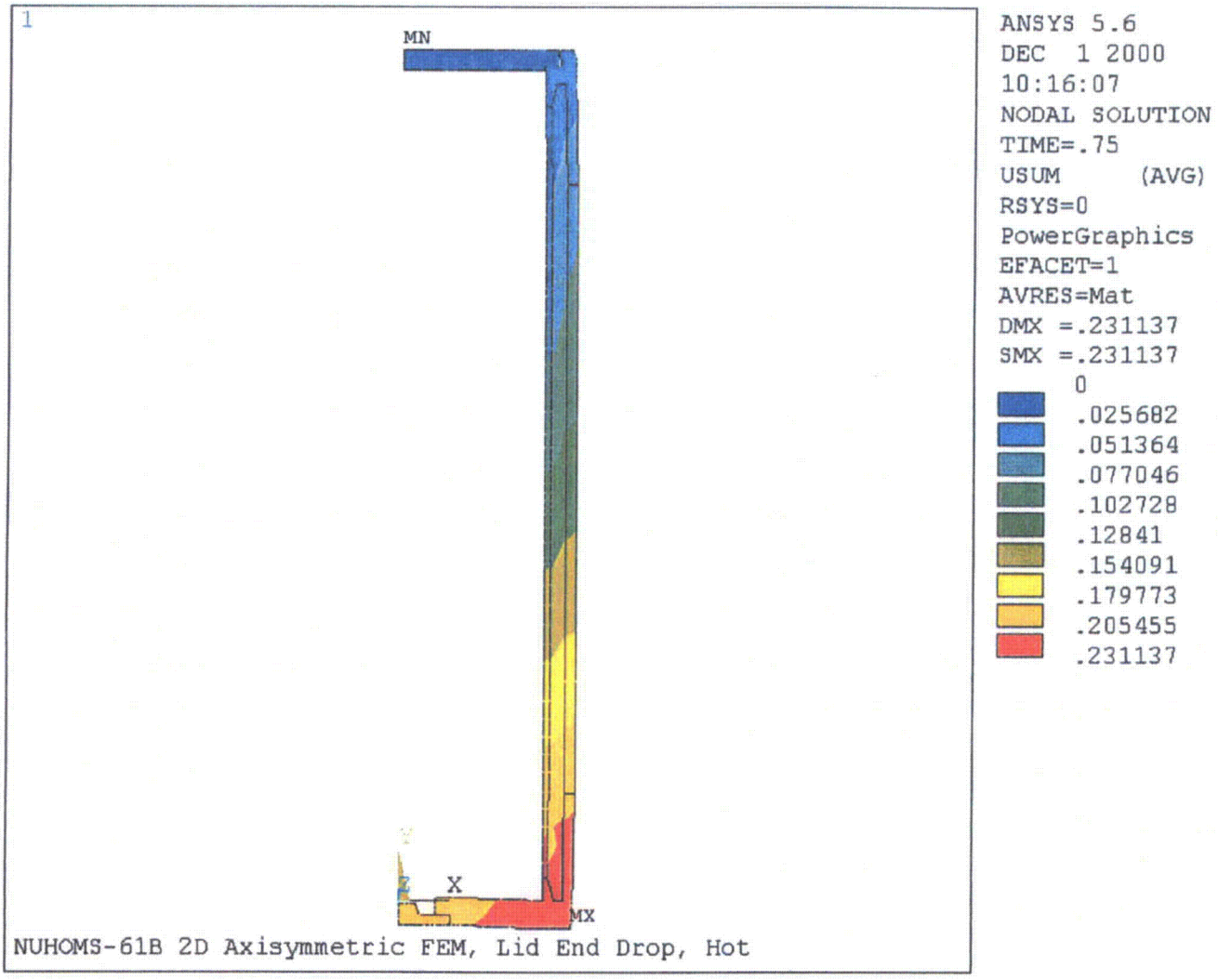

Figure 2.10.4-4
Displacement Pattern – Lid End Drop, Cold Environment Load Case

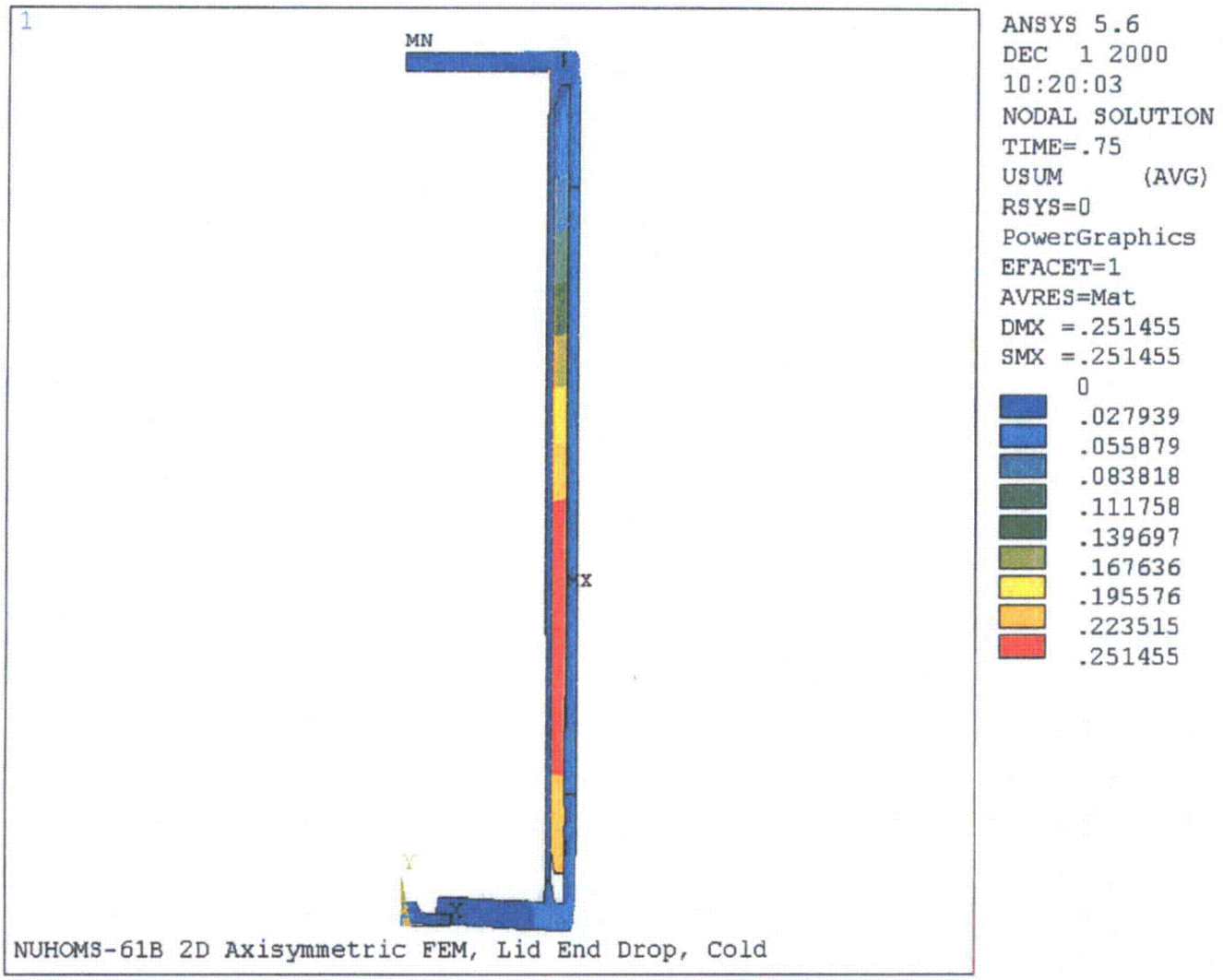

Figure 2.10.4-5
Displacement Pattern – Bottom End Drop, Hot Environment Load Case

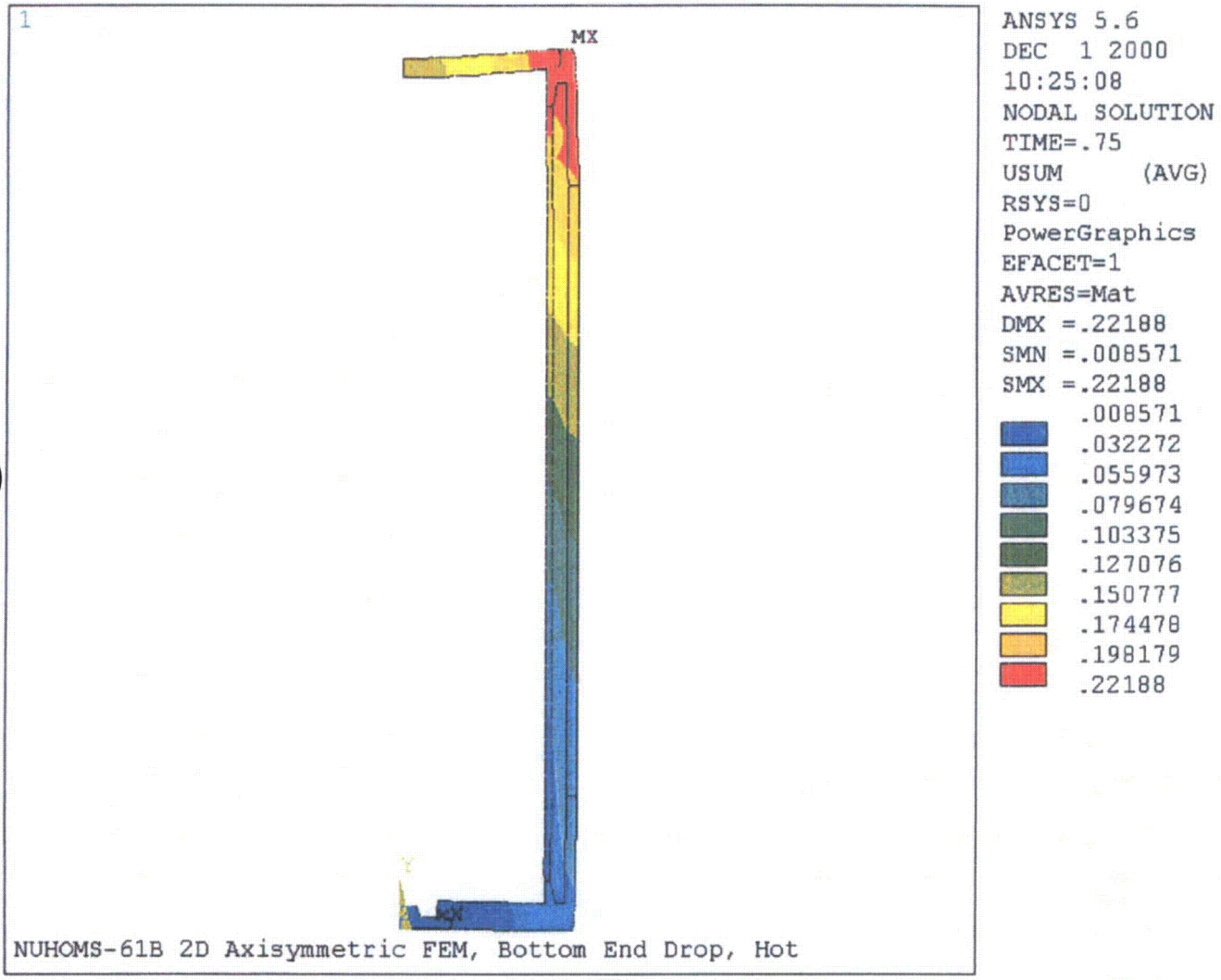

Figure 2.10.4-6
Displacement Pattern – Bottom End Drop, Cold Environment Load Case

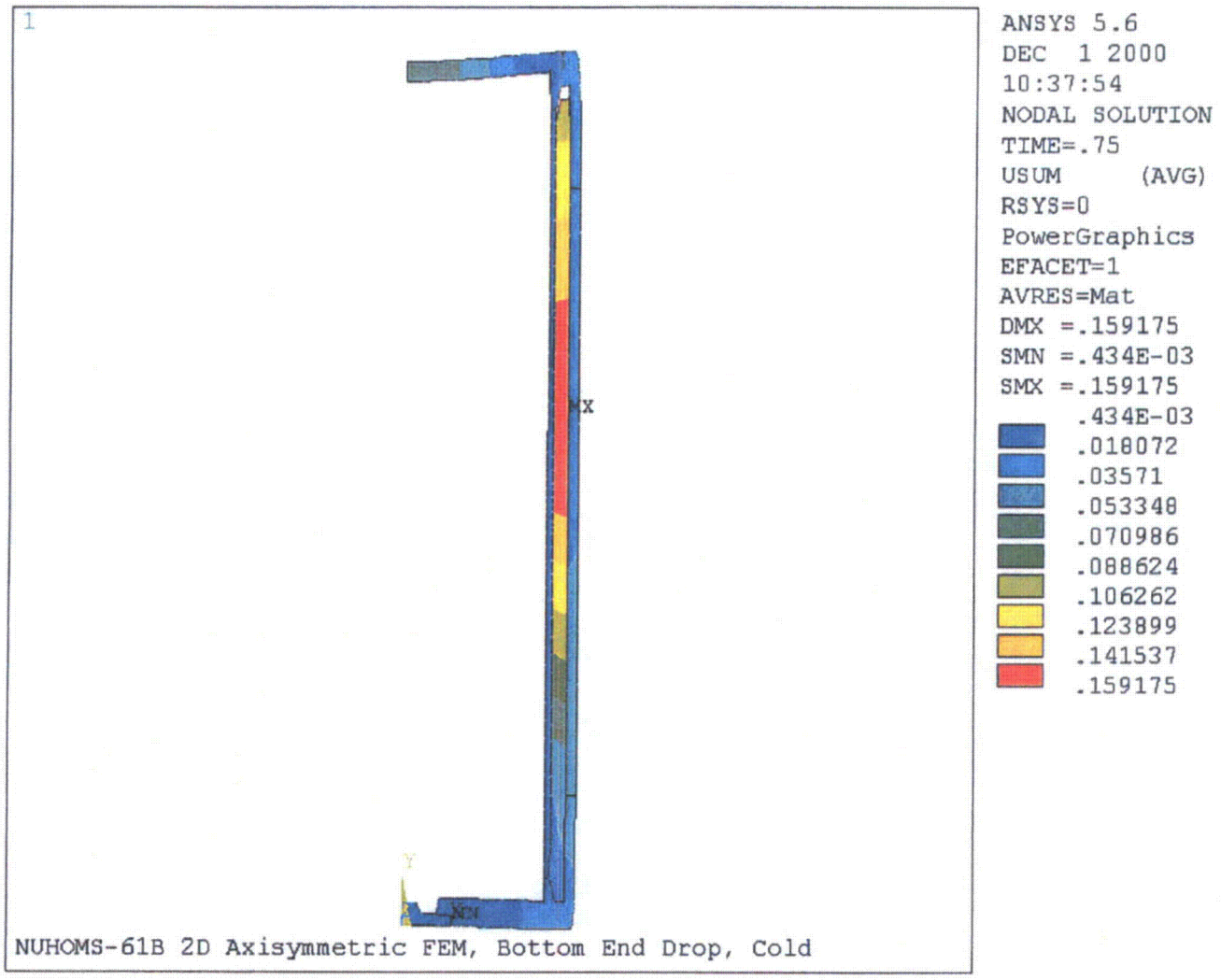

APPENDIX 2.10.5

TABLE OF CONTENTS



LIST OF FIGURES

# APPENDIX 2.10.5

# NUHOMS®-MP197 CASK INNER CONTAINMENT BUCKLING ANALYSIS

## 2.10.5.1 Introduction

The purpose of this analysis is to evaluate the structural adequacy of the NUHOMS®-MP197 cask inner shell with respect to bucking. The load cases considered in this calculation are hypothetical accident condition lid and bottom end drops. The impact loads are combined with thermal loads corresponding to a 100° F ambient environment and a -20° F ambient environment. The analysis is based on the methodology provided in ASME Code Case N-284-1 [1] and the Collapse Load Analysis described in ASME B&PV Code Appendix F [2].

During a hypothetical accident condition end drop, permanent deformation of the lead gamma shield may occur. The lead gamma shield is supported by friction between the lead and cask shells, in addition to bearing at the end of the lead column. During fabrication, a small gap may develop between the lead gamma shield and the cask structural shells due to differential thermal expansion of the dissimilar materials during cooling after the lead pour. The gap between the lead and cask shells reduces the stresses in the cask shells during the postulated end drop, while maximizing the amount of permanent deformation in the lead column (i.e. lead slump). Therefore, for the purpose of analysis, the lead is conservatively assumed to be initially in contact with both the cask inner and structural shells.

A nonlinear finite element analysis is performed in order to evaluate the buckling capacity of the inner shell of the transport cask. A 2-dimensional axisymmetric ANSYS [3] finite element model is constructed for this purpose. The results of the finite element analysis provide both stresses and displacements generated during the end drop event. The resulting stress distribution is compared with the allowable buckling stresses in both the hoop and the axial directions as dictated by ASME Code CASE N-284-1 [1]. The resulting deformation is used to perform a collapse load analysis described in ASME B&PV Code Appendix F [2].

2.10.5.2 Material Properties

The maximum temperature of the transport cask during transport in the 100° F ambient environment is 302° F (Chapter 3, Table 3-1). Properties of NUHOMS®-MP197 cask materials are taken at 300° F for both hot and cold environment cases, which is conservative. The transport cask material properties are as follows.

Outer Shell (SA-240 Type 316) @ 300° F. [4] [5] [6]

$E = 27.0\times10^{6}$ psi.
$S_y = 23.4$ ksi.
$S_u = 72.9$ ksi.
$\alpha_{70°F} = 8.5\times10^{-6}$ in./in. °F$^{-1}$
$\alpha_{300°F} = 9.2\times10^{-6}$ in./in. °F$^{-1}$
$\nu = 0.3$
$\rho = 0.29$
Elongation, $e = 40\%$

$\varepsilon$ @ $S_y = 23{,}400/27.0\times10^{6} = 0.000867$ in. in$^{-1}$.
Tangent Modulus, $E_T = (72{,}900 - 23{,}400)/(0.40 - 0.000867) = 124{,}020$ psi.

Lid Material (SA-693 Type 630, Condition H1100) @ 300° F. [4] [5] [6]

$E = 27.2\times10^{6}$ psi.
$S_y = 101.8$ ksi.
$S_u = 140.0$ ksi.
$\alpha_{70°F} = 5.89\times10^{-6}$ in./in. °F$^{-1}$
$\alpha_{300°F} = 5.90\times10^{-6}$ in./in. °F$^{-1}$
$\nu = 0.3$
$\rho = 0.29$
Elongation, $e = 14\%$

$\varepsilon$ @ $S_y = 101{,}800/27.2\times10^{6} = 0.003743$ in. in$^{-1}$.
Tangent Modulus, $E_T = (140{,}000 - 101{,}800)/(0.14 - 0.003743) = 280{,}353$ psi.

Lead (B-29) @ 300° F. [7] [8] [9]

$E = 2.06\times10^{6}$ psi.
$\nu = 0.45$
$\rho = 0.41$
$\alpha_{70°F} = 16.07\times10^{-6}$ in./in. °F$^{-1}$
$\alpha_{300°F} = 17.34\times10^{-6}$ in./in. °F$^{-1}$

Multi-linear Stress/Strain Curve:

| Strain | Stress |
|---|---|
| 0.000485 | 1,000 |
| 0.030 | 1,700 |
| 0.100 | 2,380 |
| 0.300 | 2,720 |
| 0.500 | 3,060 |

Inner Shell, Flange, Bottom, RAM Closure Plate (SA-240 Type XM-19 or SA-182 Type FXM-19) @ 300° F. [4] [5] [6]

$E = 27.0\times10^{6}$ psi.
$S_y = 43.3$ ksi.
$S_u = 94.2$ ksi.
$\alpha_{70°F} = 8.2\times10^{-6}$ in./in. °F$^{-1}$
$\alpha_{300°F} = 8.8\times10^{-6}$ in./in. °F$^{-1}$
$\nu = 0.3$
$\rho = 0.29$
Elongation, $e = 35\%$

$\varepsilon$ @ $S_y = 43{,}300/27.0\times10^{6} = 0.001604$ in. in$^{-1}$.
Tangent Modulus, $E_T = (94{,}200 - 43{,}300)/(0.35 - 0.001604) = 146{,}100$ psi.

### 2.10.5.3 Allowable Buckling Stress Determination

The following analysis, based on ASME Code CASE N-284-1 [1], is used to determine the allowable axial and hoop buckling stresses.

#### 2.10.5.3.1 Notation

The following notation is taken from Reference 1, Section –1200.

- Subscripts $\phi$ and $\theta$ = axial (maridional) and circumferential directions respectively.
- $l_\phi$ = distances between lines of support in the axial direction, use 193.50 in.
- $R$ = shell mean radius = 68.00/2 in. (inner radius) + 1.25 in. (shell thickness) = 35.25 in.
- $t$ = shell thickness, 1.25 in.
- $t_\phi$, $t_\theta$ = thickness of elements of a stiffener, in. (defaults to $t$ for unstiffened vessels).
- $M_\phi = \dfrac{l_\phi}{\sqrt{(R)(t)}}$
- $C_{\phi h}$, $C_\theta$ = elastic buckling coefficient under external pressure and axial compression respectively.
- $\sigma_{heL}$, $\sigma_{\phi eL}$ = local theoretical elastic instability stress in the hoop direction for cylinders under external pressure and axial compression respectively, psi.
- $E$ = modulus of elasticity of the material at design temperature, $27.0\times10^6$ psi. @ 300° F [5].
- $\alpha_{eL}$ = capacity reduction factor to account for the difference between classical theory and predicted instability stresses for fabricated shells.
- $\sigma_y$ = tabulated yield stress of material at design temperature, 43,300 psi. @ 300° F [5].
- $\sigma_{xa}$, $\sigma_{ha}$, allowable axial and hoop stresses for elastic buckling respectively, psi.
- $\sigma_{xc}$, $\sigma_{hc}$, allowable axial and hoop stresses for inelastic buckling respectively, psi.
- $\sigma_\phi$, $\sigma_\theta$ = calculated axial and hoop membrane stress components respectively, psi.
- $FS$ = factor of Safety, 2 for normal conditions, 1.34 for accident conditions ([1], Section – 1400 (a)).
- $K$ = the ratio of the axial membrane force per unit length to the hoop compressive membrane force per unit length, $\sigma_\phi t_\phi / \sigma_\theta t_\theta$.

2.10.5.3.2 Allowable Hoop Stress Determination

The analytical method provided in ASME Code Case N-284-1 is used to determine the allowable buckling stress with respect to external pressure of the NUHOMS®-MP197 cask inner shell.

Since the vessel is assumed to be unstiffened, only the theoretical buckling calculation for unstiffened shells or local buckling between stiffeners of stiffened shells applies ([1], Section 1712.1). Reference 1, Section –1712.2, Stringer Buckling and General instability, does not apply since it analyzes the global buckling of a stiffened vessel.

Theoretical Buckling Value

Local Buckling, external pressure, with no end pressure ([1], Section –1712.1.1 (b) (1)):

$$M_\phi = \frac{l_\phi}{\sqrt{(R)(t)}} = \frac{193.50}{\sqrt{(35.25)(1.25)}} = 29.15 \text{ in.}$$

$$\frac{R}{t} = \frac{35.25}{1.25} = 28.2, \quad 1.65\,\frac{R}{t} = 46.53$$

$$\Rightarrow 3.0 < M_\phi < 1.65\,\frac{R}{t}$$

Therefore,

$$C_{\theta r} = \frac{0.92}{M_\phi - 1.17} = \frac{0.92}{29.15 - 1.17} = 0.0329$$

$$\Rightarrow \sigma_{\theta cL} = \sigma_{rcL} = C_{\theta r}\,\frac{(E)(t)}{R} = 0.0329\,\frac{(27.0\times10^6)(1.25)}{35.25} = 31{,}481 \text{ psi.}$$

Capacity Reduction Factor

From Reference 1, Section –1511 (b), for local buckling of cylindrical shells, stiffened or unstiffened under Hoop Compression,

$$\alpha_{\theta L} = 0.8.$$

Plasticity Reduction Factor

The plasticity reduction factor is computed based on the formulae provided in Reference 1, Section –1611 (b) as follows.

$$\Delta = \frac{\alpha_{at}\sigma_{\theta L}}{\sigma_y} = \frac{(0.8)(31{,}481)}{43{,}300} = 0.582$$

Since $\Delta \leq 0.67$,

$$\eta_\theta = 1.$$

Allowable Buckling Stress

Elastic buckling interaction equations ([1], Section –1713.1.1 (b)) for normal conditions, hoop compression only:

$$\sigma_{ha} = \frac{(\alpha_{at})(\sigma_{heL})}{FS} = \frac{(0.8)(31{,}481)}{2} = 12{,}593 \text{ psi.}$$

For accident conditions,

$\sigma_{ra}$ = 12,593 psi. × (2.0 normal condition F.S. / 1.34 accident condition F.S.) = 18,796 psi.

Inelastic buckling interaction equations for hoop compression only ([1], Section –1713.2.1):

$$\sigma_{rc} = \eta_\theta \, \sigma_{ra} \, (1)(12{,}593) = 12{,}593 \text{ psi.}$$

For accident conditions,

$\sigma_{rc}$ = 12,593 psi. × (2.0 normal condition F.S. / 1.34 accident condition F.S.) = 18,796 psi.

2.10.5.3.3 Allowable Axial Stress Determination

The analytical method provided in ASME Code Case N-284-1 [1] is used to determine the NUHOMS®-MP197 cask allowable buckling axial stress.

Theoretical Buckling Value

Local Buckling ([1], Section –1712.1.1 (a)):

$$M_\phi = \frac{l_\phi}{\sqrt{(R)(t)}} = \frac{193.50}{\sqrt{(35.25)(1.25)}} = 29.15 \text{ in.}$$

$$\Rightarrow M_\phi \geq 1.73$$

Therefore,

$$C_\phi = 0.605$$

$$\Rightarrow \sigma_{\phi L} = C_\phi \frac{(E)(t)}{R} = 0.605 \frac{(27.0 \times 10^6)(1.25)}{35.25} = 579{,}255 \text{ psi.}$$

Capacity Reduction Factor

From reference 1, Section –1511 (a), for local buckling of cylindrical shells, stiffened or unstiffened under axial compression, $\alpha_{\phi L}$ is the larger of (1) and (2).

(1) Effect of *R/t*

$$\frac{R}{t} = \frac{35.25}{1.25} = 28.2$$

$$\Rightarrow \alpha_{\phi L} = MIN \left\{ \begin{array}{c} 1.52 - 0.473 \log_{10}\left(\frac{R}{t}\right) = 0.834 \\ \frac{300\sigma_y}{E} - 0.033 = 0.448 \end{array} \right\} = 0.448$$

(2) Effect of Length

$$M_\phi \geq 10 \Rightarrow \alpha_{\phi L} = 0.207$$

Therefore, $\alpha_{\phi L} = 0.448$.

Plasticity Reduction Factor

The plasticity reduction factor is computed based on the formulae provided in Reference 1, Section –1611 (a) as follows.

$$\Delta = \frac{\alpha_{\phi L}\sigma_{\phi L}}{\sigma_y} = \frac{(0.448)(579{,}255)}{43{,}300} = 5.993$$

Since $1.6 < \Delta < 6.25$,

$$\eta_\phi = \frac{1.31}{1+1.15\Delta} = 0.1660.$$

Allowable Buckling Stress

Elastic buckling interaction equations ([1], Section –1713.1.1 (a)) for normal conditions, axial compression only:

$$\sigma_{xa} = \frac{(\alpha_{\phi L})(\sigma_{\phi L})}{FS} = \frac{(0.448)(579{,}255)}{2} = 129{,}753\,\text{psi.}$$

For accident conditions,

$\sigma_{xa}$ = 129,753 psi. × (2.0 normal condition F.S. / 1.34 accident condition F.S.) = 193,661 psi.

Inelastic buckling interaction equations for axial compression only ([1], Section –1713.2.1):

$$\sigma_{xc} = \eta_\theta \sigma_{xa} = (0.1660)(129{,}753) = 21{,}539\ \text{psi.}$$

For accident conditions,

$\sigma_{xc}$ = 21,539 psi. × (2.0 normal condition F.S. / 1.34 accident condition F.S.) = 32,148 psi.

2.10.5.3.4 Summary of Allowable Buckling Stresses

The following table summarizes the allowable inelastic hoop and axial stresses for the transport cask inner shell for both normal conditions of transport and hypothetical accident conditions.

| | Normal Conditions of Transport | Hypothetical Accident Conditions |
|---|---|---|
| Maximum Allowable Hoop Stress (psi.) | 12,593 | 18,796 |
| Maximum Allowable Axial Stress (psi.) | 21,539 | 32,148 |

### 2.10.5.4 Finite Element Model

#### 2.10.5.4.1 Approach

A 2-dimensional axisymmetric ANSYS [3] finite element model, constructed primarily from PLANE42 elements, is used in this analysis. LINK1 elements are used to model the lid and RAM port cover bolts. Pre-load stresses of 87 ksi. and 25 ksi. are applied to the lid and RAM port cover bolts respectively (Appendix 2.10.2). Gap elements are used to model the interaction between the lead gamma shield and the cask inner and outer shells. The coefficient of sliding friction for lead on mild steel varies from 0.3 for lubricated surfaces to 0.95 for dry surfaces [4]. A lower bound coefficient of static friction of 0.25 is conservatively used for the buckling analysis.

In order to perform a collapse load analysis, as per ASME B&PV Code Appendix F [2], an elastic plastic analysis is required. The material properties of the lid, bottom, inner shell, and outer shell of the transport cask are modeled with bilinear stress-strain curves, while the lead material is modeled with a multilinear stress-strain curve.

The neutron shield, shield shell, trunnions and bearing block are not included in the model. The effect of the unmodeled weight is accounted for by increasing the density of the outer shell in the neutron shield region. The modified density of the outer shell in this region is computed in the following way.

The weight of the section of the outer shell, $W_{os}$, that will be given an increased density is,

$W_{os}$ = $\pi$ { [41.00 in. (outer shell o.r.)]$^2$ – [38.5 in. (outer shell i.r.)]$^2$ } × 144.0 in. (section length) × 0.29 (density) = 26,075 lb.

The weight of the entire FEM prior to density modification, $W_m$, is 128,050 lb. (Section 2.2). The actual calculated weight of the transport cask, $W_{tc}$, is 150,027 lb. (Section 2.2). However, a conservative weight of 150,320 lb. is used. Therefore, the modified density used in this analysis, $\rho_m$, is

$$\rho_m = \frac{W_{os} + (W_{tc} - W_m)}{\pi(41.00^2 - 38.50^2)\times 144} = \frac{26{,}075 + (150{,}320 - 128{,}050)}{\pi(41.00^2 - 38.50^2)\times 144} = 0.538 \text{ lb.in.}^{-3}$$

2.10.5.4.2 Lid End Drop Boundary Conditions

The weights of the transport cask internals and bottom impact limiter are accounted for by applying equivalent pressures. The actual weights of the transport cask internals and bottom impact limiter, including the thermal shield, are 88,390 lb. and 14,085 lb. respectively. The weights of the transport cask internals and bottom impact limiter, used in this analysis, are conservatively increased to 88,500 lb. and 14,200 lb. respectively. The pressure equivalent to the weight of the internals, $P_i$, is,

$$P_i = 88{,}500 / [\,\pi \times 34.00^2 \text{ (cavity inner radius [2])}\,] = 24.3689 \text{ psi.}$$

The pressure equivalent to the weight of the bottom impact limiter, including the thermal shield, $P_{bil}$, is,

$$P_{bil} = 14{,}200 / [\,\pi \times 40.50^2 \text{ (cask outer radius [2])}\,] = 2.7577 \text{ psi.}$$

The reaction pressure at the top end of the cask in the lid region is made equivalent to the weight of the lid plus the weight of the internals. The reaction pressure at the top end of the cask in the flange region is made equivalent to the weight of the entire model plus the weight of the bottom impact limiter minus the weight of the lid. The reaction pressure at the lid, $R_l$, is,

$$R_l = \frac{88{,}500 + \pi(34^2)(4.50)(0.29)}{\pi(34^2)} = 25.67 \text{ psi.}$$

The reaction pressure at the flange, $R_f$, is,

$$R_f = \frac{150{,}320 + 14{,}200 - \pi(34^2)(4.50)(0.29)}{\pi[(37.34^2 - 34.00^2) + (40.50^2 - 37.65^2)]} = 110.32 \text{ psi.}$$

These reaction pressures are applied to the finite element model and then adjusted slightly for each load case in order to balance the reaction forces at the boundary conditions.

Symmetry displacement boundary conditions are applied along the y-axis of the 2-dimensionsal axisymmetric model. A single node along the y-axis of the model at the bottom (non-impact) end of the cask is held in the axial direction. An inertial load of 100gs in the negative y-direction is also applied to the model. A plot of the finite element model and boundary conditions for the lid end drop load case is provided in Figure 2.10.5-1.

2.10.5.4.3 Bottom End Drop Boundary Conditions

The weights of the transport cask internals and top impact limiter are also accounted for by applying equivalent pressures. The actual weight of the top impact limiter is 13,782 lb. The weight of the top impact limiter used in this analysis is conservatively increased to 13,900 lb. The pressure equivalent to the weight of the internals, $P_i$, is,

$$P_i = 88{,}500 / [\, \pi \times (34.00^2 - 8.75^2) \text{ (cavity inner radius)} \,] = 26.0973 \text{ psi.}$$

The pressure equivalent to the weight of the top impact limiter, $P_{til}$, is,

$$P_{til} = \frac{13{,}900}{\pi[37.34^2 + (40.50^2 - 37.65^2)]} = 2.7362 \text{ psi.}$$

The reaction pressure at the bottom end of the cask in the central region is made equivalent to the weight of the bottom plus the weight of the internals. The reaction pressure at the bottom end of the cask in the outer region is made equivalent to the weight of the entire model plus the weight of the top impact limiter minus the weight of the bottom. The reaction pressure in the center region, $R_c$, is,

$$R_c = \frac{88{,}500 + \pi(34^2)(6.50)(0.29)}{\pi(34^2)} = 26.25 \text{ psi.}$$

The reaction pressure at the outer edge, $R_o$, is,

$$R_o = \frac{150{,}320 + 13{,}900 - \pi(34^2)(6.50)(0.29)}{\pi(40.50^2 - 34.00^2)} = 103.45 \text{ psi.}$$

These reaction pressures are applied to the finite element model and then adjusted slightly for each load case in order to balance the reaction forces at the boundary conditions.

Symmetry displacement boundary conditions are applied along the *y*-axis of the 2-dimensionsal axisymmetric model. A single node along the *y*-axis of the model at the lid (non-impact) end of the cask is held in the axial direction. An inertial load of 100*g*s in the positive *y*-direction is also applied to the model. A plot of the finite element model and boundary conditions for the bottom end drop load case is provided in Figure 2.10.5-2.

2.10.5.4.4 Thermal Loads

Two thermal load cases are applied to each drop orientation load case, yielding a total of four load combinations. The two temperature distributions applied correspond to the 100° F. and -20° F ambient temperature environments. The temperature distributions applied to the finite element model for both the 100° F hot environment condition and the -20° F cold environment condition are taken from Chapter 3.

### 2.10.5.5 FEA Results

Stress intensities and displacement patterns for the four load combinations are shown Figures 2.10.5-3 through 2.10.5-6.

#### 2.10.5.5.1 Collapse Load Determination

As per paragraph F-1340 [2], the acceptability of a component may be demonstrated by collapse load analysis. The allowable collapse load shall not exceed 100% of plastic analysis collapse load ([2], F-1341.3). The plastic analysis collapse load is defined as that determined by plastic analysis according to the criteria given in II-1430 ([2], F-1321.6(c)).

Using the methodology described in II-1430 ([2], F-1321.6(c)) (see Figures 2.10.5-7 through 2.10.5-10), the allowable collapse loads are determined. Since the load-displacement curve taken from ANSYS does not cross the line of slope $\phi$, for all load combinations, up to the 100 *g* load step, the collapse load is determined to be >100 *g*s.

#### 2.10.5.5.2 Maximum Axial and Hoop Stresses

The maximum axial and hoop stresses, in the inner shell, at the load step corresponding to 75 *g*s, is extracted from the ANSYS results files for all four load combinations. These stresses are compared to the allowable axial and hoop stresses computed above using the methodology provided in ASME Code Case N-284-1 [1].

2.10.5.5.3 Summary of Results

The following table summarizes the maximum allowable collapse load and the maximum calculated and allowable hoop and axial stresses generated in the inner shell for all four load combinations analyzed.

| Load Combination | Collapse Load | Stress Category | Maximum Stress (psi.) | Allowable Buckling Stress (psi.) |
|---|---|---|---|---|
| 75*g* Lid End Drop, Hot Environment | >100 *gs* | Axial Stress | 24,756 | 32,148 |
| | | Hoop Stress | 10,677 | 18,796 |
| 75*g* Lid End Drop, Cold Environment | > 100 *gs* | Axial Stress | 17,808 | 32,148 |
| | | Hoop Stress | 5,386 | 18,796 |
| 75*g* Bottom End Drop, Hot Environment | >100 *gs* | Axial Stress | 26,603 | 32,148 |
| | | Hoop Stress | 12,594 | 18,796 |
| 75*g* Bottom End Drop, Cold Environment | >100 *gs* | Axial Stress | 22,645 | 32,148 |
| | | Hoop Stress | 15,934 | 18,796 |

2.10.5.5.4 Elastic Buckling Stress Interaction Check

Code Case N-284, Section –1713.1 [1] details the methodology used to evaluate the combination of elastic axial and hoop stresses through the use of interaction equations. These relationships must be satisfied for all $\eta_i$.

Since the combination of the 30 foot end drop with the normal condition temperature load is considered an accident condition, a Factor of Safety (FS) of 1.34 is used ([1], Section –1400 (c)).

For all load combinations evaluated above, the calculated axial stress is greater than the calculated hoop stress. Therefore, for all load combinations, the ratio of axial to hoop stress, $K \geq 0.5$. Consequently, the following equation is considered.

$$0.5\sigma_{ha}\frac{t_\theta}{t_\phi} = (0.5)(18{,}796)\left(\frac{1.25}{1.25}\right) = 9{,}398 \text{ psi.}$$

An interaction check is required, since the calculated axial stress, $\sigma_\phi$, is greater than the above expression for all load combinations.

Consequently, the following interaction equation must hold ([1], -17131.1 (b)).

$$\frac{\sigma_\phi - 0.5\sigma_{ha}\,{}^{t_\theta}\!/_{t_\phi}}{\sigma_{xa} - 0.5\sigma_{ha}\,{}^{t_\theta}\!/_{t_\phi}} + \left(\frac{\sigma_\theta}{\sigma_{ha}}\right)^2 \leq 1.0$$

The left hand side of this interaction equation is tabulated below for the four load combinations considered.

| Load Combination | Interaction Check |
|---|---|
| Lid End Drop, Hot Environment | $0.406 \leq 1.0$ √ |
| Lid End Drop, Cold Environment | $0.128 \leq 1.0$ √ |
| Bottom End Drop, Hot Environment | $0.542 \leq 1.0$ √ |
| Bottom End Drop, Cold Environment | $0.791 \leq 1.0$ √ |

The interaction inequality holds for all load combinations.

### 2.10.5.5.5 Inelastic Buckling Stress Interaction Check

Code Case N-284, Section –1713.2 [1] details the methodology used to evaluate the combination of inelastic axial and hoop stresses through the use of interaction equations. These relationships must be satisfied when any of the values of $\eta_i < 1$. However, no interaction equations are given for meridional (axial) plus hoop compression, because it is conservation to ignore interaction of the two stress components when buckling is inelastic [1].

### 2.10.5.6 Conclusions

Based on the following results, the inner shell of the NUHOMS®-MP197 cask will not buckle during the accident condition end drop:

- The allowable collapse load, determined using the methodology described in ASME B&PV Code Appendix F [2], is greater than 100 gs, for all load combinations.
- The maximum calculated hoop and axial stresses in the inner shell, generated by the 75 *g* end drop, are less than the allowable axial and hoop stresses computed above using the methodology provided in ASME Code Case N-284-1 [1], for all load combinations.
- All interaction relations, provided in ASME Code Case N-284-1 [1], for combination of axial and hoop stresses are also satisfied.

2.10.5.7 References


1. Cases of ASME Boiler and Pressure Vessel Code, Case N-284-1, *Metal Containment Shell Buckling Design Methods*, Section III, Division 1, Class MC, 1998.

2. American Society of Mechanical Engineers, ASME Boiler and Pressure Vessel Code, Section III, along with appendices, 1998 including 1999 Addendum.

3. ANSYS User's Manual, Rev 5.6.

4. Baumeister & Marks, *Standard Handbook for Mechanical Engineers*, 7th Edition.

5. American Society of Mechanical Engineers, ASME Boiler and Pressure Vessel Code, Section II, Part D, 1998, including 1999 addenda.

6. American Society of Mechanical Engineers, ASME Boiler and Pressure Vessel Code, Section II, Part A, 1998, including 1999 addenda.

7. *An Assessment of Stress-Strain Data Suitable for Finite-Element Elastic-Plastic Analysis of Shipping Containers*, NUREG/CR-0481.

8. *Cask Design Guide*, ORNL-NSIC-68, February 1970.

9. *A Survey of Strain Rate Effects for some Common Structural Materials Used in Radioactive Material Packaging and Transportation Systems*, U.S. Energy Research and Development Administration, Battelle Columbus Laboratories, August 1976.

Figure 2.10.5-1
NUHOMS®-MP197 cask 2-Dimensional Finite Element Model
with Lid End Drop Boundary Conditions

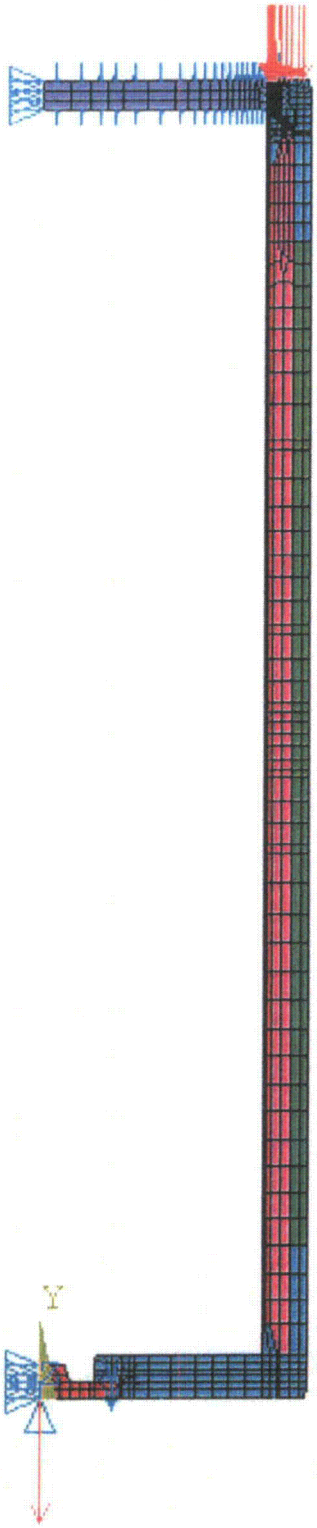

Figure 2.10.5-2
NUHOMS®-MP197 cask 2-Dimensional Finite Element Model
with Bottom End Drop Boundary Conditions

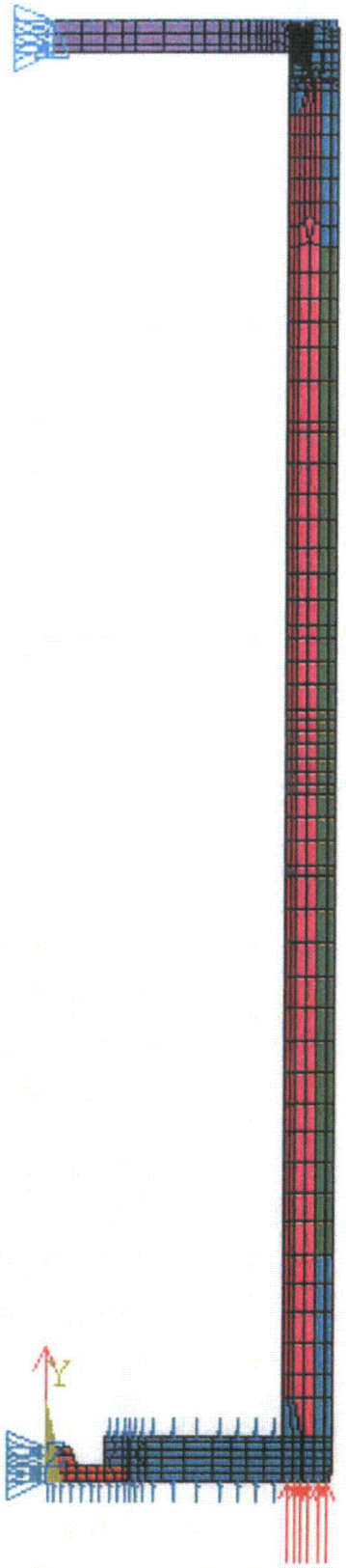

Figure 2.10.5-3
Stress Intensity – Lid End Drop, Hot Environment

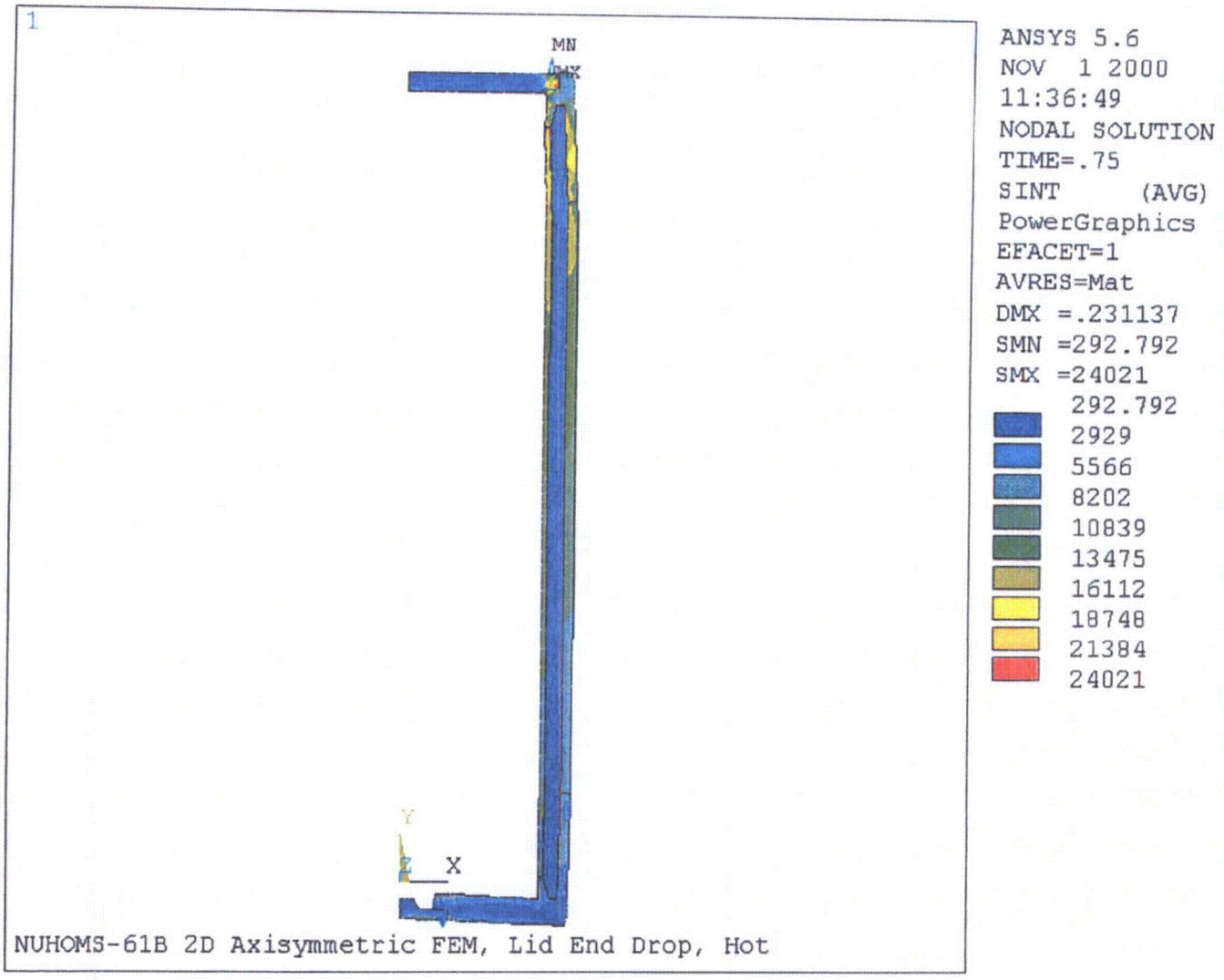

Figure 2.10.5-4
Stress Intensity – Lid End Drop, Cold Environment

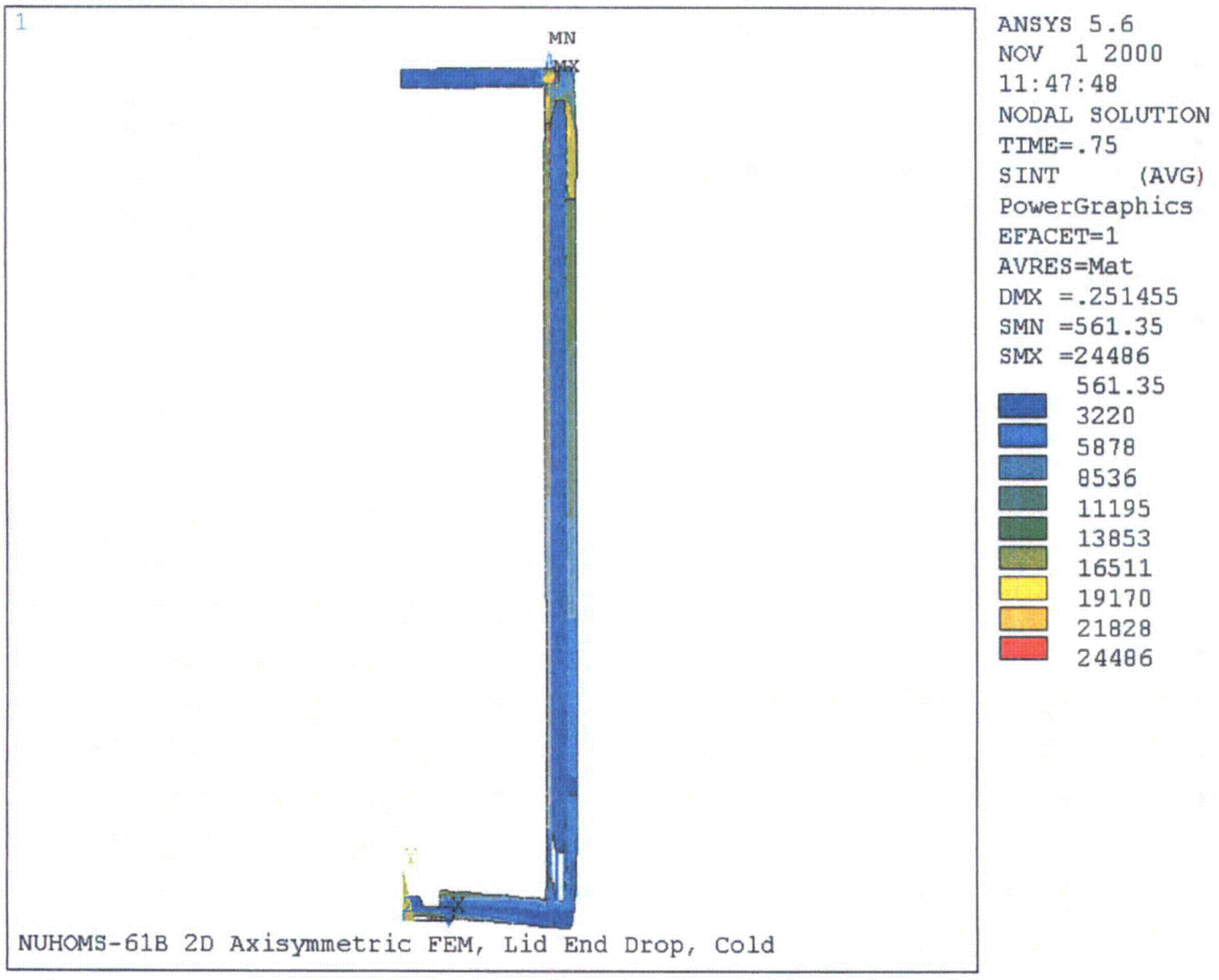

Figure 2.10.5-5
Stress Intensity – Bottom End Drop, Hot Environment

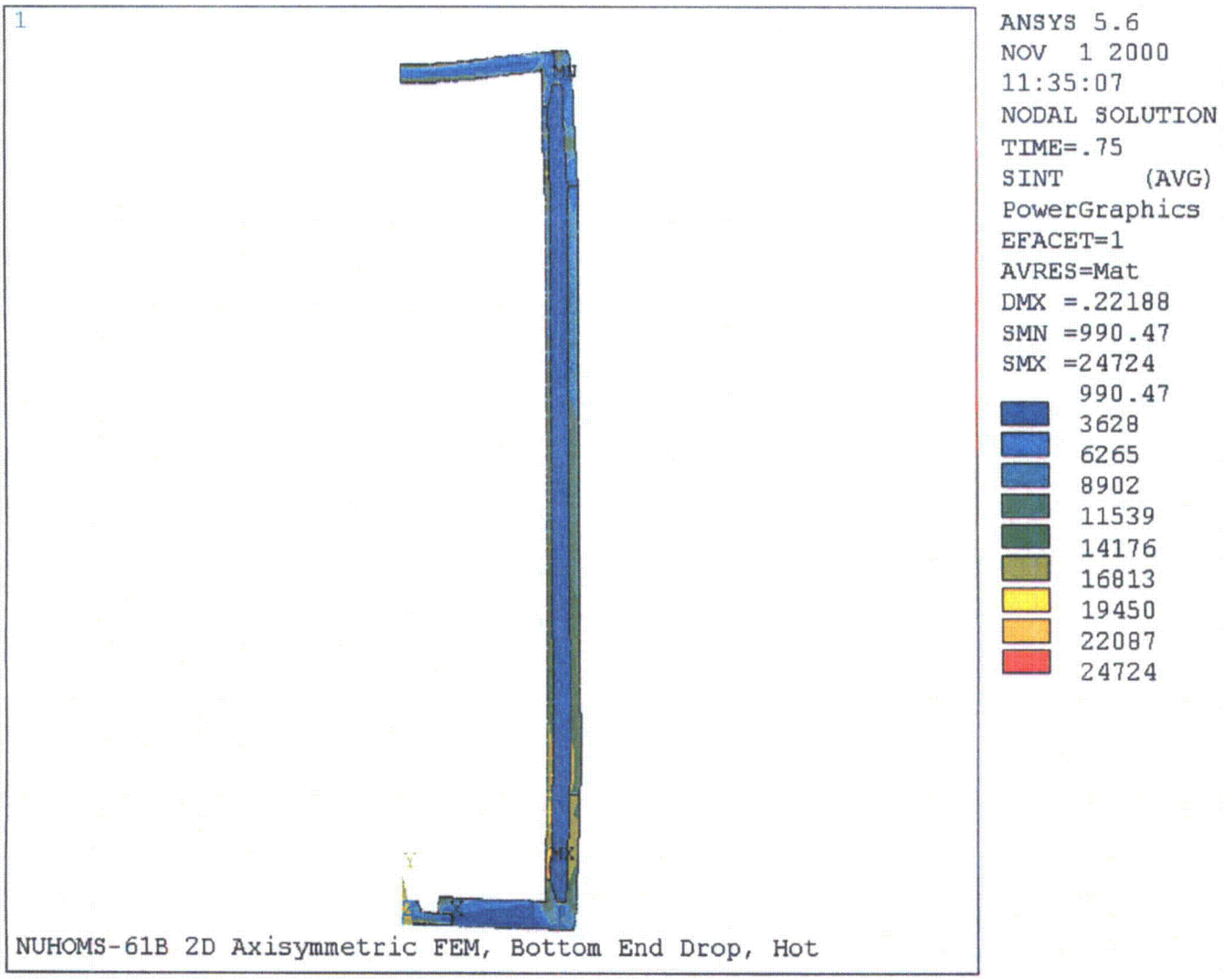

Figure 2.10.5-6
Stress Intensity – Bottom End Drop, Cold Environment

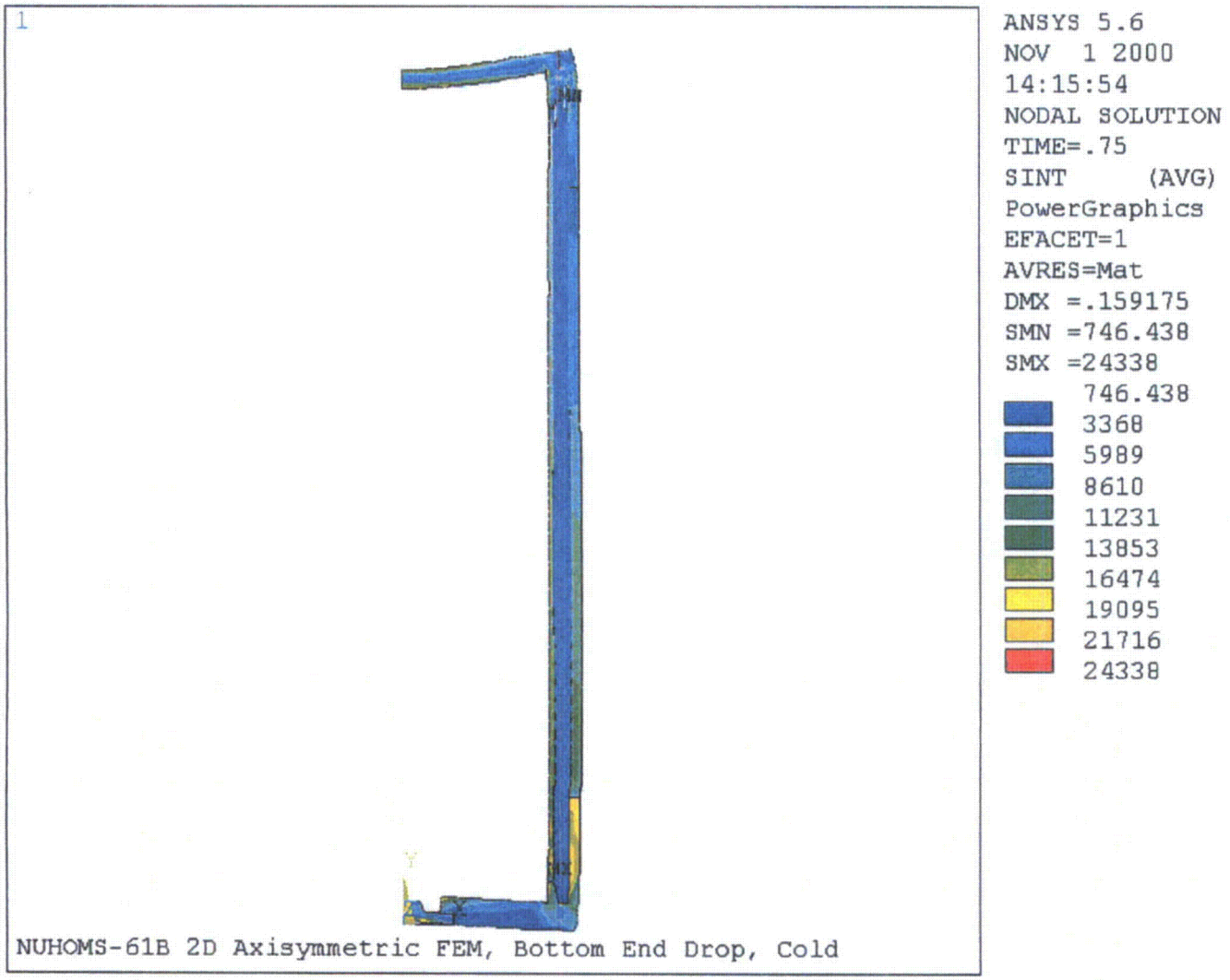

Figure 2.10.5-7
Collapse Load Determination – Lid End Drop, Hot Environment

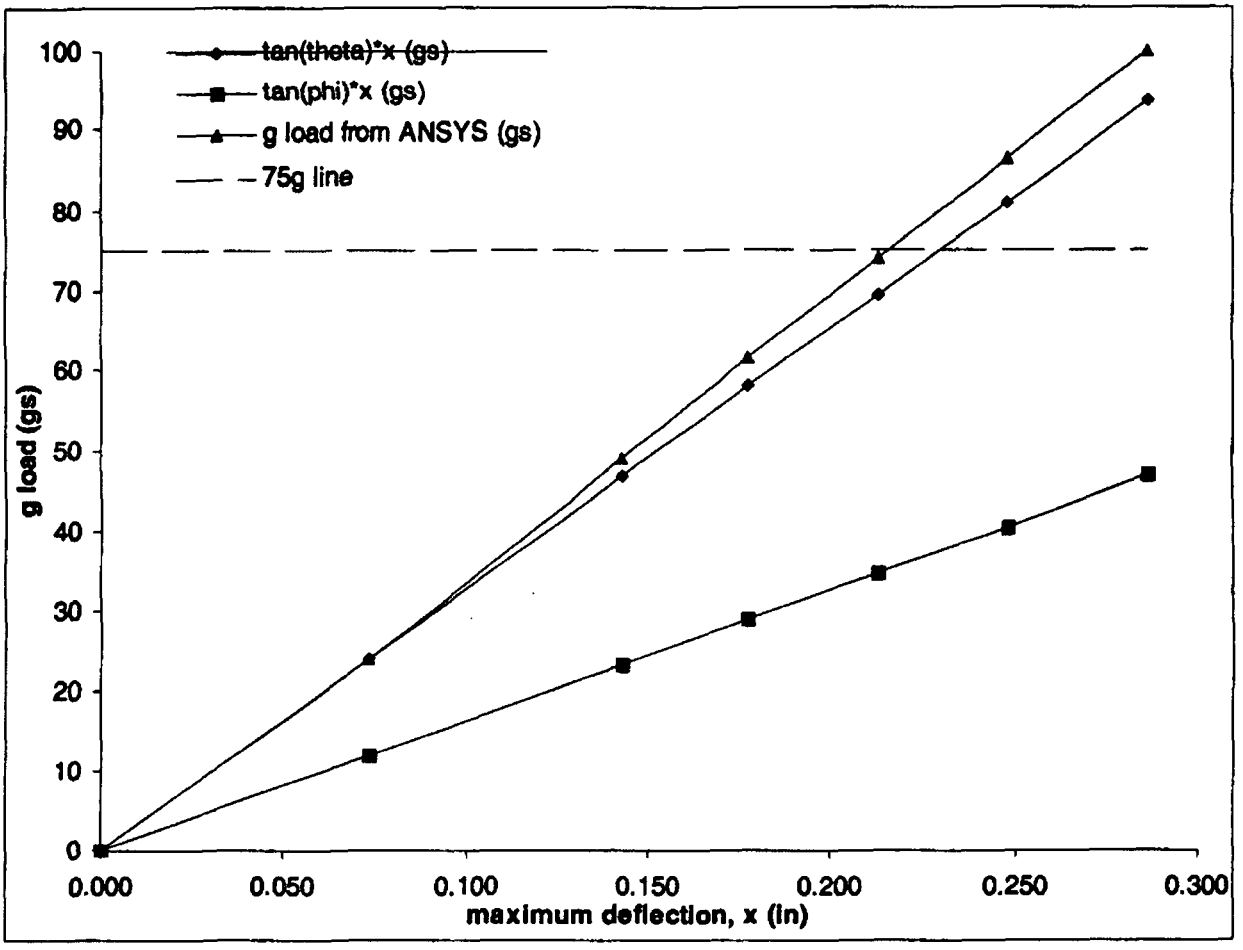

Figure 2.10.5-8
Collapse Load Determination – Lid End Drop, Cold Environment

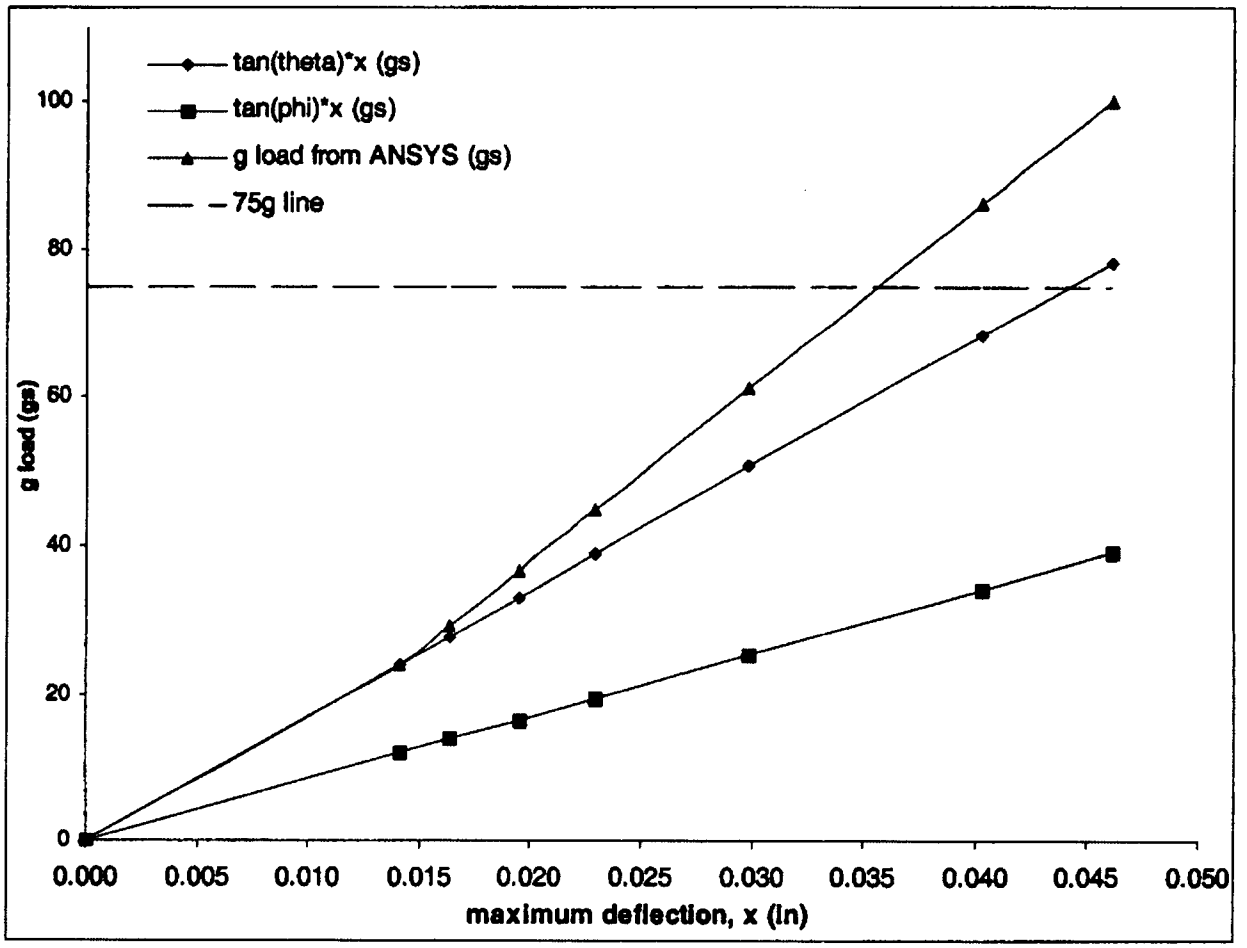

Figure 2.10.5-9
Collapse Load Determination – Bottom End Drop, Hot Environment

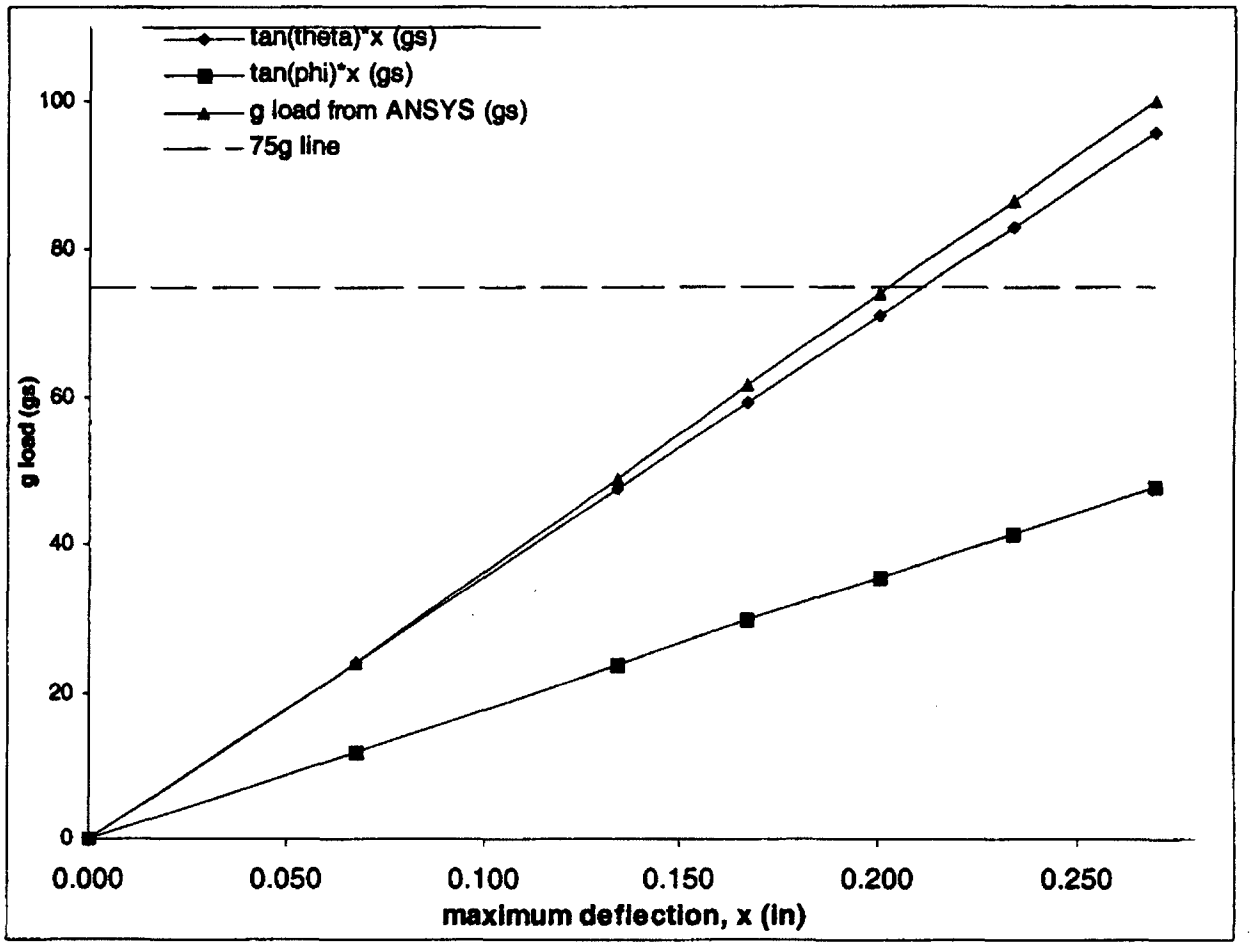

Figure 2.10.5-10
Collapse Load Determination – Bottom End Drop, Cold Environment

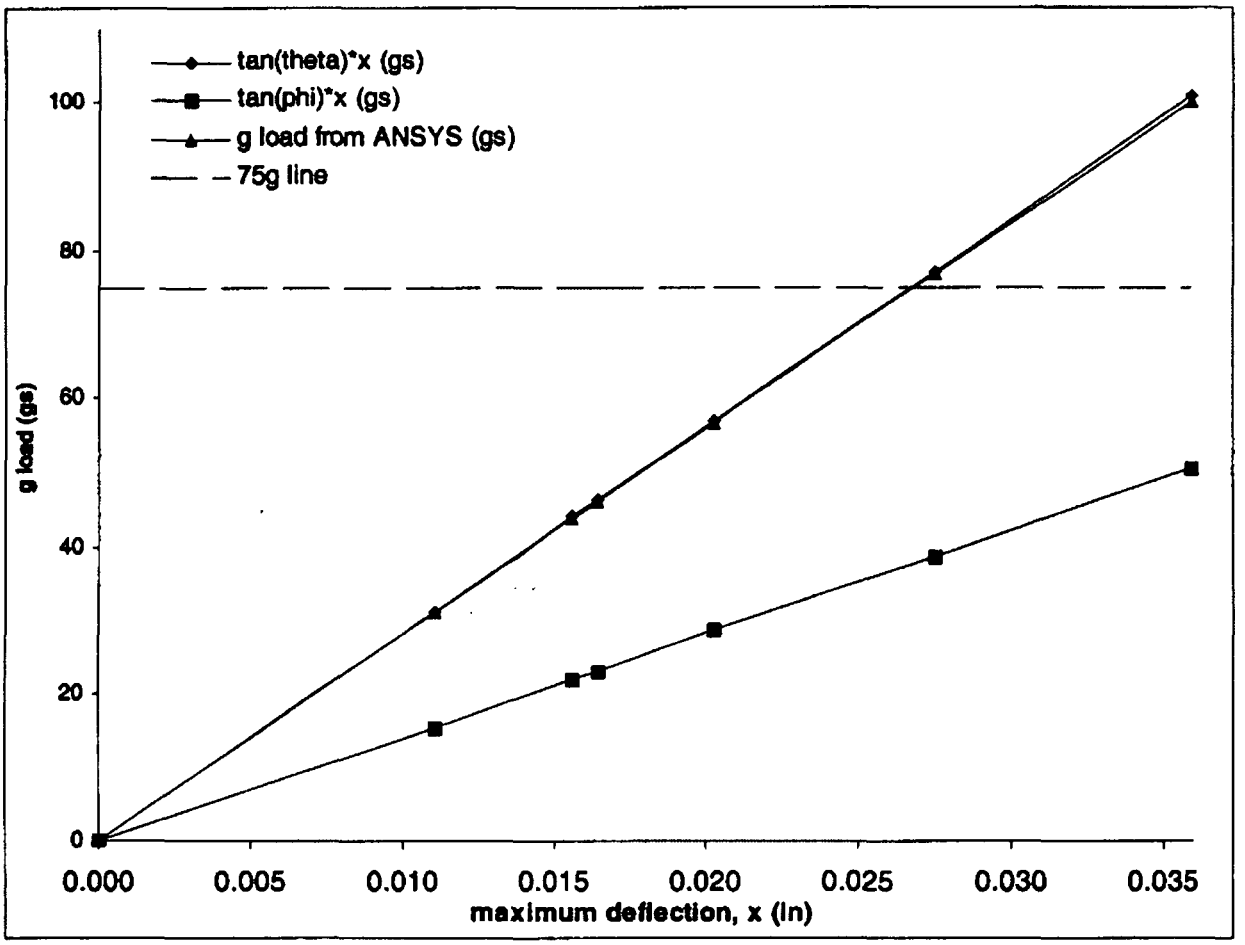

APPENDIX 2.10.6

TABLE OF CONTENTS



LIST OF FIGURES

# APPENDIX 2.10.6

# DYNAMIC AMPLIFICATION FACTOR DETERMINATION

## 2.10.6.1 Introduction

The purpose of the analysis presented in this appendix is to determine the dynamic amplification factor (DAF) for the NUHOMS®-MP197 package internals. The DAF accounts for the rigid body acceleration difference between the NUHOMS®-MP197 cask & NUHOMS®-61BT Canister and Basket during the cask drop events.

The dynamic amplification factor is taken from the results shown in Figure 2.10.6-1, which is a reproduction of figure 2.15 of NUREG/CR-3966 [1], and is a function of the ratio of the half-sine-wave impulse duration to the natural period of the structure. The dynamic amplification factor based on a half sine wave impulse is conservative relative to that of a triangular pulse.

The two components of the NUHOMS®-MP197 package internals with the longest and most significant natural periods are the Fuel Basket (with fuel assemblies) and the Canister. Each component is modeled separately. The Dynamic Amplification Factor used for the entire structure is conservatively taken to be the higher of the two individual dynamic amplification factors computed.

Two load cases will be evaluated in this analysis, one due to longitudinal loading, and one due to transverse loading. During an end drop, the fundamental natural periods of the NUHOMS®-61BT DSC components are taken to be that of simply supported cylindrical shells without axial constraint, under longitudinal vibration. The masses of the basket components and fuel assemblies are conservatively lumped together, so that an average density is used. During a side drop, the fundamental natural period of the NUHOMS®-61BT canister shell is taken to be that of a cylinder in an ovalling mode and a simply supported cylindrical shell without axial constraint.

Notation

The notation used in this analysis are taken from Blevins [2], and are as follows.

- $E$, Modulus of Elasticity, (psi).
- $f_1, f_{11}$, Fundamental natural frequency, (Hz.).
- $I$, Moment of inertia of the beam, (in.$^4$).
- $L$, Length of beam or cylindrical shell, (in.).
- $m$, Mass per unit length of the beam, (lbm.in.$^{-1}$).
- $\mu$, Mass density, (lbm.in.$^{-3}$).
- $\nu$, Poisson's ratio.
- $R$, Outer radius of the cylindrical shell, (in.).

2.10.6.2 Analysis for End Drop

The fundamental natural frequency of a simply supported cylindrical shell under axial vibration simplifies to that of a uniform beam, free axially at both ends. The fundamental natural frequency of a uniform beam free at both ends, under longitudinal vibration is as follows. ([2], p. 183, Table 8-16, frame 1)

$$f_1 = \frac{\lambda_1}{2\pi L}\left(\frac{E}{\mu}\right)^{1/2}$$

Where $\lambda_1 = \pi$.

2.10.6.2.1 Basket with Fuel Assemblies

The maximum normal conditions of transport fuel basket temperature is 578° F (Chapter 3). However, the basket material properties are taken at the average temperature of the basket, which is roughly 500° F. The modulus of elasticity is taken to be that of SA-240 Type 304 stainless steel at 500° F, or $25.8 \times 10^6$ psi. [3], since the stainless steel tubes and plates comprise the majority of the basket structure. The length of the basket is 164.00 inches.

Based on a stainless steel density of 0.29 lb. $in.^{-3}$ and an aluminum density of 0.1 lb. $in.^{-3}$ and the following component weights (Section 2.2), the average mass density, $\mu$, is calculated in the following way.

| Steel Components | Weights (lb.) |
|---|---|
| 61 fuel compartment tubes | 9,402 |
| 4 Outer 2 × 2 boxes | 1,038 |
| 5 Outer 3 × 3 boxes | 1,966 |
| type 1 Support Rails | 3,320 |
| type 2 Support Rails | 2,031 |
| Hold Down Ring | 940 |
| Inserts | 98 |
| Total Weight | 18,795 |

Steel Volume = 18,795/0.29 = 64,810 $in^3$

| Aluminum Components | Weights lb. |
|---|---|
| Aluminum Plates | 859 |
| Poison Plates | 3,264 |
| Total Weight | 4,123 |

Aluminum Volume = 4,123/0.1 = 41,230 $in^3$

Average Weight Density = 18,795 + 4,123/(64,810 + 41,230) = 0.216 $lb.in^{-3}$

Average mass density, $\mu = \frac{0.216}{386.4} = 0.000559$ lbm. in.$^{-3}$

Therefore,

$$f_1 = \frac{\pi}{2\pi(164)}\left(\frac{25.8\times10^6}{0.000559}\right)^{1/2} = 655\,\text{Hz.}$$

The natural period of the fuel compartments is then $1/f_1$ or T = 0.00153 s.

2.10.6.2.2 Canister Shell

The maximum normal conditions of transport canister temperature is 388° F (Chapter 3). However, the basket material properties are conservatively taken at 400° F. The canister shell is constructed from SA-240 Type 304, which has a modulus of elasticity of $26.5\times10^6$ psi. at 400° F [3]. The length of the canister is 195.92 inches.

The average mass density, $\mu$, is calculated in the following way.

Weight of the entire Canister = 22,467 lb. (Section 2.2)

Volume of equivalent cylinder = $(\pi/4)(67.25^2 - 66.25^2)(195.92) = 20{,}542$ in.$^3$

Average mass density, $\mu = \frac{22{,}467}{(386.4)(20{,}542)} = 0.00283$ lbm. in.$^{-3}$

Therefore,

$$f_1 = \frac{\pi}{2\pi(195.92)}\left(\frac{26.5\times10^6}{0.00283}\right)^{1/2} = 247\,\text{Hz.}$$

The natural period of the container shell is then $1/f_1$ or $T = 0.004$ s.

2.10.6.2.3 End Drop Dynamic Amplification Factor Determination

From the impact limiter analysis performed in Appendix 2.10.8, the duration of an end drop impact, $t_1$, is in the range of 0.037 seconds to 0.047 seconds, depending on the impact limiter wood properties. The minimum value of impact duration, $t_1$ = 0.037 seconds is used in DAF evaluation which is conservative. Therefore the ratio $t_1/T$ is 0.037/0.004 or 9.25. Consequently, the DAF for the basket and canister for end drop event, based on figure 2.10.6-1, is conservatively taken to be 1.10.

2.10.6.3 Analysis for Side Drop

2.10.6.3.1 Basket with Fuel Assemblies

ANSYS Modal Analysis

A finite element modal analysis is performed in order to compute the natural frequency of the NUHOMS®-61BT basket when subjected to transverse loads. The ANSYS finite element model described in Appendix 2.10.2 is used to perform the analysis. However, the canister shell and gap elements are removed from the model and the boundary conditions are applied directly to the rails. The canister shell is removed from the model, because the coupling of shell nodes to rail nodes would result in a stiffer structure and higher natural frequencies, which is less conservative.

The material properties used are based on an average basket temperature of 500° F. Weight densities are changed to mass densities ($\rho_m = \rho_w / 386.4$). The weight of the fuel assemblies and poison plates is accounted for by increasing the density of the stainless steel basket plates.

The basket is supported radially at the periphery, over a 180° section. Since an ANSYS modal analysis requires a linear model, all gap elements are replaced by couplings in the appropriate direction. The basket finite element model, including boundary conditions and couplings, is shown on Figure 2.10.6-2.

Modal Analysis Results

The natural frequencies resulting from the first 4 harmonics, computed by ANSYS, are tabulated below.

| Mode | Frequency (Hz.) |
|---|---|
| 1 | 125.53 |
| 2 | 139.95 |
| 3 | 142.11 |
| 4 | 142.40 |

Analytical Verification of Results

As an order of magnitude check, the frequency of the fundamental mode of vibration for the basket is calculated below and compared to the frequency of the first mode computed by ANSYS. The deformed shape of the first basket mode can be simplified to that of a single basket plate acting as a simply support beam under a uniform load. Roark [5], page 369, case 6, provides an equation for the natural frequency of a simply support beam with uniform *W*.

$$f = \frac{3.55}{\sqrt{\frac{5WL^3}{384EI}}}$$

Where, $W$ is the uniform load applied the beam, 4.299 lbs. [705 lb. per assembly / 164 in. per unit length of the basket], $L$ is the span of the basket plate, 6.22 in., $E$ is the modulus of elasticity of the beam, $25.8\times10^6$ psi., and $I$ is the beam moment of inertia, 0.000288 in$^4$. [$2\times(1\times0.12^3/12)$]. Therefore,

$$f = \frac{3.55}{\sqrt{\frac{5(4.299)(6.22)^3}{384(25.8\times10^6)(0.000864)}}} = 84\,\text{Hz.}$$

This value is somewhat lower than the value computed by ANSYS for the basket. The actual support conditions for the basket plate are somewhere in between simple-simple and fixed-fixed. A fixed-fixed beam's fundamental frequency is approximately double ($\sqrt{5}\times 84 = 188$ Hz.) that of a simple-simple supported beam. The ANSYS solution of 126 Hz. is somewhere between the solutions to the simple-simple and fixed-fixed analytical equations.

Conclusions

The finite element modal analysis reveals that the fundamental natural frequency of the NUHOMS®-61BT basket (with fuel) when subjected to a side drop acceleration $f_1 = 125.5$ Hz. The natural period of the basket is then $1/f_1$ or $T = 0.00797$ s.

2.10.6.3.2 Canister Shell

Two natural frequencies, each associated with a distinct mode of vibration, are evaluated for the canister. These two modes are the canister shell ovalling and bending modes

Canister Shell Ovalling Mode

The fundamental natural frequency of the canister shell ovalling (Radial-Axial) mode is determined assuming the cylindrical shell is simply supported without axial constraint. The natural frequency of the cylindrical shell ovalling mode is given by the following ([3], p. 305, Table 12-2, Frame 5).

$$f_{ij} = \frac{\lambda_{ij}}{2\pi R}\left(\frac{E}{\mu(1-\nu^2)}\right)^{1/2}$$

Where $L$ is taken to be the length between the top and bottom shield plugs, which is roughly 180 in, $E = 26.5\times10^6$ psi. (for SA-240 Type 304 stainless steel at 400° F [3]), $R$ is the average shell

radius, 33.375 in., $\nu$ is Poisson's ratio, which is 0.305 for stainless steel ([6], p. 5-6), and $\mu$ = 0.29/386.4 = 0.000751 lbm. in$^{-3}$.

$$\lambda_{ij} = \frac{\left\{(1-\nu^2)(j\pi R/L)^4 + (h^2/12R^2)\left[i^2+(j\pi R/L)^2\right]^4\right\}^{1/2}}{(j\pi R/L)^2 + i^2}$$

For the fundamental mode, $i = 2$ and $j = 1$.

$$\lambda_{ij} = \frac{\left\{(1-.305^2)(\pi\times 33.375/180)^4 + (0.5^2/12\times 33.375^2)\left[2^2+(\pi 33.375/180)^2\right]^4\right\}^{1/2}}{(\pi 33.375/180)^2 + 2^2} = 0.07679$$

$$f_{21} = \frac{0.07679}{2\pi\times 33.375}\left(\frac{26.5\times 10^6}{0.000751(1-0.305^2)}\right)^{1/2} = 72.2 \text{ Hz}$$

The natural period of the canister is then $1/f_{21}$ or $T = 0.0138$ s.

Canister Beam Bending Mode

The bending mode of the canister shell is taken to be most significant vibration mode of during a side drop event. The fundamental natural frequency of the bending mode of the canister is taken to be that of a simply supported cylindrical shell without axial constraint. This natural frequency is computed with and without the basket and fuel weights included.

Canister Beam without basket weight:

Since $L/(jR)$ = 180/(1×33.375) = 5.39 < 8.00, simple beam theory applies [2]. The fundamental natural frequency of the bending mode of a uniform beam pinned at both ends is as follows ([2], p. 108, Table 8-1, Frame 5).

$$f_1 = \frac{\lambda_1^2}{2\pi L^2}\left(\frac{EI}{m}\right)^{1/2}$$

Where, $E = 26.5\times 10^6$ psi., $\lambda_1 = \pi$, and

$$I = \frac{\pi}{64}\left(d_o^4 - d_i^4\right) = \frac{\pi}{64}\left[67.25^4 - 66.25^4\right] = 58{,}399 \text{ in.}^4.$$

The mass, m, of the canister is 0.323 lbm. in$^{-1}$ (22,467 lb. / 180 in. / 386.4 in.s.$^{-2}$, Section 2.2). Therefore,

$$f_1 = \frac{\pi^2}{2\pi \times 180^2}\left(\frac{26.5\times10^6 \times 58{,}399}{0.323}\right)^{1/2} = 106.1 \text{ Hz}$$

The natural period of the canister is then $1/f_1$ or $T = 0.0094$ s.

Canister Beam with basket weight:

Since the basket structure is stiffer ($f = 125.5$ Hz) than the canister ($f = 106.1$ Hz), during a side drop, the basket will, deflect less than the canister. This will result in a two-point contact between the basket and canister (at the basket ends). As a result, one-half of the weight of the basket and fuel will act at each contact point. One contact point is close to the end of the canister and will have no effect on the canister's behavior. The second point will be at a location roughly 16 inches from the top end of the canister. The fundamental natural frequency of the bending mode of a beam pinned at both ends and with an off-center mass is as follows ([2], p. 159, Table 8-8, Frame 5).

$$f_1 = \frac{1}{2\pi}\left\{\frac{3EI(a+b)}{a^2b^2[M+(\alpha+\beta)M_b]}\right\}^{1/2}$$

where,

$$\alpha = \frac{a}{a+b}\left[\frac{(2b+a)^2}{12b^2} + \frac{a^2}{28b^2} - \frac{a(2b+a)}{10b^2}\right],$$

$$\beta = \frac{b}{a+b}\left[\frac{(2a+b)^2}{12a^2} + \frac{b^2}{28a^2} - \frac{b(2a+b)}{10a^2}\right],$$

and $a$ and $b$ are 16.0 inches and 164.0 inches respectively. The mass of the canister, $M_b$, is 22,467 lb. / 386.4 in. s.$^{-1}$ = 58.14 lbm., and the mass of ½ of the basket and fuel, $M$, is ½(22,918 lb. + 43,005 lb.) / 386.4 in. s.$^{-1}$ = 85.30 lbm.

$$\alpha = \frac{16}{16+164}\left[\frac{(2\times164+16)^2}{12(164)^2} + \frac{16^2}{28(164)^2} - \frac{16(2\times164+16)}{10(164)^2}\right] = 0.0308$$

$$\beta = \frac{164}{16+164}\left[\frac{(2\times16+164)^2}{12(16)^2} + \frac{164^2}{28(16)^2} - \frac{164(2\times16+164)}{10(16)^2}\right] = 3.3721$$

$$f_1 = \frac{1}{2\pi}\left(\frac{3\times26.5\times10^6\times58{,}399(16+164)}{16^2\times164^2[85.30+(0.0308+3.3721)58.14]}\right)^{1/2} = 104.2 \text{ Hz}$$

The natural period of the canister is then $1/f_1$ or $T = 0.0096$ s.

2.10.6.3.3 Side Drop Dynamic Load Factor Determination

From the impact limiter analysis performed in Appendix 2.10.8, the duration of impact during a side drop, $t_1$, is in the range of 0.032 seconds to 0.038 seconds, depending on the impact limiter wood properties. It is conservative to take $t_1$ to be 0.032 seconds. The ovalling mode of the canister shell is the vibration mode with the highest natural period (0.0138 s.). Therefore the minimum ratio $t_1/T$ is 0.032/0.0138, or 2.32. Consequently, the DAF for canister during a side drop event, based on figure 2.10.6-1, is conservatively taken to be 1.10.

2.10.6.4 Conclusions

Conservatively taking the maximum dynamic amplification factor computed for each component under both longitudinal and transverse vibration, the overall dynamic amplification factor for the NUHOMS®-MP197 package internals is taken to be 1.10.

2.10.6.5 References


1. *Methods for Impact Analysis of Shipping Containers*, NUREG/CR-3966, UCID-20639, LLNL, 1987.

2. Blevins, *Formulas for Natural Frequency and Mode Shape*, Krieger Publishing Company, 1995.

3. American Society of Mechanical Engineers, ASME Boiler and Pressure Vessel Code, Section II, Part D, 1998, including 1999 Addendum.

4. ANSYS User's Manual, Rev 5.6.

5. Roark, Raymond J., *Formulas for Stress and Strain*, Fourth Edition, McGraw-Hill Book Company.

6. Baumeister, T., Marks, L. S., *Standard Handbook for Mechanical Engineers*, 7th Edition, McGraw-Hill, 1967.

FIGURE 2.10.6-1
DYNAMIC LOAD FACTOR FOR HALF SINE WAVE

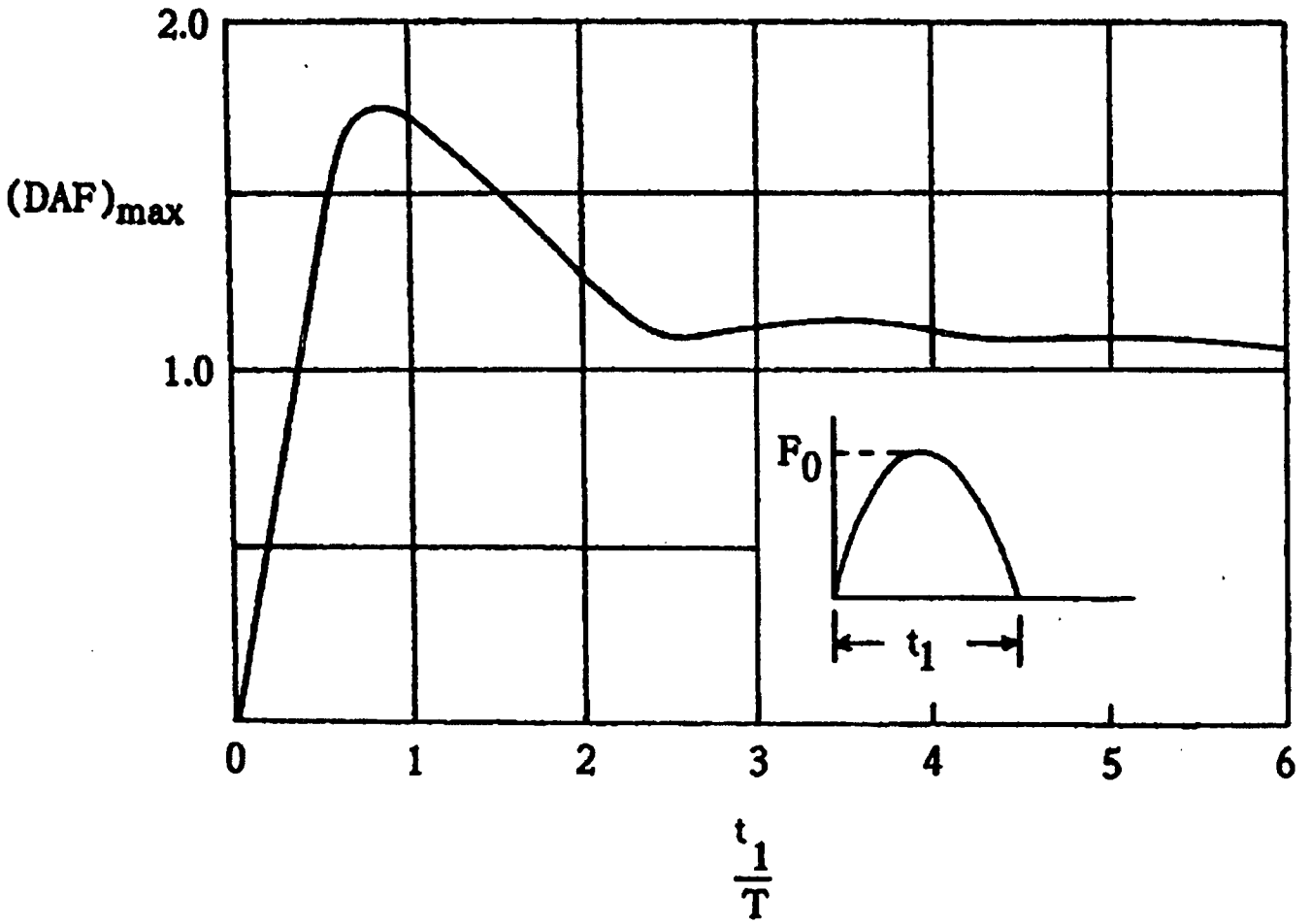


(T = Natural period of structure)

FIGURE 2.10.6-2
BASKET FINITE ELEMENT MODEL FOR MODAL ANALYSIS

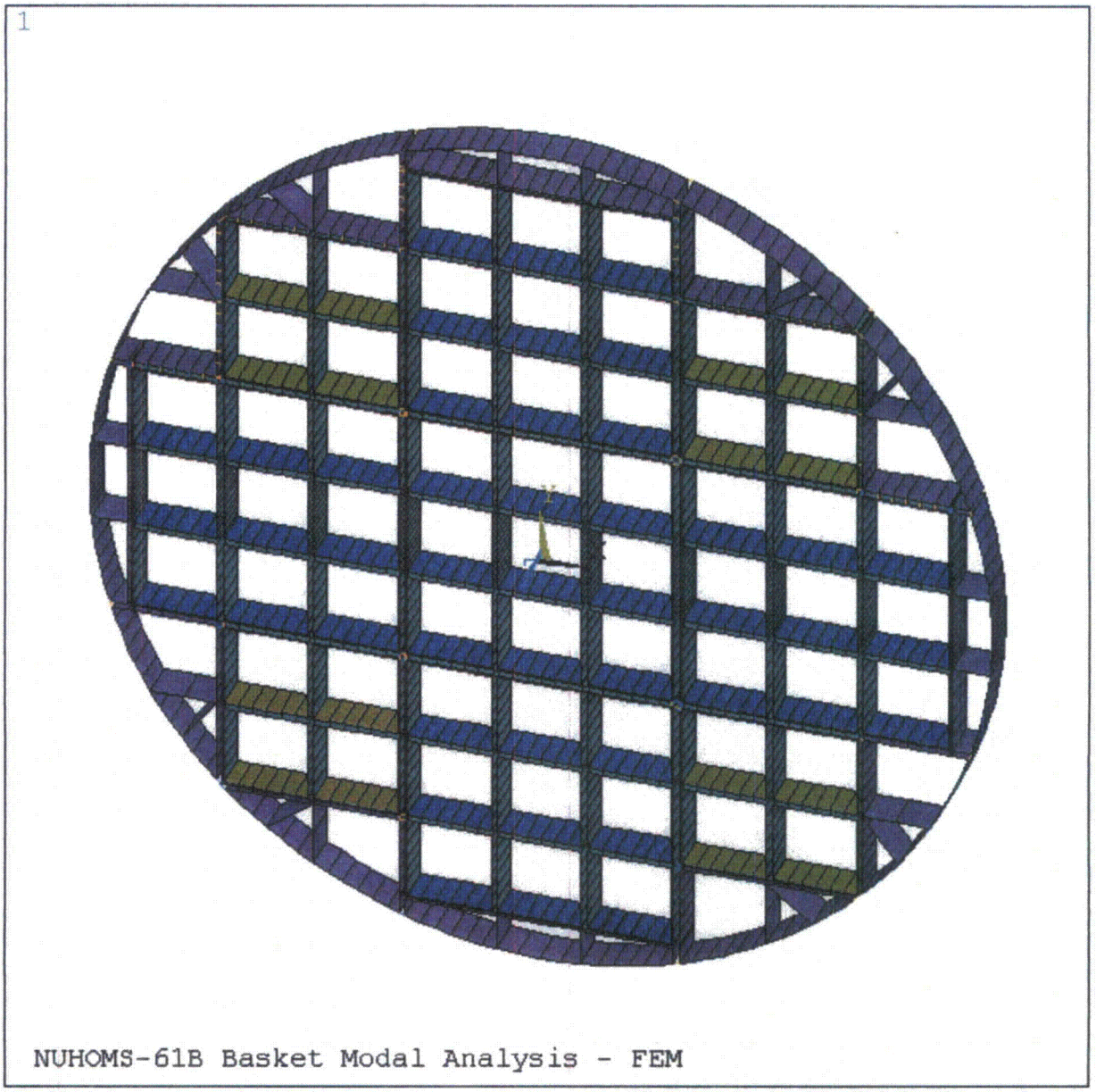

APPENDIX 2.10.7

TABLE OF CONTENTS



LIST OF TABLES



LIST OF FIGURES

# APPENDIX 2.10.7

## EVALUATION OF FUEL ASSEMBLY UNDER ACCIDENT IMPACTS

### 2.10.7.1 Introduction

This appendix evaluates the effect of NUHOMS®-MP197 cask impact (30 foot side drop or end drop) on the integrity of fuel rod cladding. The material properties of irradiated zircalloy cladding and the rod impact stress analysis approach are based on LLNL Report UCID-21246 [1]. The fracture analysis of the fuel rod cladding is based on the ASME Code, Section XI [2]. The irradiated zircalloy fracture toughness data is obtained from ASTM Special Technical Publication 551 [3]. Presented below are the analyses and results that are used to conclude that the fuel rod cladding will remain intact and retain the fuel pellets during all accident scenarios.

### 2.10.7.2 Material Properties

This section establishes the basis for assuming particular material properties. The values of some of the parameters used in the analysis are temperature dependent. The maximum temperature during the normal conditions of transport will not exceed 598° F. However, material properties are conservatively taken at 638° F. This is conservative because both yield strength and modulus of elasticity are lower at higher temperatures.

Weight Density

The weight density of both Zircalloy-2 and Zircalloy-4 is very close to the weight density of Zirconium itself. From Reference 1,

$$\rho_{tube} = 0.234 \text{ lb/in}^3$$

Young's Modulus

The Young's modulus for typical Zircalloy cladding is illustrated in Table 5 of Reference 1. Thus, at 638° F,

$$E_{tube} = 11.0 \times 10^6 \text{ psi}$$

$$E_{fuel} = 13.7 \times 10^6 \text{ psi (conservatively assume a lower value)}$$

Yield Strength

The yield strength for typical Zircalloy cladding is illustrated in Table 5 of Reference 1. Thus, at 638° F,

$$S_{yield\text{-}tube} = 83{,}710 \text{ psi}$$

2.10.7.3 30 Foot Side Drop

The fuel rod side impact stresses are computed by idealizing fuel rods as continuous beams supported at each spacer grid. Continuous beam theory is used to determine the maximum bending moments and corresponding stresses in the cladding tube. The methodology used in performing the analysis is based on work done at Lawrence Livermore National Labs [1]. The fuel gas internal pressure is assumed to be present and the resulting axial tensile stress is added to the bending tensile stress due to 75*g* load (Appendix 2.10.8). The stresses for different General Electric fuel assemblies are computed in Table 2.10.7-1. It is seen that the 35,393 psi is the highest stress and occurs in the GE9-8x8 fuel assembly. This stress is lower than the yield strength of zircalloy (83,710 psi). It is, therefore, concluded that the fuel tube will not fail and will withstand the side drop load without excessive plastic deformations. The grid supports (spacers) are expected to crush before the 75*g* load is developed and the actual tube stresses will be much lower than the above noted stress.

2.10.7.4 Bottom End Drop

In case of an end drop, the inertial forces load the rod as a column having intermediate supports at each grid support (spacer). The tube load limit is that at which the fuel rod segments between the supports become unstable.

An elastic-plastic stress analysis was performed using the ANSYS Finite Element Program [4]. A three-dimensional finite element model of the active fuel tube length was constructed using plastic PIPE20 element for cladding tube and elastic PIPE16 element for fuel. The hinge supports were modeled at each support location. The finite element model and support conditions for a typical tube model are shown in Figure 2.10.7-1. The tube and fuel nodes were coupled in *x*, *y* and *z* directions. The following material properties (at 638° F) were input as a bilinear kinematic stress-strain curve for Zircalloy cladding tube. These properties are taken from Reference 1.

Yield Strength = 83,710 psi
Ultimate Strength = 94,000 psi
Modulus of elasticity = $11.0 \times 10^6$ psi
Elongation = 1.75%
Max. elastic strain = $83,710/11.0 \times 10^6 = 0.0076$ in/in
Tangent Modulus = $(94,000 - 83,710) / (.0175 - .0076) = 1.04 \times 10^6$ psi

For fuel elements, a modulus of elasticity = $13.7 \times 10^6$ psi is conservatively used for analysis. The tube and fuel densities were modified to compensate for the extra tube length and the components which were not modeled. The calculations of equivalent tube and fuel densities are shown in Table 2.10.7-2.

In order to calculate the tube-buckling load, the large displacement option of ANSYS was used. The maximum inertia force of 200*g* was applied to the model. This load was applied gradually in a number of sub-steps. A small lateral load (0.001 lb.) was applied at the middle of the lowest segment to introduce an initial deflection and bending. The analysis stopped at the load sub-step

where the tube model became unstable and did not converge. In each case, the lowest segment became unstable as it was supporting the entire tube and fuel weights. The last converged load sub-step was taken as the plastic instability load.

The above analysis was repeated for one fuel rod of each fuel subassembly. All the input data and the resulting plastic instability loads are summarized in Table 2.10.7-2. It is seen from the above table, that GE9 8×8 fuel assembly drop is the critical as it results in the lowest plastic instability load of 128g. The allowable collapse load is calculated by using paragraph F-1340 of Reference 5.

As per paragraph F-1340 [5], the acceptability of a component may be demonstrated by collapse load analysis. The allowable collapse load shall not exceed 100% of plastic analysis collapse load ([5], F-1341.3). The plastic analysis collapse load is defined as that determined by plastic analysis according to the criteria given in Appendix II-1430 ([5], F-1321.6(c)).

Using the methodology described in Appendix II-1430 ([5], F-1321.6(c)) (see Figure 2.10.7-2), the allowable collapse loads has been determined for GE9 8×8 fuel assembly drop which is 128g. The allowable collapse loads for other fuel assemblies will be equal or higher than this load.

Since the internal pressure produces tensile stresses in the cladding, it will reduce the compressive stresses caused by the end drop impact. The pressure is therefore conservatively neglected in this analysis.

From the results in Table 2.10.7-2, it is seen that the lowest allowable tube-buckling load of 128$g$ occurs for the fuel assemblies. It may be noted that the axial stresses in fuel rods are also quite small ($128 \times 6.11 / (\pi/4)(0.400)^2 = 6{,}224$ psi). The actual end drop impact load is less than 75$g$. It is, therefore, concluded that the fuel cladding tubes will not be damaged during an end drop.

### 2.10.7.5 Brittle Fracture Evaluation

The stress intensity factor $K_I$ is calculated from tube maximum stresses under pressure and impact loads. A conservative flaw configuration is assumed in the cladding tube. Stress intensity factor for the flaw model is calculated, using the methodology given in Section XI, Article A-3000 [2]. The calculated Stress intensity factor for the flaw size should satisfy the code faulted condition criteria (Section XI, para. IWB-3612 [2]):

$$K_I < \frac{K_{Ic}}{\sqrt{2}}$$

Where, $K_I$ is the maximum applied stress intensity factor for the flaw size in faulted condition, and $K_{Ic}$ is critical fracture toughness based on fracture initiation for the corresponding crack tip temperature.

The stress intensity factor $K_I$ is calculated using the following equation (Section XI, A-3300 [2]):

$$K_1 = S_m M_m \sqrt{\frac{\pi a}{Q}} + S_b M_b \sqrt{\frac{\pi a}{Q}}$$

Where, $S_m$ and $S_b$ are the membrane and bending stresses respectively, a is the flaw depth for a surface flaw, $Q$ is the flaw shape parameter ([2], Fig. A-3300-1), $M_m$ is the correction factor for membrane stress ([2], Fig. A-3300-3), and $M_b$ is the correction factor for bending stress ([2], Fig. A-3300-5).

It is seen from Table 2.10.7-1, that the combined tensile stress of 35,393 psi, in the GE9- 8×8 fuel assembly tube, is the highest. This tube is therefore selected for a fracture evaluation. It is conservatively assumed that all the stresses are membrane stresses.

Reference 6 gives a guideline of pinhole as "included cracks of maximum width about 100 μm (0.004") but whose length could be any where between 200 –300 μm (0.008" – 0.012") and several mm". For conservatism, the following flaw size is used in the fracture evaluation:

$a$ = crack depth = 0.006 in.
$l$ = crack length = 4 mm = 0.16 in.
$t$ = tube thickness = 0.030 in.
$a/t$ = 0.006/0.030 = 0.2
$a/l$ = 0.006/0.16 = 0.0375
Zircaloy yield strength, $S_y$ = 83,710 psi
$(S_m + S_b) / S_y$ = (35,393)/ 83,710 = 0.42
Flaw shape parameter, $Q$ ([2] Fig. A-3300-1) = 0.99
Membrane stress factor, $M_m$ , ([2] Fig. A-3300-3) = 1.25

$$K_1 = (35{,}393)(1.25)\sqrt{\frac{\pi(0.006)}{0.99}} = 6{,}593 \text{ psi.in.}^{1/2} = 6.1 \text{ ksi.in.}^{1/2}$$

$K_{ic}$ at 200° F = 30.0 ksi.in.$^{1/2}$ ([7], Figure 3)

$$\text{Allowable fracture toughness} = \frac{30}{\sqrt{2}} = 21.2 \text{ ksi.in.}^{1/2}$$

Based on the above evaluations, it is concluded that the fracture toughness of the irradiated zircalloy cladding is sufficiently high to preclude a brittle fracture failure during accident conditions. Therefore, the fuel cladding tube will remain intact and retain the fuel pellets during accident conditions.

2.10.7.6 References


1. LLNL Report UCID-21246, Dynamic Impact Effects on Spent Fuel Assemblies, 10/1987.

2. ASME Boiler and Pressure Vessel Code, Section XI, 1998, including 1999 Addendum.

3. ASTM Special Technical Publication 551, Variation of Zircalloy Fracture Toughness in Irradiation, Walker and Kass, 8/1973.

4. ANSYS Engineering Analysis System User's Manual, Rev. 5.6.

5. American Society of Mechanical Engineers, ASME Boiler and Pressure Vessel Code, Section III, along with Appendices, 1998 including 1999 Addendum.

6. EPRI TR-103949, "Temperature Limit Determination for the inert Dry Storage of Spent Nuclear Fuel".

7. ASTM STP 551, 1974, "Variation of Zircaloy Fracture Toughness in Radiation", Walker and Kass.

Table 2.10.7-1
Side Drop Impact Stress Calculations

| Tube Arrays | 7×7 | 8×8 | 8×8 | 8×8 | 8×8 | 9×9 | 10×10 |
|---|---|---|---|---|---|---|---|
| GE Designation | GE2, GE3 | GE4 | GE5 | GE8 | G9, G10 | GE11, GE13 | G12 |
| MTU/Fuel Assy. | 0.1977 | 0.1880 | 0.1856 | 0.1825 | 0.1834 | 0.1766 | 0.1867 |
| No. of fuel rods | 49 | 63 | 62 | 60 | 60 | 74 | 92 |
| Max. active fuel length (in) | 144 | 146 | 150 | 150 | 150 | 146 | 150 |
| Fuel rod OD[5] (in) | 0.559 | 0.489 | 0.479 | 0.479 | 0.479 | 0.436 | 0.400 |
| Clad thick.[6] (in) | 0.030 | 0.032 | 0.030 | 0.030 | 0.030 | 0.026 | 0.024 |
| Fuel rod ID (in) | 0.499 | 0.425 | 0.419 | 0.419 | 0.419 | 0.384 | 0.352 |
| $S_y$ (psi) | 83,710 | 83,710 | 83,710 | 83,710 | 83,710 | 83,710 | 83,710 |
| No. of Spacers, $n$ | 7 | 7 | 7 | 7 | 7 | 8 | 8 |
| $L$ = length/$n$-1 | 24 | 24.3 | 25 | 25 | 25 | 20.9 | 21.4 |
| Tube, $E_1$ (psi) | $11.0\times10^6$ | $11.0\times10^6$ | $11.0\times10^6$ | $11.0\times10^6$ | $11.0\times10^6$ | $11.0\times10^6$ | $11.0\times10^6$ |
| Tube, $I_1$ (in$^4$) | .00175 | .001205 | .001071 | .001071 | .001071 | .000707 | .000503 |
| Fuel, $I_2$ (in$^4$) | .003044 | .001602 | .001513 | .001513 | .001513 | .001067 | .000754 |
| Tube $Wt, W_1$[1] | 1.85 | 1.70 | 1.55 | 1.55 | 1.55 | 1.22 | 1.04 |
| Fuel $Wt$, $W_2$[2] | 10.09 | 7.46 | 7.49 | 7.61 | 7.64 | 5.97 | 5.07 |
| Total Weight (lb) | 11.94 | 9.16 | 9.04 | 9.16 | 9.19 | 7.19 | 6.11 |
| $W$, (lb/in) | .0829 | .0627 | .0603 | .0611 | .0613 | .0492 | .0407 |
| $M = .1058wl^2$,7supp<br>$M = .1056wl^2$,8supp | 5.053 | 3.920 | 3.987 | 4.038 | 4.053 | 2.269 | 1.970 |
| $S_b$ for $1g = MC/I$ (psi) | 294.6 | 341.4 | 369.5 | 374.2 | 375.7 | 278.8 | 313.4 |
| $S_b$ for $75g$ (psi) | 22,095 | 25,605 | 27,713 | 28,065 | 28,178 | 20,910 | 23,505 |
| Pressure at 0° C, $p_0$ | 670 | 642 | 856 | 870 | 863 | 822 | 825 |
| Pressure[3] at 337° C, $p$ (psi) | 1497 | 1435 | 1913 | 1944 | 1928 | 1837 | 1843 |
| $S_{press.}$ (psi.)[4] | 6599 | 5121 | 7134 | 7273 | 7215 | 7241 | 7221 |
| $S = S_b 75g + S_{press.}$ (psi) | 28,694 | 30,726 | 34,847 | 35,338 | 35,393 | 28,151 | 30,726 |

Notes:

(1) $W_1$ = Area × 0.234 lb/in$^3$ × 158" length

(2) $W_2$ ($UO_2$) = [ MTU × 1000 (kg/MTU) × 2.2046 (lb/kg) × 270 (M.W of $UO_2$)/238 (M.W of U)] /No. of Tubes = [2501 × MTU] /No. of Tubes

(3) The max. rod temp. is 638° F, the max. rod pressure is 870 psia at 0° C. The pressure at 638° F (337°C) is $p = (337 + 273) / (0+273) \times p_0$

(4) $S_{press.}$, axial stress = $p \times D_{avg} / 4t$

(5) Includes 0.004 in. reduction in cladding OD to account for water side cladding corrosion [11].

(6)Thickness is reduced by 0.002 in. to account for corrosion [11].

Table 2.10.7-2
Fuel Rod Buckling Loads for End drop Impact

| Tube Arrays (No. of Tubes) | 7 × 7 (49) | 8 × 8 (63) | 8 × 8 (62) | 8 × 8 (60) | 8 × 8 (60) | 9 × 9 (74) | 10 × 10 (92) |
|---|---|---|---|---|---|---|---|
| GE Designation | GE2, GE3 | GE4 | GE5 | GE8 | G9, G10 | GE11, GE13 | G12 |
| Tube Length (in.) | 158 | 158 | 158 | 158 | 158 | 158 | 158 |
| Tube Active Length (in) | 144 | 146 | 150 | 150 | 150 | 146 | 150 |
| No. of Spacers | 7 | 7 | 7 | 7 | 7 | 8 | 8 |
| Length between spacers, $L$ (in.) | 24 | 24.3 | 25 | 25 | 25 | 20.9 | 21.4 |
| Cladding tube OD (in) | 0.559 | 0.489 | 0.479 | 0.479 | 0.479 | 0.436 | 0.400 |
| Cladding tube thickness (in) | 0.030 | 0.032 | 0.030 | 0.030 | 0.030 | 0.026 | 0.024 |
| Cladding Tube ID (in) | 0.499 | 0.425 | 0.419 | 0.419 | 0.419 | 0.384 | 0.352 |
| Tube Area, $A$ ($in^2$) | 0.050 | 0.046 | 0.042 | 0.042. | 0.042 | 0.033 | 0.028 |
| Fuel area, ($in.^2$) | 0.196 | 0.142 | 0.138 | 0.138 | 0.138 | 0.116 | 0.097 |
| Tube weight = $Ax$ Density[3] × 158 (lb) | 1.85 | 1.70 | 1.55 | 1.55 | 1.55 | 1.22 | 1.04 |
| Fuel Weight (lb) | 10.09 | 7.46 | 7.49 | 7.61 | 7.64 | 5.97 | 5.07 |
| Tube + Fuel Weight, (lb) | 11.94 | 9.16 | 9.04 | 9.16 | 9.19 | 7.19 | 6.11 |
| Eqv. Density Tube[1] | 0.257 | 0.253 | 0.246 | 0.246 | 0.246 | 0.253 | 0.247 |
| Eqv. Density Fuel[2] | 0.357 | 0.360 | 0.362 | 0.368 | 0.369 | 0.352 | 0.347 |
| ANSYS Plastic Instability Load ($g$) | 176 | 146 | 131 | 128 | 128 | 151 | 128 |
| Allowable Buckling $g$ Load (Fig2.10.7-2) | * | * | * | * | 128 | * | * |

* The allowable buckling g load for these assemblies will be higher or equal to 128$g$.

Notes:
(1) Eqv. Density Tube = (0.234 × Actual tube length )/ Active tube length modeled
(2) Eqv. Density Fuel = Fuel Weight /(Fuel area × Active tube length modeled)
(3) Zircaloy Density = 0.234 $lb/in.^3$

Figure 2.10.7-1

Tube and Fuel Finite Element Model - Buckling Analysis

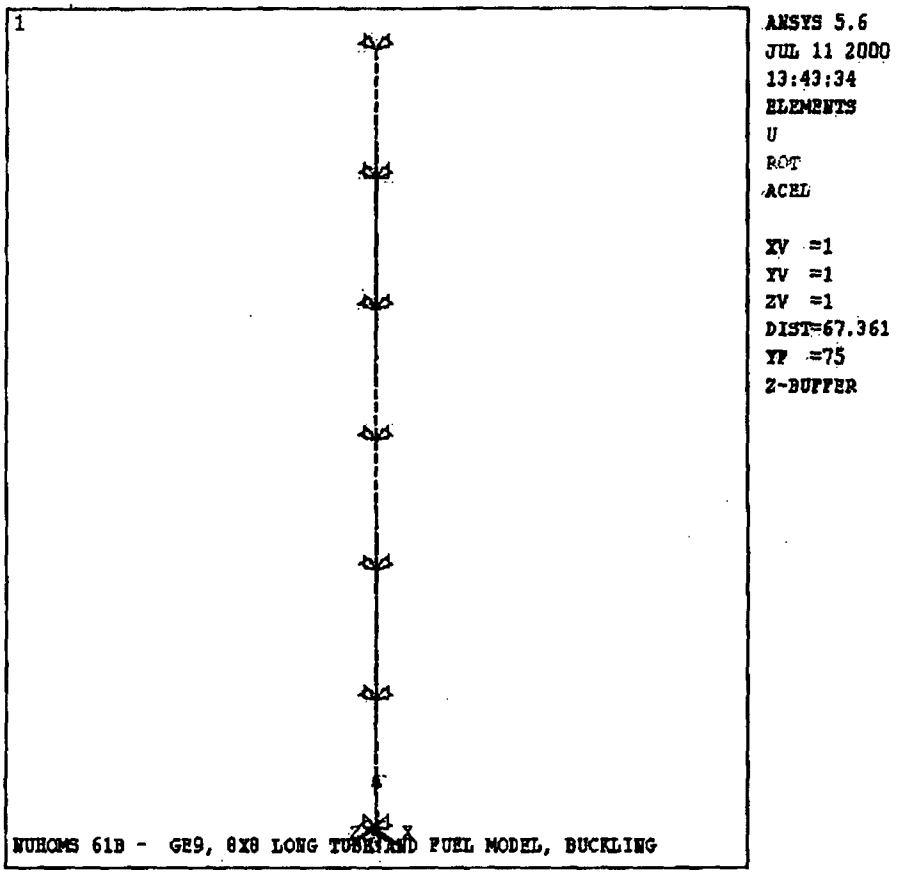

Figure 2.10.7-2

Allowable Buckling Load for G9 8 × 8 Fuel Assembly

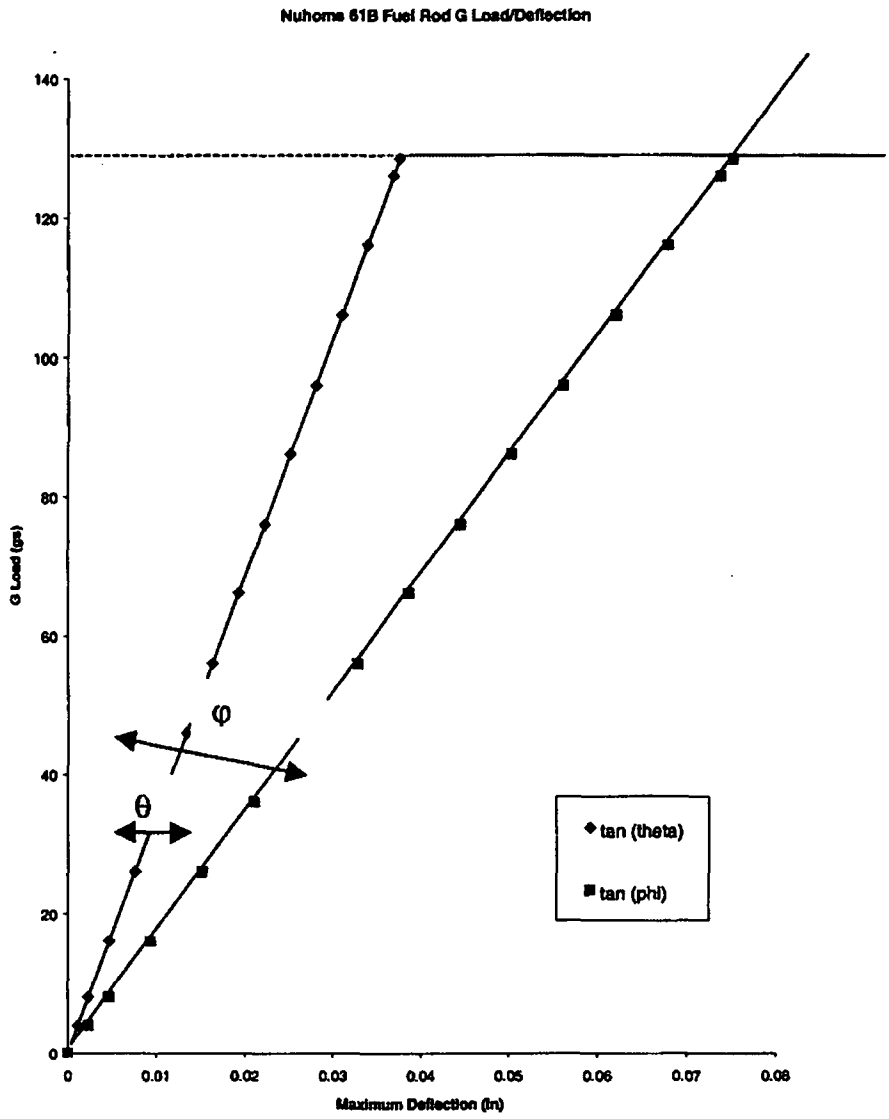

APPENDIX 2.10.8

TABLE OF CONTENTS



LIST OF TABLES

## LIST OF FIGURES

APPENDIX 2.10.8

# STRUCTURAL EVALUATION OF THE NUHOMS®-MP197 PACKAGE IMPACT LIMITERS

## 2.10.8.1 Introduction

This appendix presents the details of the structural analysis of the NUHOMS®-MP197 impact limiters. The impact limiters are designed to absorb the kinetic energy resulting from the one (1) foot and thirty (30) foot normal conditions of transport and hypothetical accident conditions free drop events specified by 10 CFR 71. Redwood and balsa wood are used as the primary energy absorption material(s) in the impact limiters. A sketch of the impact limiter is shown in Figure 2.10.8-1. A functional description of the impact limiters is given in Section 2.10.8.2. The impact limiter design criteria are described in Section 2.10.8.3.

A computer model of the NUHOMS®-MP197 Transport Packaging was developed to perform system dynamic analyses during impacts of 30 foot accident and 1 foot normal condition drops. The model was developed for use with the ADOC (Acceleration Due To Drop On Covers) computer code described in detail in Section 2.10.8.8 which determines the deformation of the impact limiters, the forces on the packaging and the packaging deceleration due to impact on an unyielding surface. Numerous cases were run to determine the effects of the wood properties and the initial drop angle. A description of the computer model, input data, analysis results and conclusions for the 30 foot accident condition and one foot normal condition free drops are given in Sections 2.10.8.4 and 2.10.8.5 respectively. The analysis of the impact limiter attachments is described in Section 2.10.8.6. A summary of results for all drop orientations is provided in Section 2.10.8.7. The forces and decelerations used in the cask body and basket structural analysis, presented in detail in Appendix 2.10.1 and Appendix 2.10.5, are given in Table 2.10.8-12 (loading values calculated in this appendix are increased for conservatism). The testing program for the NUHOMS®-MP197 wood filled limiters is discussed in Appendix 2.10.9. Test results indicate that ADOC predicts higher deceleration values, crush forces and crush depths than measured test results.

2.10.8.2 Design Description

The impact limiters absorb energy during impact events by crushing of balsa and redwood. The size, location and orientation of each wood block is selected to provide protection for the cask during all normal and hypothetical accident conditions of transport.

The top and bottom impact limiters are identical. Each has an outside diameter of 122 inches and a height of 60.75 inches. The inner and outer shells are Type 304 stainless steel joined by radial gussets of the same material. The gussets limit the stresses in the 0.25 in. thick steel outer cylinder and end plates due to pressure differentials caused by elevation and temperature changes during normal transport and provide wood confinement during impact. The metal structure positions, supports, confines and protects the wood energy absorption material. The metal structure does contribute to the energy absorbing capability of the impact limiter. However, the contribution to a side drop or oblique angles is negligible because contact starts at a single point with the unyielding surface (target) and initiates buckling of a single gusset. After the drop event is complete, relatively few gussets are buckled.

The materials and grain orientations are selected to provide acceptably low deceleration to prevent excessively high stresses in the cask during impact after the thirty foot end drop. A 2.50 inch layer of balsa wood with the grain parallel to the end of the cylindrical cask is provided on the outer face of the impact limiter to minimize decelerations after a one foot end drop.

A 18.0 inch wide ring of redwood and a 6.75 inch wide ring of balsa wood (consisting of 12 segments or blocks of wood) is located in the sides of the pie shaped compartments which surround the end of the cylindrical surface of the cask with the grain direction oriented radially. This ring of wood absorbs most of the kinetic energy during a side drop. Wood for this portion of the impact limiter was selected to absorb a large amount of energy in a relatively short crush distance.

The corners of the pie shaped compartments are filled with redwood. The primary function of the redwood block in this region is energy absorption during a 30 foot corner drop.

All wood blocks used in the impact limiters are composed of individual boards glued together with a Phenol Resorcinol Adhesive or equivalent. This adhesive is selected for its superior strength and moisture resistance. The wood blocks are assembled and glued together in accordance with an approved QA procedure. Minimum properties of the adhesive are listed in Table 2.10.8-1. Ranges of shear and tensile strengths of each type of wood are also listed. The adhesive is significantly stronger than any of the wood used in the limiter in terms of shear and tensile strength. Therefore the boards or blocks of wood will not fail along the glue joints.

The other mechanical properties of the wood used in the analysis are shown in Table 2.10.8-2. The crush strength properties used cover the range of expected values for the density and moisture content specified in the procurement specification. During procurement, wood samples are tested for density, moisture content and crush strength in accordance with an approved

sampling plan. If the density, moisture content, and crush strength are not within the specified range, the wood blocks from which samples are taken would be rejected.

During the end drop, all of the wood in the central part of the impact limiter that is directly "backed-up" by the cask body will crush. The wood in the corner and side of the limiter will tend to slide around the side of the cask since it is not supported or backed-up by the body and it will not crush or absorb energy as effectively as the wood that is backed-up. During the side or oblique drop the wood backed up by the cask will crush, while the wood beyond the end of the cask body will have a tendency to slide around the end of the cask. The analyses assume that the effectiveness of the portion of the wood that is not backed-up is 20%. Effectiveness is defined as the actual crush force developed at the target by this material divided by the theoretical force required to deflect the material. The analysis also assumes a range of wood crush strengths. When determining maximum deceleration, the maximum crush strengths are used. When determining crush depth, the minimum wood crush strengths are used.

The impact limiters are attached to the cask by twelve attachment bolts each. The attachment bolts have been sized to withstand the loads transmitted during a low angle drop slap down. This analysis is described in Section 2.10.8.6 of this Appendix.

2.10.8.3 Design Criteria

The outside dimensions of the impact limiter are sized to be within federal and state highway height and width restrictions. The balsa and redwood distribution and densities have been selected to limit the maximum cask body inertia loads due to the one foot normal condition drop and the thirty foot hypothetical accident drop so that the design criteria specified for the cask and basket (See Section 2.1) are met.

The welded stainless steel structure of the impact limiter is designed so that the wood is maintained in position and is confined during crushing of the impact limiters. The outer shell and gussets are designed to buckle and crush during impact. Local failure of the shell is allowed during impact limiter crushing. The welded stainless steel shell and its internal gussets are designed to withstand pressure differences and normal handling and transport loads with stresses limited to the material yield strength.

The impact limiters are designed to remain attached to the cask body during all normal and hypothetical accident conditions.

### 2.10.8.4 Analysis of 30 Foot Free Drop Accident Conditions

#### 2.10.8.4.1 Approach

The kinetic energy due to the hypothetical 30 ft drop accident is absorbed by crushing of the impact limiters on the ends of the packaging. The limiters contain materials, i.e. balsa and redwood, which provide controlled deceleration of the packaging by crushing between the target surface and the cask body.

The applicable regulation, 10CFR71.73, requires that the packaging be oriented for the drop so that it strikes the target in a position for which maximum damage is expected. Dynamic impact analyses were performed for various packaging orientations using the ADOC computer code described in Section 2.10.8.8. This computer code has been validated by comparing its dynamic results with those from hand calculations for relatively simple problems, comparing its calculated force-deflection curves with those obtained from static crush tests, and by correlating dynamic results with actual measured cask behavior on other programs.

#### 2.10.8.4.2 Assumptions and Boundary Conditions

The assumptions and boundary conditions are as follows:

1. The cask body is assumed to be rigid and absorb no energy. This assumption is realistic since the design criteria of Section 2.1.2 limit metal deformations to small values. All of the impact energy is therefore assumed to be absorbed by the impact limiters.

2. The crushable material is one or several anisotropic materials. The different wood regions are modeled individually.

3. The crush strengths of the wood sections are obtained from the properties parallel to and perpendicular to the grain based on the orientation of the cask at impact.

4. Each wood region is modeled as a one dimensional elastic, perfectly plastic material up to a specific locking strain. After reaching the locking strain, the stress increases linearly with the additional strain. The wood properties (modulus of elasticity, average crush strength, locking modulus, and locking strain) are taken from force-deflection curves of sample blocks of wood. Typical force-deflection curves for balsa and redwood are shown in Figures 2.10.8-1A and 2.10.8-1B. Since the locking strain varies from sample to sample, conservatively low locking strains of 80% for balsa and 60% for redwood are used.

5. The crush properties of the wood are varied with the initial angle of impact and do not change during the drop event being evaluated.

6. The cask and impact limiters are axisymmetric bodies.

7. The crushing resistance of the impact limiter shell and gussets have a negligible effect on the crush strength of the limiter and, therefore, a negligible effect on the impact forces and inertial loads.

2.10.8.4.3 Packaging Dynamic Computer Model

Figure 2.10.8-2 illustrates the computer model used for all packaging orientations. Regions I, II, and III in the model are used to delineate regions where different impact limiter materials are used. It should be noted that the properties of the three regions have been designed by choosing wood types and orientations to accommodate the crush requirements of the drop orientations. The crushable materials of Regions I, II, and III are selected to control the decelerations resulting from end, corner, and side drop orientations, respectively. Table 2.10.8-2 tabulates the wood properties that were used to describe the wood stress-strain behavior in the analysis.

A portion of the impact limiter crushable material is backed up by the cask body as it crushes against the impact surface. The remaining material overhangs the cask body and is not backed up. Backed up regions project vertically from the target footprint to the cask body, while unbacked regions do not project vertically to the cask. The effectiveness of the energy absorbing crushable material varies depending on whether it is "backed up" by the cask or is unsupported. Two cases are analyzed to bound impact limiter performance. In one case, the non-backed up material is assumed to be 20% effective and maximum wood crush strength is used (maximum of the possible range based on specified density). In the other case, the non-backed up material is also assumed to be 20% effective but the minimum wood strength is used. Evaluating impact limiter performance in this way results in a range of deceleration values, crush forces and crush depths. This, in combination with close control of wood properties during procurement, assures that the effects of wood property variations (including temperature effects) are bounded by the analyses.

2.10.8.4.4 Analysis Results Predicted by ADOC

The peak inertia loadings or cask body decelerations (in terms of *g*s) versus initial angle of impact are presented in Tables 2.10.8-3 through 2.10.8-6 for the 30 foot drop. The 30 foot drop is measured from the impact surface to the bottom of the impact limiter; the center of gravity (CG) of the cask is much higher than 30 feet. The values of crush depth vs. impact force are shown in Tables 2.10.8-7 to 2.10.8-12. Since the packaging CG is within ½ inch of the packaging center and the impact limiters are identical, these tables are valid for impacts on either end.

Based on the crush depths for the side drop from Table 2.10.8-7, the neutron shield shell will not hit the impact surface. Using maximum wood properties, the clearance after the limiters crush would be approximately 10.2 inches. Using minimum wood properties, the clearance after the limiter crush would be 9.2 inches. It is expected that the crush depth would be somewhere between the two bounding cases.

### 2.10.8.5 Analysis for One Foot Drop Normal Condition

This section describes the analysis of the NUHOMS®-MP197 for the one foot normal conditions of transport drop. The NUHOMS®-MP197 in the transport configuration is lifted and transported horizontally. Therefore, the side drop orientation is considered the only credible normal condition drop event. The accident condition analysis in Section 2.10.8.4 bound any possible accident condition drops. However, a 1 foot end drop and a 60° CG over corner drop are also evaluated for completeness. The results from the one foot, 60° corner drop are only used to compute the maximum NUHOMS®-MP197 lid bolt stress caused by a normal condition impact event.

The packaging kinetic energy is absorbed by crushing of the impact limiters. The dynamic system model of Section 2.10.8.4 was used to perform the side drop (0°) analysis using the ADOC computer program described in Section 2.10.8.9. The end drop analysis was performed assuming that the energy would be absorbed by the soft balsa wood (oriented in the weak direction) in the outer end of the limiter. This is an accurate way to determine $g$ loads on an end drop since the $g$ values can be calculated by the expression $F = Ma$ where $F$ is the crush stress times the area and $M$ is the package weight divided by the acceleration of gravity $g$.

The inertial load results of these one foot drop analyses are presented in Table 2.10.8-13. Again, two extreme cases are considered. The upper bound stiffness case assumes maximum wood crush strength and the lower bound stiffness case assumes minimum wood strength. Stress analyses in Section 2.10.1 are conservatively performed for the case(s) with maximum inertia loads resulting from upper bound stiffness cases.

### 2.10.8.6 Impact Limiter Attachment Analysis

#### 2.10.8.6.1 Approach

The impact limiter attachments are designed to keep the impact limiters attached to the cask body during all normal and hypothetical accident conditions. The loading that has the highest potential for detaching the impact limiter is the slap down or secondary impact after a shallow angle 30 foot drop. During this impact, the crushing force on the portion of the impact limiter beyond the cask body (the non backed-up area) tends to pull the limiter away from the cask. The end and corner drops are not critical cases for the impact limiter attachments since the impact force tends to push the impact limiter onto the cask in these orientations.

For the impact limiter attachment bolt analysis, maximum wood crush strengths of 2010 psi for balsa and 6500 psi for redwood are assumed. The maximum wood properties produce the highest overturning moment on the limiter. Based on the dynamic analysis performed using the ADOC code, the most severe slap down impact occurs after a shallow angle oblique impact. The calculated peak contact forces at the end of the cask body subjected to secondary impact (slap down) for the orientations analyzed are as follows.

| Drop Orientation | Impact Force (lb.×1000) |
|---|---|
| 5° | 10,200 |
| 10° | 10,116 |
| 15° | 10,222 |
| 20° | 12,343 |

Therefore, the 20° slap down impact will result in the most severe overturning moment. The peak impact force that is applied to the impact limiter is conservatively increased by roughly 33% to 16,500,000 lb. for the structural analysis of the attachment bolts.

The maximum moment applied to the impact limiter attachments is conservatively determined ignoring the mass of the impact limiter which tends to reduce the attachment forces. The resultant of the external impact force on the limiter is offset 1.42 in. from the resultant of the cask reaction force. Therefore, the net moment applied to the limiter is $16.500 \times 10^6 \times 1.42$ or $2.343 \times 10^7$ in lb. There is also a frictional force that acts to pull the impact limiter away from the cask. Assuming a frictional coefficient of 0.12 between the cask and limiter and between the limiter and impact surface, the magnitude of this force is

$$F_f = \mu R = .12(16{,}500{,}000) = 1.980 \times 10^6 \text{ lbs.}$$

The crush depth on the side is 10.03 inches. The resultant moment due to friction is

$$M_f = (1{,}980{,}000)(10.03) = 1.986 \times 10^7 \text{ in lbs.}$$

The total moment is therefore $4.329 \times 10^7$ in lbs. This moment is reacted by the twelve impact limiter attachment bolts. A free body diagram of the impact limiter is shown in Figure 2.10.8-13. It is conservatively assumed that the impact limiter pivots about the edge of the cask. The attachment bolt forces vary linearly with distance from the pivot point, so that the maximum force, $F_{max}$, occurs in the bolt farthest from the pivot point. The worst case angular orientation occurs when any one of the attachment bolts is oriented closest to the point of impact.

The attachment bolts counteract the moment applied to the impact limiter in the following way.

$$M = 84.38F_{max} + 2\frac{(78.64^2)}{84.38}F_{max} + 2\frac{(62.94^2)}{84.38}F_{max} + 2\frac{(41.50^2)}{84.38}F_{max}$$
$$+ 2\frac{(20.06^2)}{84.38}F_{max} + 2\frac{(4.36^2)}{84.38}F_{max} = 375.65F_{max}$$

Where $M$ is the moment applied to the impact limiter and $F_{max}$ is the maximum attachment bolt force, which is applied to the attachment bolt farthest from the pivot point. Therefore,

$$F_{max} = \frac{4.329\times10^7}{375.65} = 115{,}240 \text{ lbs.}$$

The stress limits for the impact limiter attachments during the accident condition free drop are taken to be $S_u$ and $0.42S_u$ for membrane plus bending and shear stresses respectively. For stress analysis, all material properties are taken at 300° F.

2.10.8.6.2 Attachment Bolt Stress

The critical tensile area of the 1.072 inch diameter attachment bolt is in the bolt shank, since the threads are 1¼-7UNC. The tensile area of the bolt is $(\pi/4)(1.072^2) = 0.903$ in$^2$. The maximum allowable stress is taken to be $S_u$ of SA-540, Grade B24 at 300° F, or 165 ksi. [4]. So the maximum attachment bolt tensile stress is 115,240/0.903/1000 = 127.7 ksi., which is less than 165 ksi.

2.10.8.6.3 Stress in Bolt Tunnel

The allowable stress for the bolt tunnel is the ultimate strength of SA-240, Type 304 at 300°F, or 66.2 ksi. [4]. The tensile force in the attachment bolt is reacted in the impact limiter shell by both the outer and inner bolt tunnels. A compressive stress is generated in the inner bolt tunnel, while a tensile stress is generated in the outer bolt tunnel. The critical cross sectional area in the outer bolt tunnel is that of the weld between the outer tunnel and the tunnel shelf. Therefore, the cross sectional area available to react the bolt force, $A_{bt}$, is that of the weld between the outer tunnel and the tunnel shelf plus the cross sectional area of the inner bolt tunnel.

$$A_{bt} = (\pi/4)\times(2.00^2 - 1.50^2) \text{ in.}^2 \text{ (inner tunnel)} + \pi\times2.50\times0.19\times\sin(45°) \text{ in.}^2 \text{ (outer tunnel)}$$
$$= 2.430 \text{ in.}^2$$

The stress generated in the inner and outer bolt tunnels, $\sigma_{bt}$, is,

$$\sigma_{bt} = 115{,}240 \text{ lb.} / 2.430 \text{ in.}^2 = 47{,}431 \text{ psi.} < 66{,}200 \text{ psi.}$$

2.10.8.6.4 Stress in Bolt Tunnel Weld

The bolt tunnel assembly is attached to the impact limiter shell by a weld at both ends of the bolt tunnel assembly plus a weld between the inner bolt tunnel and the inner shell. The cross sectional area of the weld available to react the bolt force, $A_{bt}$, is,

$$A_{bt} = \pi\times2.00\times0.25\times\sin(45°) \text{ in.}^2 \text{ (inner tunnel)} + \pi\times3.00\times0.25\times\sin(45°) \text{ in.}^2 \text{ (outer tunnel)} + 2\times24.75\times0.19\times\sin(45°) = 9.427 \text{ in.}^2$$

The stress generated in the inner and outer bolt tunnels, $\sigma_{bt}$, is,

$$\sigma_{bt} = 115{,}240 \text{ lb.} / 9.427 \text{ in.}^2 = 12{,}224 \text{ psi.} < 66{,}200 \text{ psi.}$$

2.10.8.6.5 Attachment Block Analysis

The impact limiter attachment bolts thread into attachment block that are welded to the outer shell of the NUHOMS®-MP197 cask. The material used for the attachment bolt blocks is SA-240 Type 304 with $S_u = 66.2$ ksi. at 300° F. [4]. The allowable shear stress is $0.42S_u = 27.8$ ksi., and the allowable primary plus bending stress is $S_u = 66.2$ ksi.

Attachment bolt block / cask shell weld

There is a ½ inch groove weld on all four sides of the of the attachment block between the block and the cask shell.

Weld area, $A_{weld} = (4.81 \times 4.50) - (3.81 \times 3.50) = 8.31 \text{ in}^2$.

Weld moment of inertia, $I_{weld} = \dfrac{bh^3}{12} = \dfrac{(4.81)(4.50^3)}{12} - \dfrac{(3.81)(3.50^3)}{12} = 22.91 \text{ in}^2$.

Max. moment applied to block weld, $M_{weld} = 115{,}240 \text{ lb.} \times 1.88 \text{ in.} = 216{,}650 \text{ in.lb.}$

Bending stress, $\sigma_b = \dfrac{M_{weld}c}{I_{weld}} = \dfrac{(216{,}650)(4.50/2)}{22.91} = 21{,}277 \text{ psi.}$

Shear stress, $\tau = F_{max} / A_{weld} = 115{,}240 / 8.31 = 13{,}868 \text{ psi.} < 31{,}500 \text{ psi.}$

Stress intensity, $S.I. = \sqrt{\sigma_b^2 + 4\tau^2} = \sqrt{(21{,}277)^2 + 4(13{,}868)^2} = 34{,}957 \text{ psi.} < 66{,}200 \text{ psi.}$

Minimum Engagement Length for Attachment Bolt and Block

The bolt material is SA-540, Grade B24, Class 1, with

$$S_u = 165 \text{ ksi., and}$$
$$S_y = 150 \text{ ksi at room temperature [4].}$$

The bolt block material is SA-240 Type 304 or SA-182 F304, with

$$S_u = 75 \text{ ksi., and}$$
$$S_y = 30 \text{ ksi. at room temperature [4].}$$

The minimum engagement length, $L_e$, for the bolt and flange is ([5], Page 1149),

$$L_e = \frac{2A_t}{3.146K_{n\max}\left[\frac{1}{2} + .57735n(E_{s\min} - K_{n\max})\right]}.$$

For a 1¼ - 7UNC 2A bolt,

$A_t$ = tensile stress area = 0.969 in.$^2$,
$n$ = number of threads per inch = 7,
$K_{n\,max}$ = maximum minor diameter of internal threads = 1.123 in., ([5], p. 1290).
$E_{s\,min}$ = minimum pitch diameter of external threads = 1.1476 in., ([5], p. 1290).

Substituting the values given above,

$$L_e = \frac{2(0.969)}{(3.146)1.123\left[\frac{1}{2} + .57735(7)(1.1476 - 1.123)\right]} = 0.915 \text{ in.}$$

$$J = \frac{A_s \times S_{ue}}{A_n \times S_{ui}}. \text{ [5]}$$

Where, $J$ is a factor for the relative strength of the external and internal threads, $S_{ue}$ is the tensile strength of external thread material, and $S_{ui}$ is the tensile strength of internal thread material.

$A_s$ = shear area of external threads = $3.1416\, nL_e\, K_{n\,max}\, [1/(2n) + .57735\, (E_{s\,min} - K_{n\,max})]$

$A_n$ = shear area of internal threads = $3.1416\, nL_e\, D_{s\,min}\, [1/(2n) + .57735(D_{s\,min} - E_{n\,max})]$

For a 1¼ - 7UNC 2A bolt,

$D_{s\,min}$ = minimum major diameter of external threads = 1.2314 in. ([5], p. 1290)

$E_{n\,max}$ = maximum pitch diameter of internal threads = 1.1668 in. ([5], p. 1290).

Therefore,

$$A_s = 3.1416(7)(0.915)(1.123)[1/(2\times7) + .57735\,(1.1476 - 1.123)] = 1.935 \text{ in.}^2$$

$$A_n = 3.1416(7)(0.915)(1.2314)[1/(2\times7) + .57735\,(1.2314 - 1.1668)] = 2.694 \text{ in.}^2$$

So,

$$J = \frac{1.935(165.0)}{2.694(75.0)} = 1.580$$

The required length of engagement, $Q$, to prevent stripping of the internal threads is,

$$Q = L_e J = (0.915)(1.580) = 1.446 \text{ in.}$$

The actual minimum engagement length = 3.50 in. > 1.446 in.

2.10.8.6.6 Attachment Bolt Torque

Assume a bolt tensile stress of 15,000 psi.

$$F_a = 15{,}000 \times 0.969 = 14{,}535 \text{ lb.}$$

$$Q = K D_b F_a = 0.1 \times 1.25 \times 14{,}535 = 1{,}817 \text{ in. lb.} = 151 \text{ ft. lb.}$$

Where $F_a$ is the bolt force, $Q$ is the applied torque, $K$ is the nut factor (0.1 with lubrication), and $D_b$ is the nominal bolt diameter at the threads (0.969 in. [5], p. 1266).

Specify a bolt torque of 140 to 160 ft. lb.

For a bolt torque of 140 ft. lb.,

$$F_a = \frac{Q}{KD_b} = \frac{140 \times 12}{0.1 \times 1.25} = 13{,}440 \text{ lb.}$$

For a bolt torque of 160 ft. lb.,

$$F_a = \frac{Q}{KD_b} = \frac{160 \times 12}{0.1 \times 1.25} = 15{,}360 \text{ lb.}$$

Therefore, the maximum tensile stress in the bolt is 15,360/0.903 = 17,010 psi. Which is much less than the yield strength of the bolt material at 300° F., 138,600 psi. [4].

## 2.10.8.7 Summary of ADOC Results Used for Structural Analysis

### 2.10.8.7.1 Cask Structural Analysis - *g* Load and Drop Orientation

In order to determine the cask stresses, the maximum *g* loads from ADOC runs are converted to forces and applied as quasistatic loadings on the cask body. A detailed ANSYS finite element model of the NUHOMS®-MP197 cask is used to perform this analysis.

Only the loads corresponding to the most critical normal and accident condition free drop orientations are used in the cask body analysis in Section 2.10.1. For the 30 foot accident condition drops, *g* loads corresponding to four different angles are evaluated, and for the 1 foot normal condition drops, *g* loads corresponding to two different angles are evaluated. The orientations evaluated in Section 2.10.1 are as follows.

| Drop Height (Normal / Accident) | Orientation Analyzed |
|---|---|
| 30 Foot Accident Condition Drop | 0° Side Drop |
| | 20° Slap Down |
| | 60° C.G. Over Corner Drop |
| | 90° End Drop |
| 1 Foot Normal Condition Drop | 0° Side Drop |
| | 90° End Drop |

The *g* loads corresponding to these drop orientations are provided in Tables 2.10.8-3 through 2.10.8-6, and 2.10.8-13.

The thirty foot side drop is evaluated because it produces the highest normal transverse *g* load. The 20°, thirty foot slap down is analyzed because it produces a high normal as well as rotational *g* load at the ends of the cask (second impact). Stresses in the cask and lid bolts are most sensitive to *g* loads applied in the 60° (CG over corner) direction. Consequently, the thirty foot CG over corner drop is evaluated. The highest axial *g* load occurs during a 90°, thirty foot end drop, and is therefore also evaluated.

For the normal conditions of transport one foot drops, the 0° side drop, and the 90° end drop are bounding, since they produce the highest normal *g* loads in the transverse and axial directions respectively. The 60° CG over corner drop acceleration is only used in the transport cask lid bolt analysis, since the 60° drop is the bounding orientation for the lid bolt impact load case.

When the *g* loads are applied to the cask model in Section 2.10.1, the *g* loads predicted by ADOC are increased in order to bound all drop angles, and to create conservatism. The *g* loads predicted by ADOC as well as the increased *g* loads used in the cask body analysis are shown in Figure 2.10.8-14.

Basket Structural Analysis - *g* Load and Drop Orientation

The loading conditions considered in the evaluation of the fuel basket consist of inertial loads resulting from normal handling (1 foot drop) and hypothetical accident (30 foot) drops. The inertial loads of significance for the basket analysis are those that act transverse to the cask and basket structural longitudinal axes, so that the loading from the fuel assemblies is applied normal to the basket plates and is transferred to the cask wall by the basket. The side drop will generate the highest stress in the basket, because of the inertial load caused by the fuel assemblies impacting the basket plates. For example, the maximum transverse *g* load resulting from a 0° side drop is 60 *g*s, and the maximum transverse *g* load resulting from a 5° slap down second impact is 53 *g*s. The rotational *g* loads from slap down impact will have a very small effect on the basket because the cask stiffness is much greater than the basket stiffness and the basket is enveloped by the cask. Consequently, any rotational bending affect will be absorbed by the cask body. Therefore, the basket structure is analyzed for 1 foot and 30 foot side drops. The basket structure is also analyzed for 1 foot and 30 foot end drops despite a large margin of safety. Table 2.10.8-14 lists the *g* loads used for the basket structural analysis.

## 2.10.8.8 Summary Description of ADOC Computer Code

One of the accident conditions which must be evaluated in the design of transport packagings to be used for the shipment of radioactive material is a free drop from a thirty-foot height onto an unyielding surface (10CFR71). The packaging must be dropped at an orientation that results in the most severe damage. Impact limiters are usually provided on the packaging to cushion the effects of such impact on the containment portion of the packaging. The limiters are usually hollow cylindrical cups which encase each end of the containment and are filled with an energy absorbing material such as wood or foam.

A computer code, ADOC (Acceleration due to Drop On Covers), has been written to determine the response of a packaging during impact. The analysis upon which this code is based is discussed in this section. The overall analysis of the packaging response is discussed in Section 2.10.8.8.1, and the methods used to compute the forces in the limiters as they crush are presented in Section 2.10.8.8.2.

### 2.10.8.8.1 General Formulation

The general formulation used to compute the response of the packaging as it impacts with a rigid target is discussed in this section. The assumptions upon which the analysis is based are first presented followed by a detailed development of the equations of motion used to calculate the packaging dynamic behavior. This is followed by a discussion of the numerical methods and the computer code used to implement the analysis. A significant part of the development is concerned with the prediction of forces developed in the impact limiters as the impact occurs. This aspect of the evaluation is discussed in Section 2.10.8.8.2.

Assumptions

The cask body is assumed to be rigid and axisymmetric. Therefore, all of the energy absorption occurs in the impact limiters which are also assumed to have an axisymmetric geometry. Several assumptions are made in calculating the forces which develop in the limiters as they crush. These are discussed in Section 2.10.8.8.2. Since the packaging is axisymmetric, its motion during impact will be planar. The vertical, horizontal, and rotational components of the motion of the packaging center of gravity (CG) are used to describe this planar motion.

Equations of Motion

A sketch of the packaging at the moment of impact is shown on Figure 2.10.8-3. The packaging is dropped from a height (H), measured from the lowest point on the packaging to the target. The packaging is oriented during the drop, and at impact, so that the centerline is at an angle (r) with respect to the horizontal. At the instant of impact, the packaging has a vertical velocity of

$$V_0 = \sqrt{2GH}\,. \tag{1}$$

Where $G$ is the gravitational constant.

At some time, $t$, after first impact, the packaging has undergone vertical, $u$, horizontal, $x$, and rotational, $\rho$, displacements. The location of the packaging at this time is shown on Figure 2.10.8-4. One or both of the limiters have been crushed as shown. The resulting deformations (and strains) in the limiters result in forces which the limiters exert on the packaging, thereby decelerating it. These forces, and their points of application on the packaging, are shown on Figure 2.10.8-4 as $F_{v1}$, $F_{v2}$, and $F_h$. The method used to calculate these forces and the points of application are provided in Section 2.10.8.8.2, below.

The three equations of motion of the cask are

$$M\ddot{u} + F_{v1} + F_{v2} - W = 0, \tag{2}$$

$$M\ddot{x} - F_h = 0, \text{ and} \tag{3}$$

$$J\ddot{\rho} - F_{v1}x_{v1} + F_{v2}x_{v2} + F_hY_h = 0\,. \tag{4}$$

Where, $M$ is the mass of packaging, $J$ is the polar moment of inertia of the packaging about its CG, $W$ is the packaging weight, and $\ddot{}$ denotes acceleration. At impact ($t = 0$), all of the initial conditions are zero except that $u$ = the vertical velocity.

Computer Solution

The computer code is written to compute the motion of the packaging during impact. The solution is obtained by numerically integrating the equations of motion (equations 2, 3, and 4) from the time of impact, $t = 0$, to a specified maximum time, $t_{max}$. The integrations are carried forward in time at a specified time increment, $\Delta t$. Parametric studies indicate that a time increment of 1 msec is sufficiently small so that further reduction of the time increment does not affect the results. Solutions are usually carried out to about 150 msec for the near horizontal drops and to about 50 msec for the near vertical drops. The significant motions of the packaging normally occur within these time periods.

A standard fourth order Runge Kutta numerical integration method is used to perform the numerical integrations. The following procedure is used to carry the solution from time $t_i$ to time $t_{i+1}$. Note that at time $t_i$ the displacements and velocities of the three degrees of freedom describing the motion of the CG of the packaging are known.

1. Calculate the deformation of each of the limiters based on the packaging geometry and the motion of the packaging's CG (see Section 2.10.8.8.2).

2. Calculate the forces which the limiters exert on the packaging body using the deformation of the limiters and their stress-strain characteristics (see Section 2.10.8.8.2).

3. Use Equations 2, 3, and 4 to calculate the accelerations during the time interval. Use the Runge Kutta equations to calculate the location and velocity of the cask CG at time $t_{i+1}$.

4. Go to step (1) to repeat the process until time $t_{max}$.

5. Generate the output.

Output from the code consists of:

- Problem title, packaging geometry, drop conditions, and integration data.
- Limiter geometric and material property data.
- History of packaging CG motion and amount of crushing in each of the limiters.
- Force history data.
- Plot of acceleration histories.
- Plot of maximum limiter deformations.

2.10.8.8.2 Forces in Limiters

The methods used to calculate the forces $F_{v1}$, $F_{v2}$, and $F_h$ in the limiter at a given crush depth are discussed in this section. These calculations are used to perform steps (1) and (2) above. The limiter geometry and material specification is discussed first. The general methodology used to calculate the forces are then presented which is followed with a detailed development of the equations used to calculate the force-displacement relationships.

Limiter Geometry

A sketch of the model of a limiter is shown on Figure 2.10.8-5. Regions I, II and III are used to delineate regions where different materials are used. It should be noted that the properties of the three regions are designed to accommodate the crush requirements of the three significant drop orientations. The properties of regions I, II and III are selected to control the decelerations resulting from vertical, corner, and shallow drop orientations, respectively. The properties used to describe the stress-strain behavior of each of the three materials are discussed below. The dimensions $A$ and $B$ may vary for the limiters at each end of the packaging, but $R_0$ and $R_i$ are taken to be the same for both limiters. The same material properties are used for each of the limiters.

General Approach

The ideal energy absorbing material is one that has a stress-strain curve that has a large strain region where the stress is constant. Such a material absorbs the maximum energy while minimizing force (which determines the magnitude of the deceleration). Wood, foam, and honeycomb materials exhibit such behavior and are prime candidates for impact limiter crushable material. If the constant stress region of the stress-strain curve is of primary interest, the forces may be calculated as the crush stress times the area of the surface defined by the intersection of the target and the impact limiter. This approach assumes that the crush stress, which acts normal to the crush surface, is not influenced by stresses acting in directions parallel to the crush surface (i.e., the confining stresses). This assumption is made in the computer code. The crush stress used as input to the code is selected to represent that value which is consistent with the degree of confinement afforded by the impact limiter geometry for the drop orientation considered.

Therefore, the crushable material is modeled in the code with a one dimensional (oriented normal to the crush surface) stress-strain law. The properties of the stress-strain law are selected to represent the degree of confinement provided by stresses acting in the other two dimensions. The properties of the crushable material are not modified as the packaging rotates but are selected to represent the material properties for the initial crush direction of the material.

A portion of the "crushed" area of the limiter is often not backed up by the packaging body (*i.e.*, a projection of a point in this non backed up area normal to the target (impact surface) does not intersect the cask body). The user must specify the percentage of these forces which are to be included in the calculation. The confinement provided by the overall construction of the limiter will determine the extent to which these non backed up forces are actually effective. The computer code does not perform any computations which would allow the user to judge the adequacy of the selected percentage of non backed up forces which are counted.

The evaluation of the impact area and its centroid (required to locate the impact forces) is computationally complicated because of the many variations possible in the manner in which the target intersects the limiter. This problem is resolved by dividing the surface of the limiter into many small segments. The segment is located relative to the target at each computation. If the segment's original location is below the target, then it has crushed and it contributes a force equal to the stress times its area projected on the target. The location of this force is also known. The strain at the segment may also be evaluated so that the peak strains may be determined and stresses may be evaluated for strains which fall outside of the constant crush stress region of the stress-strain law.

The forces must be calculated at each time that the solution for the packaging response is computed. The problem, therefore, is to determine the forces acting on the limiters given the current location of the packaging center of gravity. The solution for the location of the packaging center of gravity is discussed in Section 2.10.8.8.1. The procedure used to perform these computations is as follows (each of the steps is detailed below).

1. Define the location of the target relative to the limiters from the current location of the packaging center of gravity relative to the target.

2. Divide the surface of the limiter into segments and calculate the strain in a one-dimensional element spanning the distance between the center of the segment and the packaging body.

3. Compute the stress in the element from the stress-strain relationship. Multiply the stress by the area of the element projected onto the target.

4. After all of the segments on the limiter are evaluated, sum the segment forces and moments of the forces to find the total force and moment acting on the packaging.

5. Calculate the horizontal force and moment of the horizontal force.

6. Use equations 2, 3, and 4 to extend the solution to the next time step. The new solution consists of the location of the packaging CG at the new time. The above steps are then repeated. This process is continued until the specified maximum time is reached.

Details of Force Computations

Details of each of the six steps outlined above are given in this section. Note that the location of the packaging CG is known at the beginning of this computational sequence.

Deformation of the Limiter

The first step in the computation is to evaluate the location of the limiters relative to the target given the location of the packaging CG relative to the target. The limiter position relative to the target is defined by the six variables, $D_1$ through $D_6$, as shown on Figure 2.10.8-6. The location of the cask at first contact is shown on Figure 2.10.8-6a with the subscript 0 added to the $D$'s indicating initial values. The initial values of these parameters (when the lowest corner of the packaging first contacts) are found from the following geometric considerations.

$$\begin{aligned} D_{10} &= 2R_0 \cos\theta, \\ D_{20} &= 0, \\ D_{30} &= B_1 \sin\theta, \\ D_{40} &= D_{30} + D_{10} + L\sin\theta + B_2 \sin\theta, \\ D_{50} &= D_{40} - D_{10}, \\ D_{60} &= D_{30} + L\sin\theta, \end{aligned} \tag{5}$$

At a given time, $t$, the packaging CG has displaced vertically, $u$, horizontally, $x$, and has rotated, $\rho$, and reached the position shown in Figure 2.10.8-6b. Each of the six points have then fallen by an amount:

$$\Delta D = u + l\,[\sin\theta - \sin(\theta - \rho)] + r\,[\cos\theta - \cos(\theta - \rho)] \tag{6}$$

Where $l$ is the axial distance CG to point (+CG to top), and $r$ is the radial distance CG to point (+CG to impact).

Then the corner deformation, $D_2$, at time, $t + 1$, becomes

$$D_{2(t+1)} = D_{2t} + \Delta D_2.$$

Where

$$\begin{gathered} l_1 = l_2 = -yL^* - B_1, \\ l_3 = -yL^* \\ l_4 = l_5 = (l - y)L^* + B_2, \\ l_6 = (l - y)L^*, \\ r_1 = r_4 = -R_0, \text{ and} \\ r_2 = r_3 = r_5 = r_6 = R_0. \end{gathered}$$

To facilitate the computation of strains in the limiter, the position of the limiter relative to the impact surface is classified as shown in Figure 2.10.8-7. There are three possible locations of the impact surface relative to the limiter. The task is therefore to define which of the three patterns apply, and to determine the parameters $\phi$ and $\Delta$ in terms of the variables $D_1$ through $D_6$, just determined.

These deformations are next related to the three types of crush patterns for the bottom limiter shown on Figure 2.10.8-7. Crush pattern I applies when

$$D_1 < 0; D_2 < 0; D_3 > 0. \tag{8}$$

Then,

$$\Delta = -\frac{D_2}{\cos\phi}, \text{ and} \tag{9}$$

$$\phi = \cos^{-1}\frac{D_3 - D_2}{B_1}.$$

Crush pattern II applies when

$$D_1 > 0; D_2 < 0; D_3 > 0. \tag{10}$$

Then,

$$\Delta = -\frac{D_2}{\cos\phi}, \text{ and} \tag{11}$$

$$\phi = \cos^{-1}\frac{D_3 - D_2}{B_1}.$$

Crush pattern III applies when:

$$D_1 > 0; D_2 < 0; D_3 < 0. \tag{12}$$

Then,

$$\Delta = \frac{D_2}{\sin\phi}, \text{ and} \tag{13}$$

$$\phi = \sin^{-1}\frac{D_1 - D_2}{2R_0}.$$

The same set of equations applies to the top limiter if $D_1$, $D_2$, $D_3$, and $B_1$ are replaced with $D_4$, $D_5$, $D_6$, and $B_2$ in equations (8) through (13).

Strains in Limiters

The next step in the computation is to calculate strains in the limiters given the deformation defined above. The limiters are first divided into segments as shown in Figure 2.10.8-8. The number of segments used for the bottom, *NB*, and the sides, *NS*, are input by the user. Locations on the surface of the limiters are described in terms of the ($R$, $Z$, $\beta$) coordinate systems shown on the figure. Strains in the segments along the sides of the limiters are calculated based on the location of the center of the segment ($R_0$, $Z$, $\beta$). The segments at the bottom are divided into two pieces: one for $R < R_i$ (i.e. in Region 1) and the second for $R > R_i$. A strain is calculated for each of these two pieces for each segment along the bottom surface.

The strains, $\varepsilon$, are calculated as the deformation of the point normal to the crush surface, $\delta$, divided by the undeformed distance of the point from the surface of the limiter to the outer container (q), again measured normal to the crush surface. Therefore:

$$\varepsilon = \delta / q \tag{14}$$

Different equations govern each of these parameters for each of the three crush patterns as shown on Figure 2.10.8-7.

The geometry for crush pattern I is shown on Figure 2.10.8-9. Forces resulting from deformation of the side elements are neglected for this crush pattern. It may be shown that the deformation is

$$\delta = \Delta \cos\phi + (R \cos\beta - R_0) \sin\phi \tag{15}$$

The undeformed length of the element is taken measured to the plane of the packaging bottom so that

$$q = A_1 \cos\phi \tag{16}$$

The geometry for crush pattern II is shown on Figure 2.10.8-10. The deformation of the points on the bottom (a) and along the side (b) may be represented with the same equation

$$\delta = \Delta \cos\phi + (R \cos\beta - R_0) \sin\phi - Z/\cos\phi \tag{17}$$

The original length of the element depends on the intersection of the projection of the point on the impact surface with the outline of the limiter. Four points are identified as shown on Figure 2.10.8-10. The lengths are

$$q_1 = \frac{A-Z}{\cos\phi},$$
$$q_2 = \frac{X}{\sin\phi}, \qquad (18)$$
$$q_3 = \frac{B-Z}{\cos\phi}, \text{ and}$$
$$q_4 = \left[\left(R_0^2 - R^2\sin^2\beta\right)^{1/2} + R\cos\beta\right]\sin\phi.$$

Where $X = R\cos\beta + (R^2\cos^2\beta - R^2 + R_1^2)^{1/2}$.

The deformation for crush pattern III is shown on Figure 2.10.8-11. Deformations of points on the bottom of the limiter are neglected for this crush pattern. The deformation is

$$\delta = \frac{\Delta - Z/\tan\phi - R_0(1-\cos\beta)}{\sin\phi}$$

The original length is measured to, $R_i$, so that

$$q = \frac{R_0 - R_i}{\sin\phi}. \qquad (20)$$

Segment Stress

The stresses in the elements are calculated from the above strains. As mentioned above, three sets of stress-strain laws are input to the code, one for each of the regions defined in Figure 2.10.8-5.

The location of the center of the segment on the surface of the limiter is used to determine which of the three stress-strain laws is to be used. The model may be viewed as a set of one dimensional rods which run from the center of the segment, normal to the target, to another boundary of the limiter. The entire rod is given the properties which the limiter material has at the beginning point of the rod (i.e., the intersection with the target).

The stress-strain law used for the materials is shown on Figure 2.10.8-12. Each of the seven parameters shown on the figure is input to the code for each of the three regions of the limiter. The arrows on the figure indicate the load-unload paths used in the model. The step in the crush strength is built into the stress-strain law so that two crushable materials in series may be modeled. The two crush strengths should be specified as the actual crush strengths of the two materials. The first locking strain, $\varepsilon_l$, should be specified as the locking strain of the weaker material times the length of the weaker material divided by the total specimen length. The higher locking strain, $\varepsilon_L$, should be specified as the first locking strain plus the locking strain of the stronger material times its length and divided by the specimen length.

As stated above, the properties of the limiter material are not varied as the limiter crushes and the packaging rotates. Limiter materials such as wood exhibit anisotropic material properties. This must be accounted for when the properties are input to the code based on the anticipated direction of crushing. Most of the anisotropic wood data is based on tests performed in the elastic range. The following relationship has been used to represent wood properties for a loading which is applied at an angle (a) with respect to the wood grain:

$$P = \frac{P_1 \cos^4 \alpha + P_2 \sin^4 \alpha}{\cos^4 \alpha + \sin^4 \alpha} \tag{21}$$

Where $P$ is the property of interest at angle $\alpha$, and $P_1$ and $P_2$ are properties parallel and perpendicular to grain.

Evaluation of Forces

The stresses determined above are multiplied by the area of the segment projected onto the crush surface. The areas of the sidewall segments are (see Figure 2.10.8-8):

$$A_s = \frac{2R_0 B \cos(\theta - \rho)}{(NB)(NS)\tan\beta}. \tag{22}$$

The area of the bottom segments is divided into two parts, one in region I and the other in region II. These areas are

$$A_b = \frac{4R_0 L_b \sin(\theta - \rho)}{NB} \tag{23}$$

Where, $L_b = (R_i^2 - R_c^2)^{1/2}$ for region 1, and $L_b = (R_0^2 - R_c^2)^{1/2} - (R_i^2 - R_c^2)^{1/2}$ for region II.

These forces are summed for all of the elements to determine the total force acting on the packaging. The forces are also multiplied by their moment arms about the packaging CG to calculate the total moment acting on the packaging. The point on the segment is first projected, normal to the target, to evaluate whether or not it intersects the packaging body. If the projection does not intersect the packaging body, only a percentage of the force is included in the summation. The user specifies the percentage to be used.

Horizontal Force

A horizontal force develops at the limiter/target interface. This force is only considered for the bottom limiter (i.e., the first to impact) since the packaging is always close to horizontal when the top impact limiter is in contact.

The horizontal force, $F_h$, is first calculated as that required to restrain horizontal motion of the tip of the limiter.

The horizontal acceleration, $\ddot{\Delta}_H$, at the tip of the bottom limiter (point 2 on Figure 2.10.8-6) may be related to the CG motion of the packaging by

$$\ddot{\Delta}_H = \ddot{x} - \ddot{\rho}\left[\left(\gamma L^* + B_1\right)\cos\phi + R_0 \sin\phi\right] \tag{24}$$

Where $\phi = \frac{\pi}{2} - \theta + \rho$.

Equating $\Delta_H$ to zero would result in no acceleration of the tip in the horizontal direction and provides the solution for $x$ in terms of $\rho$.

Substituting this solution for $x$ into Equation (3) results in an expression for the horizontal force, $F_h$, required to restrict horizontal acceleration of the tip, in terms of the rotational acceleration, $\rho$. Finally, equation 4 is used to eliminate $\rho$ with the following result.

$$F_h = \frac{M_v W\left[\left(\gamma L^* + B_1\right)\cos\phi + R_0 \sin\phi\right]}{J_g + W\left[\left(\gamma L^* + B_1\right)\cos\phi + R_0 \sin\phi\right]^2} \tag{25}$$

Where $M_v$ is the moment due to vertical forces, which is equal to $F_{v1}x_{v1} - F_{v2}x_{v2}$, and $W$ is the packaging weight.

This force is restricted to

$$F_h < \mu F_{v1} \tag{26}$$

Where $\mu$ is the coefficient of friction specified by user.

2.10.8.9 References


1. Federal Specification MMM-A-188b.

2. Dreisback, J.F., *Balsa Wood and Its Properties*, Columbia Graphs, Columbia, CT 1952.

3. Baumeister, T., Marks, L. S., *Standard Handbook for Mechanical Engineers*, 8th Edition, McGraw-Hill, pg. 6-124.

4. American Society of Mechanical Engineers, ASME Boiler and Pressure Vessel Code, Section II, Part D, 1998, including 1999 Addenda.

5. *Machinery Handbook*, 21st Edition, Industrial Press, 1979.

Table 2.10.8 -1
Mechanical Properties of Wood and Wood Adhesive

| Minimum Properties of Adhesive | |
|---|---|
| Shear Strength by Compression Loading | 2,800 lb $in^{-2}$ [1] |
| Shear Strength by Tension Loading | 340 lb $in^{-2}$ [1] |
| Properties of Heavy Balsa (10-12 lb $ft^{-3}$) | |
| Shear Strength Parallel to Grain | 315-385 psi max. [2] |
| Tensile Strength Perpendicular to Grain | 140-160 psi [2] |
| Properties of Redwood | |
| Shear Strength Parallel to Grain | 940 psi [3] |
| Tensile Strength Perpendicular to Grain | 240 psi [3] |

Table 2.10.8-2
Typical Wood Material Properties

| Property | High Density Balsa | Redwood |
|---|---|---|
| Density | 10-12 lb $ft^{-3}$ | 18.7-27.5 lb $ft^{-3}$ |
| Parallel to Grain | | |
| Crush Stress | 1560-2010 psi | 5000-6500 psi |
| Locking Strain | 0.8 | 0.6 |
| Unloading Modulus | 32,000 psi | 1,247,000 psi |
| Locking Modulus | 10 × (max. crush stress) | 10 × (max. crush stress) |
| Perpendicular to Grain | | |
| Crush Stress | 300-420 psi | 750-975 psi |
| Locking Strain | 0.8 | 0.6 |
| Unloading Modulus | 32,000 psi | 1,247,000 psi |
| Locking Modulus | 10 × (max. crush stress) | 10 × (max. crush stress) |

Table 2.10.8-3
First Impact Maximum Inertia *g* Load versus Initial Angle of Impact
for 30 Foot Drop,
using Maximum Wood Crush Stress Properties

| Impact Angle, 30 Foot Drop | Maximum *g* Load During First Impact, Maximum Wood Properties | | | |
|---|---|---|---|---|
| | Axial | Transverse | | |
| | CG | Top | Bottom | CG |
| 0° | 3 | 60 | 59 | 59 |
| 5° | 9 | 19* | $G_{nor} = 31$<br>$G_{rot} = 50$ | 31 |
| 10° | 14 | 21* | $G_{nor} = 36$<br>$G_{rot} = 57$ | 36 |
| 15° | 21 | 24* | $G_{nor} = 43$<br>$G_{rot} = 66$ | 43 |
| 20° | 31 | 28* | $G_{nor} = 53$<br>$G_{rot} = 80$ | 53 |
| 30° | 10 | 12 | $G_{nor} = 12$<br>$G_{rot} = 25$ | 12 |
| 40° | 17 | 9 | $G_{nor} = 14$<br>$G_{rot} = 24$ | 14 |
| 45° | 24 | 7 | $G_{nor} = 17$<br>$G_{rot} = 24$ | 17 |
| 50° | 26 | 4 | $G_{nor} = 15$<br>$G_{rot} = 18$ | 15 |
| 60° | 34 | 4 | $G_{nor} = 12$<br>$G_{rot} = 10$ | 12 |
| 70° | 43 | 4 | 13 | 9 |
| 80° | 46 | 3 | 7 | 5 |
| 90° | 44 | 2 | 0 | 1 |

* Maximum acceleration occurred during second impact.

Table 2.10.8-4
Second Impact Maximum Inertia *g* Load versus Initial Angle of Impact
for 30 Foot Drop,
using Maximum Wood Crush Stress Properties

| Impact Angle, 30 Foot Drop | Maximum *g* Load During Second Impact (Top), Maximum Wood Properties | | | | | | |
|---|---|---|---|---|---|---|---|
| | Axial | Transverse | | | | | |
| | CG | Top | | | Bottom | CG |
| | | Normal | Rotational | Impact Force (lb.×1000) | | |
| 5° | 1 | 37 | 71 | 10,200 | 33 | 37 |
| 10° | 1 | 37 | 69 | 10,116 | 32 | 37 |
| 15° | 3 | 37 | 70 | 10,222 | 33 | 37 |
| 20° | 9 | 44 | 83 | 12,343 | 37 | 44 |

Table 2.10.8-5
First Impact Maximum Inertia *g* Load versus Initial Angle of Impact
For 30 Foot Drop,
Using Minimum Wood Crush Stress Properties

| Impact Angle, 30 Foot Drop | Maximum *g* Load During First Impact (Bottom), Minimum Wood Properties | | | |
|---|---|---|---|---|
| | Axial | Transverse | | |
| | CG | Top | Bottom | CG |
| 0° | 4 | 53 | 53 | 53 |
| 5° | 7 | 16* | $G_{nor} = 24$<br>$G_{rot} = 41$ | 24 |
| 10° | 11 | 19* | $G_{nor} = 29$<br>$G_{rot} = 48$ | 29 |
| 15° | 16 | 20* | $G_{nor} = 34$<br>$G_{rot} = 53$ | 34 |
| 20° | 24 | 22* | $G_{nor} = 40$<br>$G_{rot} = 62$ | 40 |
| 30° | 27 | 14 | $G_{nor} = 34$<br>$G_{rot} = 48$ | 34 |
| 40° | 15 | 8 | $G_{nor} = 13$<br>$G_{rot} = 21$ | 13 |
| 45° | 21 | 7 | $G_{nor} = 15$<br>$G_{rot} = 22$ | 15 |
| 50° | 23 | 4 | $G_{nor} = 14$<br>$G_{rot} = 17$ | 14 |
| 60° | 32 | 4 | $G_{nor} = 11$<br>$G_{rot} = 8$ | 11 |
| 70° | 41 | 4 | 13 | 8 |
| 80° | 50 | 5 | 8 | 6 |
| 90° | 34 | 2 | 0 | 1 |

* Maximum acceleration occurred during second impact

Table 2.10.8-6
Second Impact Maximum Inertia *g* Load versus Initial Angle of Impact
for 30 Foot Drop,
using Minimum Wood Crush Stress Properties

| Impact Angle 30 Foot Drop | Maximum *g* Load During Second Impact (Top), Minimum Wood Properties | | | | | | |
|---|---|---|---|---|---|---|---|
| | Axial | Transverse | | | | | |
| | C.G. | Top | | | Bottom | C.G. |
| | | Normal | Rotational | Impact Force (lb.×1000) | | |
| 5° | 1 | 35 | 69 | 9,659 | 34 | 35 |
| 10° | 1 | 32 | 64 | 8,916 | 31 | 32 |
| 15° | 3 | 32 | 61 | 8,755 | 29 | 32 |
| 20° | 7 | 36 | 69 | 10,154 | 32 | 36 |

Table 2.10.8-7
Depth of Crush versus Crush Force, 0° Impact Angle

| Maximum wood properties | | Minimum wood Properties | |
|---|---|---|---|
| Crush Depth Δ (in.) | Force (Kips) | Crush Depth Δ (in.) | Force (Kips) |
| 2.62 | 4,081 | 2.62 | 3,006 |
| 5.00 | 6,346 | 5.08 | 4,674 |
| 7.01 | 6,346 | 7.25 | 4,674 |
| 8.55 | 8,027 | 9.07 | 4,599 |
| 9.54 | 8,027 | 10.50 | 5,912 |
| 10.01 | 5,504 | 11.50 | 6,912 |
| | | 12.11 | 5,632 |

Table 2.10.8-8
Depth of Crush versus Crush Force, 20° Impact Angle

| First Impact | | | |
|---|---|---|---|
| Maximum wood properties | | Minimum wood Properties | |
| Crush Depth Δ (in.) | Force (Kips) | Crush Depth Δ (in.) | Force (Kips) |
| 5.28 | 218 | 5.29 | 167 |
| 10.51 | 598 | 10.54 | 454 |
| 15.56 | 669 | 15.66 | 528 |
| 20.32 | 13,568 | 20.51 | 10,645 |
| 22.41 | 15,386 | 22.84 | 12,050 |
| Second | | Impact | |
| Maximum wood | Properties | Minimum wood | Properties |
| Crush Depth Δ (in.) | Force (Kips) | Crush Depth Δ (in.) | Force (Kips) |
| 0.47 | 0 | 0.16 | 0 |
| 9.68 | 6,071 | 8.51 | 4,238 |
| 16.22 | 10,757 | 15.86 | 7,719 |
| 18.15 | 6,573 | 19.95 | 5,946 |

Table 2.10.8-9
Depth of Crush versus Crush Force, 45° Impact Angle

| First Impact | | | |
|---|---|---|---|
| Maximum wood properties | | Minimum wood Properties | |
| Crush Depth Δ (in.) | Force (Kips) | Crush Depth Δ (in.) | Force (Kips) |
| 5.29 | 259 | 5.29 | 199 |
| 10.55 | 899 | 10.57 | 688 |
| 15.68 | 2,023 | 15.76 | 1,551 |
| 20.41 | 4,536 | 20.64 | 3,502 |
| 24.35 | 6,184 | 24.91 | 5,365 |
| 27.08 | 7,523 | 28.20 | 6,583 |
| 28.16 | 7,292 | 30.64 | 6,110 |

Table 2.10.8-10
Depth of Crush versus Crush Force, 60° Impact Angle

| First Impact | | | |
|---|---|---|---|
| Maximum wood properties | | Minimum wood Properties | |
| Crush Depth Δ (in.) | Force (Kips) | Crush Depth Δ (in.) | Force (Kips) |
| 5.29 | 224 | 5.29 | 164 |
| 10.58 | 930 | 10.59 | 691 |
| 15.75 | 2,675 | 15.81 | 2,040 |
| 20.56 | 5,055 | 20.77 | 3,871 |
| 24.73 | 6,418 | 25.22 | 5,294 |
| 27.99 | 7,745 | 28.97 | 6,669 |
| 30.13 | 9,445 | 31.79 | 8,559 |
| 30.92 | 6,490 | 33.81 | 5,077 |

Table 2.10.8-11
Depth of Crush versus Crush Force, 80° Impact Angle

| First Impact | | | |
|---|---|---|---|
| Maximum wood properties | | Minimum wood Properties | |
| Crush Depth Δ (in.) | Force (Kips) | Crush Depth Δ (in.) | Force (Kips) |
| 5.29 | 1,194 | 5.29 | 897 |
| 10.41 | 5,269 | 10.46 | 4,106 |
| 14.83 | 9,153 | 15.11 | 7,103 |
| 18.06 | 10,243 | 18.83 | 8,504 |
| 19.90 | 12,570 | 21.41 | 12,705 |
| 20.23 | 7,981 | 22.46 | 6,695 |

Table 2.10.8-12
Depth of Crush versus Crush Force, 90° Impact Angle

| First Impact | | | |
|---|---|---|---|
| Maximum wood properties | | Minimum wood Properties | |
| Crush Depth Δ (in.) | Force (Kips) | Crush Depth Δ (in.) | Force (Kips) |
| 2.59 | 11,291 | 2.60 | 8,656 |
| 6.82 | 11,291 | 7.10 | 8,656 |
| 9.48 | 11,957 | 10.42 | 9,196 |
| 10.54 | 6,006 | 12.53 | 9,196 |
| | | 13.44 | 8,012 |

Table 2.10.8-13
Maximum Inertial *g* Load During One Foot Drop

| Impact Angle, 1 foot Drop | Maximum *g* Load During First Impact, Maximum Wood Properties | | | |
|---|---|---|---|---|
| | Axial | Transverse | | |
| | CG | Top | Bottom | CG |
| 90° | 10 | 0 | 0 | 0 |
| 60° | 5 | 1 | 3 | 2 |
| 0° | 0 | 24 | 24 | 24 |

| Impact Angle, 1 foot Drop | Maximum *g* Load During First Impact, Minimum Wood Properties | | | |
|---|---|---|---|---|
| | Axial | Transverse | | |
| | CG | Top | Bottom | CG |
| 90° | 7 | 0 | 0 | 0 |
| 60° | 5 | 1 | 2 | 2 |
| 0° | 1 | 18 | 17 | 17 |

Table 2.10.8-14
Loading Used in Cask Body and Cask Internals Analysis
(Appendices 2.10.1, 2.10.3, and 2.10.4)
versus
Maximum *g* Load Predicted by ADOC Program

| Accident Conditions (30 Foot Drops) | | |
|---|---|---|
| Drop Orientation | Max. *g* Load from ADOC | Input Loading Used in Analysis |
| End Drop on Lid and Bottom | 50*g* Axial | 75*g* Axial |
| Side Drop | 60*g* Transverse | 75*g* Transverse |
| CG over Corner Drop on Lid And Bottom | 34*g* Axial | 45*g* Axial |
| | 12*g* Transverse | 16*g* Transverse |
| | | 48*g* Resultant Vertical |
| Low Angle Slap Down on Top Impact Limiter | 31*g* Axial | 35*g* Axial |
| | 53*g* Normal | 60*g* Normal |

| Normal Conditions (1 Foot Drops) | | |
|---|---|---|
| Drop Orientation | Max. *g* Load from ADOC | Input Loading Used in Analysis |
| 90° End Drop on Lid and Bottom | 10*g* Axial | 30*g* Axial |
| 0° Side Drop | 24*g* Transverse | 30*g* Transverse |

Figure 2.10.8-1
Impact Limiter Geometry

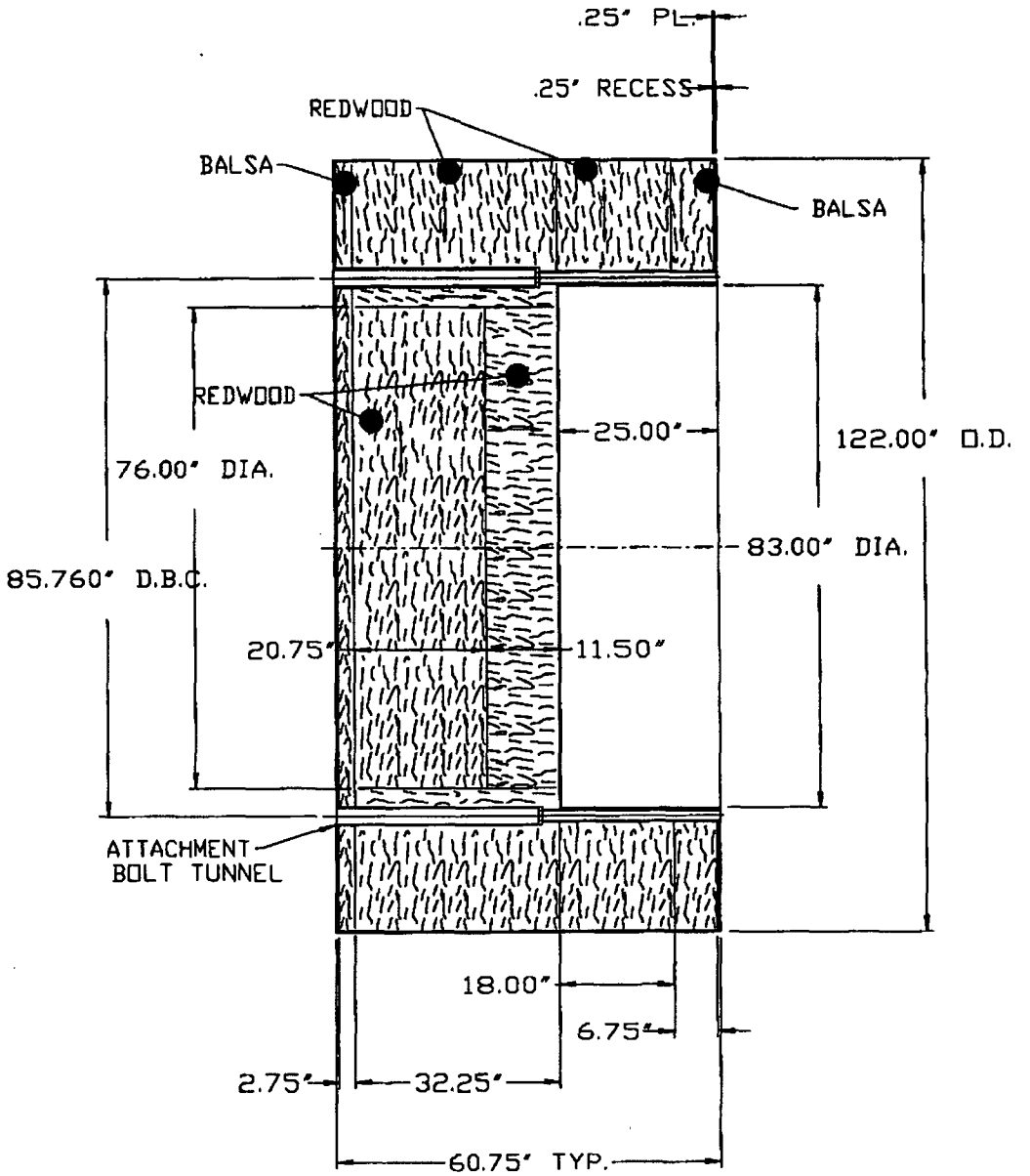

Figure 2.10.8-1A
Sample Force/Deflection Curve for Balsa

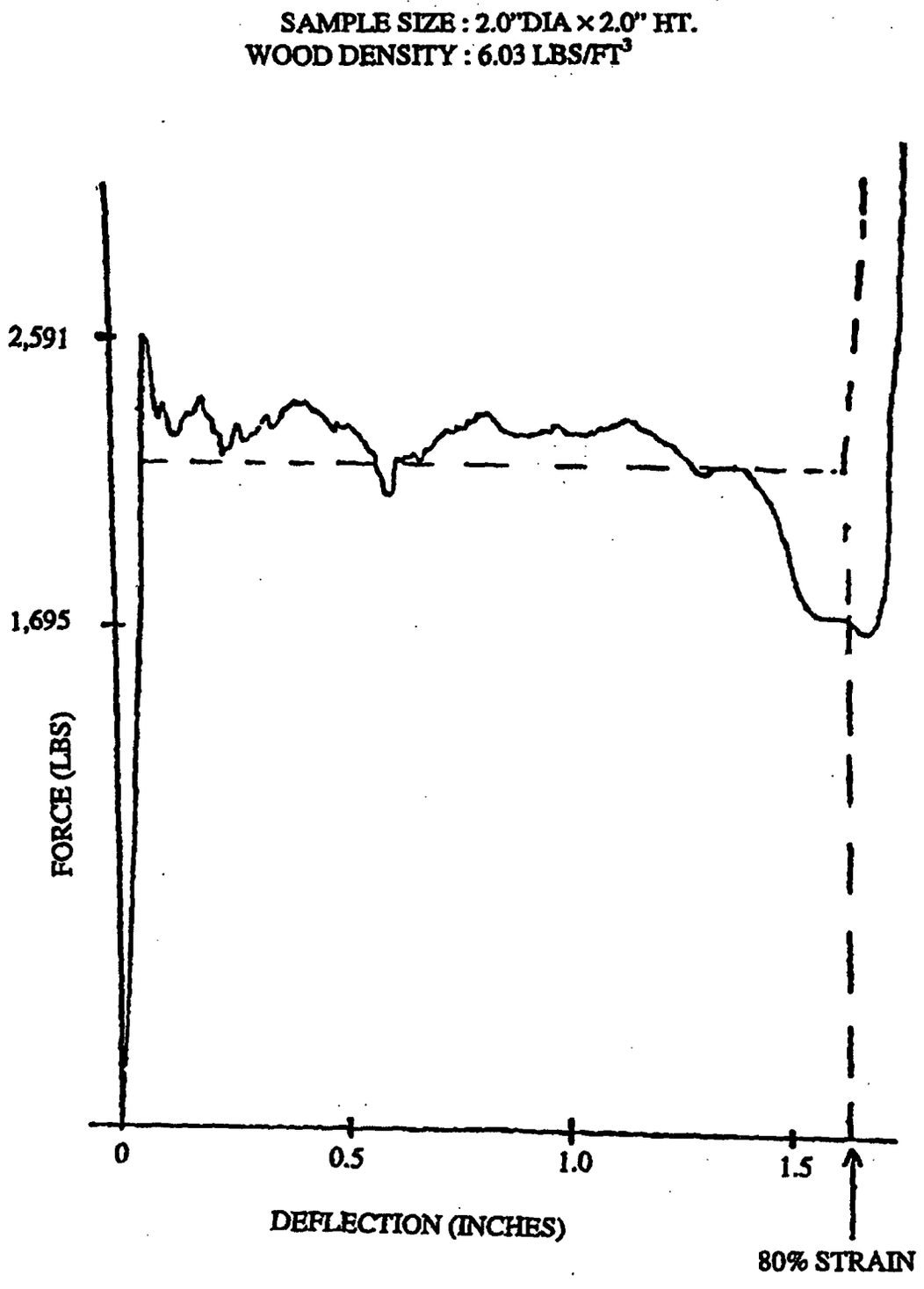

NOTE : NOMINAL SAMPLE 1.625"DIA × 1.625" HT.

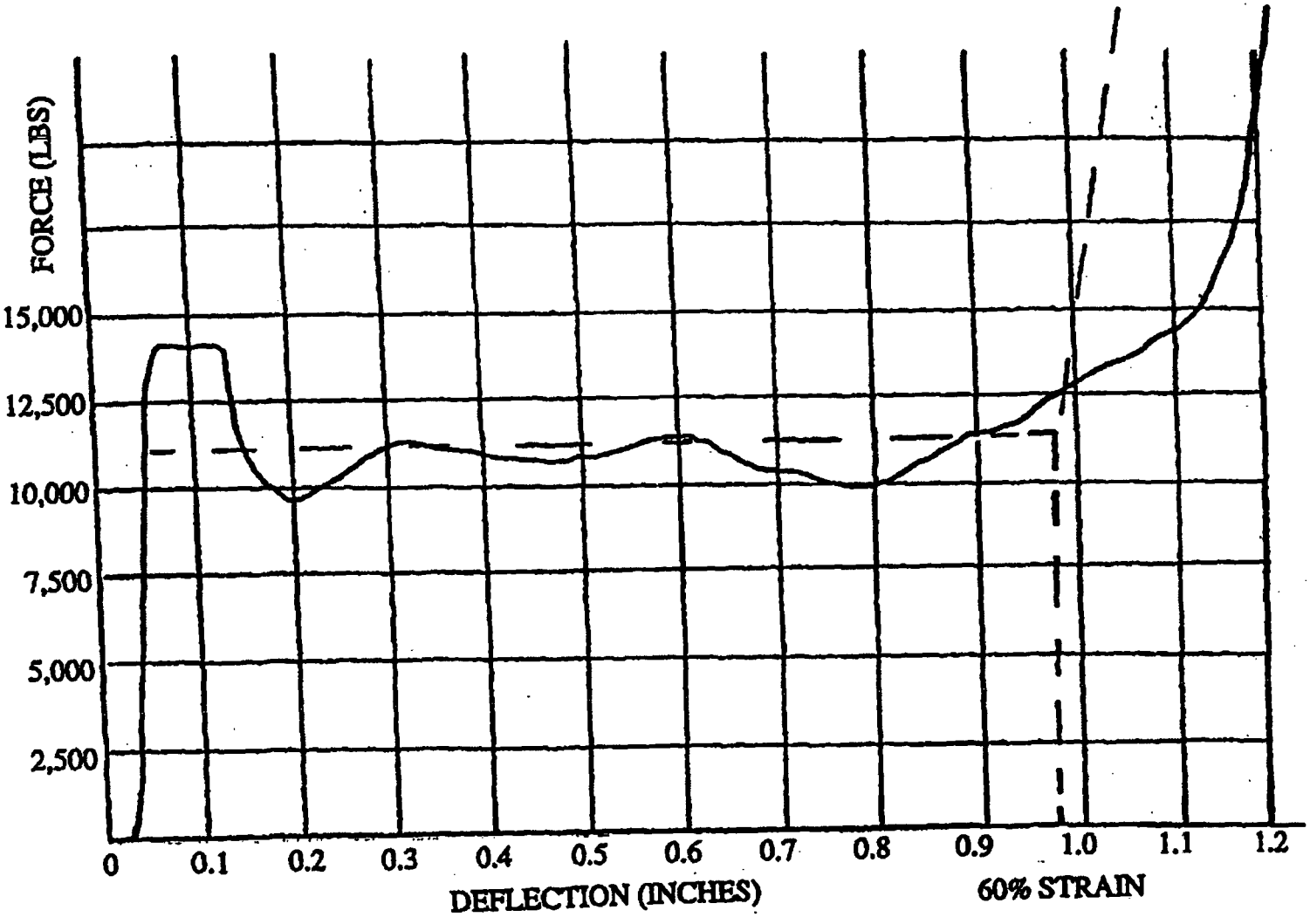


Figure 2.10.8-1B
Sample Force/Deflection Curve for Redwood

Figure 2.10.8-2
ADOC Computer Model for NUHOMS®-MP197 Transport Package

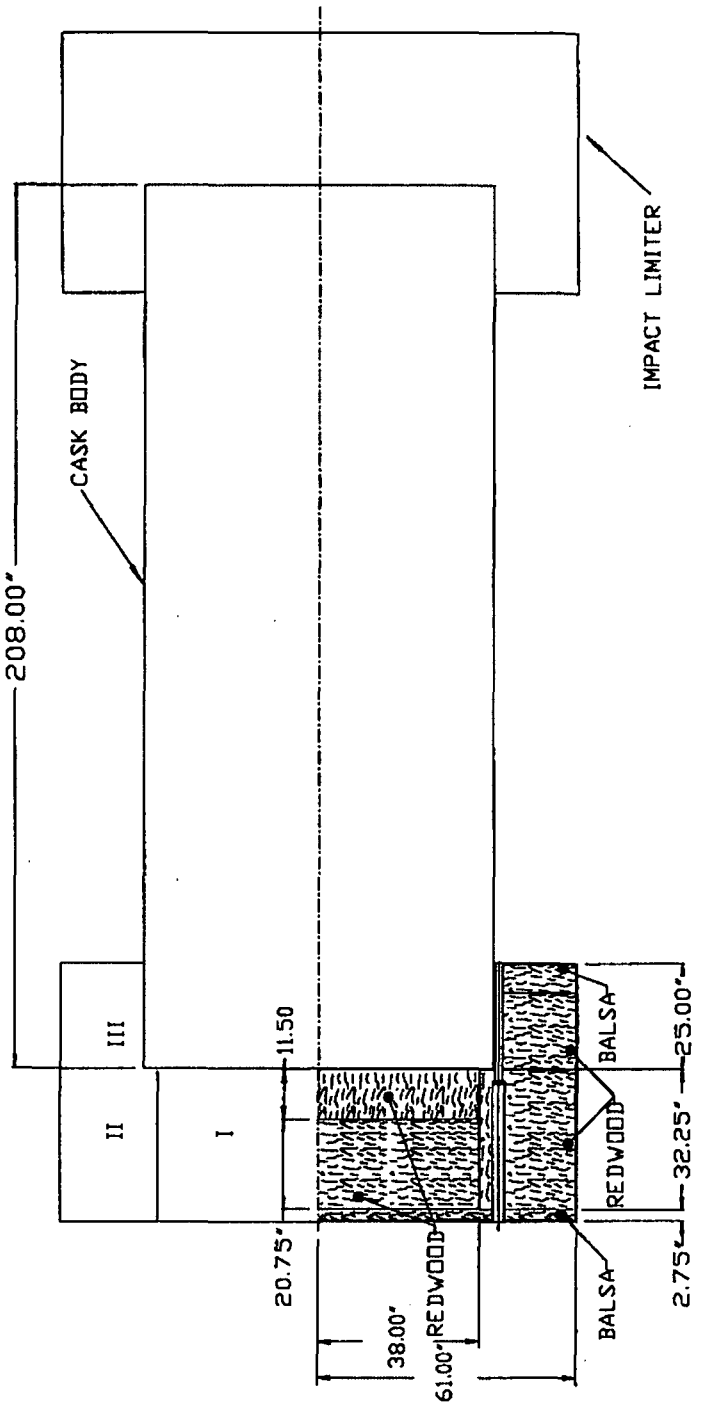

Figure 2.10.8-3
Geometry of Packaging

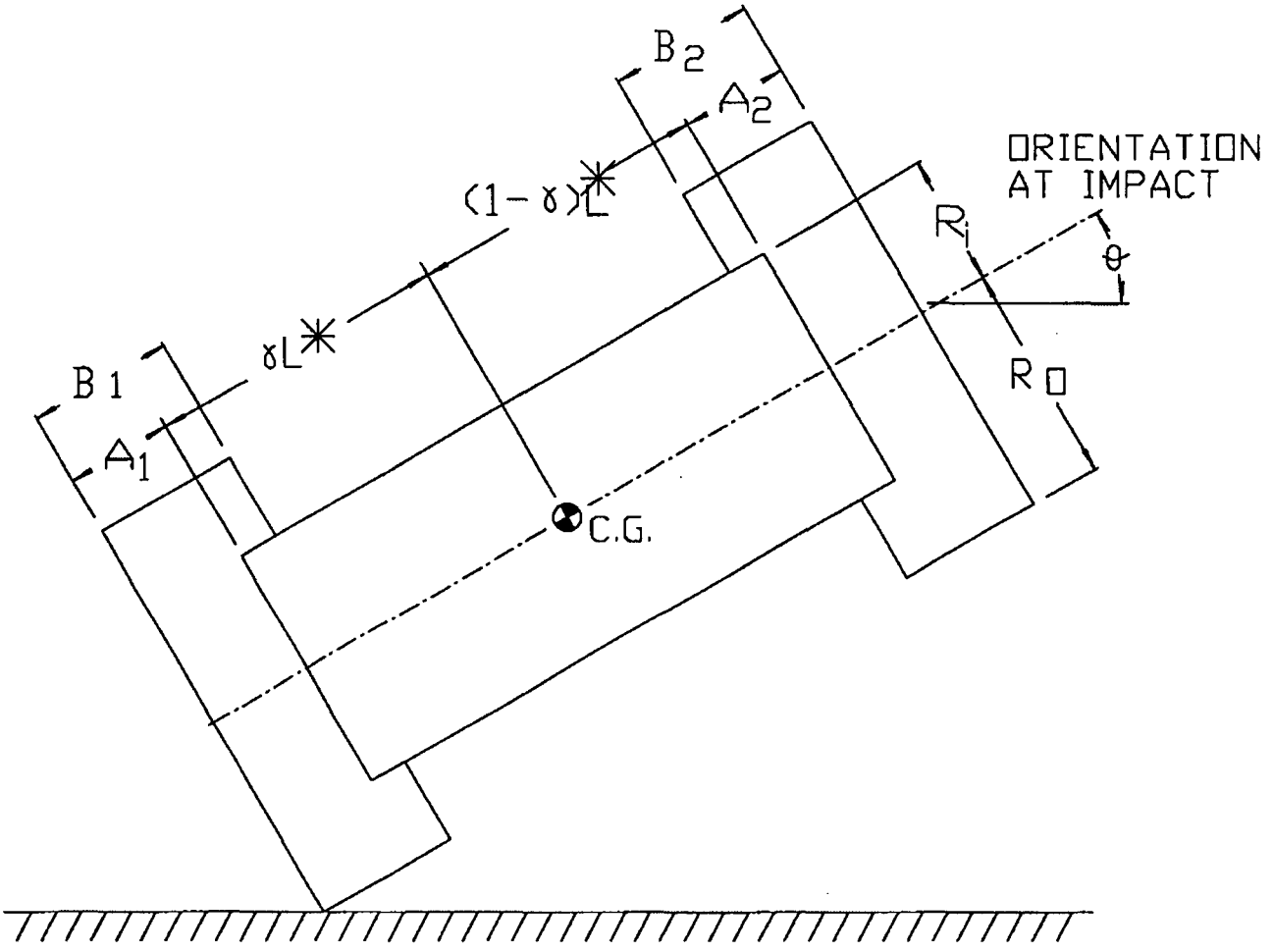

Figure 2.10.8-4
Packaging at Time, *t*

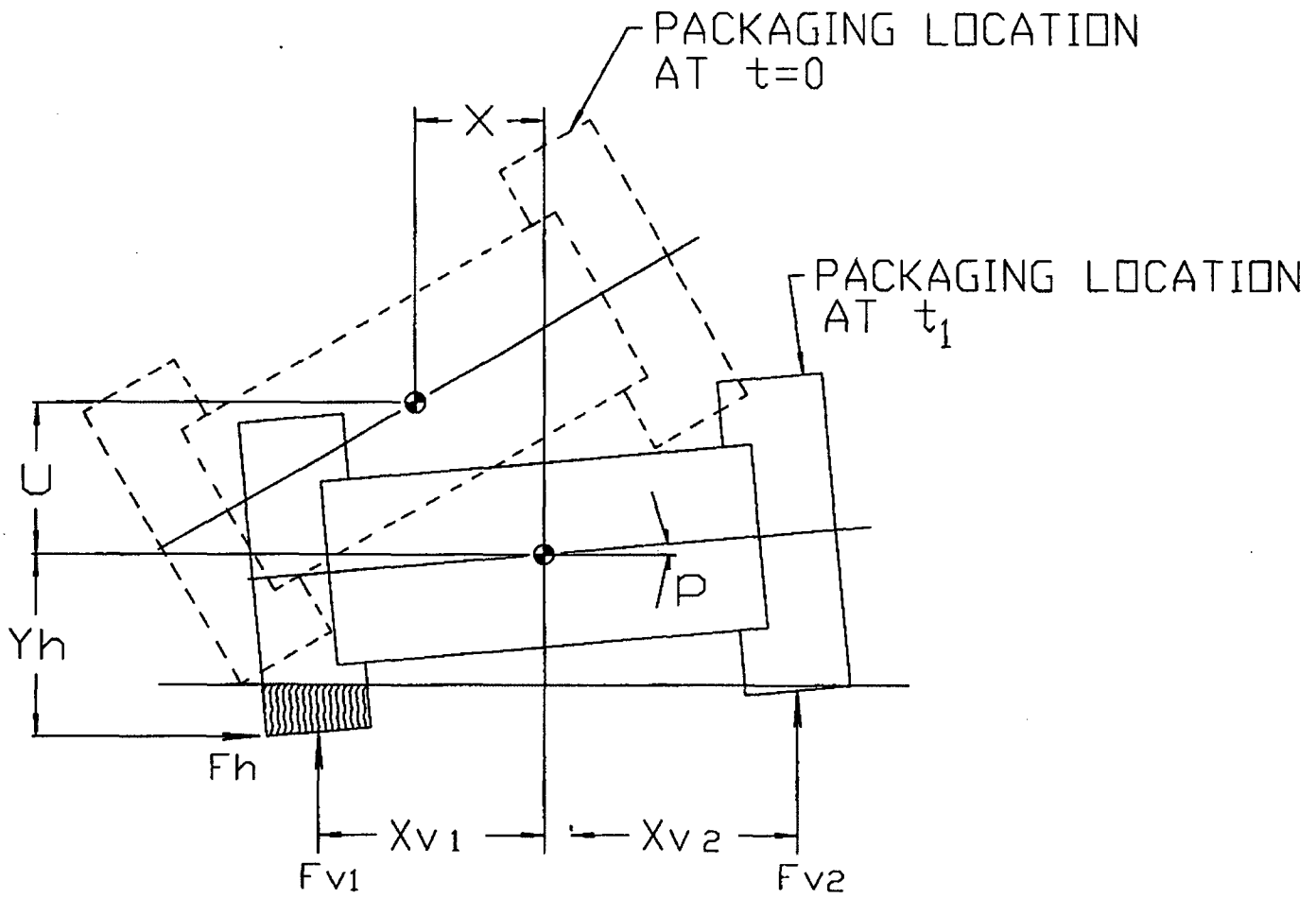

Figure 2.10.8-5
Geometry of Impact Limiter Parameters

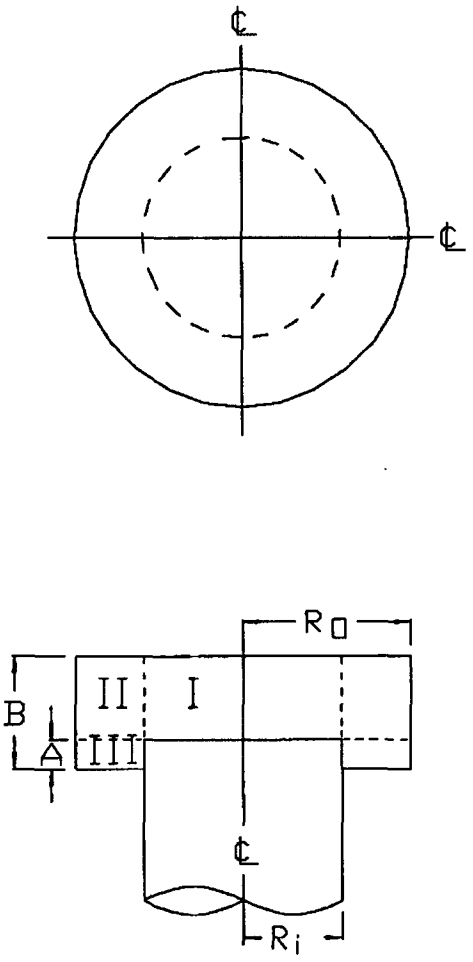

Figure 2.10.8-6
Definition of Limiter Deformation

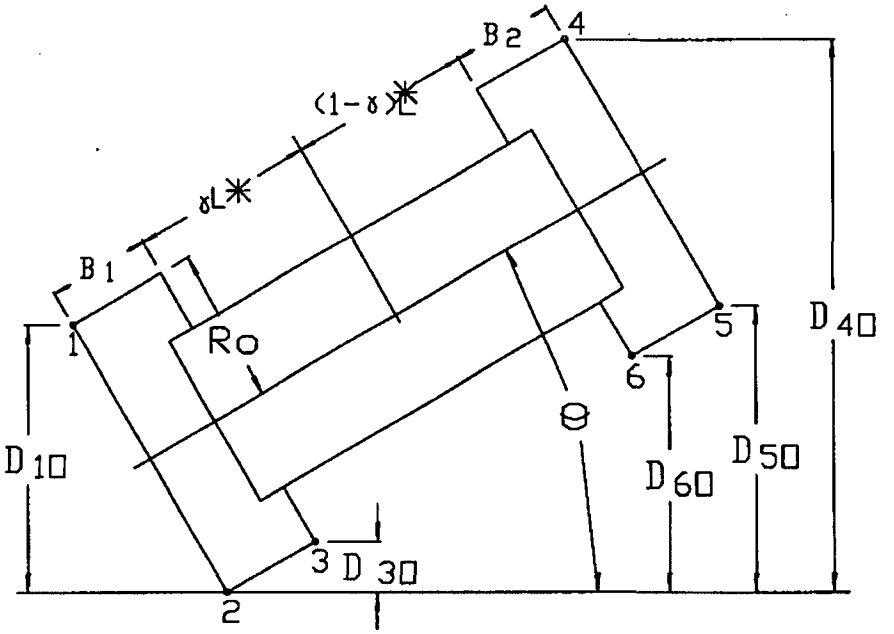


a) IMPACT LIMITER PARAMETERS AT FIRST IMPACT

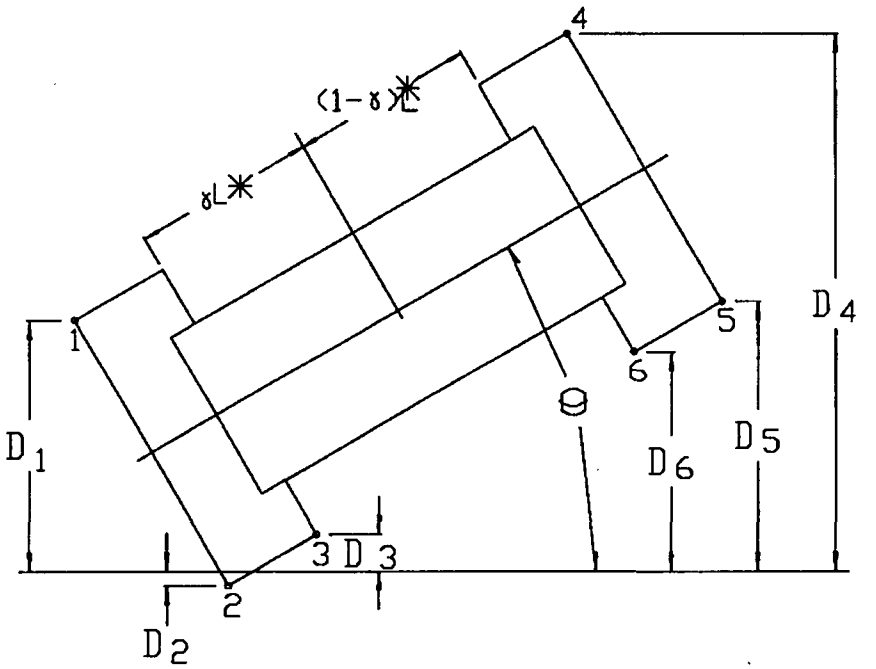


b) IMPACT LIMITER PARAMETER - GENERAL

Figure 2.10.8-7
Crush Pattern in Impact Limiter

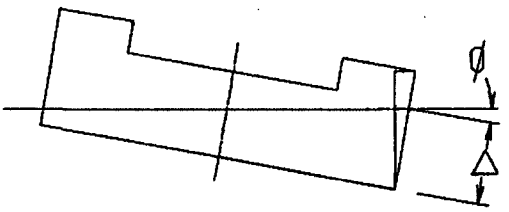


a) CRUSH PATTERN I

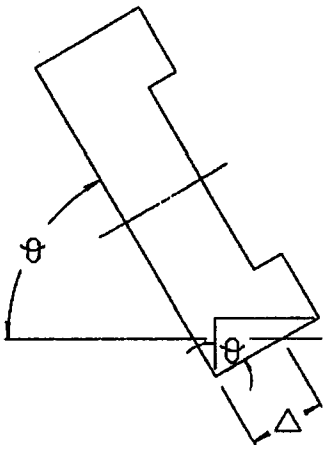


b) CRUSH PATTERN II

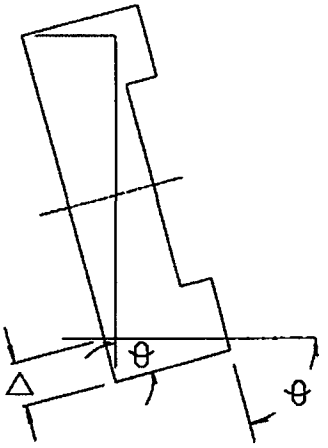


c) CRUSH PATTERN III

Figure 2.10.8-8
Impact Limiter Segments

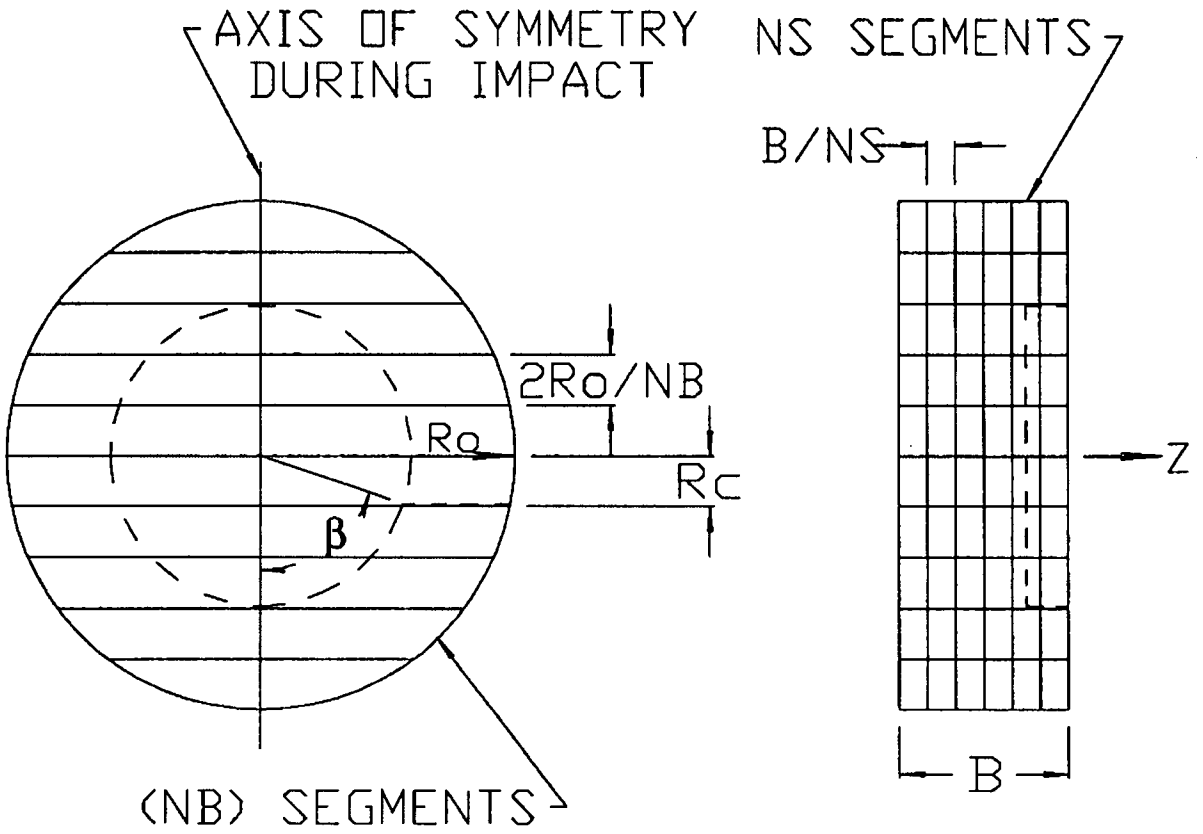

Figure 2.10.8-9
Strain Computation for Crush Pattern I

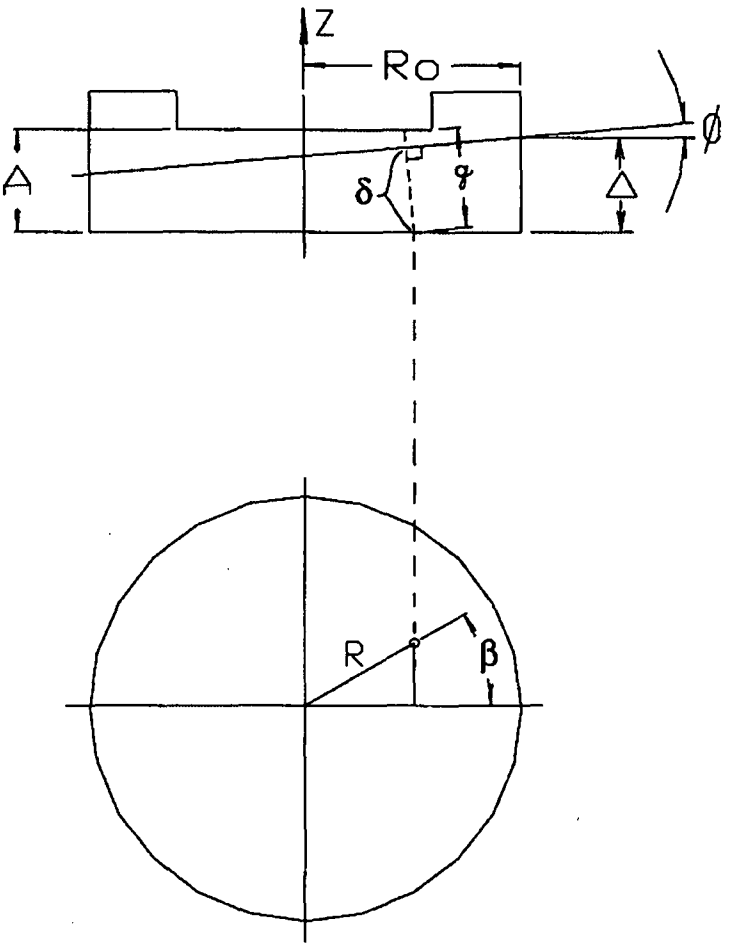

Figure 2.10.8-10
Strain Computation for Crush Pattern II

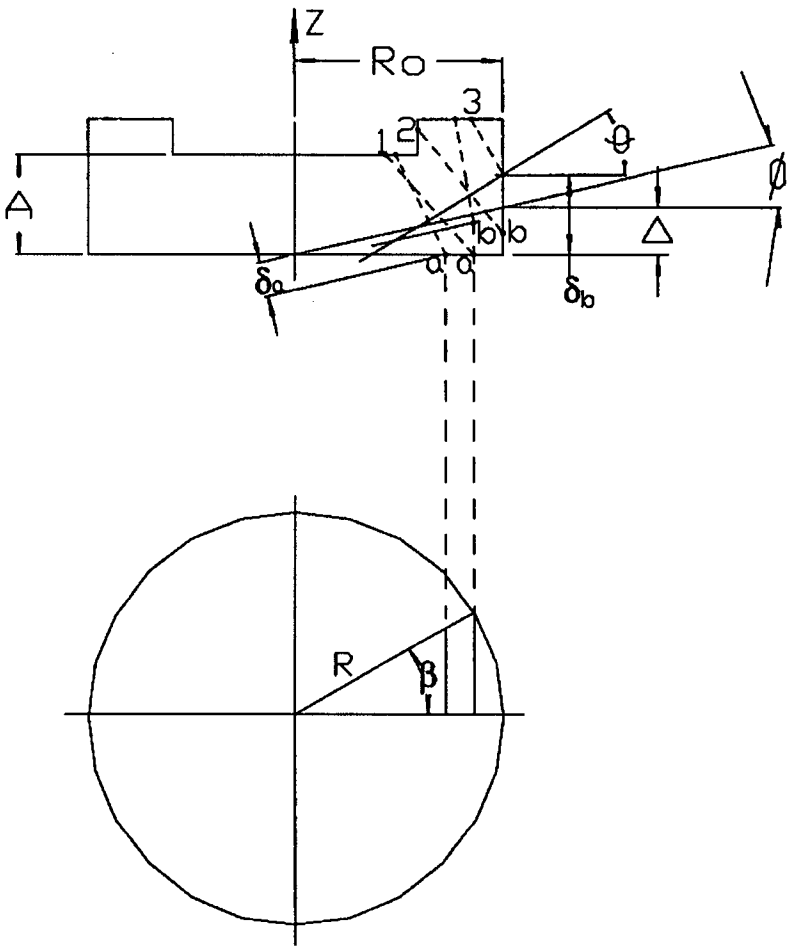

Figure 2.10.8-11
Strain Computation for Crush Pattern III

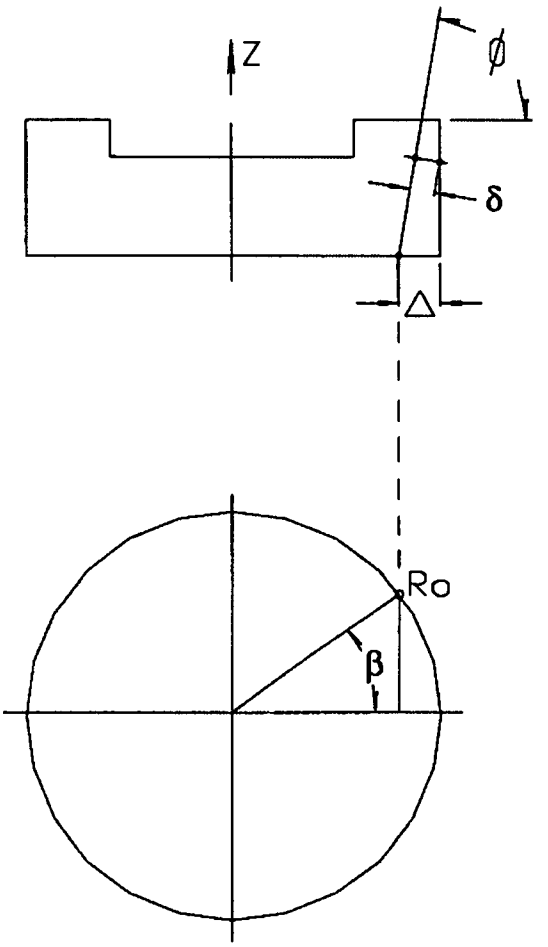

Figure 2.10.8-12
Wood Stress-Strain Curve

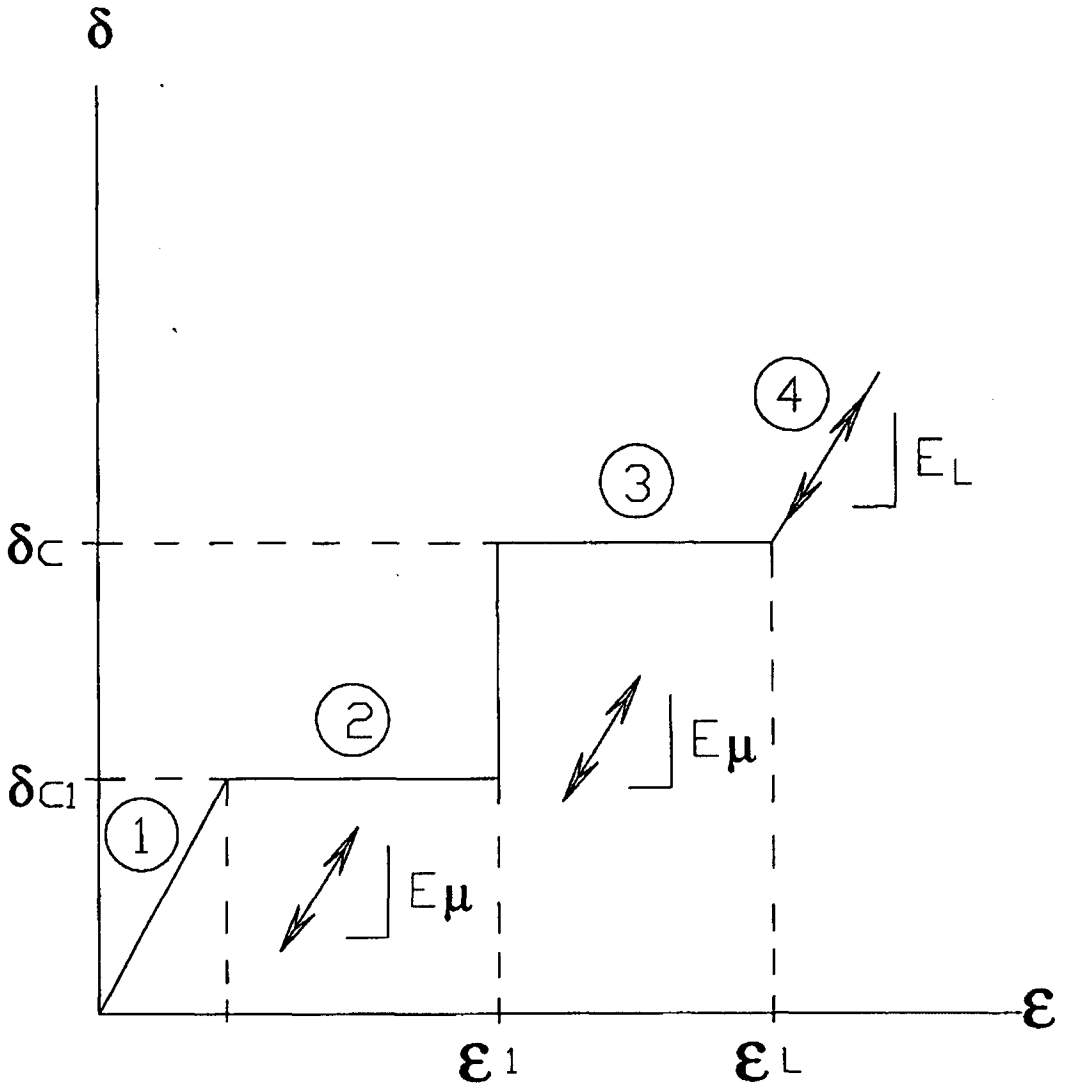

Figure 2.10.8-13
Impact Limiter Free Body Diagram during 20° Slap Down

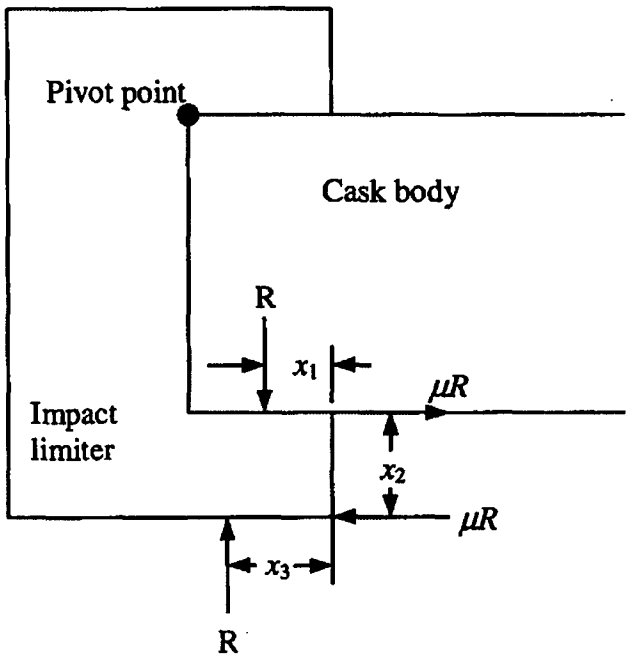


Where:

$R$ = reaction force, 16,500 kips.
$\mu$ = friction coefficient, 0.12
$x_1$ = 25.00/2 = 12.50 in.
$x_2$ = (I.L. od – I.L. id)/2 – crush depth = (122 – 83.00)/2 – 9.47 = 10.03 in.
$x_3$ = 25.00 – (209.75 – 104.60 – 94.07) = 13.92 in.

# APPENDIX 2.10.9

## TABLE OF CONTENTS



## LIST OF TABLES

LIST OF FIGURES

# APPENDIX 2.10.9

## NUHOMS®-MP197 PACKAGE IMPACT LIMITER TESTING

### 2.10.9.1 Introduction

A series of dynamic tests have been performed on one-third scale models of the NUHOMS®-MP197 cask impact limiters. The tests were performed to evaluate the effects of the 30 foot free drop hypothetical accident defined in 10 CFR 71.73(c)(1) [1]. The test results are used to verify the analyses performed for the NUHOMS®-MP197 package. The objectives of the NUHOMS®-MP197 cask impact limiter test program are:

- Demonstrate that the inertia *g* values and forces calculated in Appendix 2.10.8 and used in the analyses presented in Appendices 2.10.1 through 2.10.5 are conservative.
- Demonstrate that the extent of crush depths are acceptable, i.e., limiters do not bottom out and the neutron shield does not impact the target.
- Demonstrate the adequacy of the impact limiter enclosure.
- Demonstrate adequacy of the impact limiter attachment design.
- Evaluate the effects of low temperature (-20° F) on the crush strength and dynamic performance of the impact limiters.
- Evaluate the effects (puncture depth and shell damage) of a 40 inch drop onto a scaled six inch diameter puncture bar on a previously crushed impact limiter, as per 10 CFR 71.73(c)(3).

The four 1/3 scale impact limiters that were constructed are identified as 1, 2, 3, and 4. The various drop test orientations were performed in the following sequence.

| Test Number | Drop Orientation | Drop Height | Impact Limiter Number | Location of Impact Limiter | Comments |
|---|---|---|---|---|---|
| 1 | 0° Side Drop | 30 feet | 1 | Top | |
| | | | 2 | Bottom | |
| 2 | 20° Slap Down | 30 feet | 3 | Top ($2^{nd}$ Impact) | Limiter #1 was removed and replaced with limiter #3, entire test article rotates 180°. |
| | | | 2 | Bottom ($1^{st}$ Impact) | |
| 3 | 90° End Drop | 30 feet | 3 | Top | Limiter #2 was removed and replaced with limiter #4. Limiter #4 chilled at –20° F for 48 hours before installed to the test body. |
| | | | 4 | Bottom (Impact End) | |
| 4 | 90° End Drop | 40 inches | 3 | Top | Drop onto scaled 6 inch diameter puncture bar. |
| | | | 4 | Bottom (Puncture End) | |

The 0° side drop was performed because this orientation generates the highest transverse acceleration as well as significant deformation. The 0° side drop also provides a reasonable estimate of the likelihood of the neutron shield impacting the target.

The 20° slap down drop was chosen to be performed because the 20° orientation puts the highest load on the impact limiter attachment bolts, and stainless steel shell.

The 90° end drop orientation was chosen to be performed because the 90° orientation causes the highest axial deceleration. For the 90° end drop, the bottom impact limiter was chilled at -20° F for at lease 24 hours in order to acquire the most conservative estimate of the highest axial *g* load.

A 40 inch drop onto a 1/3 scale 6 inch diameter puncture bar was performed in accordance with 10 CFR 71.73(c)(3) in order to evaluate the effects of this drop on the NUHOMS®-MP197 transport package. Subsequent to the 30 foot end drop, the test model was dropped in the 90° end drop orientation onto the puncture bar, which was centered over test model's center of gravity. This orientation was chosen because it assures that the puncture impact absorbs 100% of the drop energy. Also the center of the impact limiter outer plate, where the puncture impact occurred, is the weakest portion of the impact limiter since there are no gussets in this location.

2.10.9.2 Scaling Relationships

The NUHOMS®-MP197 cask and impact limiter models are constructed with a geometric scale factor of $1/\lambda = 1/3$. Consequently, the following scale factors apply.

Length:

$$L_p = \lambda L_m$$

Surface area:

$$A_p = \lambda^2 A_m$$

Moment of inertia:

$$I_p = \lambda^4 I_m$$

Section modulus:

$$S_p = \lambda^3 S_m$$

Weight:

$$W_p = \lambda^3 W_m$$

Energy absorbed during drop (from same height $h$):

$$E_p = W_p h = \lambda^3 W_m h = \lambda^3 E_m$$

Velocity at beginning of impact:

$$V_p = \sqrt{2gh} = V_m$$

where $\lambda$ is the scale factor, the subscript $p$ refers to the full size, and the subscript $m$ refers to the model.

During impact, the impact limiter materials will deform or crush. Since the model and full size impact limiters are made of the same materials, they deform under the same stress,

$$S_p = S_m.$$

Therefore we have the following relationships.

Force during impact:

$$F_p = S_p A_p = S_m \lambda^2 A_m = \lambda^2 F_m$$

Deformation:

$$D_p = E_p / F_p = \lambda^3 E_m / \lambda^2 F_m = \lambda D_m$$

Impact duration:

$$T_p = D_p / V_p = \lambda D_m / V_m = \lambda T_m$$

Impact deceleration:

$$a_p = V_p / T_p = V_m / \lambda T_m = 1/\lambda a_m$$

### 2.10.9.3 Test Model Description

The test model for the dynamic tests consists of a solid carbon steel test body with an impact limiter on each end, and a thermal shield located between the bottom impact limiter and the cask body. The test model, shown in Figure 2.10.9-1, is constructed to be as close as possible to one-third of the full size packaging.

#### 2.10.9.3.1 Model Test Body

The model test body provides the proper one-third scale weight, CG location, and dimensions. The test body is 69.33 inches long with a gamma shield outside diameter of 27.33 inches. The reduced diameter portion, located in the axial center of the dummy is not important dimensionally, but is required to provide the proper overall weight and CG location. Important test model and full size packaging dimensions, weight, and CG location are provided below.

Test Model vs. Full Size Packaging

| Component | Test Model | Full Size Packaging |
|---|---|---|
| Body Length (with spacer) | 69.33 in. | 208.00 in. |
| Package Length Including Impact Limiters and Thermal Shield | 93.82 in. | 281.25 in. |
| Gamma Shield Diameter | 27.33 in. | 82.00 in. |
| Package Outer Diameter Impact Limiters and Thermal Shield | 40.67 in. | 122 in. |
| Overall Package Weight | 9,750 lb. (measured) | 266,300 lb. (calculated) |
| Overall Package C.G. Location (measured from bottom surface of cask) | 34.38 in. (measured) | 102.85 in. (calculated) |

The 1/3 scale attachment blocks are used to simulate the full scale impact limiter attachment method. The outer shell of the neutron shield is omitted from the 1/3 scale cask body. This omission is conservative, because the out shell structure would strengthen the connection between the attachment blocks and the cask body.

The attachment bolts are made of the same material specified for the full size limiters, but their dimensions are scaled down by a factor of one-third.

2.10.9.3.2 Impact Limiters

The one-third scale model impact limiters are scale models of the full size limiters with some minor exceptions. The steel impact limiter structure is the same as that described in Appendix 2.10.8; stainless steel shells closed off by flat plates and reinforced by twelve (12) radial gussets. The model and full scale configurations are almost identical, except that all linear dimensions in the model are one-third of those in the full scale impact limiter.

The spaces within the steel shells and gussets are filled with wood blocks, which are formed by gluing together a number of smaller pieces of wood. The balsa and redwood used in the model are consistent with that specified for fabrication of the full scale impact limiters. The model contains the same number of wood blocks as the full size impact limiters. The wood blocks are made up of a number of smaller pieces of wood glued together with phenol resorcinol adhesive, using the same procedure to be used on the full size impact limiters.

The differences between the model and full size limiters are as follows:

a) The nearest standard plate thicknesses corresponding to one-third scale were used. The following dimensions for the scale model impact limiter components do not exactly conform to one-third scaling:

| Component | Full-size Thickness | One-third Scale | Model Thickness |
|---|---|---|---|
| Stainless Steel Shell | 0.25 in. | 0.083 in. | 0.0897 (13 Gauge) |
| 12 Radial Gussets | 0.19 in. | 0.063 in. | 0.0598 (16 Gauge) |

b) The support angles used as legs to allow the limiters to stand upright for storage are not included on the models.

c) The fusible plugs that provide pressure relief during a fire are excluded. Only two openings diametrically opposite from each other are included in the model. Steel plugs are used instead of fusible plugs for sealing these openings and for leak testing.

d) The lifting lugs are made larger than one-third scale to facilitate lifting.

2.10.9.4 Test Description

The drop tests were performed at the Department of Energy's Hanford Site drop pad facility (Area 300), near Richland Washington. The drop test was performed in accordance with approved written procedures.

The quick release mechanism used to drop the package consists of a hydraulic piston that opens a latch, releasing a shackle that supports the test model via a rigging system. The rigging system consists of nylon straps and padded shackles, which prevent ringing of the cask body during impact.

An inclinometer was placed on the test body to measure the initial angle (± 1°) of its longitudinal axis with respect to the drop pad (i.e., impact surface). A measured line, 30 feet long (+ 3.0, -0.0 inches), was attached to the lowest point on the test dummy in order to assure the proper drop height.

The impact surface was an unyielding horizontal surface. The drop pad base consisted of an unyielding concrete pad weighing more than 250,000 lb. (weight of test dummy = 9,750 lb.) resting on bedrock. A hot rolled mild steel plate was securely attached to the concrete pad.

Accelerometers were used to measure the inertial *g* load during impact for the three 30 foot drops performed. The accelerometers were mounted to steel blocks, which were welded to the exterior of the test body at 0°, 90°, 180°, and 270° orientations at the approximate center of gravity location and adjacent to each impact limiter. The twelve (12) accelerometer locations are shown in Figure 2.10.9-2. Accelerometers were not mounted in locations that would result in certain destruction of the accelerometer. However, at least ten (10) accelerometers were used during each 30 foot drop.

The test setup for the 0° side drop is shown in Figure 2.10.9-3. For the side drop test, the accelerometers were oriented to measure accelerations in the drop direction (perpendicular to the drop pad surface).

The test setup for the 20° slap down drop is shown in Figure 2.10.9-4. The accelerometers located at the center of gravity and near the bottom impact limiter (1$^{st}$ impact) were oriented to measure accelerations 70° from the axis of the test model (perpendicular to the drop pad surface when the test model is oriented at a 20° angle). The accelerometers at the CG and near the bottom impact limiter (2$^{nd}$ impact) were oriented to measure accelerations perpendicular to the test model axis (perpendicular to the drop pad surface during slap down when the test modal axis is parallel to the drop pad surface).

The test setup for the end drop is shown in Figure 2.10.9-5. The package was oriented with the cask bottom facing down so that the impact occurred on the bottom end of the package. For the end drop test, the accelerometers were oriented to measure accelerations in the drop (axial) direction. The bottom impact limiter (impact limiter number 4) was kept in a conditioning chamber held at a temperature of -20° F for more than 48 hours. The time between removal of the impact limiter from the conditioning chamber and the test article drop was roughly 2 hours.

The test setup for the 90° puncture drop is shown in Figure 2.10.9-6. During the puncture drop the package was oriented so that the puncture bar impacted on the bottom end of the package. A scaled 6 inch diameter solid cylindrical puncture bar, 18 inches long was used. The puncture bar was constructed from mild steel and was welded to the drop pad with its long axis oriented in the vertical direction. Accelerometer data was not taken during the puncture drop.

PCB Model 350B04 accelerometers were used to measure the cask response. These transducers have a measurement range of +/- 5000*g*, and a shock limit of +/- 50,000*g*. The transducers have both electrical filtering and mechanical filtering, with a nominal frequency response of 1 – 10,000 Hz (+/- 1dB).

The lowest natural vibration frequencies of the test body, which are excited during the test, are much lower than this. These body vibrations involve small displacements (low stresses) at high frequencies, which excite the accelerometers and tend to mask the low frequency rigid body acceleration. This low frequency acceleration is masked, because both low frequency rigid body and high frequency natural vibration accelerations superimpose and the net acceleration is recorded. Filtering the data is necessary to remove these high frequency accelerations. A low pass filter is used to eliminate data above a specified cutoff frequency.

A TEAC XR-5000 14-channel instrumentation recorder was used to record the accelerometer signals.

A photograph of the accelerometer locations for each channel are shown in Figure 2.10.9-7. 1-4 are on the front (left side of cask in Figure 1), 5-8 re in the middle, and 9-12 are on the right side of the cask. Note that accelerometers 4, 8 and 12 are not visible in Figure 2.10.9-7.

The following data was measured and recorded before, during, and after each drop test.

1. Prior to each drop test.
    a. Torque of the impact limiter bolts.
    b. Impact limiter dimensions.
    c. Height from test article to drop pad.
    d. Angular orientation of the test article to the impact surface.
    e. Atmospheric condition data, *i.e.*, ambient temperature, wind speed, immediately and prior to the release of the test article.

2. During each drop test.
    a. Test article behavior on videotape.
    b. Date and time of test.
    c. Observations of damage or unexpected behavior of the test article
    d. Impact acceleration time histories and frequency responses (excluding the puncture drop test).

3. Following each drop test.
    a. Observations of the damage to the test article on features other than the limiters, *i.e.*, attachment bolts.
    b. Measurements of deformation to each impact limiter to fully describe the extent of the damage. These measurements include:
        i. Depth of external crushing on the impact limiter.
        ii. Overall thickness of each impact limiter after each test.
        iii. Width of impact footprint.

### 2.10.9.5 Test Data and Results

For purposes of reviewing test results, it should be noted that the energy to be absorbed by the scale model is approximately 1/27 of the full scale NUHOMS®-MP197 package value. The acceleration of the model is approximately three times that of the full size cask, and the crush deformation of the model limiter is approximately one-third that of the full size limiter. The impact force applied to the model is determined by multiplying the mass by the rigid body acceleration ($F = ma$). The model force is 1/9 of the full scale force.

#### 2.10.9.5.1 0° Side Drop Test

The first drop test performed was the 0° side drop. Impact limiters 1 and 2 were placed on the top and bottom of the test model respectively. Two straps, connected to the test article and to each other with padded shackles, were used to support the test model. Figure 2.10.9-8 is a photograph of the test package set up just before the 0° drop test.

Accelerometer Data

The acceleration time history plots for the 0° side drop test appeared qualitatively reasonable. The plots generally show a single rounded peak roughly 0.012 s. long, with a high frequency low amplitude signal superimposed on top of it. The measured 1/3 scale impact duration of 0.012 s. corresponds to 0.036 s. for the full size package, which is consistent with the impact duration predicted by ADOC and used to compute the Dynamic Amplification Factor in Appendix 2.10.6.

| Recorded Impact Duration (Figure 2.10.9-9) | Predicted Impact Duration From ADOC Computer Run |
|---|---|
| 0.012 seconds<br>(0.012 x 3 = 0.036 seconds) | 0.036 seconds |

A review of the acceleration data revealed that the accelerometer at location 5 recorded data inconsistent with the other eleven accelerometers. Consequently, the accelerations measured at location 5 are omitted from the data analyses for all three 30 foot drops.

Ten of the twelve accelerometers mounted to the dummy cask properly recorded acceleration data. The following table shows the transverse accelerations measured by the ten accelerometers during the 0° side drop (converted to full scale), as well as the acceleration range predicted by ADOC.

| Accelerometer Location (see figure 2.10.9-2) | | Measured Transverse Acceleration (gs) (full scale) | Average Measured Transverse Acceleration (gs) | Predicted Transverse Acceleration Range (Gs) |
|---|---|---|---|---|
| Top | 1 | 61 | 61 | 53 – 60 |
| | 2 | 62 | | |
| | 3 | 62 | | |
| | 4 | - | | |
| Center of Gravity | 5 | - | | |
| | 6 | 63 | | |
| | 7 | 62 | | |
| | 8 | 63 | | |
| Bottom | 9 | 57 | | |
| | 10 | 61 | | |
| | 11 | 58 | | |
| | 12 | 62 | | |

The accelerations measured during the side drop are at the high end of the range predicted by the ADOC computer program. The acceleration results presented in the above table are taken from the measured acceleration data filtered with a 1,000 Hz. Low pass filter. Figures 2.10.9-9 and 2.10.9-10 show the filtered acceleration time histories from accelerometers 1 and 10 respectively, which are characteristic of the acceleration plots in general. Note that the accelerations plotted in Figures 2.10.9-9 and 2.10.9-10 are for the 1/3 scale package, which is equivalent to 3 times the full scale accelerations.

Crush Depth Measurements

After the side drop test the top impact limiter (number 1) was removed from the test model body and impact limiter crush depths were measured. There was evidence of both inside and outside crushing. The following table summarizes the measured and predicted crush depths for the bottom impact limiter (slap down impact). A spring back of 0.50 inches is assumed (based of previous crush tests).

| | Impact Limiter Number 1 (Top) | Impact Limiter Number 2 (Bottom) |
|---|---|---|
| **Maximum Inside Crush Depth (in.)** | 1.44 | 1.50 |
| **Maximum Outside Crush Depth (in.)** | 0.75 | 0.75 |
| **Spring Back** | 0.50 | 0.50 |
| **Total Maximum Crush Depth (in.)** | 2.69 | 2.75 |
| **Predicted Total Maximum Crush Depth x 1/3 (in.)** | 3.34 – 4.04 | |

From the above table it can be seen that the measured crush depths are slightly less that those predicted by the ADOC computer program.

It should also be noted that the neutron shield would not contact the target during the impact. The full scale distance between the end of the outer diameter of the neutron shield and the outside diameter of the impact limiter is 15.25 inches. Therefore, a clearance of 7.00 in. (full scale, $15.25 - 2.75 \times 3 = 7.00$) would remain between the crushed plane of the impact limiter and the neutron shield, based on the measured crush depth.

Damage Assessment

Both impact limiters remained attached to the cask during and after the side drop impact. All impact limiter attachment bolts remained intact, except for two bolts on the top impact limiter. These two bolts, located at 15° and 45° with respect to vertical, failed in shear.

Only a single small opening in the stainless steel impact limiter shell was evident. This opening consisted of a tear in the weld between the outer flat plate and the cylindrical shell of the impact limiter. The tear was roughly 0.25 inches wide and 6 inches long. Despite this tear, all impact limiter wood remained completely confined within the shell.

Figures 2.10.9-11 and 2.10.9-12 are photographs of the dummy cask and impact limiters after the 0° side drop.

### 2.10.9.5.1 20° Slap Down Test

The second drop test performed was the 20° slap down drop. Impact limiters 3 and 2 were placed on the top and bottom of the test model respectively. The cask was oriented such that the bottom end (with thermal shield) impacted the drop pad first. A two point strap rigging system was used to lift the test model by two lifting lugs. The two legs of the rigging system join at a single point that was shackled to the quick release mechanism. Figure 2.10.9-13 is a photograph of the test package set up just before the 20° slap down test.

Accelerometer Data

The acceleration time history plots for the 20° slap down test appeared qualitatively reasonable. The plots measured by the accelerometers located near the bottom impact limiter (first impact) generally show a single rounded peak roughly 0.016s. long, with a high frequency low amplitude signal superimposed on top of it.

The plots measured by the accelerometers located at the package center of gravity generally show two rounded peaks roughly 0.016s. (first impact), and 0.009 s. (second impact) long, with the second peak higher than the first. The plots at the center of gravity also show significant ringing of the cask throughout both impacts.

The plots measured by the accelerometers located near the top impact limiter (second impact) generally show a single rounded peak roughly 0.009s. long, with a high frequency low amplitude signal superimposed on top of it.

The following table shows the transverse accelerations measured by eleven accelerometers during the 20° slap down (converted to full scale), as well as the acceleration ranges predicted by ADOC. The measured and predicted accelerations are broken down into those generated during the initial impact and those generated during the second (slap down) impact. In addition, both the normal acceleration (translational only) at the package CG, and the rotational component of the transverse acceleration at the impact end (top or bottom) are reported.

**Measured versus Predicted Accelerations during First Impact**

| Accelerometer Location (see figure 2.10.9-2) | | Measured Acceleration (gs) | Average Measured Acceleration (gs) | Predicted Acceleration Range (gs) |
|---|---|---|---|---|
| Normal Transverse Acceleration at Package CG (1st Impact) | 5 | - | 17 | 40 – 53 |
| | 6 | 17 | | |
| | 7 | 16 | | |
| | 8 | 18 | | |
| Rotational Acceleration at Bottom Impact Limiter (1st Impact) | 9 | 13 | 19 | 62 – 80 |
| | 10 | 21 | | |
| | 11 | 21 | | |
| | 12 | 22 | | |

**Measured versus Predicted Accelerations during Second Impact**

| Accelerometer Location (see figure 2.10.9-2) | | Measured Acceleration (gs) | Average Measured Acceleration (gs) | Predicted Acceleration Range (gs) |
|---|---|---|---|---|
| Normal Transverse Acceleration at Package CG (1st Impact) | 5 | - | 32 | 36 – 44 |
| | 6 | 32 | | |
| | 7 | 32 | | |
| | 8 | 32 | | |
| Rotational Acceleration at Top Impact Limiter (2nd Impact) | 1 | 53 | 53 | 69 – 83 |
| | 2 | 52 | | |
| | 3 | 56 | | |
| | 4 | 51 | | |

The exact locations of the accelerations at the "Top" and "Bottom", reported in the table above, correspond to the locations of the reaction forces applied to the top and bottom impact limiters by the drop pad. These locations are computed by the ADOC computer program, which is described in detail in Appendix 2.10.8. Since the accelerometers mounted near the top and bottom impact limiters are not located at the impact limiter reaction point, the measured top and bottom accelerations, reported in the table above, are adjusted so that a proper comparison with the predicted accelerations can be performed. The locations of the reaction forces with respect to the package center of gravity for both impact limiters are provided in the following table. These locations are computed by the ADOC computer code (see Appendix 2.10.8), and are adjusted to 1/3 scale.

**Distance Between Impact Limiter Reaction Forces and Package CG Location**

| | Maximum Wood Properties (in.) | Minimum Wood Properties (in.) | Average Value (in.) |
|---|---|---|---|
| Bottom Impact Limiter (First Impact) | 30.2 | 30.4 | 30.3 |
| Top Impact Limiter (Second Impact) | 31.3 | 31.7 | 31.5 |

The distance between the accelerometers mounted near the top and bottom impact limiters and the center of gravity of the package are as follows.

**Distance between Accelerometer Locations and Package CG Location**

| | Distance to CG (in) |
|---|---|
| Bottom Accelerometer (First Impact) | 22.38 |
| Top Accelerometer (Second Impact) | 22.45 |

Since the relationship between transverse acceleration and the distance to the rotation point (CG location) is linear ($\alpha = \omega r$), the transverse acceleration at the reaction force locations can be computed by linear interpolation in the following way:

$$\textit{acceleration at top reaction location} = \textit{measured top acceleration} \times \frac{31.5}{22.45}$$

$$\textit{acceleration at bottom reaction location} = \textit{measured bottom acceleration} \times \frac{30.3}{22.38}$$

The accelerations measured during the slap down drop are low relative to the range predicted by the ADOC computer program. The acceleration results presented in the above table are taken from the measured acceleration data filtered with a 1,000 Hz. Low pass filter. Figures 2.10l.9-14, 2.10.9-15, and 2.10.9-16 show the filtered acceleration time histories from accelerometers 1, 8, an 10 respectively, which depict the general behavior of the acceleration histories at the top,

CG, and bottom of the package. Note that the accelerations plotted in Figures 2.10.9-14, 2.10.9-15 and 2.10.9-16 are for the 1/3 scale package, which is equivalent to 3 times the full scale accelerations.

Crush Depth Measurements

After the slap down test the impact limiters were removed from the test model body and their crush depths were measured. There was evidence of both inside and outside crushing. The following table summarizes the measured and predicted crush depths for the top and bottom impact limiter. A spring back of 0.50 inches is assumed (based of previous crush tests).

| | Impact Limiter Number 3 (Top) | Impact Limiter Number 2 (Bottom) |
|---|---|---|
| **Maximum Inside Crush Depth (in.)** | 2.42 | 0.42 |
| **Maximum Outside Crush Depth (in.)** | 1.80 | 4 |
| **Spring Back** | 0.50 | 0.50 |
| **Total Maximum Crush Depth (in.)** | 4.72 | 4.92 |
| **Predicted Total Maximum Crush Depth x 1/3 (in.)** | 7.47 – 7.61 | 6.05 – 6.65 |

From the above table it can be seen that the measured crush depths are less that those predicted by the ADOC computer program.

It should also be noted that the neutron shield would not contact the target during the impact. Since the crush pattern on the top and bottom impact limiters occur at a 20° angle, and only at the outer edge, there is no possibility of the neutron shield impacting the target during the slap down impact.

Damage Assessment

Both impact limiters remained attached to the cask during and after the slap down impact. All impact limiter attachment bolts remained intact, except for four bolts on the top impact limiter (slap down side). Four bolts located 90° apart from each other, starting with the bolt located 45° from vertical, failed in shear. No two adjacent bolts failed.

No openings in the stainless steel impact limiter shell were evident, and no welds in the shell failed. The impact limiter wood remained completely confined within the shell.

Figures 2.10.9-17 and 2.10.9-18 are photographs of the dummy cask and impact limiters after the 20° slap down drop.

2.10.9.5.2 90° End Drop Test

The third drop test performed was the 90° end drop. Impact limiters 3 and 4 were placed on the top and bottom of the test model respectively. The cask was oriented such that the bottom end impacted the drop pad. Two straps were attached to the test article's top two lifting lugs and to the quick release mechanism with padded shackles. Figure 2.10.9-19 is a photograph of the test package set up just before the 90° end drop test.

Accelerometer Data

The acceleration time history plots for the 90° end drop test appeared qualitatively reasonable. The plots generally show a single rounded peak 0.010 s. long, with a high frequency low amplitude signal superimposed on top of it. The measured 1/3 scale impact duration of 0.010 s. corresponds to 0.030 s. for the full size package, which is consistent with the impact duration predicted by ADOC and used to compute the Dynamic Amplification Factor in Appendix 2.10.6.

The following table shows the axial acceleration measured by nine accelerometers, during the 90° end drop, as well as the range of axial acceleration predicted by ADOC (accelerometers at locations 1 and 3 were removed from the package, because of interference with the rigging system in the vertical orientation).

| Accelerometer Location (see figure 2.10.9-2) | | Measured Axial Acceleration (gs) | Average Measured Axial Acceleration (gs) | Predicted Axial Acceleration Range (gs) |
|---|---|---|---|---|
| Top | 1 | - | 65 | 44 – 50 |
| | 2 | 63 | | |
| | 3 | - | | |
| | 4 | 68 | | |
| Canter of Gravity | 5 | - | | |
| | 6 | 65 | | |
| | 7 | 66 | | |
| | 8 | 66 | | |
| Bottom | 9 | 63 | | |
| | 10 | 63 | | |
| | 11 | 62 | | |
| | 12 | 70 | | |

The higher than predicted accelerations are attributed to the fact that the bottom impact limiter was chilled to –20° F prior to the drop test. The crush strength of balsa and redwood increases as temperature decreases.

The acceleration results presented in the above table are taken from the measured acceleration data filtered with a 1,000 Hz. Low pass filter. Figures 2.10.9-20 and 2.10.9-21 show the filtered acceleration time histories from accelerometers 7 and 11 respectively, which are characteristic of the acceleration plots in general. Note that the accelerations plotted in Figures 2.10.9-20 and 2.10.9-21 are for the 1/3 scale package, which is equivalent to 3 times the full scale accelerations.

Crush Depth Measurements

After the end drop test the crush depths of the bottom impact limiter were measured. There was evidence of both inside and outside crushing. The following table summarizes the measured and predicted crush depths for the bottom impact limiter (impact limiter 4). A springback of 0.50 inches is assumed.

| | Impact Limiter Number ? (Top) |
|---|---|
| **Maximum Inside Crush Depth (in.)** | 1.75 |
| **Maximum Outside Crush Depth (in.)** | 0.25 |
| **Spring Back** | 0.50 |
| **Total Maximum Crush Depth (in.)** | 2.50 |
| **Predicted Total Maximum Crush Depth x 1/3 (in.)** | 3.51 – 4.48 |

The relatively low crush depth measured after the 90° end drop, compared with predicted values can be attributed to the fact that the bottom impact limiter was chilled to -20° F prior to the drop test.

Damage Assessment

Both impact limiters remained attached to the cask during and after the end drop impact, and all impact limiter attachment bolts remained intact.

No openings in the stainless steel impact limiter shell were evident, and no welds in the shell failed. The impact limiter wood remained completely confined within the shell.

Figures 2.10.9-22 and 2.10.9-23 are a photographs of the test dummy and impact limiters after the 90° end drop.

2.10.9.5.4 Puncture Drop Test

The final drop test performed was the puncture drop. In order to simulate the proper sequence of accident events specified in 10 CFR 71.73, the impact limiters used for the end drop test were left on the dummy cask without adjustment or tightening of the attachment bolts. Two straps, attached to top two lifting lugs, were used to support the test model in the 90° vertical orientation with the test model's bottom end facing down. The puncture bar impacted impact limiter 4, which was previously crushed during the 90° end drop. No accelerometer data was taken, since the purpose of the puncture drop is to obtain impact limiter damage only. Figure 2.10.9-6 depicts the test setup up for the 90° puncture drop test.

Test Results

The puncture bar impacted the test package squarely in the center of the outer flat surface of the bottom impact limiter shell. The puncture bar cleanly punched through the outer stainless steel shell of the impact limiter and was imbedded in the impact limiter wood. The test package came to rest in the vertical position, perfectly balanced on top of the puncture bar.

The puncture bar sheared a circular section, roughly 2 inches in diameter, of the outer shell of the bottom impact limiter. No other sections of the impact limiter were damaged, and no welds on the impact limiter shell were broken. The impact limiter wood remained completely contained by the impact limiter shell, and no impact limiter wood could be seen at the puncture point.

The puncture bar was stopped by a thin wedge of impact limiter wood that was compacted between the top of the puncture bar and the inner shell of the impact limiter. The puncture bar did not penetrate the inner stainless steel shell of the impact limiter or the aluminum thermal shield.

Both impact limiters remained attached to the cask during the puncture drop event, and no additional impact limiter attachment bolts were damaged.

Figure 2.10.9-24 is a photograph of the test dummy and impact limiters after the puncture drop.

2.10.9.6 Conclusions

The predicted performance of the impact limiters in terms of accelerations and crush depths agrees well with the measured data. Table 2.10.9-1 summarizes the maximum inertial loads measured during the dynamic testing program, as well as the maximum inertial loads computed by ADOC and used in the NUHOMS®-MP197 transport package structural analysis. Table 2.10.9-1 demonstrates that the inertial loads calculated in Appendix 2.10.8 are reasonable and that the inertial loads used in the analyses in Appendices 2.10.1 through 2.10.5 are conservative.

The results of the dynamic tests demonstrate that:

- The crush depths do not result in lockup of the wood in the limiters.
- The crush depths for the 0° side drop case would not result in the neutron shield impacting the target.
- The predicted performance of the impact limiters in terms of decelerations and crush depths agrees well with the measured data.
- The impact limiter enclosure is structurally adequate in that it successfully confines the wood inside the steel shell.
- The impact limiter attachment design is structurally adequate in that the attachment bolts hold the impact limiters on the ends of the cask during all drop orientations.
- The effects of low temperature (-20° F) on the crush strength of the impact limiters is minor, and is bounded by the conservative accelerations and forces used in the analysis in Appendices 2.10.1 through 2.10.5.
- A 40 inch drop onto a scaled six inch diameter puncture bar, as per 10 CFR 71.73(c)(3), does not significantly destroy the impact limiter. The impact limiter and attachments remain firmly secured to the cask, and the impact limiter wood is confined.

2.10.9.7 References

1. 10 CFR PART 71, Packaging and Transportation of Radioactive Material.

TABLE 2.10.9-1

Comparison of Calculated vs. Measured *g* loads

| 30 foot Drop Orientation | Average *g* Load Measured by Drop Test (Appendix 2.10.9) | *g* Load Computed by ADOC (Appendix 2.10.9) | Input Loading Used in Stress Analysis** (Appendix 2.10.1) |
|---|---|---|---|
| 0° Side Drop | 61*g* Transverse | 53*g* – 60*g* Transverse | 75g Transverse |
| 20° Side Drop | 32*g* Normal | 36g – 44*g* Normal | 60*g* Normal |
| | 53*g* Rotational | 69g – 83g Rotational | 196g Rotational |
| 90° End Drop | 65*g* Axial | 46g – 50*g* Axial | 75*g* Axial |

** Conservatively Using Higher *g* loads

Figure 2.10.9-1

One-Third Scale Test Model

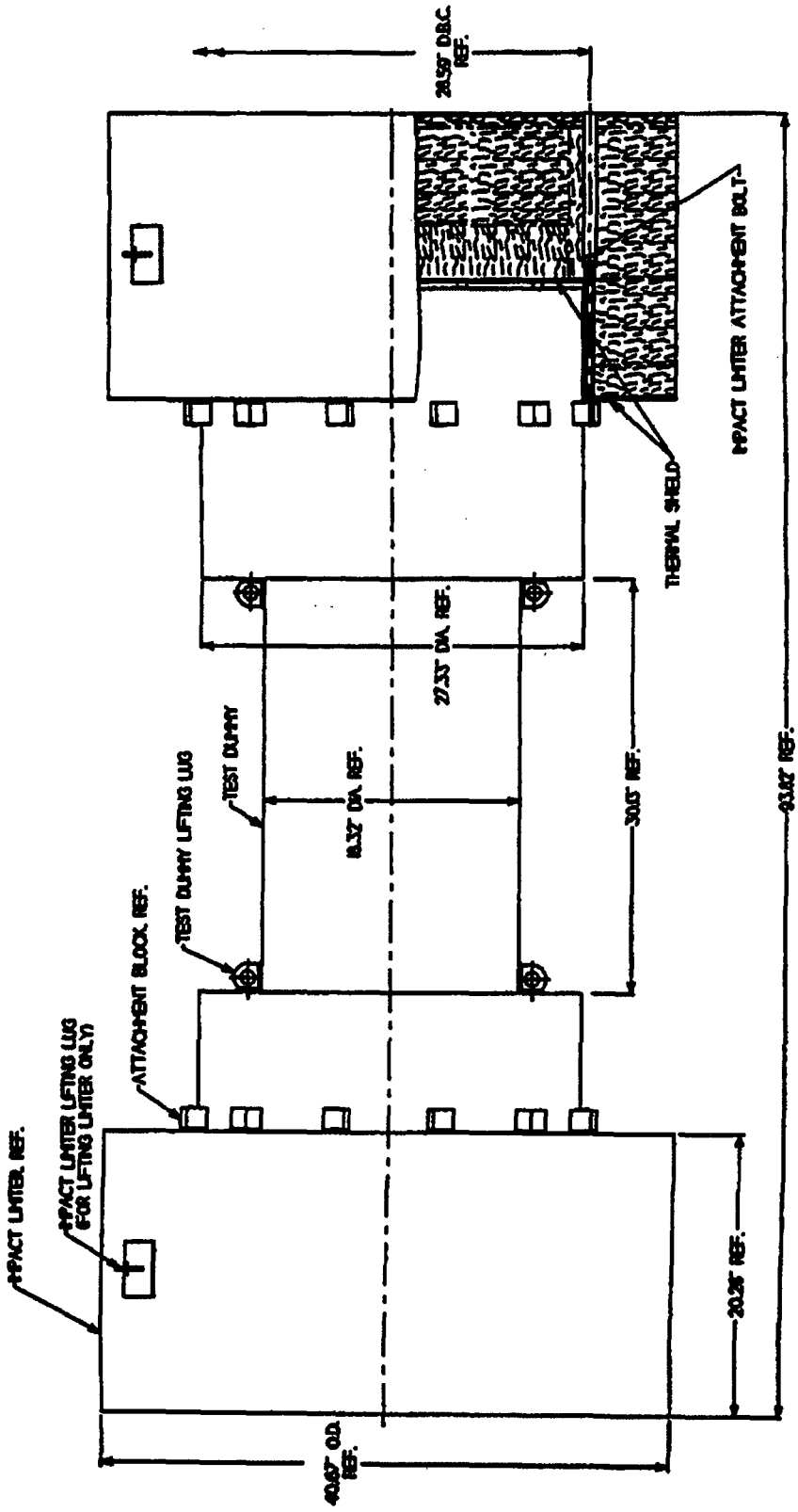

Figure 2.10.9-2

Accelerometer Locations

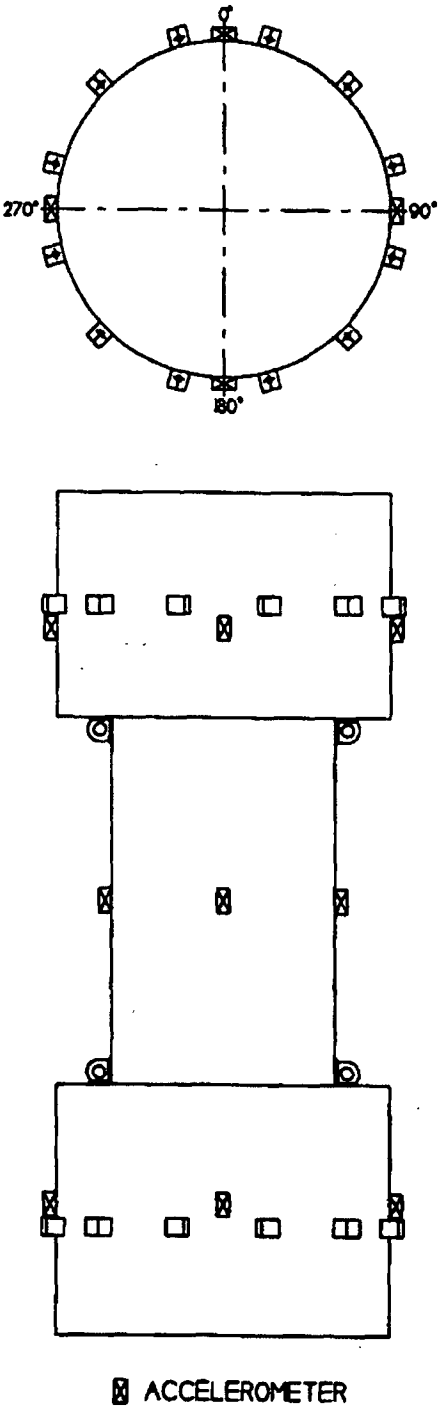

Figure 2.10.9-3

NUHOMS®-MP197 Scale Model 0° Side Drop Test Setup

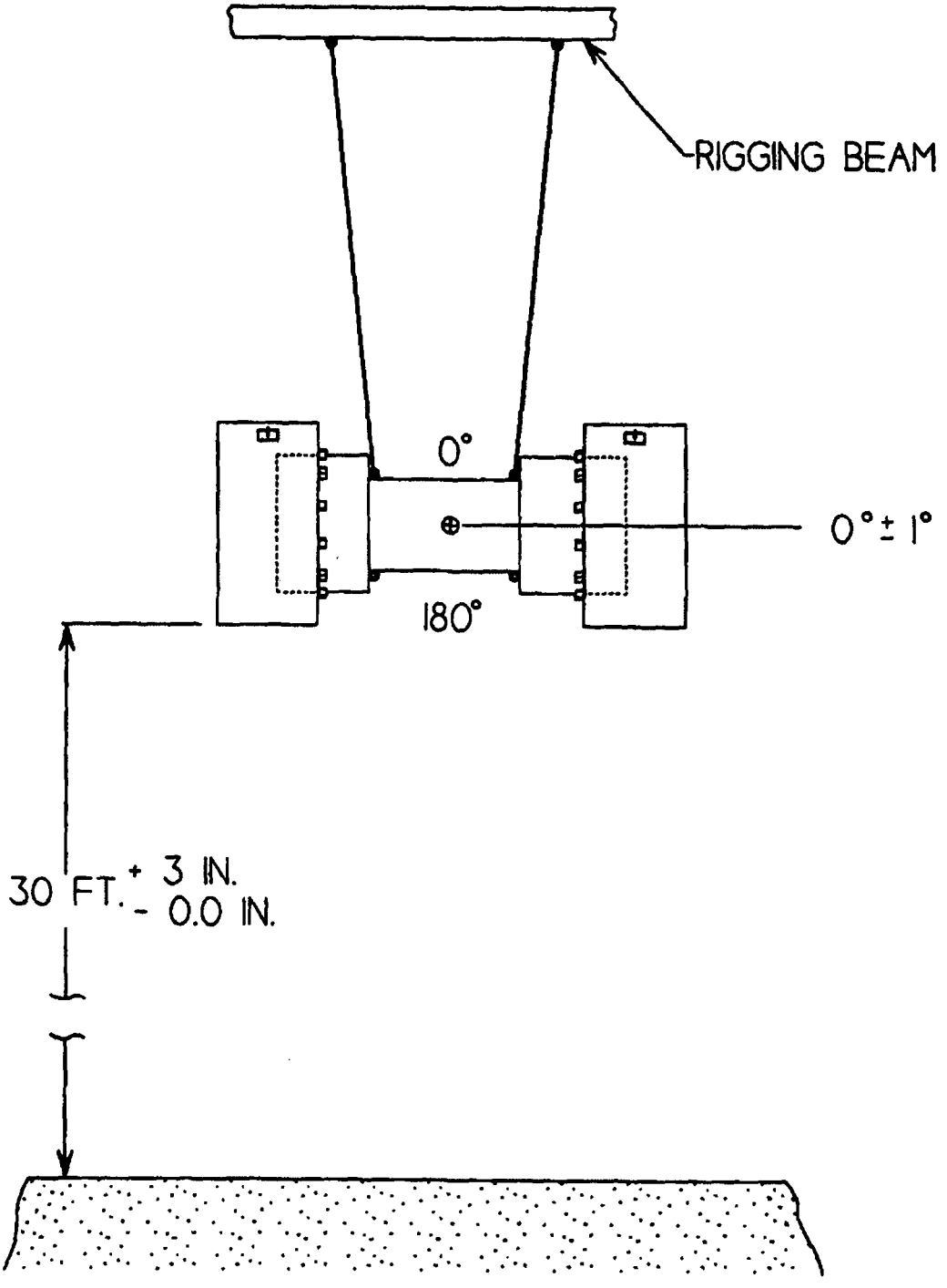

Figure 2.10.9-4

NUHOMS®-MP197 Scale Model 20° Slap Down Test Setup

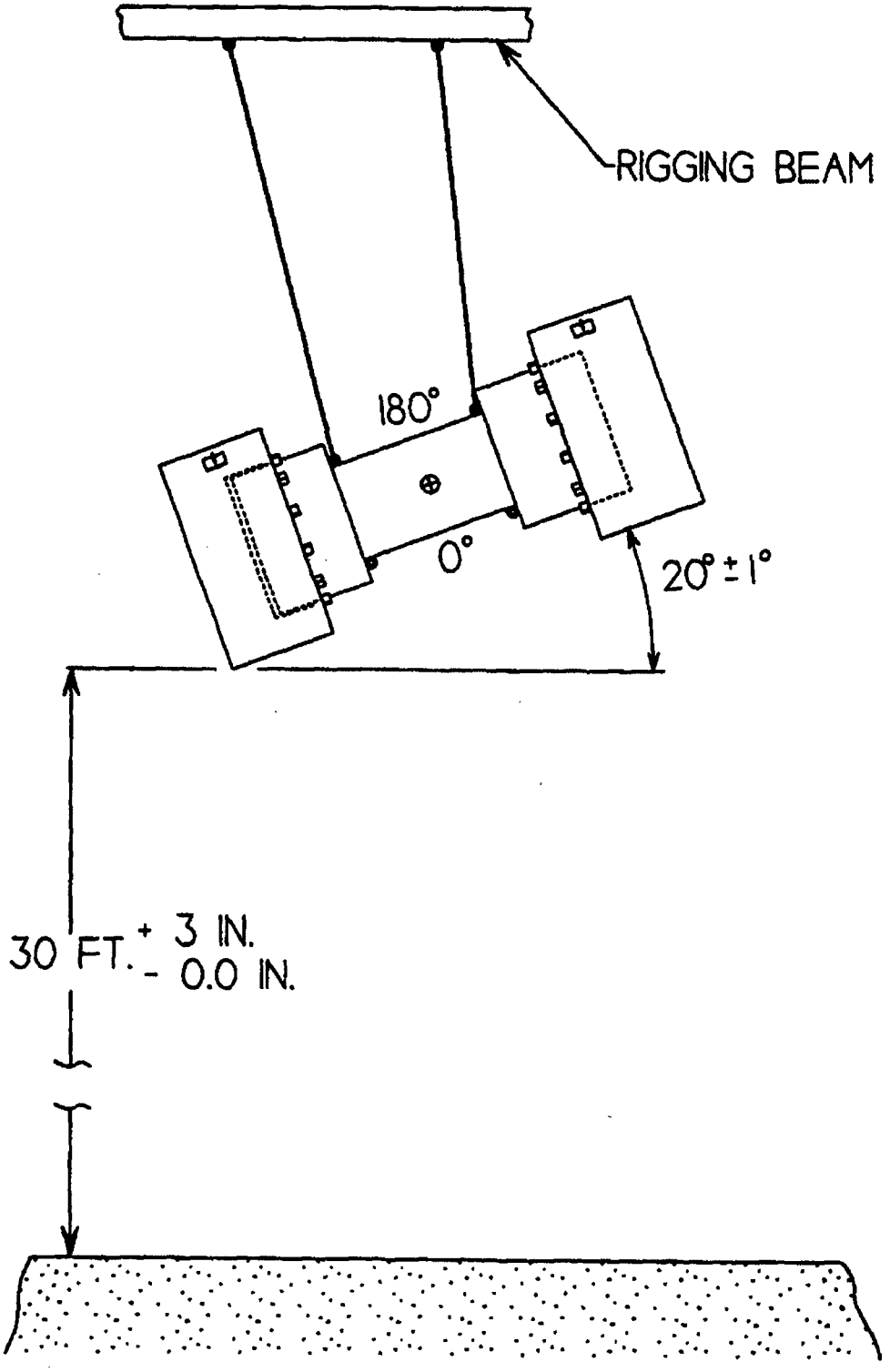

Figure 2.10.9-5

NUHOMS®-MP197 Scale Model 90° End Drop Test Setup

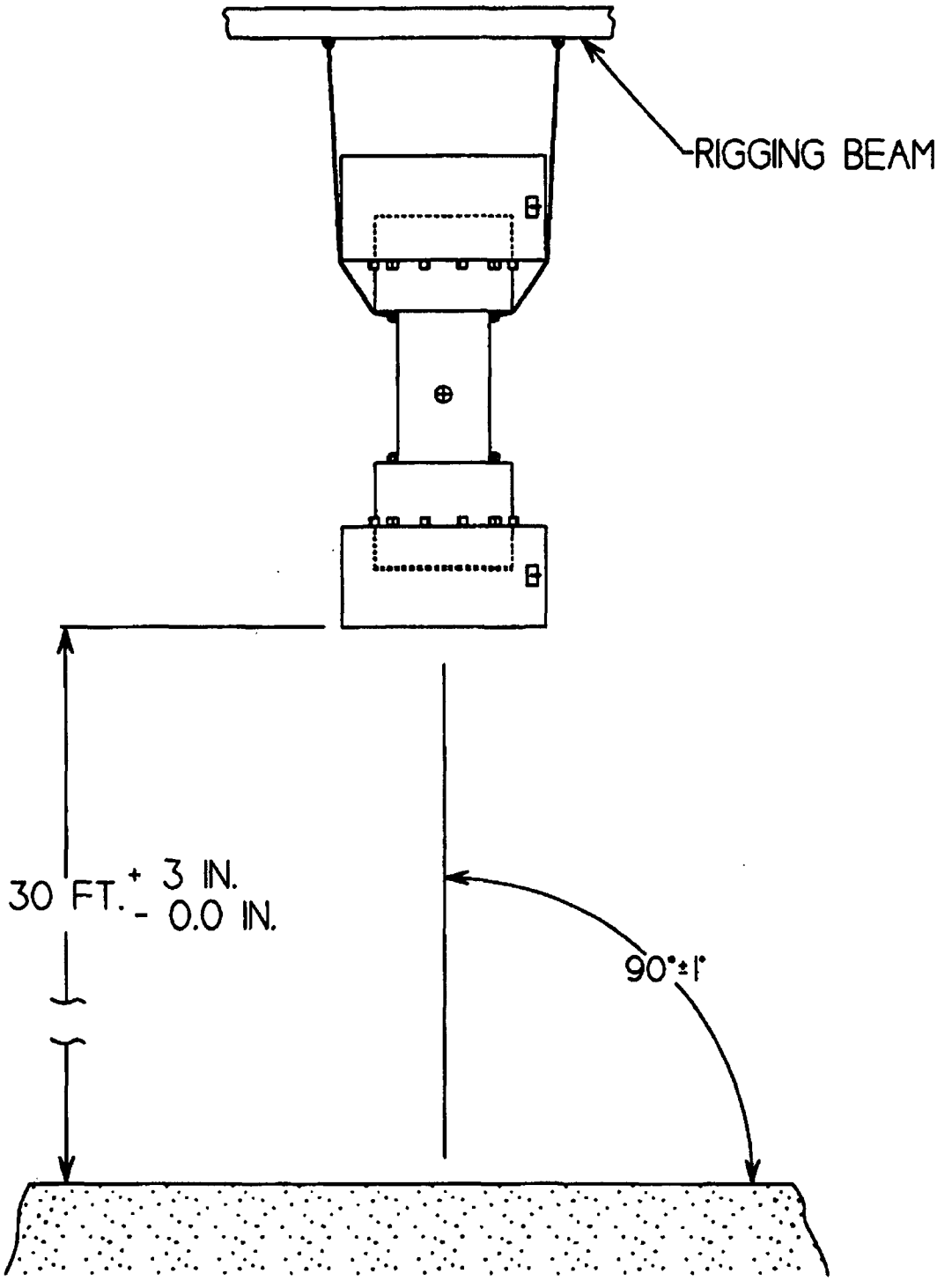

Figure 2.10.9-6

NUHOMS®-MP197 Scale Model Puncture Drop Test Setup

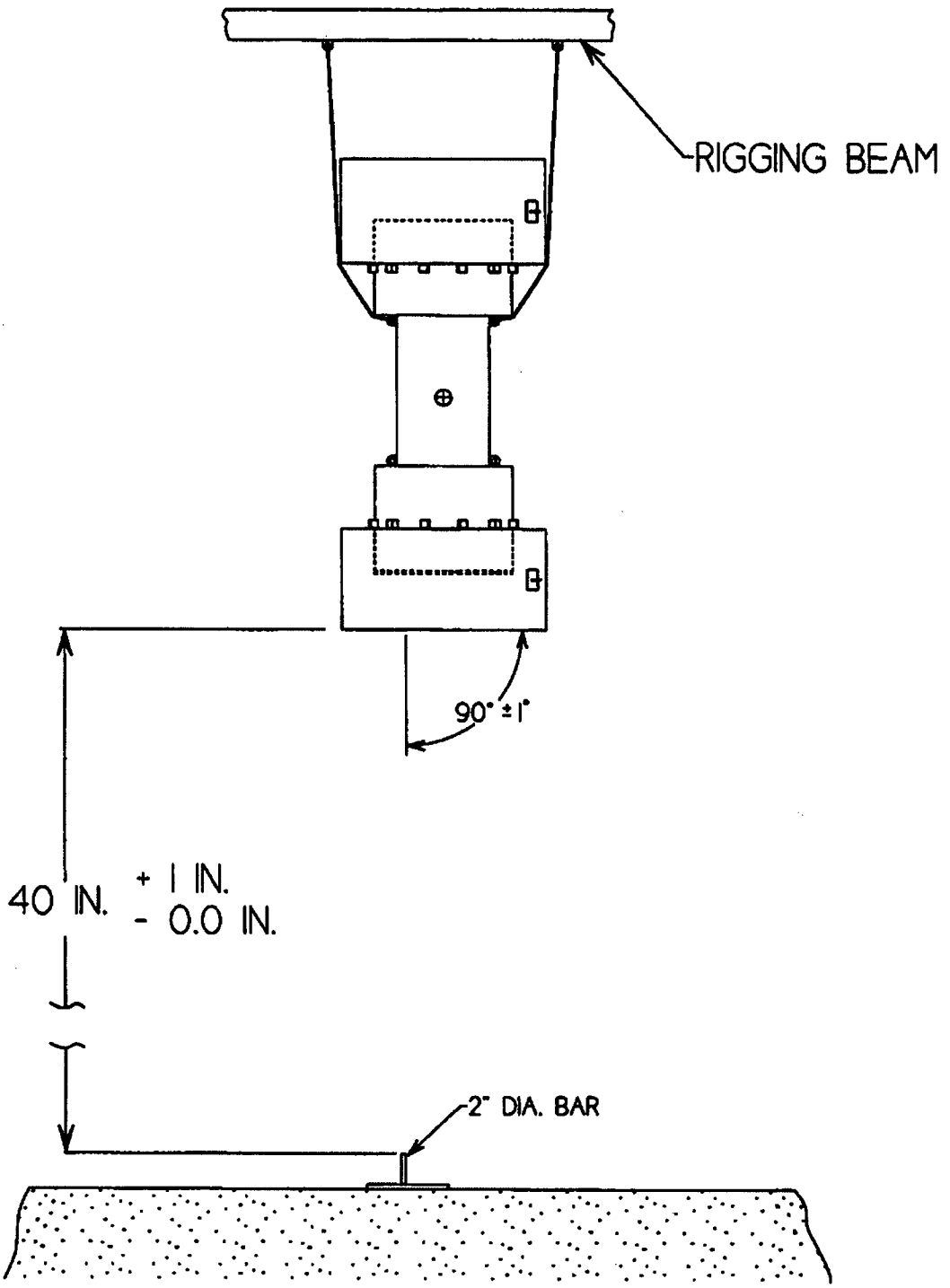

Figure 2.10.9-7

Test Article and Accelerometer locations

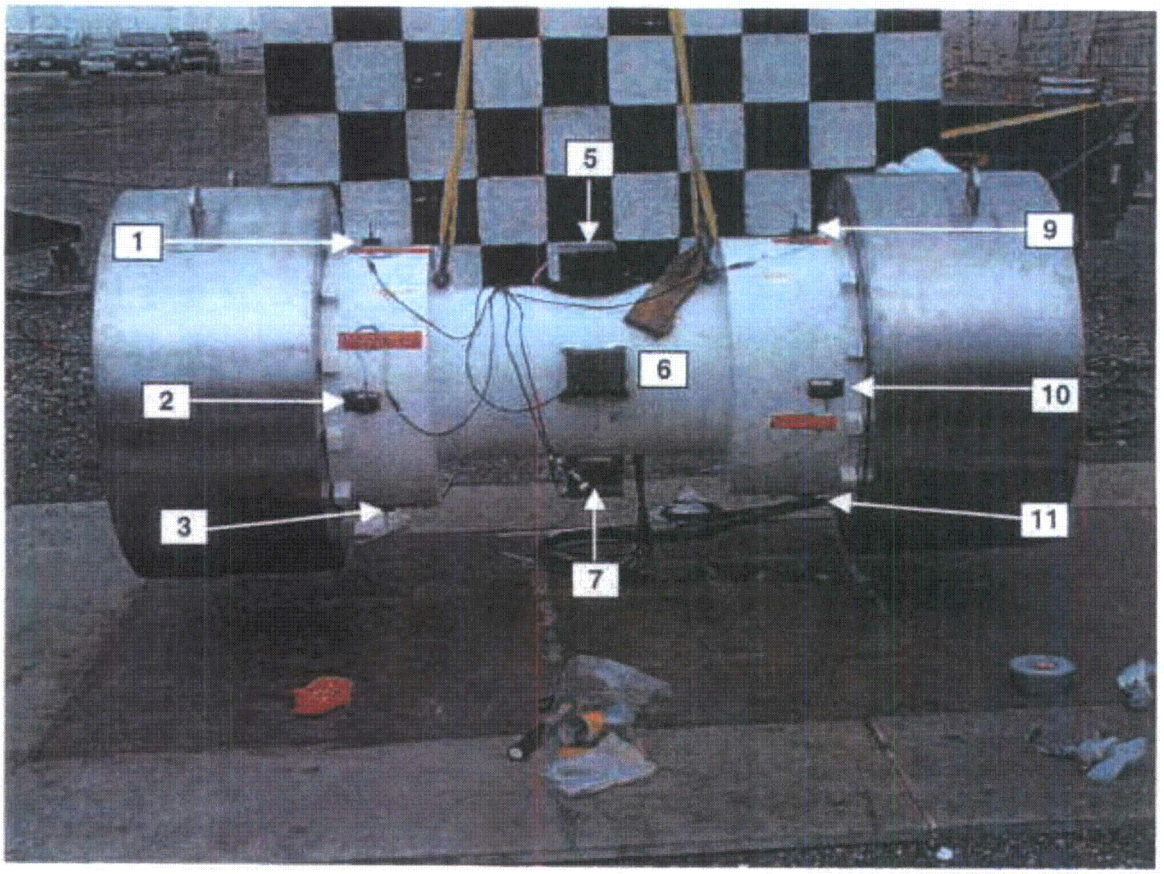

Figure 2.10.9-8

0° Side Drop Test Setup

Figure 2.10.9-9

Acceleration Time History, with 1,000 Hz. Low-Pass Filter, 0° Side Drop,
Accelerometer 1 (Top)

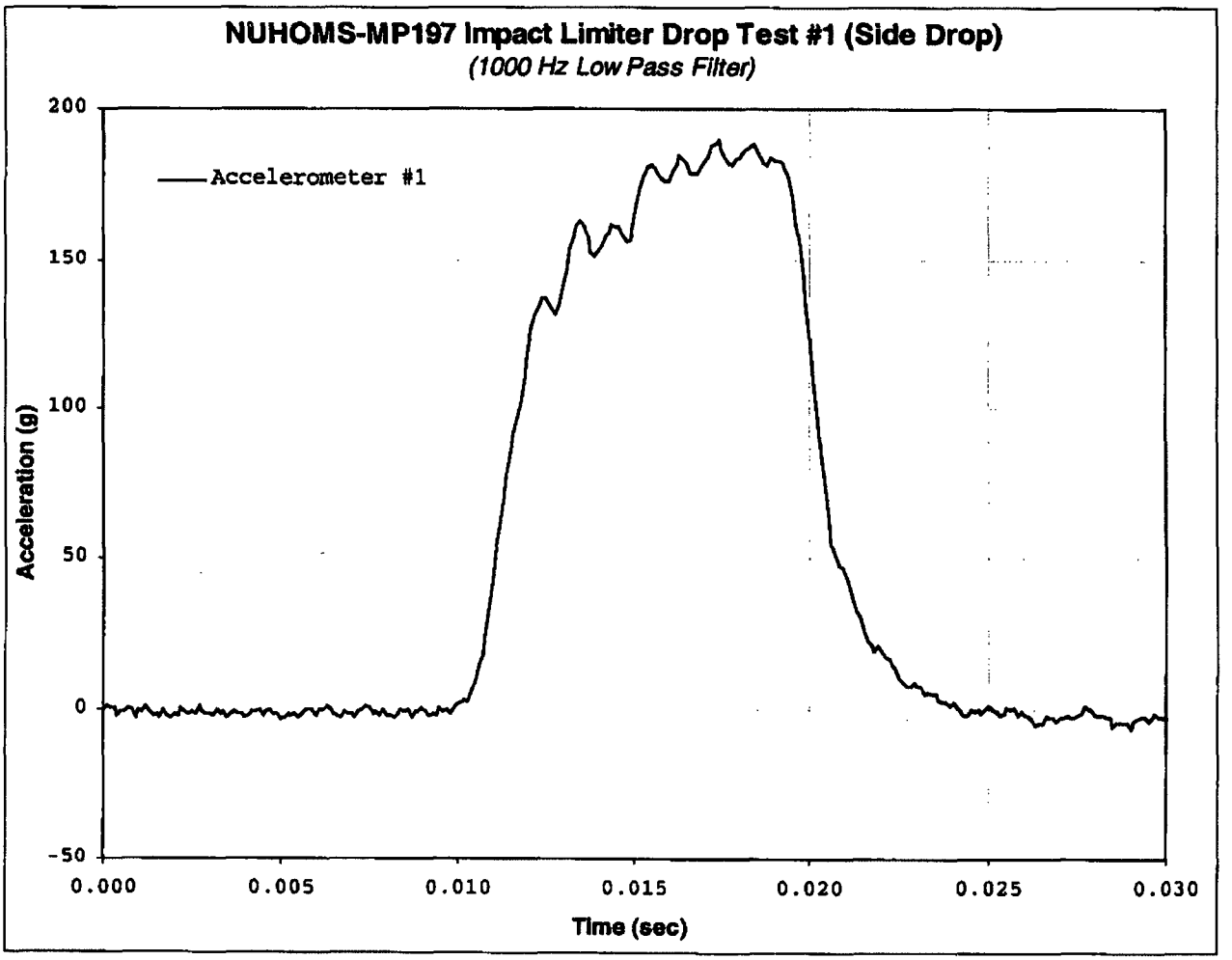

Figure 2.10.9-10

Acceleration Time History, with 1,000 Hz. Low-Pass Filter, 0° Side Drop,
Accelerometer 10 (Bottom)

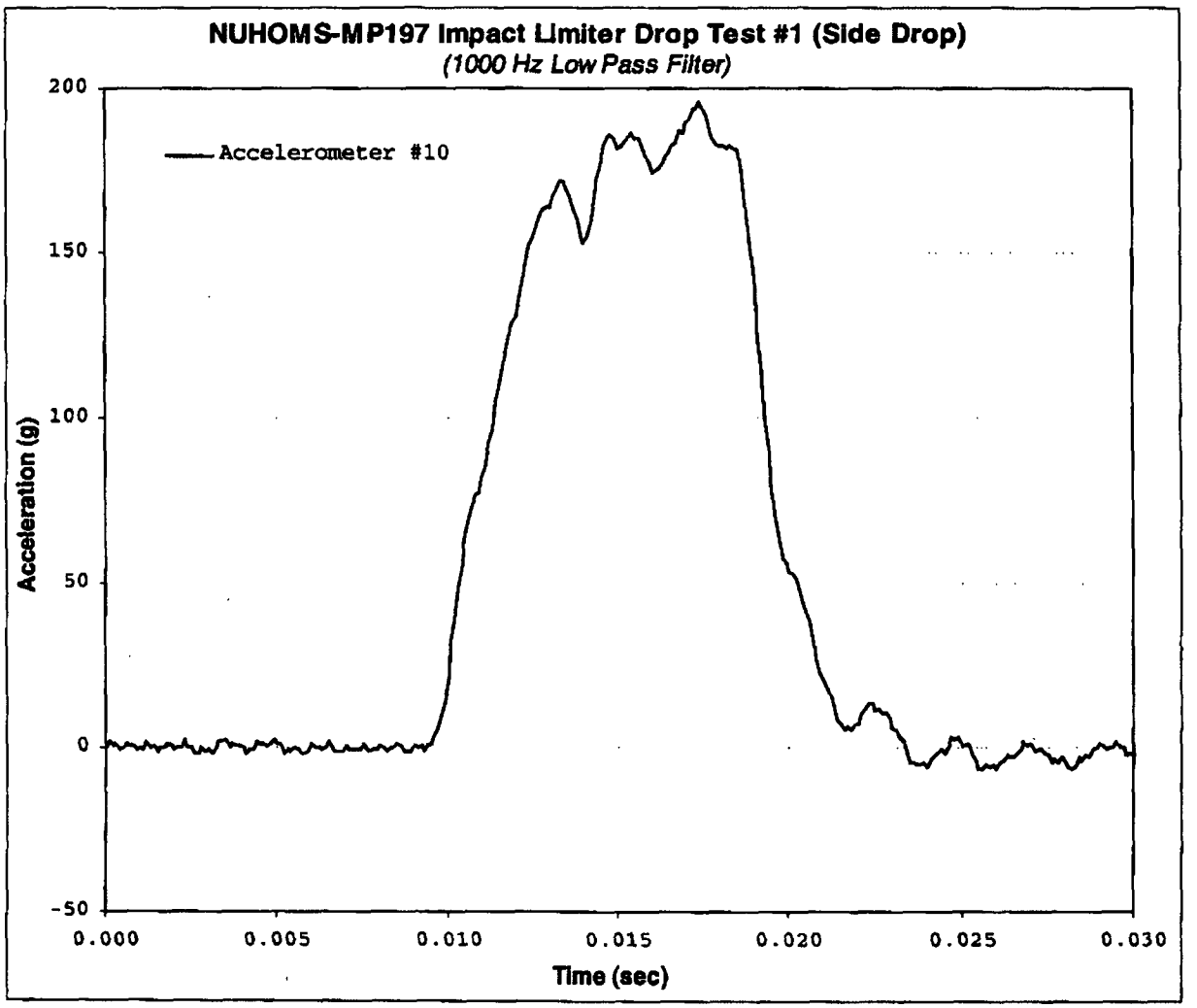

Figure 2.10.9-11

NUHOMS®-MP197 Cask Dummy and Impact Limiters After 0° Side Drop

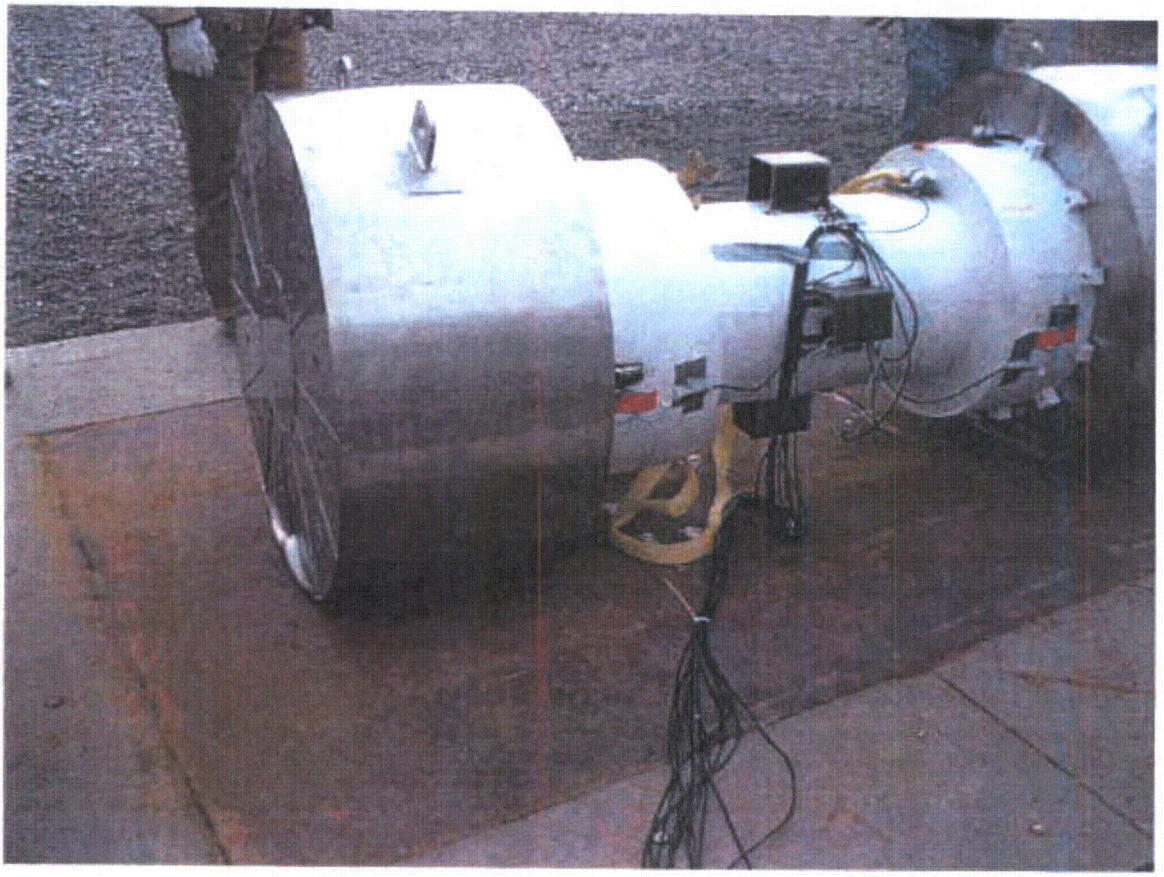

Figure 2.10.9-12

NUHOMS®-MP197 Cask Dummy and Impact Limiters After 0° Side Drop

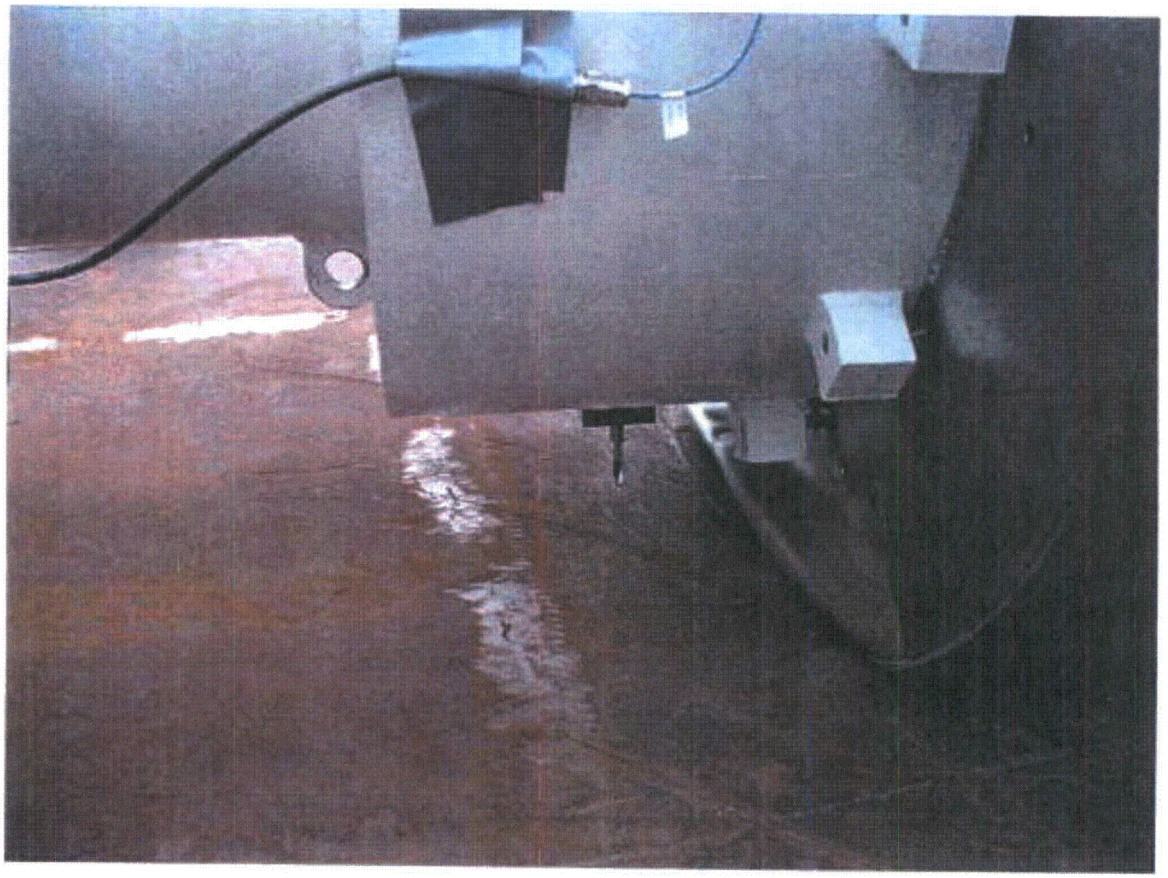

Figure 2.10.9-13

20° Slap Down Test Setup

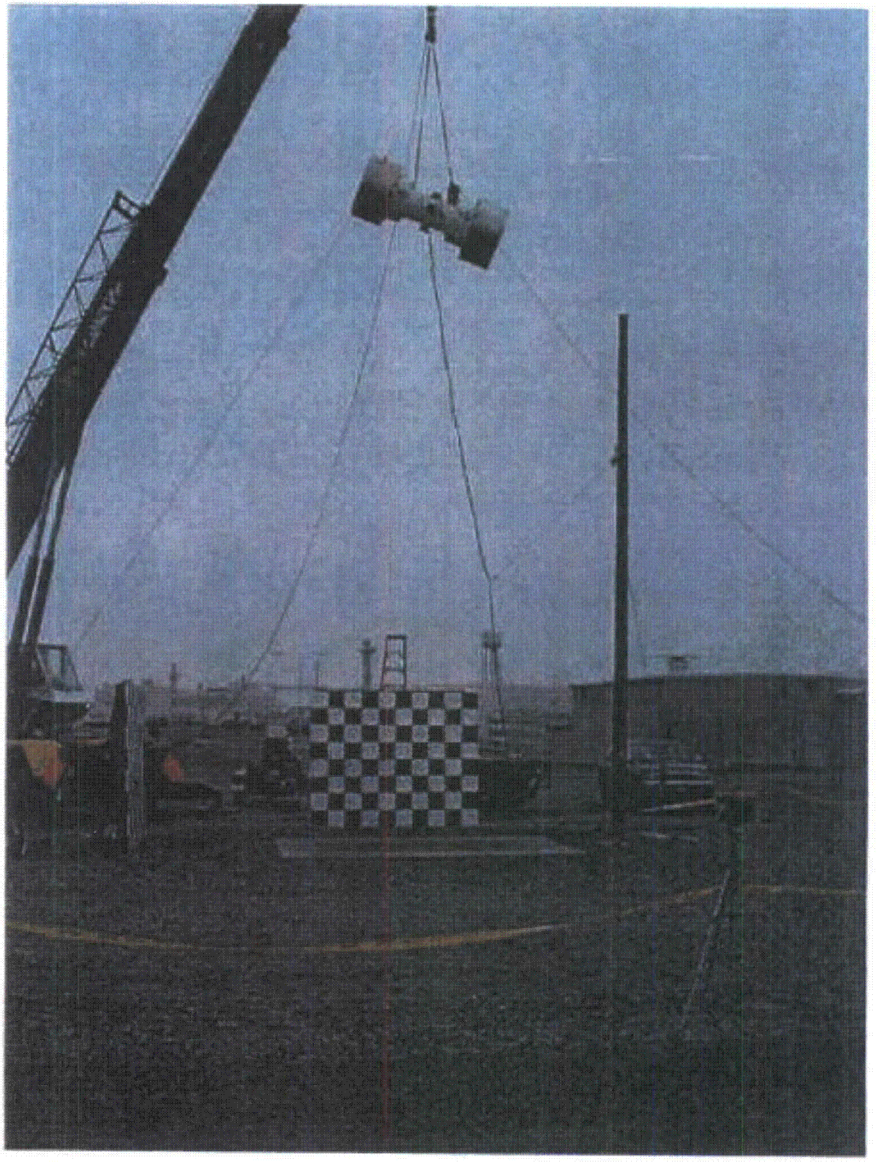

Figure 2.10.9-14

Acceleration Time History, with 1,000 Hz. Low-Pass Filter, 20° Slap Down Drop, Accelerometer 1 (Top / Second Impact)

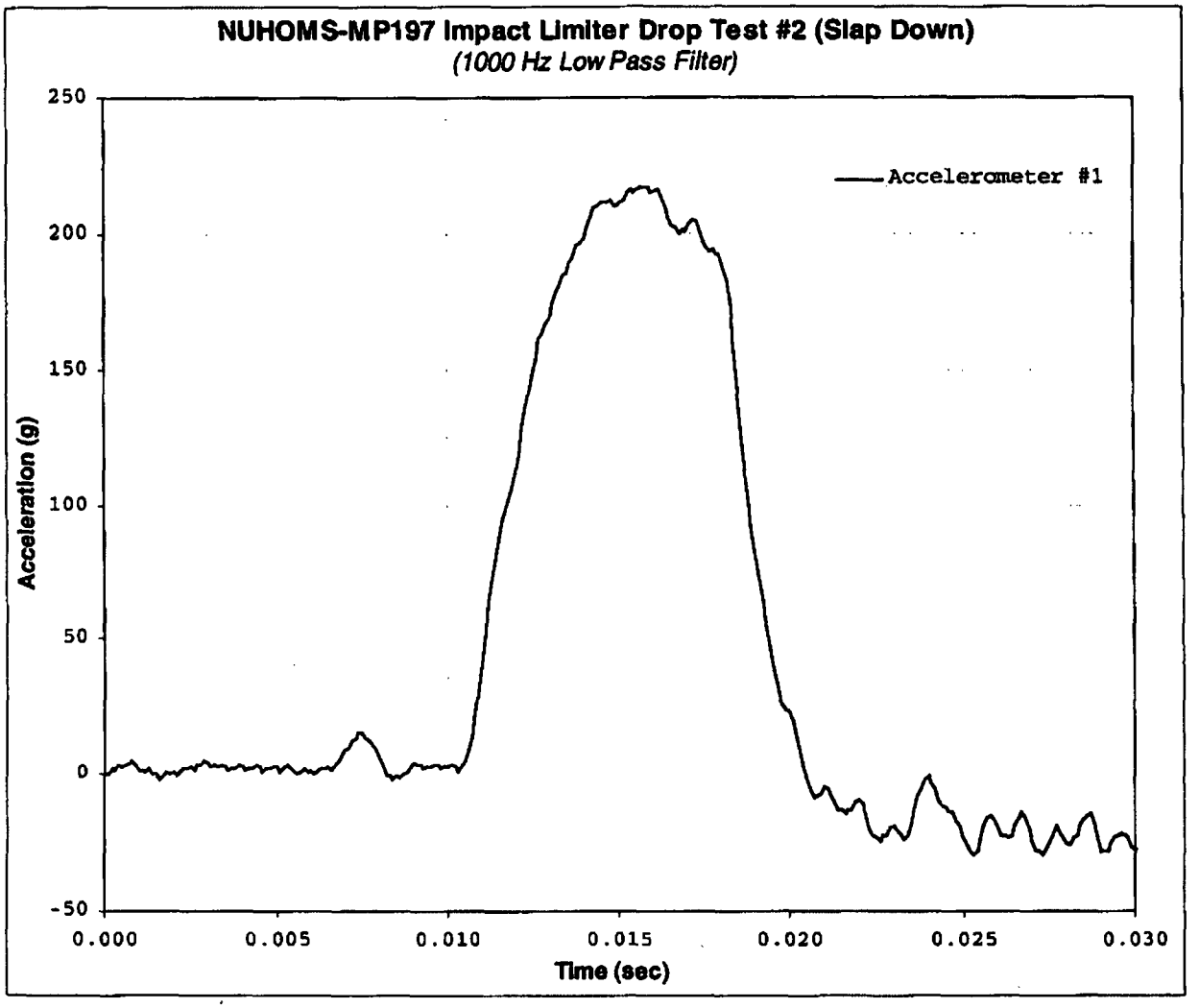

Figure 2.10.9-15

Acceleration Time History, with 1,000 Hz. Low-Pass Filter, 20° Slap Down Drop, Accelerometer 8 (Center of Gravity)

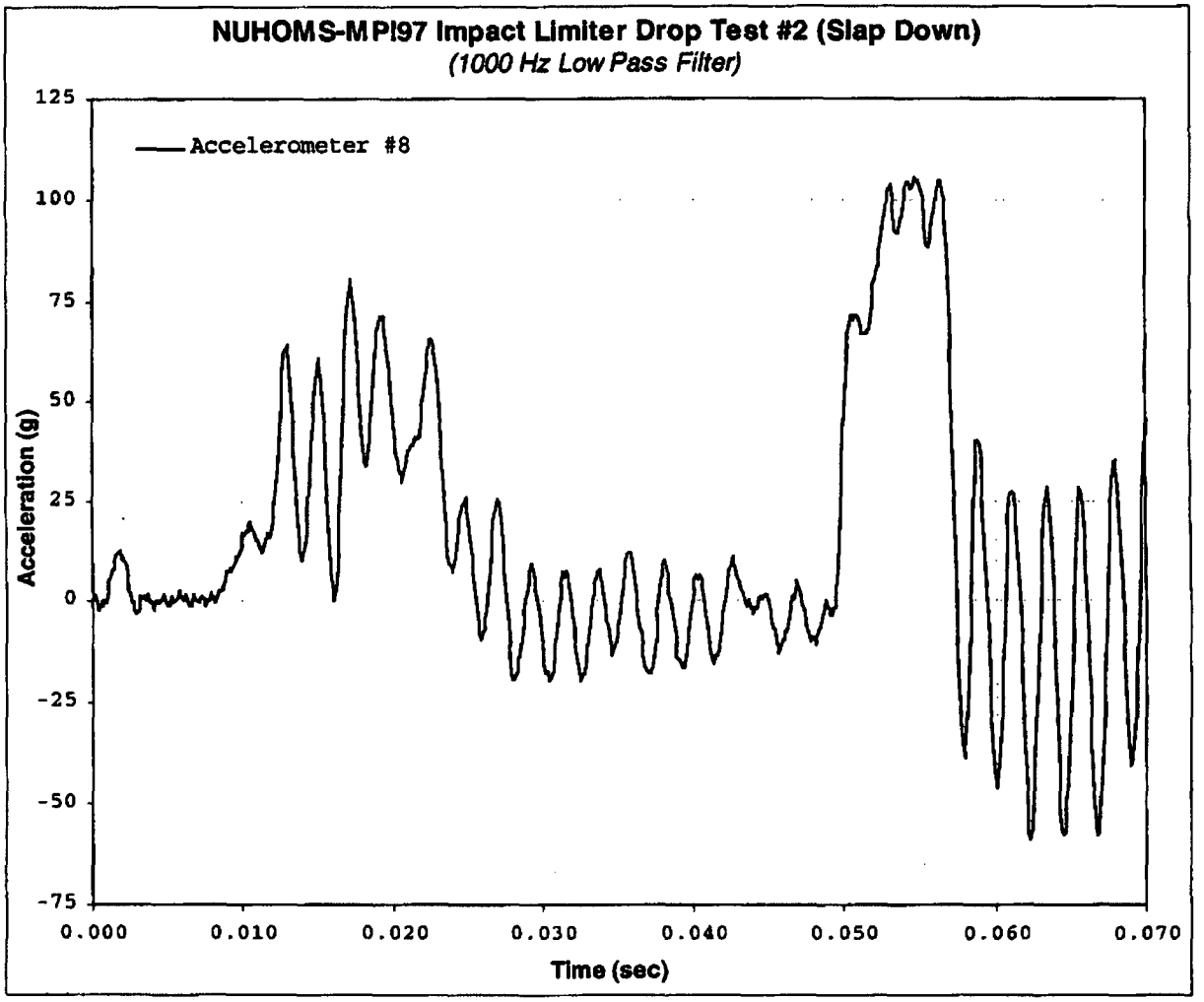

Figure 2.10.9-16

Acceleration Time History, with 1,000 Hz. Low-Pass Filter, 20° Slap Down Drop,
Accelerometer 10 (Bottom / First Impact)

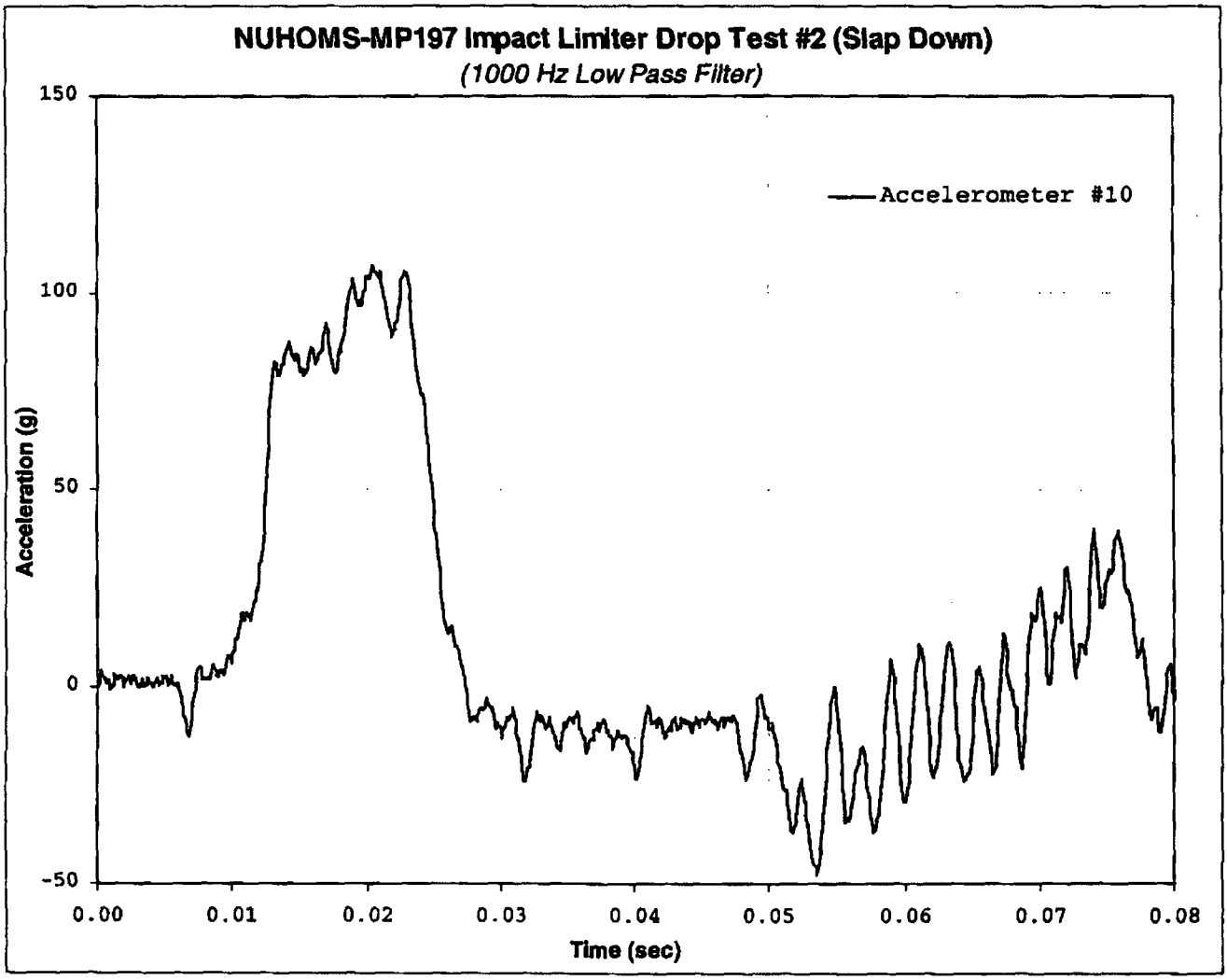

Figure 2.10.9-17

NUHOMS®-MP197 Cask Dummy and Impact Limiters After 20° Slap Down Drop

Figure 2.10.9-18

NUHOMS®-MP197 Cask Dummy and Impact Limiters After 20° Slap Down Drop

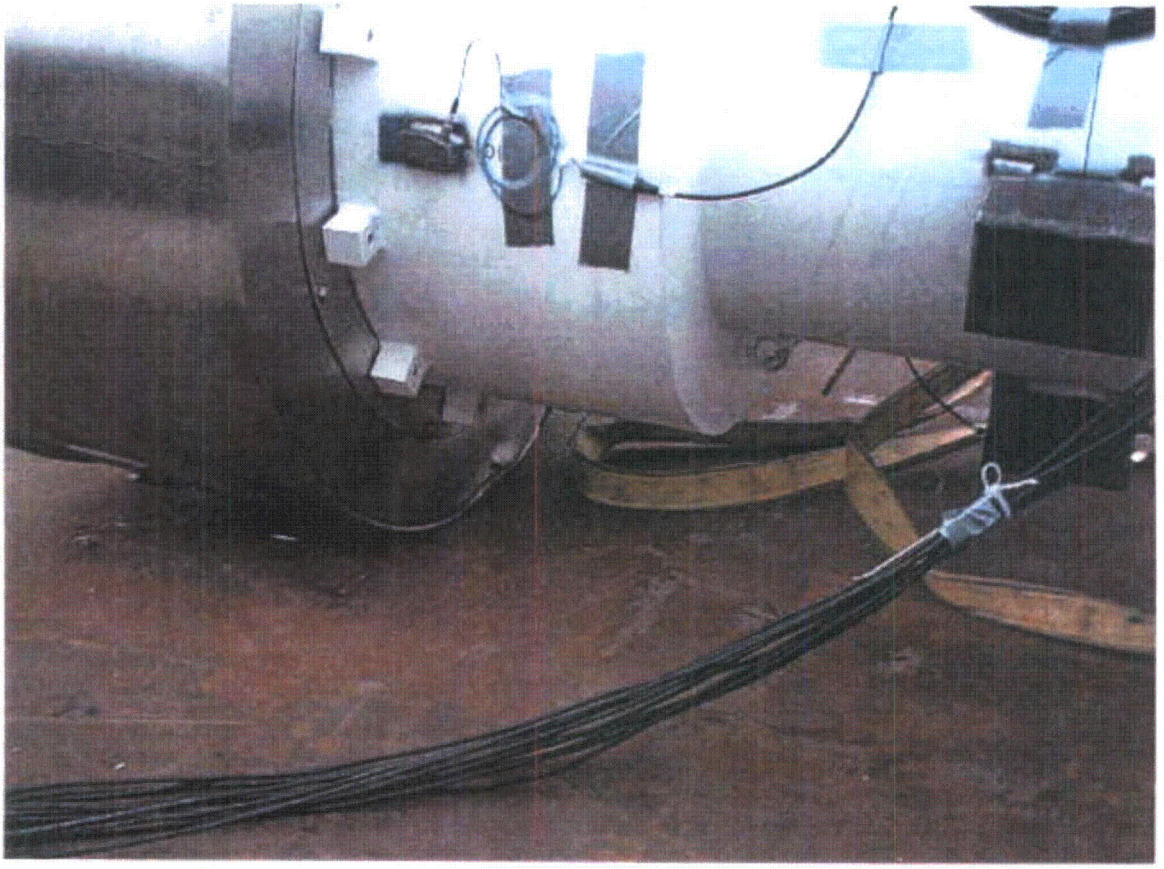

Figure 2.10.9-19

90° End Drop Test Setup

Figure 2.10.9-20

Acceleration Time History, with 1,000 Hz. Low-Pass Filter, 90° End Drop,
Accelerometer 7 (Center of Gravity)